CELLULAR DETERMINANTS OF RALTEGRAVIR EXPOSURE

Thesis submitted in accordance with requirements of the University of Liverpool for the degree of Doctor of Philosophy

Darren Moss

May 2012

This thesis is the results of my own work. The material contained within the thesis has not been presented, either wholly or in part, for any other degree or qualification.

Darren Moss

This research was carried out in the

Liverpool HIV Pharmacology Group

Department of Molecular and Clinical Pharmacology

University of Liverpool, UK

TABLE OF CONTENTS

ACKNOWLEDGEMENTS

The studies presented in this thesis were carried out in the Department of Molecular and Clinical Pharmacology, University of Liverpool. Financial support was provided by Merck Sharp and Dohme for which I am extremely grateful.

Thank you to all the people in the HIV pharmacology group, for providing all the support and encouragement that helped me complete this thesis.

Thank you to my supervisors, Andrew Owen and David Back, for the valuable guidance and advice which was essential throughout my studies.

Thank you to Neill and Phil, for putting up with my stream of stupid questions and for always being supportive when things got tough.

Thank you to Jay Dogg, for teaching me new words that I never knew (Horrendi = plural of horrendous) and for putting up with my constant (affectionate) bullying.

Thank you to Marco, for all the coffee and laughs, and for all the never-ending encouragement you gave me.

Thank you to Paul, for letting me beat you at Street Fighter so many times, and for being a good friend.

Thank you, Mum and Dad. Without you I would never have made it to University and so this thesis is yours also.

Thank you, Mel. You have given me endless loving support during these three years. Also, your great cooking probably stopped me dying of malnutrition!

ABBREVIATIONS

3TC	Lamivudine
μCi	Microcurie(s)
μg	Microgram(s)
μL	Microlitre(s)
μM	Micromolar
μmol	Micromole(s)
Ω	Ohms
A-to-B	Apical to basolateral
ABC	ATP-binding cassette transporter
ADAM	Advanced dissolution, absorption and metabolism
ADME	Absorption, distribution, metabolism and elimination
ADP	Adenosine diphosphate
AHA	Aminohippuric acid
AI	Attachment inhibitor
AIDS	Acquired immunodefiency syndrme
APV	Amprenavir
ARV	Antiretroviral
ATP	Adenosine triphosphate
ATV	Atazanavir
AUC	Area under the curve
AZT	Zidovudine
B/P	Blood to plasma ratio
B-to-A	Basolateral to aplical
bid	Twice-daily
BBB	Blood–brain barrier
BCP	1-bromo-3-chloropropane
C_{12hr}	Concentration 12 hours post-dose
C_{24hr}	Concentration 24 hours post-dose
$CaCl_2$	Calcium chloride
CAR	Cellular accumulation ratio

CAR	Constitutive androstane receptor
°C	Degree Celsius
C_{av}	Average concentration
CCR5	Chemokine (C-C motif) receptor 5
CXCR4	Chemokine (C-X-C motif) receptor 4
CD4	Cluster of differentiation 4
cDNA	Complementary DNA
CI	Confidence Intervals
Ci	Curie(s)
Cl	Clearance
Cl_{int}	Intrinsic clearance
Cl_R	Renal clearance
C_{max}	Maximum concentration
C_{min}	Minimum concentration
CNS	Central nervous system
cRNA	Complementary RNA
CSF	Cerebrospinal fluid
C_{trough}	Trough concentration
CV%	Coefficient of variation
CYP	Cytochrome P450
d4T	Stavudine
ddH_20	Double deionised water
ddI	Didanosine
DLV	Delavirdine
DMEM	Dulbecco's Modified Eagle Medium
dNTP	Deoxy nucleoside triphosphate
DNA	Deoxyribonucleic acid
dQ	Change in drug concentration
DRV	Darunavir
dt	Change in time
E3S	Estrone 3-sulphate
EC	Extracellular

EFV	Efavirenz
ETR	Etravirine
ETV	Etravirine
F	Bioavailability
FDA	Food and drug administration
FI	Fusion inhibitors
fL	Femtolitre(s)
FPV	Fosamprenavir
FTC	Emtricitabine
f_u	Free fraction
g	Gram(s)
g	Gravitational force
GALT	Gut-associated lymphoid tissue
GI	Gastrointestinal
GLY	Glycyl-sarcosine
GMR	Geometric mean ratio
gp41	Glycoprotein 41
gp120	Glycoprotein 120
gp160	Glycoprotein 160
h	Hour(s)
hr	Hour(s)
HAART	Highly active antiretroviral therapy
HBSS	Hank's Balanced Salt Solution
HEPES	4-(2-hydroxyethyl)-1-piperazineethanesulfonic acid
HIV	Human immunodeficiency virus
HLM	Human liver microsome
HPLC	High performance liquid chromatography
IC	Intracellular
IC_{50}	Concentration required to produce 50% inhibition
IC_{95}	Concentration required to produce 95% inhibition
IDV	Indinavir
Ind_{max}	Maximum induction
INI	Integrase inhibitor

IQ	Inhibitory quotient
IQR	Inter-quartile range
IVIVE	*In vitro in vivo* extrapolation
logP	Partition coefficient
K_a	Absorption rate constant
KCl	Potassium chloride
kD	KiloDalton
kg	Kilograms
K_i	Inhibitory constant
K_m	Michaelis constant
kV	KiloVolts
L	Litre(s)
Log	Logarithm to the base 10
LC-MS/MS	Liquid chromatography-triple quadrupole
LogP	Log partition coefficient
$LogP_{app}$	Apparent log partition coefficient
$LogP_{o:w}$	Log partition coefficient between octanol and water
LPV	Lopinavir
LTR	Long terminal repeats
M	Molar
mCi	Millicurie(s)
mg	Milligram(s)
$MgCl_2$	Magnesium chloride
$MgSO_4$	Magnesium sulphate
MIC	Minimum inhibitory concentration
min	Minute(s)
mL	Millilitre(s)
mM	Millimolar
mmol	Millimole(s)
mol	Mole(s)
mRNA	Messenger RNA
MS	Mass spectrometry
MTC	Maximum tolerated concentration

MTT	3-(4,5-dimethylthiazol-2-Yl)-2,5-diphenyltetrazolium bromide
MVC	Maraviroc
NaCl	Sodium chloride
NFV	Nelfinavir
ng	Nanogram(s)
nL	Nanolitre(s)
nm	Nanometer(s)
nM	Nanomolar
nmol	Nanomole(s)
NNRTI	Non-nucleoside reverse transcriptase inhibitor
NPC	Nuclear pore complex
NR	Nuclear receptor
NRTI	Nucleoside reverse transcriptase inhibitor
NtRTI	Nucleotide reverse transcriptase inhibitor
NVP	Nevirapine
OAT	Organic anion transporter
OCT	Organic cation transporter
OF	Objective function
qid	Once daily
PAMPA	Parallel artificial membrane permeability assay
P_{app}	Apparent permeability
PBMC	Peripheral blood mononuclear cell
PBPK	Physiologically-based pharmacokinetic
PCR	Polymerase chain reaction
PD	Pharmacodynamic
PG	Pharmacogenetics
pH	$-\log_{10}$ hydrogen ion concentration
PI	Protease inhibitor
PIC	Pre-integration complex
pl	Picolitre(s)
PK	Pharmacokinetic(s)
PK-PD	Pharmacokinetic-phamacodynamic
pKa	acid dissociation constant

pmol	Picomole(s)
PRO	Probenecid
PXR	Pregnane X receptor
QC	Quality control
RAL	Raltegravir
RNA	Ribonucleic acid
rpm	Revolutions per minute
RPMI	Roswell Park Memorial Institute Medium
RPV	Rilpivirine
RT	Reverse Transcriptase
RTV	Ritonavir
s	Second(s)
sec	Second(s)
SD	Standard Daviation
SE	Standard error
SLC	Solute carrier transporter
SLCO	Solute carrier organic anion transporter
SNP	Single nucleotide polymorphism
SQV	Saquinavir
$t_{1/2}$	Half-life
T-20	Enfuvirtide
TAR	Tariquidar
TDF	Tenofovir disoproxil fumarate
TDP	Tenofovir diphosphate
TDM	Therapeutic drug monitoring
TEA	Tetrethyl ammonium
TEER	Trans-epithelial electrical resistance
TFV	Tenofovir
TPV	Tipranavir
UGT	UDP-glucuronosyltransferase
UV	Ultraviolet
UV-vis	Ultraviolet-visible
VER	Verapamil

V_{max}	Maximum Velocity
vs	Versus
Vss	Volume of distribution

PUBLICATIONS

Moss DM, Siccardi M, Murphy M, Piperakis MM, Khoo SH, Back DJ, Owen A. Divalent metals and pH alter raltegravir disposition in vitro. Antimicrob Agents Chemother, 2012, 56(6): 3020-3026.

Moss DM, Kwan WS, Liptrott NJ, Smith DL, Siccardi M, Khoo SH, Back DJ, Owen A. Raltegravir is a substrate for SLC22A6: A putative mechanism for the interaction between raltegravir and tenofovir. Antimicrob Agents Chemother, 2011, 55(2): 879-887.

Siccardi M, D'Avolio A, Rodriguez-Novoa S, Cuenca L, Simiele M, Baietto L, Calcagno A, **Moss D**, Bonora S, Soriano V, Back DJ, Owen A, Di Perri G. Intrapatient and interpatient pharmacokinetic variability of raltegravir in the clinical setting. Ther Drug Monit, 2012, 34(2): 232-5.

Siccardi M, D'Avolio A, Nozza S, Simiele M, Baietto L, Stefani FR, **Moss D**, Kwan WS, Castagna A, Lazzarin A, Calcagno A, Bonora S, Back D, Di Perri G, Owen A. Maraviroc is a substrate for OATP1B1 in vitro and maraviroc plasma concentrations are influenced by SLCO1B1 521 T>C polymorphism. Pharmacogenet Genomics, 2010, 20(12): 759-65.

COMMUNICATIONS

Moss DM, Siccardi M, Khoo SH, Back DJ, Owen A. The interplay between raltegravir solubility, tablet dissolution, metal binding, charge state and cell permeability. 13th International Workshop on Clinical Pharmacology of HIV Therapy, Barcelona, April 2012, abstract 27.

Moss D, Murphy M, Back D, Owen A. Magnesium inhibits raltegravir cell membrane permeability: elucidating the interaction between raltegravir and antacids in vivo. 17th International Conference on Cytochrome P450, Manchester, June 2011, abstract 3047.

Moss D, Murphy M, Siccardi M, Khoo S, Back D, Owen A. Influence of pH on Transcellular Permeability of Raltegravir: Unravelling the Interaction with Antacids and Food. 18th Conference on Retroviruses and Opportunistic Infections, Boston, February 2011, abstract N117.

Moss D, Liptrott N, Khoo S, Back D, Owen A. Inhibition of SLCO22A1 by antiretroviral drugs: potential for drug-drug interaction in patients. 7th Annual PRISM conference, Lancaster, Septermber 2010.

Moss D, Liptrott N, Khoo S, Back D, Owen A. Influence of SLC22A6 by antiretroviral drugs: potential for drug-drug interactions in patients. DMDG Open Meeting, Canterbury, September 2010.

Moss D, Kwan WS, Liptrott N, Siccardi M, Anstee D, Khoo S, Back D, and Owen A. Raltegravir is a substrate for the influx transporters OAT1 and PEPT1 and the efflux transporter Pgp but is not transported by OATP1A2, OATP1B1, OATP1B3, OCT1, NTCP, or PEPT2. 17th Conference on Retroviruses and Opportunistic Infections, San Francisco, February 2010, abstract 613.

Liptrott N, **Moss D**, Back D, Owen A, Khoo S. Interactions between Tenofovir (TFV) and Nevirapine (NVP) in CD4+ T cells and Monocyte Derived Macrophages Restrict their Intracellular Accumulation. 2nd HIV Symposium, London, June 2010.

Else L, Liptrott N, **Moss D**, Dutton J, Fraser W, Kakude T, Mrus J, Back D. Evaluating the effect of gender on darunavir and ritonavir exposure in HIV infected subjects (a post-hoc analysis of the GRACE PK sub-study). 11th International Workshop on Clinical Pharmacology of HIV Therapy, Sorrento, April 2010, abstract 11.

Siccardi M, **Moss D**, Kwan WS, D'Avolio A, Bonora S, Khoo S, Back D, Di Perri G, and Owen A. Solute carrier organic anion transporter 1B1 (SLCO1B1) mediates transport of maraviroc using a X. leavis model. 17th Conference on Retroviruses and Opportunistic Infections, San Francisco, February 2010, abstract 599.

Siccardi M, D'Avolio A, Nozza S, Bonora S, Castagna A, Baietto L, Stefani FR, **Moss D**, Calcagno A, Scinadra M, Lazzarin A, Back D, Owen A, Di Perri G. Is maraviroc a substrate for SLCO1B1? 10th International Workshop on Clinical Pharmacology of HIV Therapy, Amsterdam, April 2009, abstract P-02.

Kwan WS, **Moss D**, Hartkoorn R, Salcedo-Sora E, Bray P, Khoo S, Back D, Owen A. Determining the substrate specificity of SLCO1B3 for antiretroviral drugs using a X. laevis model. British Pharmacology Society Winter Meeting, Brighton, December 2008, abstract P050.

Southall R, Shaw L, Dilworth C, **Moss D**, Little C, Butler P, Dykstra P, Gill H. Development of a high throughput assay for the screening of mechanism-based cytochrome P450 inhibition. SBS 13th Annual Conference and Exhibition, Montreal, April 2007.

ABSTRACT

HIV infection remains a worldwide concern and new drug treatments are required to tackle drug resistance and to reduce drug-associated host toxicity. Raltegravir, a new anti-HIV drug which targets the HIV integrase enzyme, is now being used in anti-HIV treatment and has shown impressive efficacy and low toxicity. However, the drug shows high pharmacokinetic (PK) variability between subjects and it has been difficult to associate PK parameters with treatment outcome. The aim of this thesis was to improve the current understanding of the factors influencing raltegravir PK and cellular exposure using *in vitro* and *in silico* techniques.

It is unknown whether efflux transporter ABCB1 influences raltegravir disposition. Chapter 2 confirmed raltegravir efflux transport by ABCB1 and found that raltegravir was unable to inhibit or induce ABCB1 activity. Cellular toxicity of raltegravir was also assessed and shown to be minimal. Although ABCB1-mediated transport was confirmed, transport was low compared to control substrates and ABCB1 is unlikely to influence raltegravir *in vivo*.

The influence of influx transporters on raltegravir disposition has not previously been determined and may help explain variable raltegravir PK. Chapter 3 investigated raltegravir influx transport using the *Xenopus laevis* oocyte expression system and also investigated SLC22A1 inhibition by raltegravir. Raltegravir concentration was increased in oocytes expressing influx transporters SLC22A6 and SLC15A1. Raltegravir did not inhibit the transport of tetraethylammonium by SLC22A1.

Chapter 4 investigated in more detail raltegravir influx transport by kidney-expressed SLC22A6. Raltegravir K_m and V_{max} for SLC22A6 were 150 μM and 36 pmol/oocyte/hr, respectively, in the oocyte expression system. Competition between tenofovir and raltegravir for SLC22A6 transport was assessed (IC_{50} values of 27.3 μM and 14.0 μM for tenofovir and raltegravir, respectively). Inhibitors of SLC22A6 and SLC15A1 were unable to alter raltegravir accumulation in peripheral blood mononuclear cells (PBMC), suggesting these transporters are not important in raltegravir PBMC exposure.

Chapter 5 investigated the physicochemical characteristics of raltegravir. An increase in pH led to increased raltegravir solubility and tablet breakdown, decreased lipophilicity and, at low raltegravir concentrations, decreased cell permeation. Raltegravir pKa was calculated as 6.7. At pH 7.4, raltegravir Caco-2 cell membrane permeation was also shown to decrease in the presence of 25 mM divalent metals magnesium and calcium but not in the presence of 25 mM monovalent metal potassium, suggesting that divalent metal-containing products may reduce raltegravir intestinal absorption when co-administered.

Data from Chapter 5 and from literature was used to create a PK simulation modelling program (Simcyp) to help explain and predict the effects of food, pH-altering agents and divalent metal cation-containing products on raltegravir PK (Chapter 6). Simulated data correlated well with real PK values (AUC +4% deviation, C_{trough} -30% deviation, C_{max} +3% deviation). Increased gastrointestinal pH, the presence of ingested divalent metals and an increased gut transit time were all associated with raltegravir PK exposure.

The investigations in this thesis have improved our understanding of the factors influencing raltegravir cellular exposure. Transporters such as ABCB1 and SLC22A6 may play a role in raltegravir PK. However, they are unlikely to fully explain high raltegravir PK variability. Factors such as gastrointestinal pH and divalent metals influence raltegravir physicochemical properties and human trial studies are now underway to define their role in the high inter-patient and intra-patient PK variability seen in people receiving raltegravir.

Chapter 1

General Introduction

Table of Contents

1.1 HIV and AIDS: the current situation

Autoimmune deficiency syndrome (AIDS) remains a serious concern for worldwide public health. AIDS is caused by the human immunodeficiency virus (HIV). Unlike some other infectious diseases, HIV uses no animal to transmit the disease between humans and is instead directly spread between humans by sexual intercourse, blood transfusions, needle sharing and general blood to blood contact. Therefore, HIV has been able to spread from its site of origin in Africa to virtually all the countries in the world.

According to the 2011 UNAIDS report (www.unaids.org), an estimated 34 million people were living with HIV worldwide at the end of 2010, which is 17% higher than in 2001. This figure is a message of both concern and hope: the number of new HIV infection cases remains high, but the yearly number of AIDS-related deaths has reduced to 1.8 million in 2010 from a peak of 2.2 million in 2005. This reduction in AIDS-related deaths is a result of multiple factors, including improved education and increased availability of antiretroviral treatment to HIV patients in developing countries. This emphasises the essential and continuing role that antiretroviral drugs play in reducing HIV-related mortality and transmission worldwide.

1.2 Pathogenesis of HIV-1 infection

1.2.1 The structure and genome of an HIV-1 virion

The HIV-1 virion was first described in 1983 (Barre-Sinoussi *et al.*, 1983) and a description of HIV-2 followed in 1986 (Clavel *et al.*, 1986). HIV is approximately 120nM in diameter and has a spherical shape (Briggs *et al.*, 2006). Contained within the virion are two identical single-stranded RNA strands which are enclosed within a conical antigen named p24. Surrounding p24 is the spherical matrix antigen p17 which maintains the shape of the virion. The outer surface consists of a lipid bilayer taken from a host cell membrane and this contains both host cell proteins and viral proteins gp41 and gp120 (Figure 1.1). Various viral proteins are contained in the core antigen including reverse transcriptase, integrase, protease, vpr, vif, nef and the nucleocapsid proteins p7 and p6. Table 1.1 gives information on the locations and functions of the different viral proteins.

The HIV-1 genome is RNA-based and contains 9749 nucleotides (Ratner *et al.*, 1985) arranged into 9 genes (*pol, gag, env, nef, tat, rev, vpu, vpr* and *vif*) encoding 18 proteins (Figure 1.2). These genes can be divided into structural genes which are essential for viral replication (*gag*, *pol* and *env*) and accessory genes which are not absolutely required for HIV replication *in vitro* (*nef*, *tat*, *rev*, *vpu*, *vpr* and *vif*).

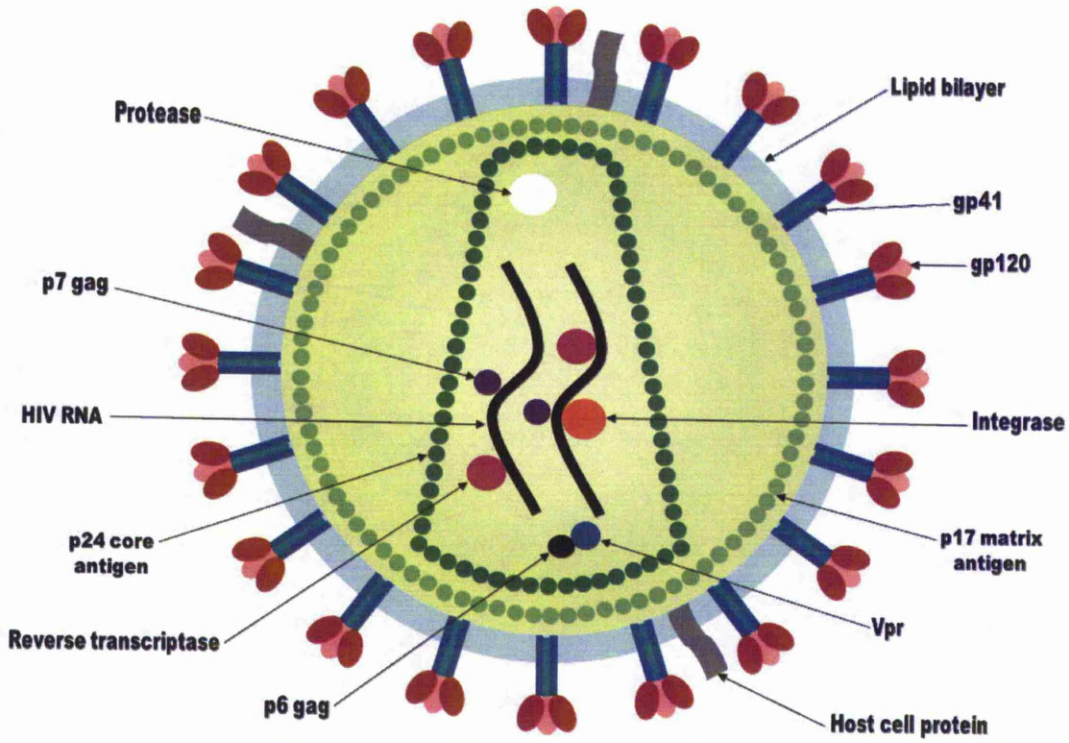

Figure 1.1. The structure of the HIV-1 virion.

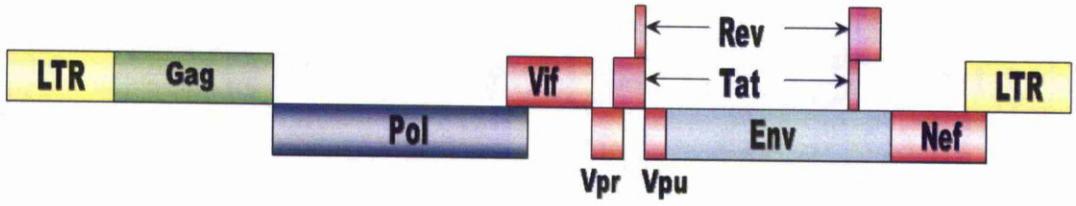

Figure 1.2. The HIV-1 genome.

Name	Size	Function	Localization
Gag			
MA	p17	Membrane anchoring, env interaction, nuclear transport of viral core	Virion
CA	p24	Core capsid	Virion
NC	p7	Nucleocapsid, binds and protects RNA	Virion
	p6	Binds Vpr	Virion
Pol			
PR	p15	Gag/Pol cleavage and maturation	Virion
RT	p66, p51	reverse transcription, RNAse H activity	Virion
RNAse H	p15	degrades the RNA after DNA synthesis	Virion
IN	p31	DNA provirus integration	Virion
Env	gp120, gp41	External viral glycoproteins which bind to CD4 and secondary receptors	Plasma membrane, virion envelope
Tat	p16, p14	Viral transcriptional transactivator	Primarily in nucleolus/ nucleus
Rev	p19	RNA transport, stability and utilisation factor	Shuttling between nucleolus and cytoplasm
Vif	p23	Promotes virion maturation and infectivity	Cytoplasm, virion
Vpr	p10-15	Promotes nuclear localisation of pre-integration complex, inhibits cell division, arrests infected cells at G2/M	Virion, nucleus
Vpu	p16	Promotes extracellular release of viral particles, degrades CD4 in the ER	Integral membrane protein
Nef	p25-p27	CD4 and class I MHC down-regulation	Primarily in nucleolus/ nucleus

Table 1.1. The proteins produced by the HIV-1 genome and their known function.

1.2.2 HIV-1 replication

HIV-1 is a group VI lentivirus in the family *retroviridae*. The processes undertaken by HIV-1 to replicate itself have been extensively studied, although further research is still ongoing. Figure 1.3 shows a simplified version of the HIV-1 replication cycle.

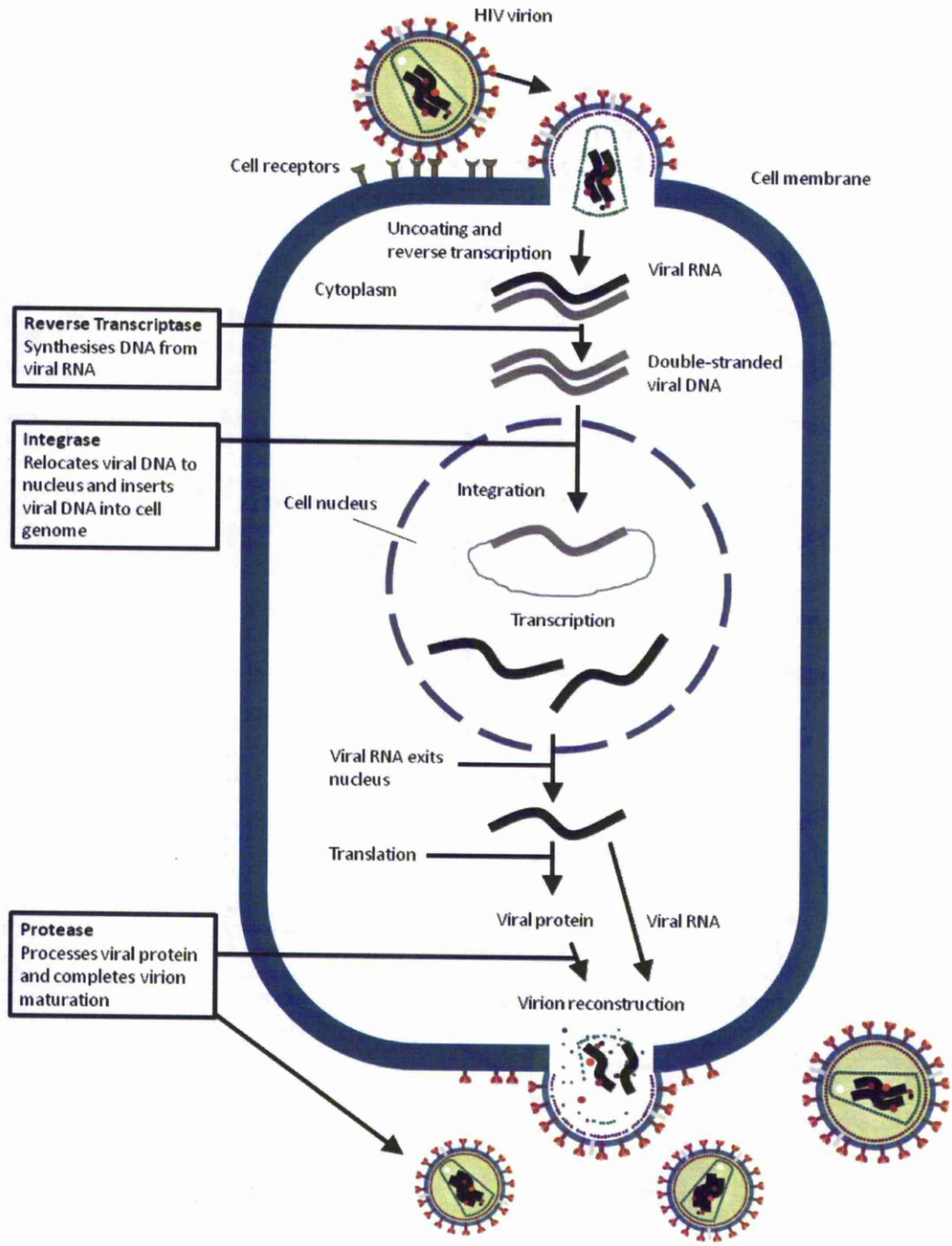

Figure 1.3. The replication cycle of HIV-1. Boxes on the left detail the roles of essential viral proteins reverse transcriptase, integrase and protease.

HIV entry into CD4+ macrophages and T cells begins with the adsorption of the HIV gp120 to a CD4 receptor on the cell surface (Chan *et al.*, 1998; Wyatt *et al.*, 1998). This gp120-CD4 interaction has a high binding affinity but also requires HIV gp41 binding to the chemokine receptor CXCR4 (Feng *et al.*, 1996) or CCR5 (Deng *et al.*, 1996). Dual-tropic HIV strains have also been isolated which are able to use either CXCR4 or CCR5 for cell entry (Doranz *et al.*, 1996). The HIV peptide gp41 can then puncture the cell membrane and the HIV virion fuses with the host membrane, releasing the viral nucleoplasmid into the cell. The nucleoplasmid then uncoats, discharging the single stranded viral RNA and various viral proteins into the cell cytoplasm (Aiken, 2006). The single stranded viral RNA is then used to produce double stranded viral cDNA by the viral enzymes reverse transcriptase and RNAse H. This copying process is error-prone, resulting in about 1 to 10 errors per round of replication (Isel *et al.*, 2010). This feature, along with the fecundity of HIV, allows for rapid mutation and adaptation of the virus in response to antiretroviral treatment. The double stranded viral cDNA is relocated into the nucleus and integrated into the host cell genome by the viral enzyme integrase (see Section 1.3 for a detailed overview of integration).

Once integrated, the viral cDNA is termed the provirus and may remain dormant in this form for long periods. Several factors can affect the activation state of the HIV provirus, most importantly the location of the provirus in the cell genome and the abundance of cellular transcription factors (Bisgrove *et al.*, 2005). The provirus is efficiently expressed when integrated into actively transcribed areas of the cell genome. A cellular transcription factor important for HIV provirus transcription is NF-κB, which is upregulated in activated T cells (Hiscott *et al.*, 2001).

When the provirus is initially transcribed, viral mRNA is spliced to produce the viral proteins rev and tat. Working with the cellular cofactor Cyclin T1 (Wei *et al.*, 1998), tat binds to the LTR transactivation region of the provirus and upregulates HIV proviral DNA transcription. The viral protein rev binds to the rev response element in the viral *env* gene and similarly upregulates transcription. Rev is also a nuclear export factor and is important for switching the expression of regulatory viral proteins to the structural and enzymatic proteins (Pollard *et al.*, 1998).

The env gp160 is cleaved by the viral protease enzyme to form gp41 and gp120 which are both localised to an area of the inner cell surface (Adamson, 2012). Gp41 anchors gp120 to the membrane of the infected cell. Other proteins, including incompletely spliced polypeptides gag and gag-pol, also associate with the inner layer of the cell membrane along with unspliced HIV genomic RNA. The forming virion begins to bud from the cell, taking with it the cell membrane and associated cellular membrane proteins and carbohydrate chains (Spearman, 2006). Eventually an immature virion is released from the cell and the enclosed protease enzyme completes maturation by splicing the polypeptides to form working proteins. These virions are now able to infect new host T cells and macrophages, completing the replication cycle. Potentially billions of new HIV virions are created every day in an infected individual and this astronomical rate of replication puts enormous pressure on the individual's immune system, allowing the virus population to evolve resistance to antiretroviral drugs, neutralising antibodies and cytotoxic T cell attack.

1.3 Integration: an essential step in HIV-1 replication

HIV-1 is a retrovirus, characterised by the ability to convert its RNA genome into DNA and then integrate this DNA into the host cell genome. The integration of viral DNA is essential for HIV-1 to replicate *in vivo* and *in vitro* (Bouyac-Bertoia *et al.*, 2001).

1.3.1 The HIV-1 integrase protein: structure and function

HIV-1 integrase is a 32 kDa protein which is involved in the preparation and integration of viral DNA into the host cell genome. Approximately 40–100 integrase molecules are packaged within each HIV particle (Pommier *et al.*, 2005). The integrase gene is located in the pol region of the HIV-1 genome and is initially expressed as a polyprotein containing immature integrase, reverse transcriptase and protease. This polyprotein is cleaved by protease in a budded virion to produce mature enzymes. The active integrase enzyme involved in viral DNA integration is believed to be a pair of covalently-bound polypeptide dimers, but other multimer forms may be important for other stages in the HIV life cycle (Chiu *et al.*, 2004). The 3D crystal structure of the complete integrase enzyme has recently been described (Hare *et al.*, 2010).

Integrase contains three functionally distinct regions: the N-terminal domain, the catalytic core domain and the C-terminal domain (Figure 1.4). The N-terminal domain includes a HHCC motif containing a single zinc atom. This motif is involved in the formation of integrase multimers via zinc coordination and is also seen to

promote concerted integration of the viral DNA into the host genome. The C-terminal domain performs metal-independent non-specific DNA binding. It is the least conserved region of integrase, most likely due to the lack of specific DNA binding (Chiu *et al.*, 2004). An SH3 fold is present in this region and is believed to interact with reverse transcriptase. The catalytic core domain contains several conserved regions which are essential for integrase activity. HIV integrase has a structure which is similar to other retroviral integrase enzymes (Chiu *et al.*, 2004) and contains a DDE three amino acid motif. Alteration of any of these residues results in total loss of integrase activity and a subsequent elimination of viral replication. These three conserved amino acids coordinate an interaction with two divalent metal cations, believed to be Mg^{2+} or Mn^{2+} (Asante-Appiah *et al.*, 1997; Espeseth *et al.*, 2000). The binding of these metal cations to the integrase enzyme brings about a major conformational change to the enzyme (Asante-Appiah *et al.*, 1997) and a reduced susceptibility to proteolysis (Asante-Appiah *et al.*, 1998).

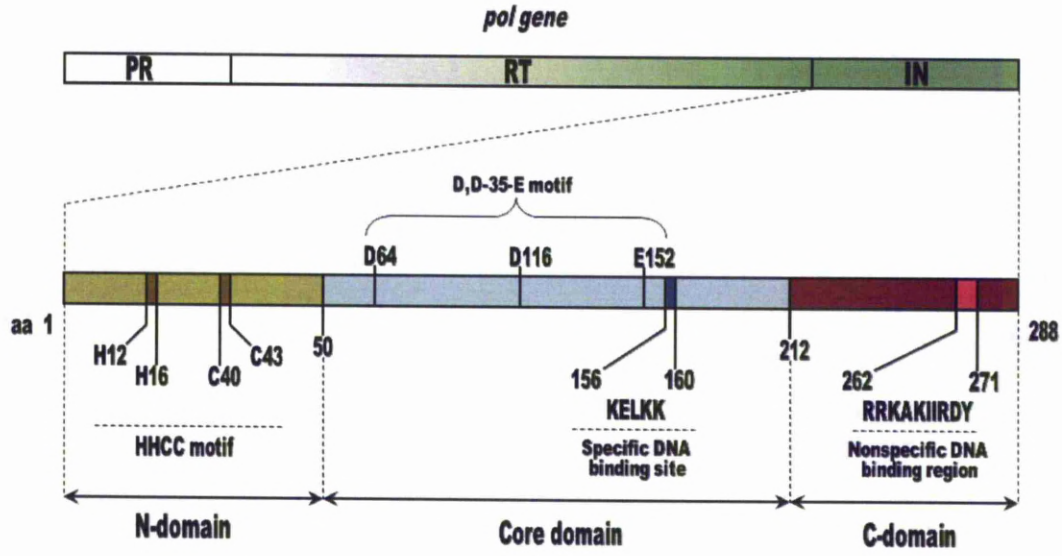

Figure 1.4. The integrase gene.

Integrase performs at least three essential functions in the HIV-1 replication cycle: 3'-processing, nuclear relocation and strand transfer of viral DNA (Krishan *et al.*, 2012). The 3'-processing stage follows the production of viral DNA by reverse transcriptase and involves endonucleolytic cleavage of GT nucleotides at the 3' site of the conserved CA region in the long terminal repeats (LTR). This creates CA-3'-hydroxyl ends on the viral DNA, providing the nucleophile groups required in the later strand transfer stage.

Viral DNA must be relocated to the site of the host DNA for successful integration. A potential barrier to this relocation is the cell nuclear envelope, which surrounds the host cell genome in non-dividing cells (Krishan *et al.*, 2012). The nuclear membrane is present in most eukaryotic cells in order to separate the nuclear contents from the cytoplasm (Mekhail *et al.*, 2010). Molecules of less than 40 kDa are able to passively diffuse across the membrane but transport of large or hydrophilic materials such as RNA and protein are regulated by the nuclear pore complex (NPC).

Many viruses are unable to infect non-dividing cells (Roe *et al.*, 1993) or are shown to infect non-dividing cells less effectively than cells which are actively dividing (Katz *et al.*, 2005; Lewis *et al.*, 1992). HIV is able to infect both dividing and non-dividing cells with similar efficacy (Lewis *et al.*, 1992) due to the ability of HIV integrase to form a viral DNA-bound pre-integration complex (PIC) with various viral (Fassati *et al.*, 2003; Reil *et al.*, 1998) and cellular (Farnet *et al.*, 1997) co-factors. This facilitates nuclear relocation of viral DNA.

Strand transfer occurs in the nucleus and is the ligation of the 3'-processed viral DNA into the host cell chromosome, resulting in a 5' viral CA base pair overhang and a cellular DNA five base gap on each side of the inserted viral genome. These overhangs and gaps are believed to be repaired by cellular DNA repair enzymes.

1.4 Anti-HIV chemotherapy

1.4.1 The basic principles of anti-HIV chemotherapy

The current strategy used with anti-HIV therapy is to use drugs to target and inhibit critical stages in the HIV replication process, thus preventing more HIV from being produced (Figure 1.5).

The immediate goals of anti-HIV therapy are to cause the greatest possible reduction in viral load and to prevent further virus-induced damage to the host immune system. When successful, these factors help bring about anti-HIV therapy's ultimate goals; immune system reconstitution and an increase in both the length and quality of the HIV-infected person's life. From an epidemiological viewpoint, anti-HIV therapy and the subsequent reduction in viral load reduce the risk of transmitting the virus to non-infected individuals and children born to HIV-positive mothers (Sturt *et al.*, 2010).

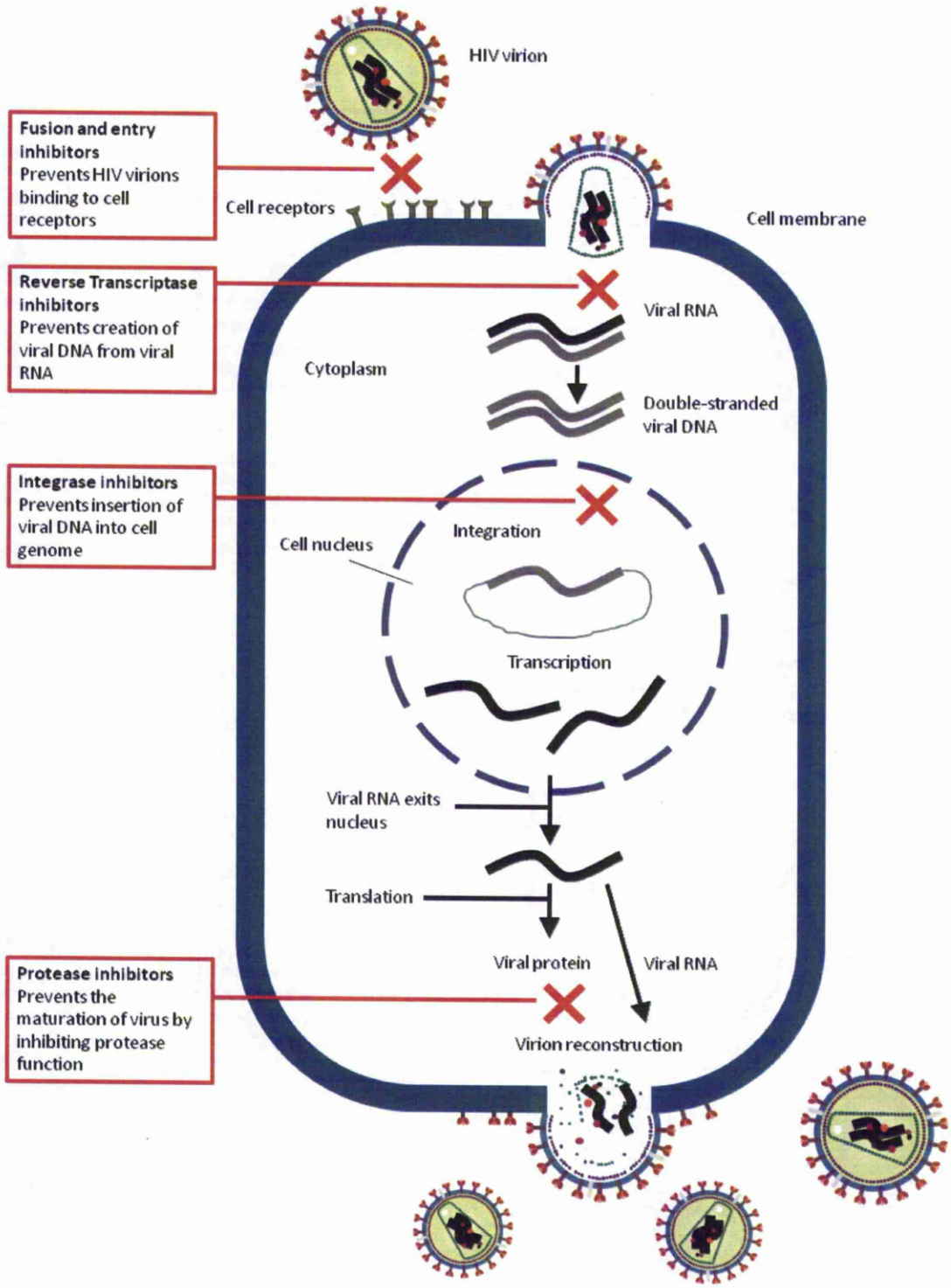

Figure 1.5. The main classes of antiretroviral drugs and how they inhibit the HIV replication cycle.

1.4.2 Drugs used in anti-HIV chemotherapy

There are currently 25 anti-HIV drugs approved by the FDA and several more in various stages of development. Table 1.2 gives a list of the currently approved drugs, where each drug is classified by its mechanism of action. Details of the mechanism of action and general characteristics of each drug class are detailed below and examples from drug classes are shown in Figure 1.6.

Type	Drug	Abbrev.	Trade Name	Manufacturer
NRTIs	Emtricitabine	FTC	Emtriva™	Gilead
	Lamivudine	3TC	Epivir™	GSK
	Zidovudine	AZT	Retrovir™	GSK
	Didanosine	ddI	Videx™	BMS
	Tenofovir	TFV/TDF	Viread™	Gilead
	Stavudine	d4T	Zerit™	BMS
	Abacavir	ABC	Ziagen™	GSK
NNRTIs	Delavirdine	DLV	Rescriptor™	Pfizer
	Efavirenz	EFV	Sustiva™	BMS/MSD
	Nevirapine	NVP	Viramune™	Boehringer Ingelheim
	Etravirine	ETR	Intelence™	Tibotec
	Rilpivirine	RPV	Edurant™	Tibotec
PIs	Tipranavir	TPV	Aptivus™	Boehringer Ingelheim
	Amprenavir	APV	Agenerase™	GSK
	Darunavir	DRV	Prezista™	Tibotec
	Indinavir	IDV	Crixivan™	MSD
	Saquinavir	SQV	Invirase 500™	Roche
	Lopinavir/ritonvir	LPV	Kaletra™	Abbott
	Ritonavir	RTV	Norvir™	Abbott
	Atazanavir	ATV	Reyataz™	BMS
	Fosamprenivir	FPV	Telzir™	GSK
	Nelfinavir	NFV	Viracept™	Roche/Pfizer
FIs	Enfuvirtide	T-20	Fuzeon	Roche
AIs	Maraviroc	MVC	Celsentri™	Pfizer
INIs	Raltegravir	RAL	Isentress™	MSD

Table 1.2. Current anti-HIV drugs approved by the FDA. NRTIs = nucleoside and nucleotide reverse transcriptase inhibitors; NNRTIs = non-nucleoside reverse transcriptase inhibitors; PIs = protease inhibitors; FIs = fusion inhibitors; AIs = attachment inhibitors; INIs = integrase inhibitors.

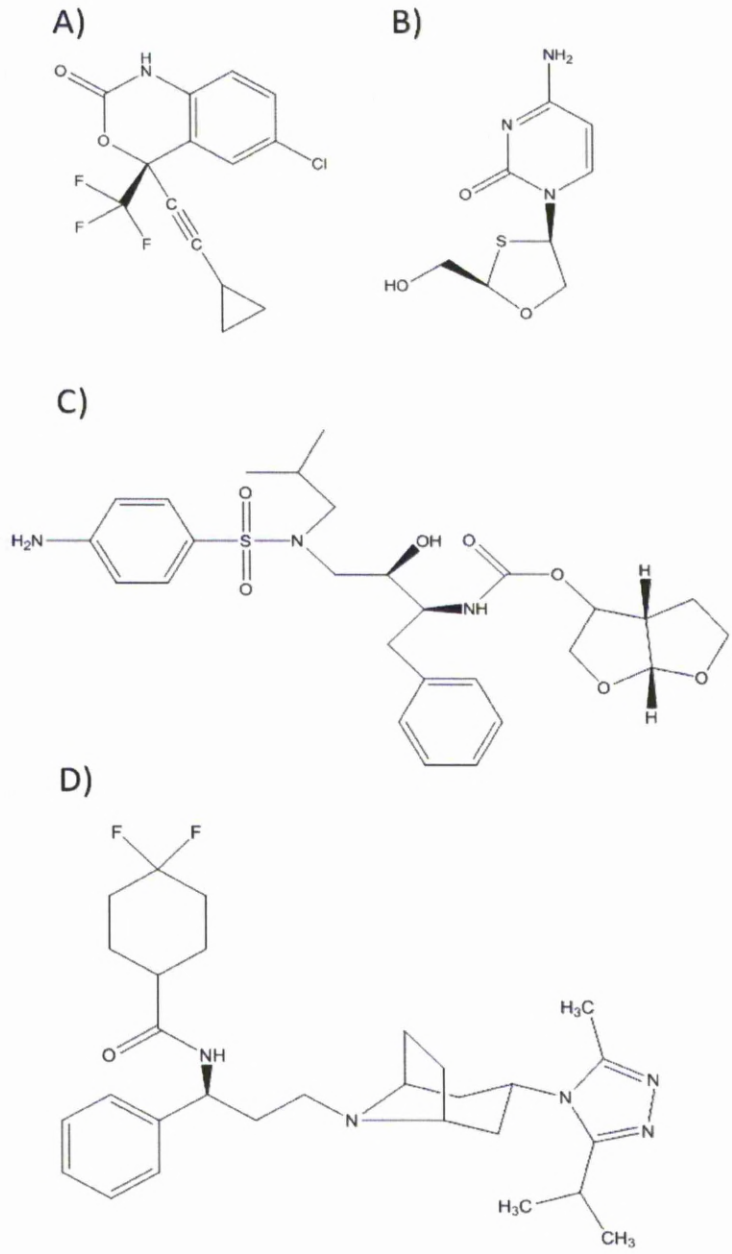

Figure 1.6. Examples of drugs from the major anti-HIV drug classes. The NNRTI efavirenz (A) is highly lipophilic (logP of 4.46) and blocks the hydrophobic pocket within the polymerase domain of the p66 HIV reverse transcriptase subunit. The NRTI lamivudine (B) resembles a deoxynucleotide and arrest HIV DNA synthesis. The PI darunavir (C) contains polypeptide-like regions and blocks the active site of HIV protease. The attachment inhibitor maraviroc (D) resembles HIV gp41 and

prevents the binding of gp41 with the cellular chemokine CCR5. The structure of raltegravir, the only integrase inhibitor currently used in anti-HIV therapy, is shown in Section 1.6.1.

1.4.3 Nucleoside and nucleotide reverse transcriptase inhibitors

Nucleoside and nucleotide reverse transcriptase inhibitors (NRTIs and NtRTIs, respectively) are analogues of the naturally occurring deoxynucleotides needed to synthesize the viral DNA. They compete with the natural deoxynucleotides for incorporation into the growing viral DNA chain but lack a 3'-hydroxyl group and therefore arrest the viral DNA synthesis once incorporated. The different NRTIs mimic only one of the four nucleotides used in DNA synthesis; adenine, thymine, cytosine or guanine. When co-administering different NRTIs to HIV patients, it is essential to use NRTIs that mimic different nucleotides to avoid cross-resistance.

1.4.4 Non-nucleoside reverse transcriptase inhibitors

Non-nucleoside reverse transcriptase inhibitors (NNRTIs) work in a non-competitive manner by binding to reverse transcriptase at a location other than the enzyme's active site. Specifically, the drugs block the hydrophobic pocket within the polymerase domain of the p66 RT subunit (Waters *et al.*, 2007). A hypersensitivity rash can result from the use of NNRTIs and hepatitis can occur in patients with a high CD4+ T-cell count (van Leth *et al.*, 2005). Once these immune system responses have been observed, the NNRTI cannot be used further in the patient's treatment.

1.4.5 Protease inhibitors

Protease inhibitors (PIs) act by blocking HIV protease, a viral enzyme that cleaves the HIV-1 gag and gag-pol polyprotein backbone at nine specific cleavage sites to produce shorter, functional proteins. The crystal structure of protease (Navia *et al.*, 1989) was used to develop compounds which would fit directly into the enzyme's active site. The previously released drugs inhibited reverse transcriptase so the discovery of PIs was a major boost in the management of HIV infection and led to the development of **H**ighly **A**ctive **A**nti**R**etroviral **T**herapy (HAART; Section 1.4.9). Unfortunately, most of the PIs developed so far exhibit adverse effects and can interact with other medications via inhibiting or inducing drug metabolising enzymes and drug transporters (Profit *et al.*, 1999) (Granfors *et al.*, 2006). The PI ritonavir is a particularly potent inhibitor of cytochrome P450 (CYP) 3A4, resulting in increased exposure of drugs metabolized by this enzyme (Kharasch *et al.*, 2008) (Decker *et al.*, 1998). This property has been utilised to augment the bioavailability of PIs (CYP3A4 substrates) and ritonavir-mediated "boosting" is used for currently licensed PI-containing HAART regimens (Merry *et al.*, 1997). Cobicistat, a potent and selective inhibitor of human CYP3A4 which displays no anti-HIV activity, is currently under investigation for use as a replacement for ritonavir in PI-containing HAART (Mathias *et al.*, 2010). PIs are generally highly bound to plasma protein and therefore show poor passage into compartments such as cerebrospinal fluid (Kim *et al.*, 1998), potentially resulting in the creation of sanctuary sites for HIV-1 replication.

1.4.6 Fusion inhibitors

Fusion inhibitors prevent fusion of the HIV virion with the host cell membrane and therefore prevent release of the nucleocapsid into the target cell. Currently, the polypeptide drug enfuvirtide is the only licensed fusion inhibitor available for HIV treatment. Enfuvirtide acts by binding to the HR1 region of gp41, preventing the fusion of the virion with the cell surface (Joly *et al.*, 2010). The large size and protein-like characteristics of enfuvirtide mean that the drug cannot be orally administered due to enzymatic degradation in the intestine. Therefore, enfuvirtide must be administered parenterally. This, coupled with high costs, has limited the use of the drug to "salvage" therapies for patients with multi-drug resistant HIV infection.

1.4.7 Attachment inhibitors

Attachment inhibitors prevent the HIV virion from binding to the target cell. Maraviroc is the only licensed attachment inhibitor and works by binding to the cellular chemokine receptor CCR5, blocking its interaction with HIV gp41 without activating the receptor (Corbeau *et al.*, 2009). CXCR4-tropic HIV, which is not susceptible to maraviroc treatment, is more lytic to T cells *in vitro* and is temporally associated with the development of AIDS (Daar *et al.*, 2007). Therefore, patients require a HIV tropism test prior to starting therapy with maraviroc to ensure they don't harbour CXCR4-tropic HIV. The cost and time required to conduct the tropism test has limited the widespread use of this drug.

1.4.8 Integrase inhibitors

Integrase inhibitors act by targeting and disrupting the function of the viral integrase enzyme (Pommier *et al.*, 2005). The term "integrase inhibitors" currently covers a broad range of compounds which all inhibit the ability of integrase to function but which have different mechanisms of action (Ingale *et al.*, 2011). The recently approved drug, raltegravir, inhibits integrase strand transfer (Section 1.3.1), but there are also various 3'-processing and multimerisation inhibitors which are currently in development. A more complete discussion on the mechanism of action and drug properties of raltegravir is continued in Section 1.5.

1.4.9 The concepts of highly active antiretroviral therapy and therapeutic drug monitoring

Despite huge successes in the treatment of HIV infection, it is now accepted that current HIV drugs cannot eradicate the virus from the body (Eisele *et al.*, 2012). This means that, unless more advanced treatments are developed, HIV-positive patients must continue taking anti-HIV therapy for life. This presents serious problems because patients must remain adherent to the drugs to prevent emergence of resistance and are also at risk of experiencing adverse drug reactions. All currently licensed anti-HIV drugs are associated with some form of adverse drug reaction but toxicities are more common and/or severe with some drug classes than with others.

Due to the high replication rate of the virus and the inefficient proof-reading ability of reverse transcriptase, HIV is able to rapidly become resistant to anti-HIV drugs via genetic mutation. This has led to the simultaneous use of multiple anti-HIV drugs

with HAART. This limits the virus's ability to become resistant to the treatment because resistance would require simultaneous mutation of all drug targets. The use of HAART has been extremely successful in reducing the occurrence of drug-resistant HIV in patients (Lehman *et al.*, 2009). However, resistance can still emerge when plasma exposure to one or more of the drugs within a regimen falls below the minimum therapeutic concentrations. Currently, WHO guidelines recommend first-line HAART should consist of the NRTIs tenofovir and emtricitabine and also a third drug of a different drug class (www.who.com). The third drug in first-line HAART can be the NNRTI efavirenz, the integrase inhibitor raltegravir or the ritonavir-boosted PIs atazanavir or darunavir.

The issues surrounding adverse drug reactions (particularly concentration-dependent toxicities) and drug resistance have led to the implementation of therapeutic drug monitoring (TDM) in some settings (Back *et al.*, 2001). TDM involves measuring anti-HIV drug concentrations in the blood plasma of the patient during treatment and using that information to help understand key issues such as viral load, development of drug resistance, and drug-induced patient toxicity. TDM is a useful surrogate for physicians to assess whether their patients are adherent to their regimens.

An example of a typical drug concentration profile from human plasma is shown in Figure 1.7. There exists a minimum inhibitory concentration (MIC) for each drug, determined *in vitro* and confirmed in patients, which is the lowest drug concentration that completely suppresses viral replication. There is also a range of drug concentrations in the plasma below the MIC where only partial viral suppression is achieved, resulting in positive selection of drug-resistant virus. The range of drug

concentrations between the MIC and the maximum concentration before host toxicity is called the "therapeutic window" of the drug. The maximum tolerated concentration before host toxicity (MTC) divided by the MIC is the drug's therapeutic index. Drugs with a high therapeutic index are often favoured in drug development, as the drugs are generally safer to use.

There are standard pharmacokinetic (PK) parameters that are determined from concentration time plots, such as C_{max} (the maximum concentration of drug achieved during the dose interval), C_{trough} (the concentration of drug just before taking another dose) and Area Under the Curve (AUC, the area under the plot of plasma concentration of drug against time after drug administration). The C_{max} and AUC values are often used to predict host toxicity (Forni *et al.*, 2010) and the C_{trough} value is important in relation to the emergence of drug resistance during HAART (Rizk *et al.*, 2012). The values of these PK parameters vary from patient to patient (inter-patient variability) and also in the same patient over time (intra-patient variability). These variations result from multiple factors, such as age, genetics, disease and interactions with other substances, which can impact the Absorption, Distribution, Metabolism and Excretion (ADME) of a drug.

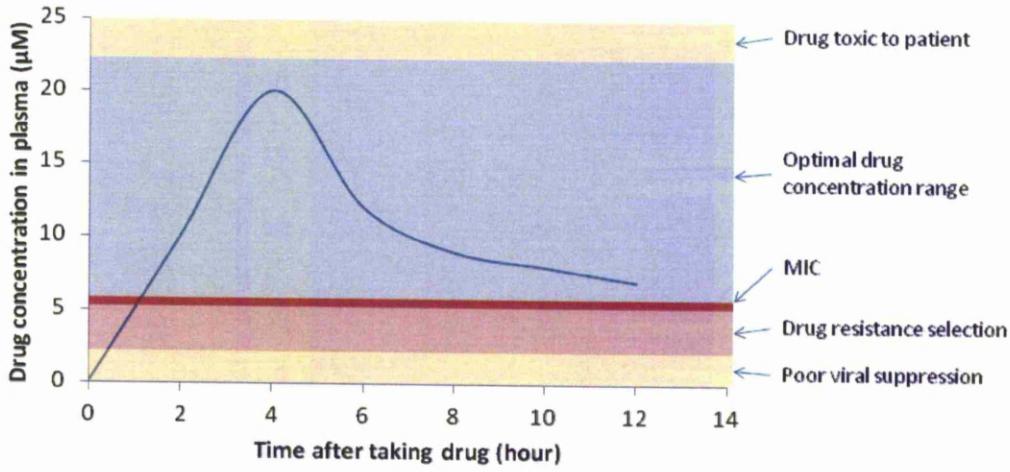

Figure 1.7. A typical drug concentration profile from human plasma. Shown is the minimum inhibitory concentration (MIC), the lowest drug concentration required to completely inhibit viral replication and prevent drug resistance selection.

1.5 Pharmacological factors relevant to HIV therapy

As described in Section 1.4.9, the desirable and undesirable effects of a drug are often linked to the concentration of drug at the site of action and in the various compartments of the body. Drug exposure in the body is the result of the interplay of several individual factors which are encompassed in the ADME properties of a drug. Elimination of a drug is determined by drug metabolism (usually in the liver or gut) and drug excretion (usually by the liver or kidney). A major determinant of the ADME properties of a drug is its affinity for drug metabolism enzymes and drug transporters.

1.5.1 Drug-metabolising enzymes

Drug metabolism is the biochemical modification of pharmaceutical compounds through specialized enzymatic systems, usually with the goal of converting lipophilic compounds to more hydrophilic metabolites. These metabolites are usually more soluble and as such are more readily cleared from the body, usually via biliary excretion or via the kidneys. The principle site of drug metabolism is usually the liver, although drug metabolism enzymes are also expressed at various levels in other tissues, including the gastrointestinal (GI) tract, kidney, lung, brain and skin (Krishna *et al.*, 1994). Drug-metabolising enzyme reactions can be separated into two distinct groups: phase I (nonsynthetic) reactions and phase II (synthetic) reactions.

Phase I reactions include hydrolysis, reduction and oxidation of a drug and occur in the cellular endoplasmic reticulum membrane. The most intensively studied group of

phase I enzymes are the CYP450 enzymes, which are involved in the metabolism of the majority of drugs used in HAART (with the exception of NtRTIs and raltegravir). Phase II reactions include glucuronidation, glycosidation, sulfation, methylation, acetylation, amino acid conjugation and glutathione conjugation and occur in the cell cytosol.

1.5.2 Drug transporters

Membrane-bound drug transporters are classified into two groups; the ATP-binding cassette (ABC) and solute-carrier (SLC) protein families (Rees *et al.*, 2009; Roth *et al.*, 2012). Both families of drugs require ATP to function, although SLC transporters do not use ATP directly and instead utilise a proton gradient created by separate ATP-consuming proton pumps.

Drug transporting proteins are located on both the cell's plasma membrane and the membranes of internalised compartments such as the mitochondria (Leung *et al.*, 2007). The proteins function by transporting endogenous and xenobiotic molecules across membranes, often against a concentration gradient. Generally, ABC transporters move drugs out of the cell (efflux transporters) and SLC transporters concentrate drugs into the cell (influx transporters), although certain transporters, such as human equilibrative nucleoside transporter family (SLC29), are capable of moving substrates in both directions (Young *et al.*, 2008). Cells in different tissues often express distinct and/or varying levels of drug transporters (Bleasby *et al.*, 2006) and this can lead to directed drug distribution and an increased concentration of drug in different organs and compartments in the body (Table 1.3).

Gene	Protein	Aliases	Tissue in humans
ABCB1	ABCB1	P-gp, MDR1	Intestine, liver, kidney, brain, placenta, adrenal gland, testes
ABCB4	ABCB4	MDR3	Liver
ACB11	ACB11	BSEP	Liver
ABCC1	ABCC1	MRP1	Intestine, liver, kidney, brain
ABCC2	ABCC2	MRP2	Intestine, liver, kidney, brain
ABCG2	ABCG2	BCRP	Intestine, liver, breast, placenta
SLCO1A2	SLCO1A2	OATP1A2, OATPA	Brain
SLCO2B1	SLCO2B1	OATPB	Intestine, liver, kidney, brain
SLCO1B1	SLCO1B1	OATP1B1, OATPC	Liver
SLCO1B3	SLCO1B3	OATP1B3, OATP8	Liver
SLC10A1	SLC10A1	NTCP	Liver, pancreas
SLC15A1	SLC15A1	PEPT1	Intestine, kidney
SLC15A2	SLC15A2	PEPT2	Kidney
SLC22A1	SLC22A1	OCT1	Liver
SLC22A2	SLC22A2	OCT2	Kidney, brain
SLC22A3	SLC22A3	OCT3	Skeletal muscle, liver, placenta, kidney, heart
SLC22A6	SLC22A6	OAT1	Kidney, brain
SLC22A7	SLC22A7	OAT2	Liver, kidney
SLC22A8	SLC22A8	OAT3	Kidney, brain

Table 1.3. Major drug transporters expressed in humans.

A possible misunderstanding when discussing drug transporters is the assumption that efflux transporters are associated with removal of drug from the body and influx transporters with the accumulation/maintenance of drug in the body. This relationship is not always correct, as the effect of a transporter on drug disposition will depend on which cellular surface the transporter is located. As an example, enterocyte cells in the small intestine provide a controlling barrier for drug absorption from the gut (Figure 1.8). Efflux transporters on the apical (lumen-facing)

surface (ABCB1, ABCC2, ABCC4, and ABCG2) decrease substrate absorption from the lumen, whereas efflux transporters on the basolateral (blood-facing) surface (ABCC1, ABCC3 and ABCC5) increase substrate absorption. Similarly, influx transporters on the apical (SLCO1A2, SLCO2B1, SLC22A3) and basolateral (SLC22A1, SLC22A2, SLC22A7) surface work to increase and decrease luminal substrate absorption, respectively (Kis *et al.*, 2010a).

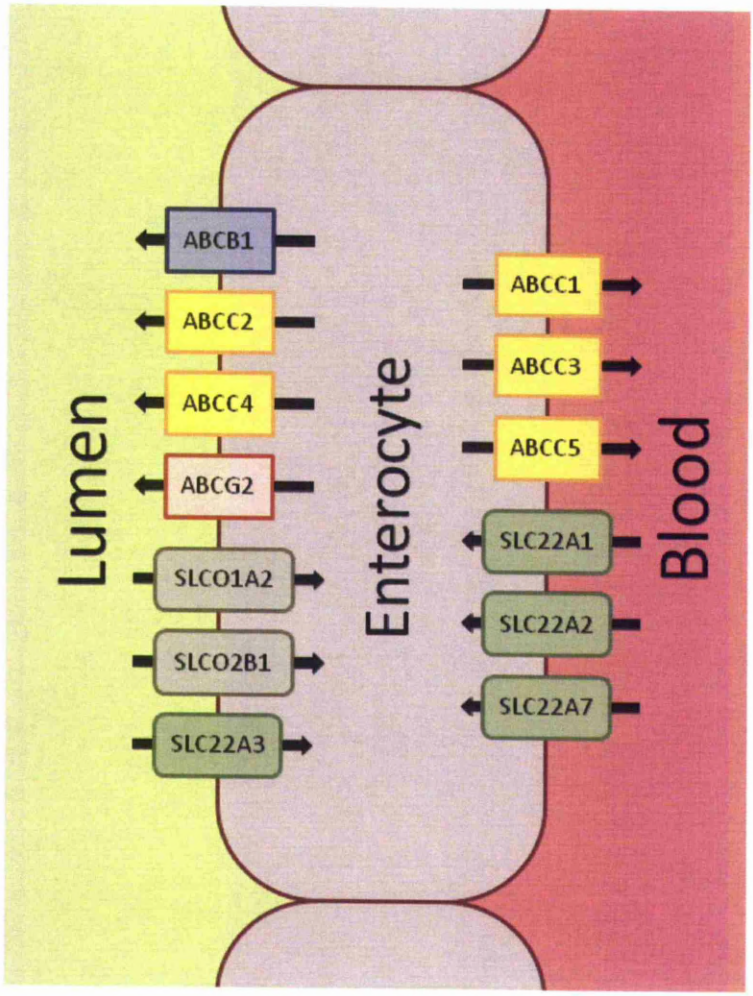

Figure 1.8. The expression and location of several drug-transporting proteins in enterocyte cells.

It is increasingly accepted that drug transporters play a major role in the disposition of several antiretroviral drugs (Kis *et al.*, 2010a). The impact of drug transporters on raltegravir disposition is integral to the work in this thesis and the topic is covered in detail in the experimental Chapters 2, 3 and 4.

1.5.3 Drug interactions

Due to the life-long nature of HAART (Section 1.4.9) and the high likelihood of HIV-positive patients using drugs to treat co-morbidities, the amount and variety of drugs that a HIV-positive patient must take during their life is high. This increases the risk of the patient experiencing a drug interaction, some of which can be serious and even life-threatening.

A drug interaction is defined as an interaction between a drug and another co-administered substance which alters the pharmacokinetic or pharmacodynamic characteristics of the drug. The drug can be described as the "perpetrator" (causes the interaction) or the "victim" (effected by the interaction), although interactions are often more complicated and both substances can affect each other.

The definition "drug interaction" is applied to interactions of the drug with another drug (drug-drug interaction), ingested food or liquid, or any other substance. The substance can interact directly (direct binding to the drug; displacing drug from plasma protein; etc) or indirectly (altering metabolism enzyme and transporter protein expression levels or activity; altering GI pH, fat content or emptying time; etc).

Inhibition of drug-metabolising enzymes and drug transporters

Substances that can directly inhibit the activity of drug-metabolising enzymes and drug transporters are potentially capable of altering the PK of substrates for these proteins. Inhibition is usually described as reversible or irreversible (Lin *et al.*, 1998). Reversible inhibition usually involves direct competition for the enzyme/transporter and does not normally damage the protein. Irreversible inhibition involves permanent or semi-permanent reduction in enzyme/protein activity and can result from non-competitive binding of inhibitor (binding at a location other than the enzyme/transporter active site). As an example, tariquidar is not a substrate of ABCB1 but is able to potently and irreversibly inhibit the ATPase activity of the transporter (Fox *et al.*, 2007).

As discussed in Section 1.4.5, inhibition of drug metabolising enzymes can actually be used as a treatment strategy to increase concentrations of CYP3A4-metabolised drugs, such as the use of ritonavir in HAART to decrease the clearance rate of PIs (Merry *et al.*, 1997). However, the usual goal in drug discovery is to avoid inhibiting major drug-metabolising enzymes and drug transporters and therefore reduce the chance of causing drug interactions.

Induction of drug-metabolising enzymes and drug transporters

Substances that can induce the expression level of drug-metabolising enzymes and drug transporters are potentially capable of altering the PK of substrates for these proteins. Expression of metabolism enzymes and drug transporters are regulated by

nuclear receptors, ligand-activated transcription factors such as the pregnane X receptor (PXR) and constitutive androstane receptor (CAR), which are important in the context of induction. As an example, the antibiotic rifampin is able to induce expression of CYP3A4 via activation of PXR (Li *et al.*, 2006) and this can result in increased clearance of CYP3A4 substrates such as lopinavir (Decloedt *et al.*, 2011), where rifampin treatment caused a 4.8-fold decrease in median plasma concentration.

The induction potential of drugs is often not detected during *in vitro* drug discovery as induction is "indirect" and often requires extended time periods to allow for protein expression. Furthermore, the correlation between *in vitro* induction data and *in vivo* reality is often not clear, with varying concentrations of drug in different tissues resulting in localised induction effects. For example, 10 μM nelfinavir induced *ABCB1* mRNA 4-fold in isolated human hepatocytes (Dixit *et al.*, 2007). However, ABCB1 protein induction was not detected in the liver of rats dosed with 175 mg/kg/day nelfinavir after 14 days treatment (Huang *et al.*, 2001), although expression of ABCB1 protein was increased 83% in rat intestine. The absence of ABCB1 induction in rat liver may be explained by lower nelfinavir concentrations being reached in the liver compared to in the lumen. In the same study, amprenavir 450 mg/kg/day caused an increase in hepatic CYP3A4 of 151% but did not alter intestinal CYP3A4 protein levels.

Displacement of highly protein-bound drugs

Plasma protein binding is a major determinant and a potential limiting factor in the metabolism and excretion of highly protein-bound drugs (Boffito *et al.*, 2003). Both

drug metabolism and drug transport is prevented by drug-protein binding (Bow *et al.*, 2006). Any administered xenobiotic which inhibits the binding of a drug to plasma protein has the potential to increase the volume of distribution (redistribution of drug into tissues). However, several drug interactions originally believed to be controlled by plasma protein displacement, such as the increase in free phenytoin concentrations in plasma when co-administered with valproic acid (Tsanaclis *et al.*, 1984), are likely to also involve other mechanisms such as inhibition of drug metabolism (Rolan, 1994).

Alteration of gastrointestinal pH

The pH of the GI tract is an important factor in the absorption of many drugs, potentially altering drug release, solubility, chemical stability, charge state and/or intestinal permeability (Charman *et al.*, 1997). Ionic drugs with a pKa within the physiological pH range are susceptible to alterations in GI pH because drugs with an ionic charge are less able to permeate the intestinal wall without active transport. Any drug or substance which alters the pH of the GI tract is therefore capable of causing drug interactions of susceptible drugs. As an example, the anti-HIV drug atazanavir is a weak base with a pKa of 4.3 (Kis *et al.*, 2010b) and shows reduced solubility at higher pH. The gastric pH-reducing drugs omeprazole and famotidine decreased the bioavailability of atazanavir by 48% and 62%, respectively (Klein *et al.*, 2008). The effect of pH on drug disposition is integral to the investigations in this thesis and is discussed in more detail in Chapters 5 and 6.

The binding of drugs to metal ions

Metal ions are present in ingested food, liquids, multivitamin tablets and certain antacid treatments. There are known drug interactions where the presence of certain metal ions in the gastrointestinal tract alters the usual absorption profile of a drug (Lober *et al.*, 1999) (Patel *et al.*, 2011), presumably by binding of the metal ion to the drug and formation of a drug-metal complex which is less able to cross the intestinal epithelium. Binding of the metal ion to the drug can also reduce the activity of drugs and this interaction is characteristic of several antibiotics (Seedher *et al.*, 2010). The effect of metal binding on drug disposition is integral to the investigations in this thesis and is discussed in more detail in Chapters 5 and 6.

1.6 Raltegravir and other integrase inhibitors

Raltegravir (Isentress®), previously known as MK-0518, is an integrase inhibitor used in the treatment of HIV-infected patients (Okeke *et al.*, 2011). The drug was given an accelerated release approval by the FDA in October 2007 to be used as part of HAART for treatment-experienced patients with multidrug resistant HIV-1. However, it is now also used in treatment-naive patients (Markowitz *et al.*, 2009). Raltegravir is also effective at preventing HIV-2 viral replication (Smith *et al.*, 2011) and this allows it to be used as a part of treatment in HIV-2 infected patients.

1.6.1 Raltegravir chemistry and physicochemical properties

Raltegravir is formulated for HIV treatment as a potassium salt and has a molecular weight of 482.51 for the salt form and 444.42 for the free drug. The empirical formula of raltegravir potassium is $C_{20}H_{20}FKN_6O_5$ and the structural formula is shown in Figure 1.9. The full chemical name of raltegravir potassium is N-[(4-fluorophenyl)methyl]-1,6-dihydro-5-hydroxy-1-methyl-2-[1-methyl-1-[[(5-methyl-1,3,4-oxadiazol-2-yl)carbonyl]amino]ethyl]-6-oxo-4-pyrimidinecarboxamide mono-potassium salt.

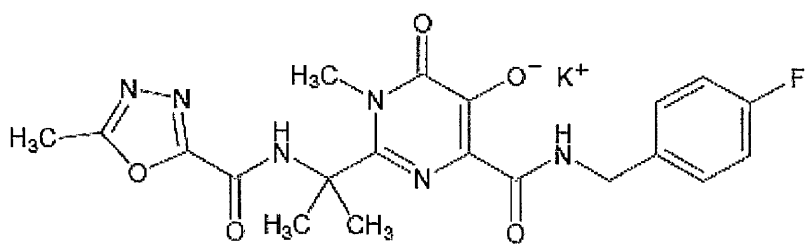

Figure 1.9. Structural formula of raltegravir potassium salt.

The raltegravir potassium salt is an off-white powder with hydrophilic properties. The drug is soluble in water, somewhat soluble in methanol, very slightly soluble in acetonitrile and ethanol and insoluble in isopropanol. Raltegravir is moderately bound to human plasma at 83%. Outside of our investigations, the logP or logD of raltegravir has not been reported.

Further information on the physicochemical properties of raltegravir has been discovered during investigations for this thesis. These investigations are detailed in Chapter 5.

1.6.2 Raltegravir pharmacodynamics

Raltegravir inhibits the catalytic activity of HIV integrase by blocking the integration of HIV-1 cDNA into the host cell genome (Figure 1.5). Integration of viral cDNA is essential for HIV replication and the action of raltegravir effectively terminates the HIV life cycle. There is no known homologue of integrase expressed in humans, which reduces the risk of raltegravir-induced cellular toxicity.

Raltegravir can only bind to integrase once the enzyme is both bound to HIV DNA and has performed 3' processing on the HIV DNA (Section 1.3.1) (Pommier *et al.*, 2005). 3'-processing of HIV DNA occurs inside the infected cell and this strongly suggests that intracellular permeation of raltegravir is a prerequisite for effective inhibition of integrase. Therefore, factors which dictate intracellular drug concentrations of raltegravir, such as cell membrane permeability and the actions of

drug transporters, could play a crucial role in raltegravir pharmacokinetics and pharmacodynamics.

The mechanism of action of raltegravir is distinct from all other antiretrovirals and displays synergistic activity when combined in HAART treatment (Hicks *et al.*, 2009). Furthermore, an investigation into the effect of raltegravir on HIV decay kinetics (the speed at which HIV viral load decreases following initiation of therapy) showed raltegravir monotherapy reduced HIV viral load more rapidly compared with efavirenz monotherapy over the 10-day trial (Murray *et al.*, 2007). This suggests that raltegravir could be useful in initial therapy to treat patients with an extremely high HIV viral load.

The inhibitory action of raltegravir is observed at very low concentrations of drug. The IC_{50} of raltegravir *in vitro* was 2-7 nM (Temesgen *et al.*, 2008) and the IC_{95} of raltegravir in cell cultures was 19 nM and 33 nM using 10% foetal bovine serum or 50% human serum, respectively. Several completed or ongoing phase II and phase III trials have shown raltegravir to be a potent inhibitor of HIV-1 replication with an impressive safety profile (Grinsztejn *et al.*, 2007) (Markowitz *et al.*, 2007) (Steigbigel *et al.*, 2008). Moreover, raltegravir has shown non-inferiority to the NNRTI efavirenz in combination therapy (Lennox *et al.*, 2009).

As is seen with all other antiretroviral drugs, mutations in the HIV genome have been identified which confer resistance to raltegravir. The major mutation pathways G140S/Q148H and N155H confer around 8-fold and 14-fold raltegravir resistance, respectively, using purified integrase *in vitro* (Malet *et al.*, 2008). Crossover

resistance between raltegravir and NRTIs, NNRTIs and PIs have not been observed, although cross resistance with other integrase inhibitors in clinical development, such as elvitegravir, have been demonstrated (Hazuda, 2010).

1.6.3 Raltegravir metabolism and transport

The metabolism of raltegravir has been extensively studied *in vitro* (Kassahun *et al.*, 2007) (Iwamoto *et al.*, 2008a). The main route of raltegravir metabolism is glucuronidation via uridine 5'-diphospho-glucuronosyltransferase (UGT) 1A1 and to a lesser extent by UGT1A9 and UGT1A3. All other UGT enzymes screened showed no contribution to raltegravir metabolism. Raltegravir was not a substrate or an inhibitor of cytochrome P450 enzymes 1A2, 2C9, 2D6, 2C19, 3A4, 2C8 and 2B6 and did not induce CYP3A4 expression in primary human hepatocytes. These results suggest that drug-drug interactions between cytochrome P450 substrates/inhibitors and raltegravir is unlikely.

The oral bioavailability of raltegravir is estimated to be at least 32%, based on the fraction of drug excreted in the urine (Kassahun *et al.*, 2007). PK studies in healthy volunteers showed that radioactively labelled raltegravir was excreted in the faeces (61.4% of total excreted drug) and the urine (38.6% total excreted drug). Raltegravir and its inactive glucuronide, named M2, constituted 28% and 72% of the dose excreted in urine, respectively. The dose excreted in faeces was wholly in the form of parent raltegravir.

Interestingly, a study in rats showed that raltegravir is the only product excreted in the rat faeces, whereas a parallel study using bile duct-cannulated rats showed that the majority of dose in the bile was in the M2 glucuronide form (Kassahun *et al.*, 2007). This suggests that the majority of the dose eliminated via the liver in rats is being glucuronidated but that this glucuronide undergoes subsequent hydrolysis in the gut to form the parent compound. This raises the possibility that raltegravir undergoes enterohepatic recirculation in rats but this has not been conclusively demonstrated *in vivo*.

Outside of the investigations in this project, there have been little published data on the interaction between raltegravir and drug transporters and only ABCB1 has been investigated in any detail. In a directional transport study conducted by Merck (unpublished data), raltegravir yielded efflux ratios (B-to-A / A-to-B) of 11.1, 7.1 and 9.4 in LLC-PK1 cells expressing human, mouse and rat ABCB1, respectively. The non-expressing control LLC-PK1 cells showed no directional transport and the positive control drug verapamil gave efflux ratios in ABCB1-overexpressing cells of 5.2 (human), 5.1 (mouse), and 4.1 (rat). These data indicate that raltegravir is a substrate of ABCB1 in the three species, although this was determined in only one experimental system and used an ABCB1-overexpressing cell line. Transport of raltegravir by ABCB1 at more physiological levels has not previously been determined but is investigated in this thesis.

1.6.4 The effect of demographic factors and special populations on raltegravir PK

Demographic factors

There have been no confirmed relationships established between raltegravir PK and demographic factors sex, age, race or body mass index (Brainard *et al.*, 2011c; Iwamoto *et al.*, 2008d). A significant decrease in raltegravir C_{12hr} in females compared to males (24.7 ng/mL versus 58.0 ng/mL, p = 0.007) seen by Iwamoto *et al* has not been repeated in subsequent studies and was possibly due to the small female sample size of 6 subjects. In a study using HIV-infected patients, Siccardi et al (2012) found no significant difference in C_{trough} levels between females and males (median, 288 ng/mL versus 243 ng/mL, p = 0.45) and neither age (p = 0.78) or body weight (p = 0.36) were correlated to raltegravir concentrations (Siccardi *et al.*, 2012a).

Hepatic and renal impairment

The primary route of raltegravir elimination is glucuronidation via the liver (Kassahun *et al.*, 2007) and the impact of moderate hepatic impairment on raltegravir PK has been evaluated (Iwamoto *et al.*, 2009a). The effect of severe renal impairment on raltegravir PK was also assessed in the same study. There was no clinically significant effect of moderate hepatic impairment or severe renal impairment on raltegravir PK, meaning that the drug can be taken by these special populations without dose adjustments. However, raltegravir PK in subjects with severe hepatic impairment has not been investigated.

UGT1A1 and UGT1A9 polymorphisms

Raltegravir is a UGT1A1 substrate and the primary route of raltegravir metabolism in humans is believed to be via this enzyme. There are known polymorphisms associated with UGT1A1 which reduce enzyme activity. Therefore, there is the potential that genetic polymorphisms in *UGT1A1* could affect raltegravir PK or PD properties.

The impact of the homozygous *UGT1A1*28* polymorphism (rs8175347) on single dose 400mg raltegravir PK was determined in healthy subjects (Wenning *et al.*, 2009b). When comparing homozygous *UGT1A1*28* versus wild type *UGT1A1*1*, the geometric mean ratio (GMR) (90% CI) of the $AUC_{0-\infty}$, C_{max} and C_{12hr} was 1.41(0.96, 2.09), 1.40 (0.86, 2.28) and 1.91 (1.43, 2.55), respectively. A separate study assessed the impact of UGT1A1*28 and UGT1A1*6 (rs4148323) polymorphisms on raltegravir PK in HIV-infected Japanese patients and found no association (Hirano *et al.*, 2011).

Raltegravir is also metabolised by UGT1A9, although the rate of metabolism was less than half that seen using UGT1A1 *in vitro* (Kassahun *et al.*, 2007). A clinical study assessed the impact of 102 single nucleotide polymorphisms (SNPs) on raltegravir PK in HIV patients, which included SNPs in *UGT1A1* and *UGT1A9* (Arab-Alameddine *et al.*, 2012). A SNP in *UGT1A9* (rs72551330, *UGT1A9*3*), when present a homozygous mutation, showed a study-wide association with increased raltegravir bioavailability. However, the homozygous *UGT1A9*3* mutation was only found in a single individual from the 219 HIV infected patients screened and

statistical significance could not be confirmed. Furthermore, the rarity of this SNP reduces its usefulness in predicting raltegravir PK.

1.6.5 Raltegravir tissue distribution

The distribution of raltegravir into various tissues in the body is an important factor to understand, as insufficient concentrations of drug in HIV sanctuary sites such as cerebrospinal fluid, genital tract and the gut could lead to drug resistance. There have been studies determining tissue distribution of raltegravir, which are detailed below.

Penetration of raltegravir into the male genital tract has been assessed in 10 HIV-infected men (Barau *et al.*, 2010). Patients were taking raltegravir 400 mg twice-daily for 24 weeks before samples were taken. Five hours post-dose, median raltegravir concentrations in semen and blood plasma were 345 (range, 83-707) ng/mL and 206 (106-986) ng/mL, respectively, with a semen/blood plasma ratio of 1.42 (0.5 to 6.7). This suggested that the raltegravir concentration in semen was generally comparable to the concentration in blood plasma, although variability in both compartments was high.

Another study using 10 HIV-infected men investigated the concentration of raltegravir in seminal fluid (Hasan *et al.*, 2012). Patients were taking raltegravir 400 mg twice-daily as part of HAART and a full concentration time curve was obtained in both blood plasma and semen. The GMR (CV%) semen/blood plasma ratio was 3.19 (41%).

Penetration of raltegravir into the female genital tract has been assessed in 14 HIV-infected women using raltegravir 400 mg twice-daily as part of HAART (Clavel *et al.*, 2011). Median raltegravir concentrations in cervicovaginal fluid and blood plasma were 235 (IQR, 135-775) ng/mL and 93 (48-167) ng/mL, respectively, with a cervicovaginal fluid/blood plasma ratio of 2.3 (1.4 to 4.1).

Penetration of raltegravir into the cerebrospinal fluid has been assessed in 16 HIV-infected individuals using raltegravir 400 mg twice-daily as part of HAART (Yilmaz *et al.*, 2009). Median raltegravir concentrations in cerebrospinal fluid and blood plasma were 18.4 (range, <2-126.0) ng/mL and 448 (37-5180) ng/mL, respectively, with a cerebrospinal fluid/blood plasma ratio of 0.03 (0.01 to 0.61). Importantly, raltegravir cerebrospinal fluid concentrations were lower than the IC_{95} determined for raltegravir *in vitro* (15.9 ng/mL) (Iwamoto *et al.*, 2008d) in around 50% of patients.

The concentration of raltegravir in maternal blood, cord blood and infant blood was determined in a study using 8 HIV-infected pregnant females during delivery (Clarke *et al.*, 2012). Each female had received at least two weeks of raltegravir 400 mg twice-daily prior to delivery. Samples were taken one hour post-delivery for maternal and cord blood and 23 hours post-delivery for infant blood. The geometric mean (CV%) maternal, cord and infant raltegravir concentrations were 1270 (108%), 1284 (70.5%) and 424 (76.7%), respectively. No adverse effects were noted in infants which could be attributed to raltegravir. These results suggest raltegravir could be a candidate for use during late pregnancy and during delivery, as the drug showed good placenta barrier penetration and no obvious detrimental effects on the infant.

The concentration of raltegravir in gut-associated lymphoid tissue (GALT) was determined in 14 healthy male volunteers given raltegravir 400 mg for seven days (Patterson *et al.*, 2012). Analysis of PK data showed that raltegravir AUC was 99-fold higher in the terminal ileum compared to blood plasma. The authors suggested that raltegravir was concentrating in the GALT following drug absorption and therefore raltegravir could be beneficial for use in pre-exposure prophylaxis. However, the high drug concentrations taken with the terminal ileum samples could have been unabsorbed drug which had travelled through the intestine and further investigation is needed to confirm the hypothesis given by the author.

1.6.6 Raltegravir drug-drug interactions

A summary of clinical drug interaction studies investigating the impact of co-administered drugs on raltegravir PK (Table 1.4) and the impact of raltegravir on co-administered drugs (Table 1.5) is given.

There have been a number of studies undertaken to evaluate the PK interactions between raltegravir and co-administered drugs. Several of these studies have shown raltegravir metabolism and disposition to be largely unaffected. For example, boceprevir (da Silva *et al.*, 2010), etravirine (Anderson *et al.*, 2008a), lopinavir (Rhame *et al.*, 2008), darunavir (Anderson *et al.*, 2008c) and rifabutin (Brainard *et al.*, 2009) did not significantly alter raltegravir plasma concentrations. In addition, despite ritonavir being an inducer of both ABCB1 (Dixit *et al.*, 2007) and UGT1A1 (Foisy *et al.*, 2008), the drug did not cause a significant reduction in raltegravir plasma

concentration (Iwamoto *et al.*, 2008c). However, there are interactions with other co-administered drugs that have a more marked effect on raltegravir disposition.

Raltegravir is a substrate for UGT1A1 and therefore co-administered compounds which alter UGT1A1 functionality have the potential to alter raltegravir PK. Atazanavir is an inhibitor of UGT1A1 (Zhang *et al.*, 2005) and co-administration of atazanavir (400 mg once-daily) with raltegravir (100 mg single dose) resulted in an increase in raltegravir plasma AUC, C_{max} and C_{min} of 72%, 53% and 95%, respectively (Iwamoto *et al.*, 2008b). This interaction was also confirmed in a separate study (Zhu *et al.*, 2009). Efavirenz and rifampin are inducers of UGT1A1 expression (Hariparsad *et al.*, 2004; Xie *et al.*, 2003) and have been shown to decrease raltegravir plasma exposure (Iwamoto *et al.*, 2008c; Wenning *et al.*, 2009a).

Omeprazole (Iwamoto *et al.*, 2009b) and famotidine (Rhame *et al.*, 2009) are treatments used to increase gastric pH and both increased raltegravir exposure. However, Maalox antacid, which also increases gastric pH, caused a reduction in raltegravir C_{12hr} (Kiser *et al.*, 2010). Therefore, it was not completely clear if increasing gastric pH was leading to an increase or decrease in raltegravir exposure. These interactions are discussed and investigated further in Chapter 5.

Several interactions affecting raltegravir exposure have no clear explanation. For example, fosamprenavir (Luber *et al.*, 2009), pravastatin (van Luin *et al.*, 2010) and maraviroc (Andrews *et al.*, 2010) all decreased raltegravir exposure and all are not known to induce UGT1A1. One intriguing interaction is that of tenofovir disoproxil fumarate (tenofovir DF) causing a moderate increase in raltegravir AUC and C_{max} by

49% and 64%, respectively (Wenning *et al.*, 2008). Although the increase in raltegravir plasma concentration is unlikely to have any important clinical significance (no increase in toxicity is expected) the mechanism of the interaction was unexplained at the outset of this thesis. Interestingly, tenofovir is an anionic compound when charged and is therefore a substrate of organic anion uptake transporters SLC22A6 and SLC22A8 (Uwai *et al.*, 2007) and this led to the investigations detailed in Chapter 4.

Raltegravir does not inhibit cytochrome P450 enzymes or induce CYP3A4 expression, therefore the potential of raltegravir to alter another drug's exposure is believed to be low. However, raltegravir has been shown to decrease the exposure of atazanavir (Iwamoto *et al.*, 2008b), fosamprenavir (Luber *et al.*, 2009), maraviroc (Andrews *et al.*, 2010), and tenofovir (Wenning *et al.*, 2008), and to increase the exposure of rilpivirine (Crauwels *et al.*, 2012). The mechanisms controlling these interactions are not known.

Co-administered drug/dose and schedule	Raltegravir dose and schedule	Overall effect on raltegravir	GMR (90% CI) of raltegravir PK parameter values with/without co-administered drug			Reference
			AUC*	C_{max}	C_{12h}	
Maalox antacid 30 mL single dose	400 mg single dose	Decrease	0.96 (0.62-1.50)	1.53 (0.90-2.60)	0.33 (0.26-0.42)	(Kiser *et al.*, 2010)
Atazanavir 400 mg qd	100 mg single dose	Increase	1.72 (1.47-2.02)	1.53 (.111-2.12)	1.95 (1.30-2.92)	(Iwamoto *et al.*, 2008b)
Atazanavir 300 mg bid	400 mg bid	Increase	1.54 (1.14-2.08)	1.39 (0.99-1.96)	1.48 (1.08-2.02)	(Zhu *et al.*, 2010)
Atazanavir/ritonavir 300/100 mg qd	400mg bid	Increase	1.41 (1.12-1.78)	1.24 (0.87-1.77)	1.77 (1.39-2.25)	(Iwamoto *et al.*, 2008b)
Boceprevir 800 mg tid	400 mg single dose	No change	1.01 (0.85-1.20)	1.09 (0.89-1.33)	ND	(da Silva *et al.*, 2010)
Darunavir/ritonavir 600/100 mg bid	400 mg bid	No change	0.71 (0.38-1.33)	0.67 (0.33-1.37)	1.38 (0.16-12.1)	(Anderson *et al.*, 2008b)
Efavirenz 600 mg qd	400 mg single dose	Decrease	0.64 (0.52-0.80)	0.64 (0.41-0.98)	0.79 (0.49-1.28)	(Iwamoto *et al.*, 2008c)
Etravirine 200 mg bid	400 mg bid	No change	0.90 (0.68-1.18)	0.89 (0.68-1.15)	0.66 (0.34-1.26)	(Anderson *et al.*, 2008a)
Famotidine 20 mg single dose†	400 mg bid	Increase	1.45 (1.09-1.93)	1.60 (1.11-2.30)	1.06 (0.84-1.35)	(Rhame *et al.*, 2009)
Fosamprenavir 1400 mg qd	400 mg bid	Decrease	0.63 (0.40-0.99)	0.72 (0.41-1.26)	0.62 (0.43-0.89)	(Luber *et al.*, 2009)
Lopinavir/ritonavir 200/50 mg bid	400 mg bid	No change	1.03 (0.64-1.64)	0.99 (0.56-1.76)	0.70 (0.53-091)	(Rhame *et al.*, 2008)
Maraviroc 300 mg bid	400 mg bid	Decrease	0.63 (0.44-0.90)	0.67 (0.41-1.08)	0.72 (0.58-0.91)	(Andrews *et al.*, 2010)
Omeprazole 20 mg qd	400 mg single dose	Increase	3.12 (2.13-4.56)	4.15 (2.82-6.10)	1.46 (1.10-1.93)	(Iwamoto *et al.*, 2009b)
Pravastatin 40 mg qd	400 mg bid	Decrease	1.13 (0.77-1.65)	1.31 (0.81-2.13)	0.59 (0.39-0.88)	(van Luin *et al.*, 2010)
Rifabutin 300 mg qd	400 mg bid	No change	1.19 (0.86-1.63)	1.39 (0.87-2.21)	0.80 (0.68-0.94)	(Brainard *et al.*, 2011b)
Rifampin 600 mg qd	400 mg single dose	Decrease	0.60 (0.39-0.91)	0.62 (0.37-1.04)	0.39 (0.30-0.51)	(Wenning *et al.*, 2009a)
Rifampin 600 mg qd	800 mg bid	Decrease	1.27 (0.94-1.71)	1.62 (1.12-2.33)	0.47 (0.36-0.61)	(Wenning *et al.*, 2009a)
Rilpivirine 25 mg qd†	400 mg bid	Increase	1.09 (0.81-1.47)	1.10 (0.77-1.58)	1.27 (1.01-1.60)	(Crauwels *et al.*, 2012)
Ritonavir 100 mg bid	400 mg single dose	No change	0.84 (0.70-1.01)	0.76 (0.55-1.04)	0.99 (0.70-1.40)	(Iwamoto *et al.*, 2008c)
Tenofovir 300 mg qd	400 mg bid	Increase	1.49 (1.15-1.94)	1.64 (1.16-2.32)	1.03 (0.73-1.45)	(Wenning *et al.*, 2008)
Tipranavir/ritonavir 500/200 mg bid	400 mg bid	Decrease	0.76 (0.49-1.19)	0.82 (0.46-1.46)	0.45 (0.31-0.66)	(Hanley *et al.*, 2009)

Table 1.4. Effect of co-administered agents on raltegravir pharmacokinetics in healthy subjects (unless otherwise stated). qd = once-daily, bid = twice-daily, tid = three times-daily. * $AUC_{0\text{-}12hr}$ for multiple dose raltegravir, $AUC_{0\text{-}\infty}$ for single dose raltegravir. † HIV-infected patients used in the study.

Co-administered drug/dose and schedule	Raltegravir dose and schedule	Overall effect on co-administered drug	GMR (90% CI) of co-administered drug PK parameter values with/without raltegravir			Reference
			AUC*	C_{max}	C_{trough}‡	
Abacavir 600 mg qd†	400 mg bid	No change	1.03 (0.95-1.12)	1.06 (0.96-1.18)	0.83 (0.66-1.10)	(Jackson *et al.*, 2009)
Atazanavir 300 mg bid	400 mg bid	Decrease	0.83 (0.78-0.89)	0.89 (0.84-0.94)	0.71 (0.65-0.78)	(Iwamoto *et al.*, 2008b)
Etravirine 200 mg bid	400 mg bid	No change	1.10 (1.03-1.16)	1.04 (0.97-1.12)	1.17 (0.65-0.78)	(Anderson *et al.*, 2008a)
Fosamprenavir 1400 mg bid	400 mg bid	Decrease	0.64 (0.47-0.88)	0.73 (0.53-1.01)	0.57 (0.43-0.76)	(Luber *et al.*, 2009)
Lamotrigine 100 mg single dose	400 mg bid	No change	0.99 (0.96-1.01)	0.94 (0.89-0.99)	ND	(van Luin *et al.*, 2009)
Lopinavir/ritonavir 200/50 mg bid	400 mg bid	No change	0.99 (0.87-1.12)	0.97 (0.87-1.08)	1.04 (0.73-1.46)	(Rhame *et al.*, 2008)
Maraviroc 300 mg bid	400 mg bid	Decrease	0.86 (0.80-0.92)	0.80 (0.67-0.94)	0.90 (0.85-0.96)	(Andrews *et al.*, 2010)
Methadone 40-60 mg qd	400 mg bid	No change	1.00 (0.93-1.09)	1.00 (0.94-1.07)	ND	(Anderson *et al.*, 2010)
Midazolam 2 mg single dose	400 mg bid	No change	0.92 (0.82-1.03)	1.03 (0.87-1.22)	ND	(Iwamoto *et al.*, 2008a)
Pravastatin 40 mg qd	400 mg bid	No change	0.96 (0.83-1.11)	1.04 (0.85-1.26)	ND	(van Luin *et al.*, 2010)
Rilpivirine 25 mg qd†	400 mg bid	Increase	1.12 (1.05-1.19)	1.12 (1.04-1.20)	1.03 (0.96-1.12)	(Crauwels *et al.*, 2012)
Tenofovir 300 mg qd	400 mg bid	Decrease	0.90 (0.82-0.99)	0.77 (0.69-0.85)	0.87 (0.74-1.02)	(Wenning *et al.*, 2008)

Table 1.5. Effect of raltegravir on co-administered drug pharmacokinetics in healthy subjects (unless otherwise stated). qd = once-daily, bid = twice-daily. * $AUC_{0\text{-}12hr}$ for twice-daily dose drug, $AUC_{0\text{-}24hr}$ for once-daily dose drug, $AUC_{0\text{-}48hr}$ for lamotrigine and $AUC_{0\text{-}\infty}$ for raltegravir single dose. ‡ C_{trough} is C_{12hr} for twice-daily drugs and C_{24hr} for once-daily drugs. † HIV-infected patients used in the study.

1.6.7 Other integrase inhibitors in development

Raltegravir is currently the only integrase inhibitor available for use in anti-HIV therapy. However, there are several integrase inhibitors in pre-clinical and clinical development which may become an important part of future HAART. Drugs that

inhibit the 3'-processing activity of integrase, such as the styrylquinoline carboxamides (Langford *et al.*, 2008), have been investigated. However, interest in 3'-processing inhibitors has diminished following the success of the less toxic strand transfer inhibitors. Recent investigations have introduced a new class of integrase inhibitor which prevents the binding of LEDGF/p75, an important co-factor in the pre-integration complex (Cherepanov *et al.*, 2003), to integrase (Christ *et al.*, 2010). Initial efficacy data for LEDGF/p75-integrase binding inhibitors is promising, although these drugs are only in the early stages of development. The most developed and most promising of the new integrase inhibitors are based on the mechanism of action of raltegravir and are elvitegravir and dolutegravir.

Elvitegravir

Elvitegravir is a potent HIV integrase inhibitor currently in late-stage clinical development. Similarly to raltegravir, elvitegravir contains a β-hydroxy-ketone structural motif and shows specific inhibition of strand transfer (Shimura *et al.*, 2009). Despite having similar mechanisms of action and sharing certain elements of chemical structure, the physicochemical properties of elvitegravir are noticeably different from raltegravir. Elvitegravir is highly lipophilic (logD of 4.5 at pH 6.8) and is extremely highly bound to human plasma protein (99.4% bound).

The drug shows potent inhibition of HIV-1 (mean IC_{50} of 0.04-0.55 ng/mL) and HIV-2 (mean IC_{50} of 0.61-1.2 ng/mL) replication *in vitro* and this effect is synergistic when used in combination with other antiretroviral classes (Ledford *et al.*, 2007). There is significant cross-over in resistance mutations for elvitegravir and

raltegravir (Van Wesenbeeck *et al.*, 2011) which limits the use of elvitegravir in HIV-positive patients resistant to raltegravir.

The metabolism of elvitegravir and raltegravir are noticeably different. Elvitegravir is primarily metabolised by CYP3A4 and shows minor (less than 10%) metabolism by UGT1A1 (Ramanathan *et al.*, 2007b). The extent of CYP3A4 metabolism is so great that it is necessary to co-administer the drug with ritonavir, in a similar procedure to that used with the HIV protease inhibitors (Section 1.4.5). The co-administered ritonavir inhibits CYP3A4 and causes a reduction in elvitegravir clearance, resulting in greatly increased bioavailability and drug exposure. When co-administered with 100 mg ritonavir, 50 mg elvitegravir once-daily caused a 1.99 log reduction in HIV-1 RNA load in HIV-infected HAART-naive patients over a ten-day treatment course, whereas 800 mg elvitegravir twice-daily taken without ritonavir caused a 1.91 log reduction (DeJesus *et al.*, 2006).

A large-scale non-inferiority study in HIV-positive treatment-experienced patients confirmed that ritonavir-boosted elvitegravir had a similar efficacy and safety profile to raltegravir (Molina *et al.*, 2012). Considering that elvitegravir is given once-daily and raltegravir is given twice-daily, the authors suggest that replacing raltegravir with elvitegravir in HAART regimens may increase patient adherence. However, raltegravir does not require ritonavir boosting and therefore avoids the risk of ritonavir-related adverse drug reactions.

Dolutegravir

Dolutegravir is a strand transfer inhibitor in late-stage clinical development. The drug has a similar mechanism of action to elvitegravir and raltegravir, shows a superior binding affinity for the integrase enzyme active site (Hightower *et al.*, 2011) and has displayed high anti-HIV activity *in vitro* (Kobayashi *et al.*, 2011) and *in vivo* (van Lunzen *et al.*, 2012).

The major advantage of dolutegravir is that current treatment used in trials is based on a once-daily dosing regimen without the requirement for ritonavir boosting. Also, dolutegravir has demonstrated activity *in vivo* against HIV which is resistant to raltegravir (Song *et al.*, 2010).

1.7 Raltegravir pharmacokinetics issues requiring investigation

This thesis aimed to use *in vitro* techniques to investigate the factors involved in determination of raltegravir cellular exposure, thus increasing our understanding of the mechanisms that control raltegravir PK in the body. The issues of interest discussed in this section are investigated in more detail throughout the thesis and therefore are given here only as a brief introduction.

1.7.1 High variability in raltegravir PK

Raltegravir plasma PK profiles are characterised by their high variability. Table 1.6 shows a selection of trials using healthy, fasted subjects taking a single 400 mg raltegravir dose. In this table the C_{max}, $AUC_{0-\infty}$ and C_{trough} vary with a range of 5.4-fold, 3.9-fold and 4.1-fold, respectively. This variability is observed between patients and also within patients over multiple doses (Cattaneo *et al.*, 2012). For example, a study determining raltegravir plasma concentrations obtained results with an inter-patient coefficient of variation percentage (CV%) for AUC, C_{max} and C_{trough} of 160%, 166% and 290%, respectively (Fayet Mello *et al.*, 2011). Another study measuring raltegravir PK variability found C_{trough} levels had an inter-patient CV% of 110% and an intra-patient CV% of 245%, suggesting in this case an even higher variability in the same patient compared to between patients (Siccardi *et al.*, 2012a). The causes of such high variability in raltegravir PK are not fully understood but a reduction in variability was seen when raltegravir was taken with treatments which increased gut pH (Iwamoto *et al.*, 2009b).

Understanding what causes high variability in raltegravir PK has been a primary goal during the author's investigations. The failure rate of raltegravir therapy in HIV-infected patients is low, although drug failure does occur. Furthermore, drug failure is not always associated with a genetic drug resistance development. Over half (141 of 255) of HIV-infected patients who failed raltegravir therapy in a recent multicenter drug study had HIV with no detectable integrase resistance mutations (Geretti *et al.*, 2012), and a smaller study found that 18% (2 of 11) of patients who failed raltegravir therapy had no evidence of HIV integrase mutations (da Silva *et al.*, 2010). High variability in raltegravir PK has led to difficulty in establishing a reliable pharmacokinetic-pharmacodynamic (PK-PD) relationship for raltegravir, it is important that investigations are undertaken so that this variability can be explained and appropriate clinical strategies can be developed.

Trial conditions			Geometric mean PK data			
Dose regimen	Subject number	Sex	C_{max} (uM)	AUC (uM/hr)	C_{trough} (nM)	Reference
400 mg single dose	12	Male	10.63	24.61	81.3	(Iwamoto *et al.*, 2008d)
400 mg single dose	6	Male	2.25	10.78	338.7	(Wang *et al.*, 2011)
400 mg single dose	14	Mixed	2.88	11	80.6	(Iwamoto *et al.*, 2009b)
400 mg single dose	12	Mixed	1.96	6.3	76.7	(Kiser *et al.*, 2010)

Table 1.6. Examples of raltegravir PK parameters from studies using healthy, fasted subjects.

1.7.2 Unexplained drug-drug interactions

Raltegravir is metabolised primarily by UGT1A1 (Kassahun *et al.*, 2007) and the induction or inhibition of UGT1A1 is assumed to be the cause of certain drug-drug

interactions affecting raltegravir PK. However, several interactions between raltegravir and concomitant drugs have been discovered which cannot be explained by the involvement of UGT1A1 (Section 1.6.6). Furthermore, it is not understood how raltegravir alters the exposure of certain co-administered drugs. A clearer understanding of the factors influencing raltegravir PK may help to explain these moderate drug interactions.

1.7.3 Raltegravir and drug transporters

Previous investigations have confirmed the route of metabolism of raltegravir (Section 1.6.3). However, the involvement of human drug transporters in raltegravir absorption, disposition and excretion had not been rigorously investigated at the outset of this thesis. An in-house bidirectional transport investigation by Merck suggested that raltegravir was substrate of the efflux transporter ABCB1, yielding efflux ratios of 11.1 in ABCB1-over-expressing LLC-PK1 cells (Section 1.6.3). However, human drug trials do not support this hypothesis. For example, ritonavir, a potent ABCB1 inhibitor, had only a minimal effect on raltegravir PK (Iwamoto *et al.*, 2008c). Further investigations into the transport of raltegravir by ABCB1 are clearly justified. Also, the effects that influx transporters have on raltegravir disposition are unknown and may aid our understanding of raltegravir PK in patients. The impact of drug transporters on raltegravir disposition is a key area of investigation in this thesis and is explored further in Chapters 2, 3 and 4.

1.7.4 The effects of food, metal cations and gastrointestinal pH on raltegravir exposure

It has become clear from clinical studies that raltegravir PK can be affected by food intake (Brainard *et al.*, 2011a), pH-altering agents (Iwamoto *et al.*, 2009b), and metal cation-containing products (Kiser *et al.*, 2010) and these studies are reviewed in detail in Chapter 5. Environmental factors such as these are more likely than genetic factors to explain raltegravir intra-patient PK variability. The impact of pH and metal cations on raltegravir disposition are investigated further in Chapters 5 and 6.

1.8 Aims of the thesis

Chapter 2 confirmed whether raltegravir is transported by the drug efflux transporter ABCB1 *in vitro*, and whether raltegravir is able to inhibit or induce ABCB1 activity. Cellular toxicity of raltegravir was also assessed.

Chapter 3 investigated the ability of influx transporters to transport raltegravir and other anti-HIV drugs *in vitro* using the *Xenopus laevis* oocyte expression system. The ability of raltegravir and other anti-HIV drugs to inhibit influx transporter SLC22A1 was also assessed.

Chapter 4 investigated in more detail the transport of raltegravir by influx transporter SLC22A6. Kinetic parameters K_m and V_{max} were also determined. The competition between tenofovir and raltegravir for SLC22A6 transport was assessed and results were used to calculate IC_{50} values.

Chapter 5 moved away from the impact of drug transporters and investigated the effect of pH on raltegravir lipophilicity, solubility and cell membrane permeation. Raltegravir pKa was also determined. The effect of metal cations on raltegravir Caco-2 cell membrane permeation was also assessed.

Chapter 6 used the PK simulation modelling program Simcyp to help explain and predict the effects of food, pH-altering agents and divalent metal cation-containing products on raltegravir PK. The *in vitro* data from Chapter 5 was added to this model.

Chapter 7 briefly summarised the investigations in Chapters 2 to 6 and discussed how the data have improved our understanding of the factors and mechanisms which determine raltegravir cellular exposure. Suggestions are given about how these investigations can be continued.

Chapter 2

Interactions between raltegravir and drug efflux transporter ABCB1

Table of Contents

2.1 INTRODUCTION

The US Food and Drug Administration (FDA) request that potential commercial drugs are screened for their substrate affinity and inhibitory potential of drug efflux transporter ABCB1 (Huang *et al.*, 2007). ABCB1 is a cell membrane-bound ATP-binding cassette (ABC) transporter which utilizes energy (from ATP hydrolysis) to actively transport xenobiotics out of the cell (Leschziner *et al.*, 2007). The protein contains two connected six-transmembrane-spanning domains and two nucleotide binding domains. ATP is dephosphorylated to produce energy, allowing for the active transport of substrates from the cytoplasm, through the cell membrane and into the extracellular domain (Figure 2.1). In doing this, ABCB1 can influence xenobiotic absorption through the gut and aid xenobiotic elimination via the liver and kidney, potentially averting xenobiotic-induced cellular toxicity. This protective function of ABCB1 may have originated as a physiological defence mechanism against xenotoxins of natural origin from plants, fungi and bacteria (Ames *et al.*, 1990).

ABCB1 is expressed in several pharmacologically-important tissues which determine drug ADME properties, such as the mucosal surface epithelial cells in the intestine (Lindell *et al.*, 2003), the biliary canalicular surface of hepatocytes in the liver (Thiebaut *et al.*, 1987) and the brush border membrane of renal proximal tubular cells in the kidney (Ernest *et al.*, 1997). Generally, drug elimination is aided by the activity of ABCB1, as drug is prevented from being absorbed in the gut or removed from the blood into bile and/or urine for excretion.

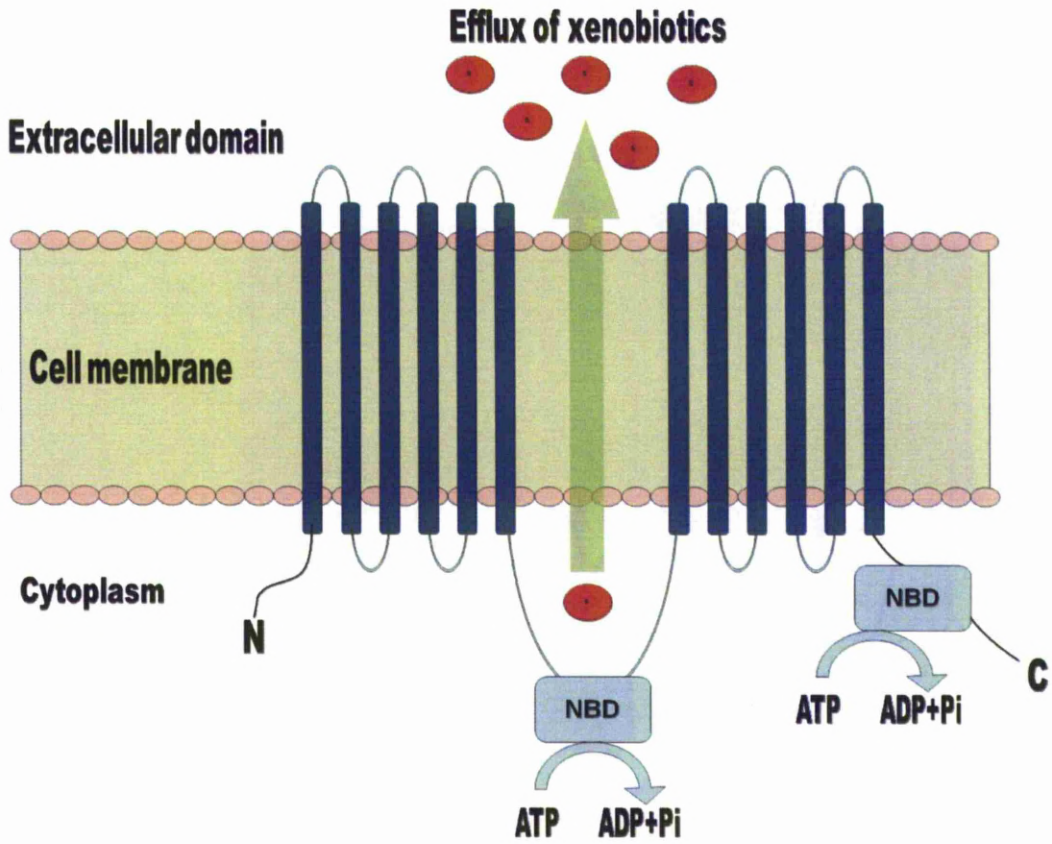

Figure 2.1. Xenobiotic efflux transporter ABCB1.

Importantly, ABCB1 is expressed in several tissues believed to be important sanctuary sites for HIV replication, such as the placenta trophoblast (Nakamura *et al.*, 1997), the endothelial cells in the testes (Cordon-Cardo *et al.*, 1989) and the luminal membrane of capilliary endothelial cells in the brain (Schinkel, 1999). It is hypothesised that the action of ABCB1 prevents certain antiretroviral drugs from sufficiently penetrating these tissues (Choo *et al.*, 2000), therefore providing a location where HIV is able to replicate and develop drug resistance.

ABCB1 is also expressed at varying levels in CD4+ T-cells and monocytes/macrophages (Drach *et al.*, 1992), both of which are viral targets for HIV (Fauci *et al.*, 1998) and are therefore important targets for antiretroviral drugs.

Antiretroviral drugs (with the exception of enfuvirtide and maraviroc) require intracellular access to their targets to elicit their inhibitory effects (Khoo *et al.*, 2002) and low intracellular drug concentrations in these cells may lead to incomplete viral suppression and subsequent resistance development by HIV (Jones *et al.*, 2001).

ABCB1 is believed to play a key role in the disposition and drug interaction profiles of many antiretroviral compounds. ABCB1 is able to transport the PIs saquinavir (Janneh *et al.*, 2005), ritonavir (Kim *et al.*, 1998), indinavir (Lee *et al.*, 1998), nelfinavir (Choo *et al.*, 2000), amprenavir (Choo *et al.*, 2000), lopinavir (Janneh *et al.*, 2007), atazanavir (Bousquet *et al.*, 2008), tipranavir (Orman *et al.*, 2008) and darunavir (Kwan *et al.*, 2009) *in vitro*. Lower intracellular accumulation of protease inhibitors has been seen in peripheral blood mononuclear cells (PBMCs) with higher levels of ABCB1 expression (Meaden *et al.*, 2002). As a drug class, the PIs show varying levels of inhibition and induction of ABCB1, with the most potent inhibitor being ritonavir (Sankatsing *et al.*, 2004). The NNRTIs efavirenz, nevirapine, delavirdine and etravirine are not substrates for ABCB1 *in vitro* (Janneh *et al.*, 2009; Scholler-Gyure *et al.*, 2009; Stormer *et al.*, 2002) but efavirenz, nevirapine and delavirdine appear to cause varying levels of inhibition (Storch *et al.*, 2007) and induction (Stormer *et al.*, 2002; Weiss *et al.*, 2008) of ABCB1 *in vitro.* Generally, NRTIs are not known to be potent ABCB1 substrates, inhibitors (Storch *et al.*, 2007) or inducers (Weiss *et al.*, 2008), although abacavir (Shaik *et al.*, 2007) and the prodrug tenofovir disoproxil fumarate (van Gelder *et al.*, 2002) appear to be ABCB1 substrates *in vitro*. The CCR5 receptor antagonist maraviroc is also transported by ABCB1 *in vitro* (Zembruski *et al.*, 2011).

The interactions between ABCB1 and HIV integrase inhibitors do not appear to be as uniform as with other antiretroviral classes (generally, PIs are ABCB1 substrates, NNRTIs are not, etc) and investigations detailing these interactions are still ongoing. The integrase inhibitor elvitegravir has been determined as a substrate of ABCB1 and an inhibitor of ABCB1 and ABCG2 *in vitro* (Zembruski *et al.*, 2011). Elvitegravir has also been shown to induce the production of mRNA coding for ABCB1 as well as mRNA for ABCC3, ABCG2, influx transporter SLCO1B1 and metabolism enzymes CYP3A4 and CYP2B6 in LS180 cells *in vitro* (Zembruski *et al.*, 2011). It is unclear whether ABCB1 plays an important role in elvitegravir disposition *in vivo*. The interactions between ABCB1 and dolutegravir have not been published.

Previous review papers have claimed that raltegravir is an ABCB1 substrate (Cocohoba *et al.*, 2008), referencing ultimately to the drug package insert. However, to the author's knowledge no published work had described an investigation of raltegravir transport by ABCB1 prior to the work published from this thesis.

One study showed that several lead-compound strand transfer inhibitors were able to inhibit ABCB1 activity and induce ABCB1 protein expression *in vitro*, although raltegravir was not tested (Cianfriglia *et al.*, 2007). Nine quinolonyl diketo acid derivatives were found to inhibit ABCB1-mediated doxorubicin efflux from KB-V1 MDR cells and to induce ABCB1 protein expression in CEM cells, evaluated by the modulation of anti-ABCB1 UIC2 monoclonal antibody binding. The chemical structures of the quinolonyl diketo acid derivatives were not provided, although both these compounds and raltegravir share the same mechanism of action by preventing

HIV integrase strand transfer. Therefore, it is possible that raltegravir shares the same "off-target" effects as the quinolonyl diketo acid derivatives and is able to inhibit and/or induce ABCB1.

The work in this chapter investigated the extent of raltegravir transport by ABCB1 *in vitro* in T-lymphoblastoid and gut cell lines and *ex vivo* in PBMCs. A cellular toxicity assay was utilized to select non-cytotoxic concentrations of raltegravir for use in these experiments. Additionally, ABCB1-mediated transport of rilpivirine, an NNRTI which has recently been licensed for use in HAART, has not been fully investigated. Therefore, rilpivirine was also investigated in this study.

2.2 METHODS

2.2.1 Materials

CEM and CEM_{VBL100} cells were donated by Ross Davey, Bill Walsh Cancer Research Laboratories (St' Leonards, Australia). Caco-2 cells were purchased from the European Collection of Cell Cultures (Salisbury, UK). CellFix was purchased from Becton Dickinson (Oxford, UK). UIC2 (anti-ABCB1) antibody was purchased from Immunotech (Marseilles, France). IgG2a and IgG1 negative control antibodies and goat anti-mouse IgG2a:RPE were purchased from Serotech Ltd. (Oxford, UK). QCLR-1 (anti-MRP1) antibody was purchased from Merck (New Jersey, USA). Goat anti-mouse IgG:FITC was purchased from Sigma (Poole, UK). [^{3}H]Raltegravir (specific activity = 32.85 Ci/mmol) and non-radiolabeled raltegravir sodium salt were gifts from Merck (New Jersey, USA). [^{3}H]Digoxin (specific activity = 0.039 Ci/mmol) was purchased from Perkin Elmer (Massachusetts, USA). [^{3}H]Saquinavir (specific activity = 1 Ci/mmol) and [^{3}H]lopinavir (specific activity, 5 Ci/mmol) were purchased from Moravek Biochemicals (California, USA). [^{14}C]Mannitol was purchased from American Radiolabelled Chemicals (Missouri, USA). Saquinavir was a gift from Roche (Sussex, UK). [^{3}H]Rilpivirine (specific activity = 20 mCi/mmol) and non-radiolabelled rilpivirine were gifts from Tibotec (Mechelen, Belgium). Lopinavir was a gift from Abbott (Illinois, USA). Tariquidar (XR9576) was purchased from Xenova (Sloane, UK). Ficoll-Paque PLUS was purchased from GE Healthcare (Buckinghamshire, UK). Ultima Gold scintillation fluid was purchased from Perkin Elmer (Boston, USA). All other drugs and reagents were obtained from Sigma (Poole, UK).

2.2.2 Cell culture

2.2.2.1 Culture of CEM and CEM_{VBL100} T-cells

CEM and CEM_{VBL100} cells were maintained in cell culture medium (Roswell Park Memorial Institute medium (RPMI), 10% [vol/vol] FCS) prior to the experiment in a CO_2 incubator (37 °C, 5% CO_2). CEM cells are a wild type T-lymphoblastoid cell line. CEM_{VBL100} cells are CEM cells which have increased ABCB1 expression. All cell culture procedures were performed in a sterile environment.

2.2.2.2 Treatment of CEM and CEM_{VBL100} T-cells

High expression of ABCB1 in CEM_{VBL100} was maintained by incubating cells with 100 ng/mL vinblastine (RPMI, 10% [vol/vol] FCS) for 72 hours (37 °C, 5% CO_2). Vinblastine is toxic to CEM cells and is also a substrate for ABCB1, therefore incubation of cells with vinblastine leads to the selection of cells with higher ABCB1 expression. This treatment was repeated every eight weeks to maintain high ABCB1 expression.

2.2.2.3 Freezing and thawing of CEM and CEM_{VBL100} cell stocks

CEM and CEM_{VBL100} cells were maintained in cell culture medium (RPMI, 10% [vol/vol] FCS) prior to establishing cryopreserved cell stocks. Cells were added to a 50mL skirted tube and centrifuged (800 g, 4°C, 5 minutes). Supernatant fraction was replaced with cell freezing solution (RPMI, 10% [vol/vol] FCS, 10% [vol/vol]

DMSO) to achieve a final cell density of 5 x 10^6 cells/mL. After gentle mixing, cell solutions were aliquoted into ice-cold cryovials and placed in a minus 20°C freezer for two hours. Following this, vials were transferred to a sealed styrofoam box (to avoid lysis associated with rapid freezing), placed in a minus 80°C freezer and left overnight. On the following morning, cells were transferred to a storage box in the minus 80°C freezer until required.

When removed from the minus 80°C freezer, cells were rapidly thawed by hand and added to 50 mL cell culture medium (RPMI, 10% [vol/vol] FCS) and centrifuged (800 g, 4°C, 5 minutes). Supernatant fraction was removed, cells were resuspended in fresh cell culture medium (RPMI, 10% [vol/vol] FCS) and used to begin a fresh cell culture.

2.2.2.4 Culture of Caco-2 cells

Caco-2 cells are human epithelial colorectal adenocarcinoma cells and are widely utilised in cell culture to represent the enterocyte cells of the small intestine. Cells were maintained in cell culture medium (Dulbecco's Modified Eagle Medium (DMEM), 15% [vol/vol] FCS) prior to the experiment. Once a cell confluence level of 70-80% was reached, Caco-2 cells were washed three times with Hank's Balanced Salt Solution (HBSS, 37°C) and incubated with trypsin-EDTA solution (37°C, 5 minutes). Flasks were gently tapped to remove Caco-2 cells and cell culture medium was added to neutralise the trypsin (DMEM, 15% [vol/vol] FCS). Cells were added to a 50mL skirted tube and centrifuged (800 g, 4°C, 5 minutes). Supernatant fraction was removed and replaced with fresh cell culture medium (DMEM, 15% [vol/vol]

FCS) to a final density of 5 x 10^5 cells/mL. Cells were seeded into new culture flasks at a density of 1 x 10^5 cells/cm^2.

Cells were purchased at passage 18 and used to create frozen stocks (Section 2.2.2.5). All cell culture procedures were performed in a sterile environment and all Caco-2 cells used in experiments were between passage numbers 20 to 30.

2.2.2.5 Freezing and thawing of Caco-2 cell stocks

Caco-2 cells were maintained in cell culture medium (DMEM, 15% [vol/vol] FCS) prior to the creation of frozen cell stocks. Once a cell confluence level of 70-80% was reached, Caco-2 cells were washed three times with HBSS (37°C) and incubated with trypsin-EDTA solution (37°C, 5 minutes). The flasks were gently tapped to remove Caco-2 cells and cell culture medium was added to neutralise the trypsin (DMEM, 15% [vol/vol] FCS). Cells were added to a 50 mL skirted tube and centrifuged (800 g, 4°C, 5 minutes). Supernatant fraction was replaced with Caco-2 cell freezing solution (DMEM, 15% [vol/vol] FCS, 10% [vol/vol] DMSO) to achieve a final cell density of 5 x 10^6 cells/mL. After gentle mixing, cell solutions were aliquoted into ice-cold cryovials and placed in a minus 20°C freezer for two hours. Following this, vials were transferred to a sealed styrofoam box to avoid rapid freezing of cells, placed in a minus 80°C freezer and left overnight. On the following morning, cells were transferred to a storage box in the minus 80°C freezer until required.

When removed from the minus 80°C freezer, cells were rapidly thawed by hand and added to 50 mL cell culture medium (DMEM, 15% [vol/vol] FCS) and centrifuged (800 g, 4°C, 5 minutes). Supernatant fraction was discarded, cells were resuspended in fresh cell culture medium (DMEM, 15% [vol/vol] FCS) and used to begin a fresh Caco-2 cell culture.

2.2.3 Detection of ABCB1 and ABCC1 expression in CEM and CEM_{VBL100} cells

CEM and CEM_{VBL100} cells were diluted in 1:10 Cell Fix and incubated (1 x 10^6 cells/mL, 30 minutes, 4°C). Cells were dispensed into vials (1 mL, 1 x 10^6 cells/mL, n = 2 replicates for each cell line) and centrifuged (800 g, 22°C, 5 minutes).

Following centrifugation, supernatant fraction was discarded and 1 mL 1 x PBS was added to each well. For ABCB1 detection, cells were centrifuged (800 g, 22°C, 5 minutes), supernatant fraction was discarded and cells were resuspended in 100µL primary ABCB1 antibody UIC2 or 100 µL isotype control IgG2a (2.5 µg/mL antibody dilution in 1 x PBS) and incubated in darkness (60 minutes, 22°C). For ABCC1 detection, cells were centrifuged (800 g, 22°C, 5 minutes), supernatant fraction was discarded and cells were resuspended in 100 µL primary ABCC1 antibody QCLR-1 or 100 µL isotype control IgG1 (2.5µg/mL antibody dilution in 1xPBS) and incubated in darkness (60 minutes, 22°C). Cells were washed three times with 1 mL 1 x PBS and centrifuged (800 g, 22°C, 5 minutes). Supernatant fraction was discarded and cells were resuspended in 100 µL secondary antibody (2.5 µg/mL antibody dilution in 1 x PBS) and incubated in darkness (60 minutes, 22°C). Cells were washed three times with 1 mL 1 x PBS and centrifuged (800 g,

22°C, 5 minutes). A volume of 100 µL 1:10 Cell Fix was added to each vial and the contents transferred to separate FACS tubes for analysis using a Coulter Epics XL-MCL flow cytometer. Data are presented as relative fluorescence units ± SD (RFU, median fluorescence minus that of the isotype control, n = 2).

2.2.4 Evaluation of the toxicity of raltegravir in Caco-2 and CEM cells

The cellular toxicity of raltegravir was determinate using the MTT assay, with modifications (Mosmann, 1983). CEM and Caco2 cells (100 µL, 2 x 10^5 cells/mL) were incubated in a 96-well Nunc flat-bottom plate (37°C, 5% CO_2, 120 hours) with 0, 0.01, 0.1, 1, 10 and 100 µM raltegravir. To validate the study, the cytotoxic control compounds epirubicin and vinblastine were incubated (0, 0.1, 1, 10, 100 µM) with CEM and Caco-2 cells, respectively. The solvent vehicle used to dissolve the drugs was sterile water (1% [vol/vol] final concentration) and control cells were incubated with 1% sterile water to act as drug-free controls.

Following incubation, plates were centrifuged (800 g, 5 minutes, 22°C), the supernatant fraction discarded and replaced with a 3-(4,5-dimethylthiazol-2-Yl)-2,5-diphenyltetrazolium bromide (MTT) solution (1 mg/mL MTT, 100 µL, HBSS). Plates were wrapped in metal foil and incubated (37°C, 5% CO_2, 2 hours).

Following incubation, cell lysis buffer (50% [vol/vol] dimethylformamide in distilled water, 20% [wt/vol] SDS) was added to wells and plates were incubated on a mechanical shaker (60 rpm, 22°C, 2 hours) to allow the cells to lyse. Plates were loaded into a GENios Microplate Reader (TECAN®) and absorbance at 570 nm was

determined. Data are expressed as percentage cell viability compared to vehicle control cells (n = 6 experimental replicates) ± SD. These data were used to determine the IC_{50} (concentration of drug needed to reduce absorbance by half) of raltegravir and the control drugs using Graphpad Prism 5.

2.2.5 Evaluation of the effects of tariquidar on raltegravir, saquinavir, lopinavir and rilpivirine accumulation in CEM and CEM_{VBL100} cells

CEM and CEM_{VBL100} cells of a constant cell density (1 mL, 2.5 x 10^6 cells/mL) were incubated (37°C, 5% CO_2) for 30 minutes in cell culture medium (RPMI, 10% [vol/vol] FCS) containing either [^{3}H]raltegravir (1 μM, 0.2 μCi/mL), [^{3}H]saquanavir (1 μM, 0.2 μCi/mL), [^{3}H]lopinavir (1 μM, 0.5 μCi/mL) or [^{3}H]rilpivirine (25 μM, 0.5 μCi/mL). A separate incubation was undertaken where CEM_{VBL100} cells were preincubated prior to the substrate addition in cell culture medium containing the potent non-competitive ABCB1 inhibitor, tariquidar (RPMI, 10% [wt/vol] FCS, 300 nM tariquidar, 30 minutes). Tariquidar was also included during the 30 minute substrate incubation. Following incubation, cells were centrifuged (800 g, 1°C, 1 minute), 100 μL supernatant fraction aliquots were taken, added to scintillation vials and used to calculate extracellular drug concentrations. The remaining supernatant fraction was discarded and cells were washed with ice-cold HBSS and centrifuged (800 g, 1°C, 1 minute). This HBSS wash was repeated a total of three times, after which the HBSS was discarded and 100 μL tap water was added to lyse the cells. Cells were vortexed for five minutes and samples were added to scintillation vials. Four millilitres of scintillation fluid was added to scintillation vials, which were then loaded into a liquid scintillation analyzer (TRI-CARB®). Using supernatant fraction

and intracellular radioactivity readings, cellular accumulation ratios (CAR; ratio of drug concentration in the cell pellet compared with drug concentration in the supernatant fraction ± SD, assuming 1 pL volume per cell) were calculated for drugs in each cell line.

2.2.6 The effect of tariquidar on the bidirectional transport of raltegravir and digoxin using a Caco-2 monolayer

Caco-2 monolayer experiments were performed as previously described (Hubatsch *et al.*, 2007), with modifications. Figure 2.2 shows the layout of a cell monolayer grown on a polycarbonate transwell. When confluent, Caco-2 cells were removed from cell culture flasks (Section 2.2.2.4) and seeded onto polycarbonate membrane transwells at a density of 5 X 10^5 cells/cm^2 (DMEM, 15% [vol/vol] FCS) and incubated (37°C, 5% CO_2) for 24 hours. Following this incubation, media was replaced to remove dead cells and to prevent the formation of multiple layers of cells settling on the filter. Media was then changed every two to three days and plates were used in experiments after a total of 21 days from initial seeding. Monolayer integrity was checked using a MillicellERS instrument (Millipore) to determine the trans-epithelial electrical resistance (TEER) across the monolayer. A TEER of more than 600 μΩ was deemed acceptable.

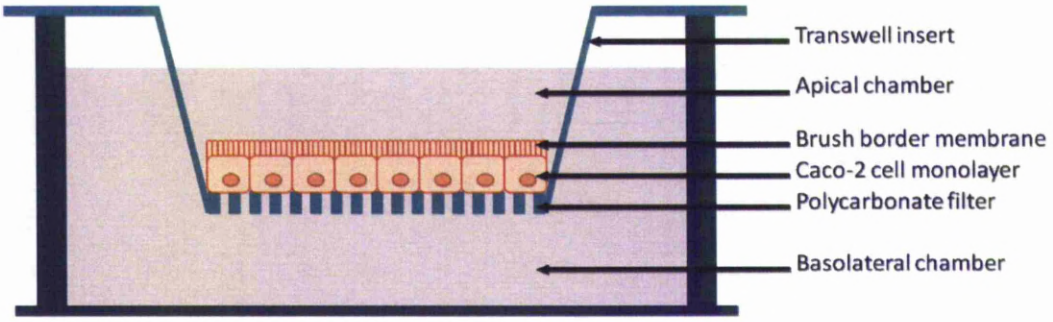

Figure 2.2. An experimental set-up used in bidirectional drug transport assays. A Caco-2 cell monolayer is grown on a semi-permeable polycarbonate filter over 21 days and drug permeability through the monolayer is determined in both directions.

On the day of the experiment, the TEER was assessed and the media in each plate was replaced with warm transport buffer (HBSS, 25 mM HEPES, 0.1% [wt/vol] bovine serum albumin, pH 7) and allowed to equilibrate (37°C, 30 minutes). For inhibition studies this transport buffer contained tariquidar (300 nM). The transport buffer in the apical (for apical-to-basolateral (A-to-B) transport) and basolateral (for basolateral-to-apical (B-to-A) transport) chambers was replaced with transport buffer containing either the test drug [^{3}H]raltegravir or the control ABCB1 substrate [^{3}H]digoxin (1 μM, 0.33 μCi/mL) with or without 300 nM tariquidar. Samples (50 μL) were taken from the receiver compartment at 0, 30, 60, 90, 120 and 180 minutes and replaced with an equal volume of transport buffer. Samples were analysed using a liquid scintillation counter (TRI-CARB®). Data were used to determine apparent permeability (P_{app}, cm/s) for each direction and efflux ratio (ratio of basolateral to apical P_{app} compared with apical to basolateral P_{app}). P_{app} was calculated using the following equation as described previously (Elsby *et al.*, 2008):

$$P_{app} \times 10^{-6} = \frac{(dQ / dt) \times V}{A \times C_0}$$

dQ / dt is the change in drug concentration in the receiver chamber over time (nM/s); **V** is the volume in the receiver compartment (mL); **A** is the total surface area of the transwell membrane (cm^2); C_0 is the initial drug concentration in the donor compartment (nM); and P_{app} is the apparent permeability ($x10^{-6}$ cm/s).

2.2.7 Isolation of peripheral blood mononuclear cells from human blood and the influence of ABCB1 inhibition

Venous blood samples (60 mL) were obtained from healthy volunteers via venipuncture and mixed in heparin-containing blood sample tubes. Blood (10 mL) was carefully layered onto Ficoll reagent (5 mL) and centrifuged (800 g, 30 minutes, 4°C, no brake on deceleration). Following centrifugation, plasma was discarded and the PBMC layer was carefully transferred to a sterile 50 mL skirted tube using a sterile plastic pipette. HBSS (25 mL) was added to PBMCs and tubes were centrifuged (800 g, 5 minutes, 4°C). Supernatant fraction was discarded and the wash procedure was repeated. PBMCs were resuspended in HBSS, ensuring that different patient samples were not mixed together. Cells were used immediately for cellular accumulation studies as described in Section 2.2.8.

2.2.8 Accumulation of raltegravir in peripheral blood mononuclear cells

Accumulation of raltegravir in PBMCs was determined using the same method as used in Section 2.2.5, with slight modifications. Briefly, cells of a constant cell density (1 mL, 5 x 10^6 cells/mL) were incubated (37°C, 5% CO_2) for 30 minutes in cell culture medium (RPMI, 10% [vol/vol] FCS) containing [^{3}H]raltegravir (1 μM, 0.2 μCi/mL). Separate incubations were undertaken where cells were preincubated prior to substrate addition with cell culture medium (10% [vol/vol] FCS) containing tariquidar (300 nM, 30 minutes). Tariquidar was again also included during the 30 minute substrate incubation. Cells were washed and treated for analysis as described in Section 2.2.5. Using supernatant fraction and intracellular radioactivity readings, CARs were calculated for raltegravir as described in Section 2.2.5. Data are expressed as mean CAR (n = 4 biological replicates, n ≥ 3 experimental replicates per biological replicate) ± SD.

2.2.9 Inhibition of ABCB1 by raltegravir, verapamil and tariquidar using CEM and CEM_{VBL100} cells

CEM and CEM_{VBL100} cells of a constant cell density (1 mL, 2.5 x 10^6 cells/mL) were incubated (37°C, 5% CO_2) for 30 minutes in cell culture medium (RPMI, 10% [vol/vol] FCS) containing control ABCB1 substrate [^{3}H]digoxin (1 μM, 0.2 μCi/mL). Separate incubations were undertaken where CEM_{VBL100} cells were preincubated for 30 minutes prior to the substrate addition with RPMI 1640 medium (10% [vol/vol] FCS) containing either raltegravir (2.5 μM, 25 μM, or 250 μM), the non-specific transport inhibitor, verapamil (30 μM), or the potent non-competitive

ABCB1 inhibitor, tariquidar (300 nM). Again, inhibitors were also included during the 30 minutes of substrate incubation. Cells were washed and treated for analysis as described in Section 2.2.5. Using supernatant fraction and intracellular radioactivity readings, CARs were calculated for digoxin as described in Section 2.2.5.

2.2.10 Modulation of vinblastine toxicity in CEM_{VBL100} cells by raltegravir

CEM and CEM_{VBL100} cells of a constant cell density (100 µL, 2 x 10^5 cells/mL) were incubated in 96-well Nunc flat-bottom plates (37°C, 5% CO_2, 120 hours) with cell culture medium (RPMI, 10% [vol/vol] FCS) containing a concentration range from 0 to 2000 ng/mL of the cytotoxic compound, vinblastine. Separate incubations were undertaken where CEM_{VBL100} cells were incubated in 96-well Nunc flat-bottom plates (37°C, 5% CO_2, 120 hours) containing 0 to 2000 ng/mL vinblastine with the addition of raltegravir (1 µM, 10 µM, or 100 µM). The solvent vehicle used to dissolve the drugs was sterile water (1% [vol/vol] final concentration) and control cells were incubated with 1% water to act as drug-free controls. An MTT assay was conducted using the treated cells and results were determined using Graphpad Prism essentially as described in Section 2.2.4.

2.2.11 Induction of ABCB1 by raltegravir in Caco-2 monolayers

Caco-2 monolayers were created as described in Section 2.2.6, with modifications. During the last three days of the 21-day monolayer maturation, a selection of cells were incubated (DMEM, 15% [vol/vol] FCS) containing raltegravir (20 µM).

Monolayer integrity was checked using a MillicellERS instrument (Millipore) to determine the TEER across the monolayer. A TEER of more than 600 μΩ was deemed acceptable. In addition to TEER, [^{14}C]Mannitol, which is not permeable through a cell membrane, was also added to each well during the experiment to confirm monolayer integrity.

On the day of the experiment, the TEER was assessed and the media in each plate was replaced with warm transport buffer (HBSS, 25 mM HEPES, 0.1% [wt/vol] bovine serum albumin, pH 7) and allowed to equilibrate (37°C, 30 minutes). The transport buffer in the apical (for A-to-B transport) and basolateral (for B-to-A transport) chambers was replaced with transport buffer containing the ABCB1 substrate, [^{3}H]lopinavir (1 μM, 0.5 μCi/mL), and [^{14}C]mannitol (3.6 μM, 0.2 μCi/mL). Samples (50 μL) were taken from the receiver compartment at 0 and 60 minutes. Samples were analysed using a liquid scintillation counter (TRI-CARB®). Data were used to determine apparent permeability (P_{app}, cm/s) and efflux ratio (ratio of basolateral to apical P_{app} compared with apical to basolateral P_{app}) as described in Section 2.2.6.

2.2.12 Statistical analysis

Data were analysed using SPSS 15.0 for Windows. All data were tested for normality using the Shapiro-Wilk test. An independent *t* test was used to determine the significance of normally distributed data and the Mann Whitney U test was used for all other data. A two-tailed p value of < 0.05 was accepted as being statistically significant.

2.3 RESULTS

2.3.1 ABCB1 and ABCC1 expression levels in CEM and CEM_{VBL100} cells

Expression of ABCB1 (Figure 2.3) and ABCC1 (Figure 2.4) in CEM and CEM_{VBL100} cells were determined using flow cytometry. Data are presented as relative fluorescence units (RFU) ± SD. ABCB1 expression was 158-fold higher in CEM_{VBL100} cells compared to CEM cells (RFU of 158.0 ± 3.0 versus 1.0 ± 0.3, $p < 0.05$). No difference in ABCC1 expression was seen between CEM_{VBL100} and CEM cells (RFU of 2.0 ± 0.1 versus 2.1 ± 0.2, $p = 1.00$).

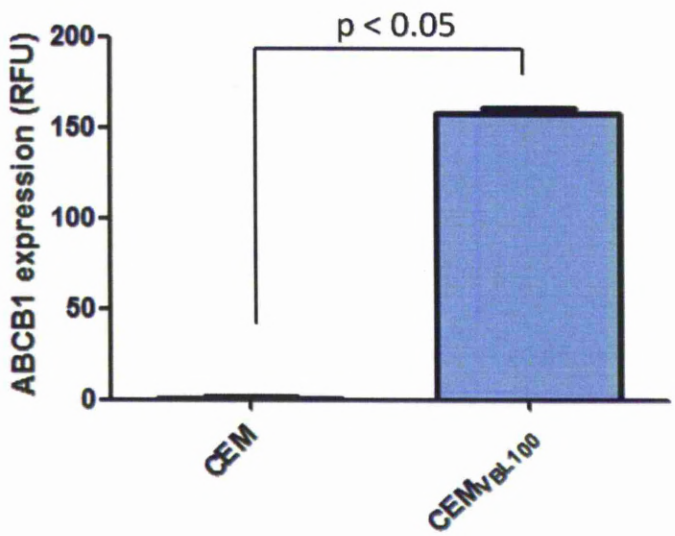

Figure 2.3. Expression of ABCB1 in CEM and CEM_{VBL100} cells. Data are expressed as RFU (median fluorescence minus that of the isotype control, n = 2 experimental replicates) ± SD.

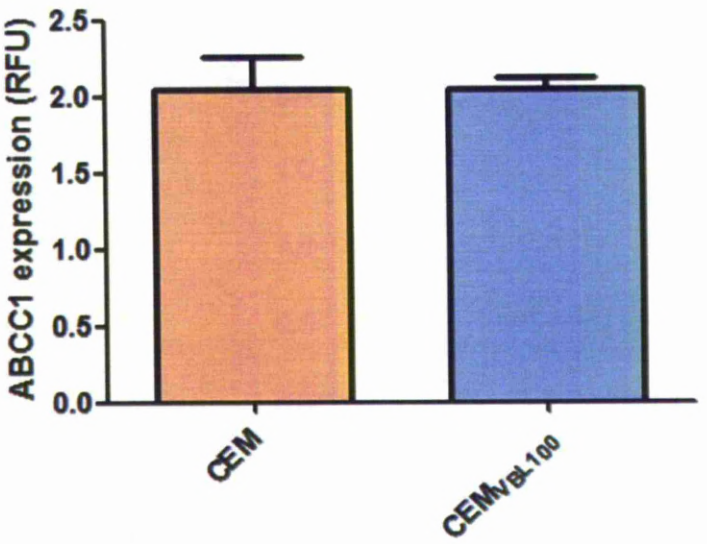

Figure 2.4. Expression of ABCC1 in CEM and CEM_{VBL100} cells. Data are expressed as RFU (median fluorescence minus that of the isotype control, n = 2 experimental replicates) ± SD.

2.3.2 Cytotoxicity of raltegravir in CEM and Caco-2 cells

Raltegravir showed no cellular toxicity in Caco-2 (Figure 2.5) and CEM (Figure 2.6) cells at any concentration tested. Cell viability (percentage mean viability compared to drug-free control cells ± SD, n = 6 experimental replicates) appeared unaffected by raltegravir concentrations up to 100 μM in Caco-2 (104.9% ± 12.7) and CEM (113.9% ± 13.0) cells. Due to the absence of any raltegravir-induced cytotoxicity at the screened concentration range, an IC_{50} value could not be calculated from the slope. The cytotoxic compounds vinblastine and epirubicin were used at up to 100μM concentration to significantly reduce cell viability in Caco-2 (13.2% ± 5.9 at 100 μM, p = 0.04) and CEM (9.5% ± 2.7 at 100 μM, p = 0.04) cells, respectively. The calculated IC_{50} values for vinblastine and epirubicin were both 1.0 μM. The

vehicle used to deliver drugs was sterile water (1% final concentration) which had no significant affect on cell viability.

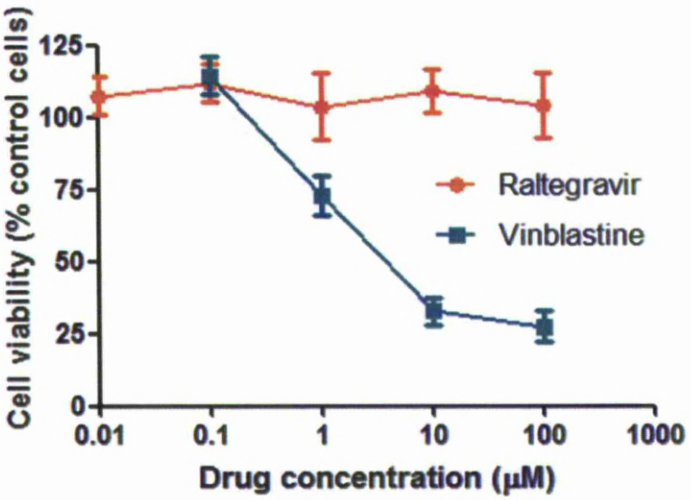

Figure 2.5. Cellular toxicity of raltegravir and vinblastine in Caco-2 cells. Data expressed as cell viability (percentage mean viability compared to drug-free control cells, n=6 experimental replicates) ± SD.

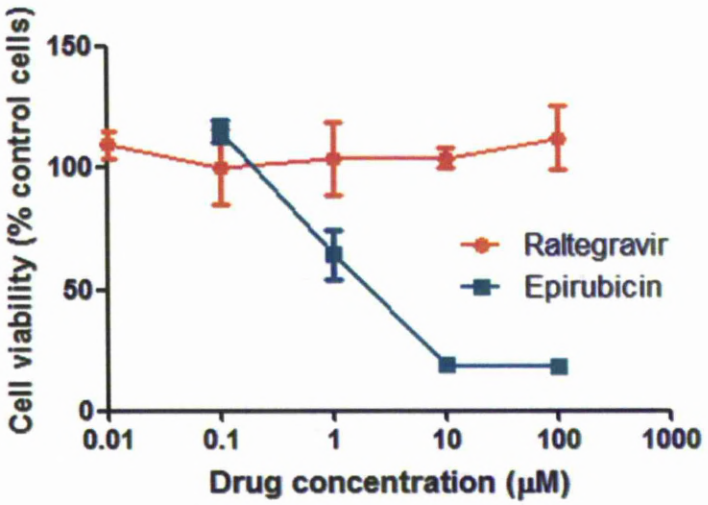

Figure 2.6. Cellular toxicity of raltegravir and epirubicin in CEM cells. Data expressed as cell viability (percentage mean viability compared to drug-free control cells, n=6 experimental replicates) ± SD.

2.3.3 The effect of tariquidar on raltegravir, saquinavir, lopinavir and rilpivirine accumulation in CEM and CEM_{VBL100} cells

The cellular accumulation of raltegravir (Figure 2.7), saquinavir (Figure 2.8), lopinavir (Figure 2.9) and rilpivirine (Figure 2.10) were determined using CEM cells and ABCB1-overexpressing CEM_{VBL100} cells. The effect of the ABCB1 inhibitor tariquidar on cellular accumulation in CEM_{VBL100} cells was also investigated. Data are expressed as mean CAR ± SD. Raltegravir CAR was significantly lower in ABCB1-expressing CEM_{VBL100} cells compared to CEM cells (1.4 ± 0.2 versus 2.1 ± 0.2, $p = 0.02$). Raltegravir CAR in CEM_{VBL100} cells was significantly increased when cells were incubated with tariquidar (2.0 ± 0.4, $p = 0.042$).

The protease inhibitors saquinavir and lopinavir are confirmed ABCB1 substrates and were used to validate the experiment. Saquinavir CAR was significantly lower in ABCB1-overexpressing CEM_{VBL100} cells compared to CEM cells (19.0 ± 5.6 versus 37.5 ± 2.1, $p = 0.021$). Saquinavir CAR in CEM_{VBL100} cells was significantly increased when cells were incubated with tariquidar (37.8 ± 8.5, $p = 0.021$). Lopinavir CAR was significantly lower in ABCB1-expressing CEM_{VBL100} cells compared to CEM cells (8.4 ± 1.3 versus 15.1 ± 2.6, $p = 0.021$). Lopinavir CAR in CEM_{VBL100} cells was significantly increased when cells were incubated with tariquidar (17.8 ± 0.9, $p = 0.034$).

The NNRTI rilpivirine has recently been accepted for use in HAART. Transport of rilpivirine by ABCB1 has not been fully investigated and therefore the drug was investigated in this study. Rilpivirine CAR was unchanged in ABCB1-overexpressing CEM_{VBL100} cells compared to CEM cells (74.4 ± 9.2 versus 70.9 ±

5.5, p = 0.56). Rilpivirine CAR in CEM_{VBL100} cells was unchanged when cells were incubated with tariquidar (72.1 ± 7.2, p = 0.72).

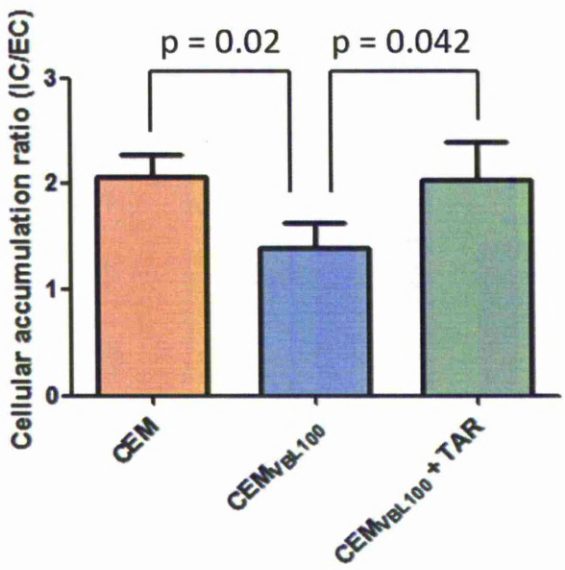

Figure 2.7. Raltegravir (1 μM) accumulation in CEM, CEM_{VBL100}, and CEM_{VBL100} cells treated with 300 nM tariquidar (TAR). Data are expressed as mean CAR (n = 4 biological replicates, n = 3 experimental replicates per biological replicate) ± SD.

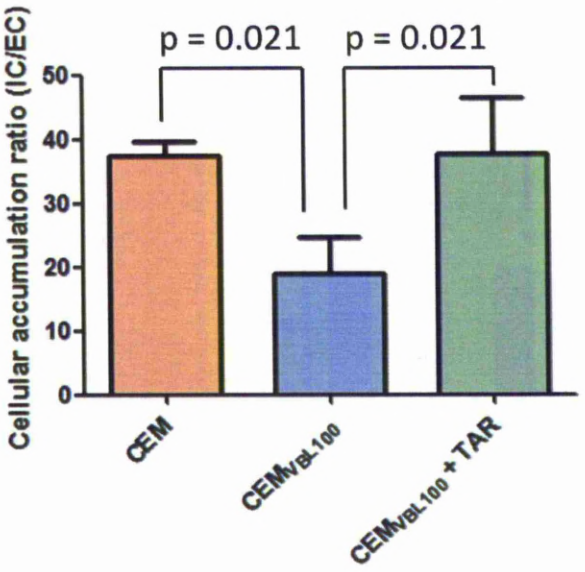

Figure 2.8. Saquinavir (1 μM) accumulation in CEM, CEM_{VBL100}, and CEM_{VBL100} cells treated with 300 nM tariquidar (TAR). Data are expressed as mean CAR (n = 4 biological replicates, n = 3 experimental replicates per biological replicate) ± SD.

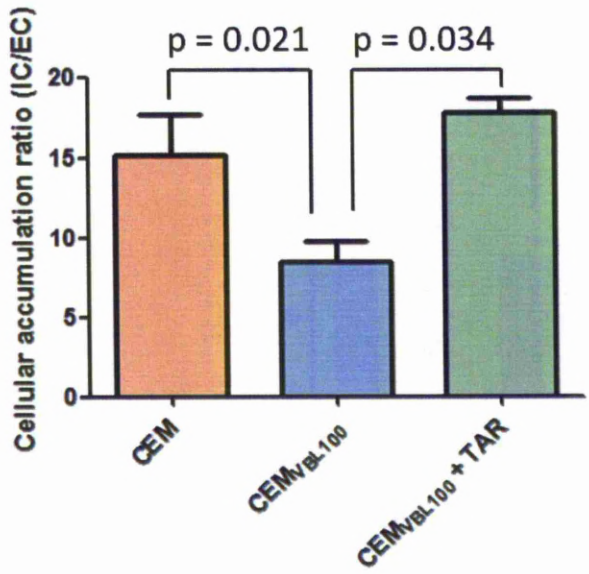

Figure 2.9. Lopinavir (1 μM) accumulation in CEM, CEM_{VBL100}, and CEM_{VBL100} cells treated with 300 nM tariquidar (TAR). Data are expressed as mean CAR ($n \geq 3$ experimental replicates) ± SD.

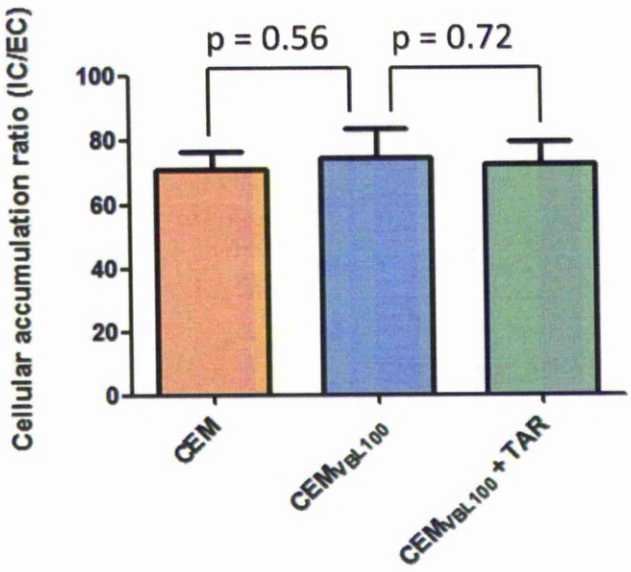

Figure 2.10. Rilpivirine (25 μM) accumulation in CEM, CEM_{VBL100}, and CEM_{VBL100} cells treated with 300 nM tariquidar (TAR). Data are expressed as mean CAR ($n \geq 3$ experimental replicates) ± SD.

2.3.4 The effect of tariquidar on the bidirectional transport of raltegravir and digoxin using a Caco-2 monolayer

The amount of drug entering the receiver compartment over a 180 minute incubation period is shown for raltegravir without (Figure 2.11) and with (Figure 2.12) tariquidar-mediated ABCB1 inhibition. The same results are presented for the positive control ABCB1 substrate, digoxin, without (Figure 2.13) and with (Figure 2.14) ABCB1 inhibition. Data are expressed as mean drug amount in receiver well (pmol, n = 3 experimental replicates) ± SD.

The P_{app} values obtained for raltegravir and digoxin with and without tariquidar are given in Figure 2.15. Data are expressed as mean P_{app} ($x10^{-6}$ cm/s) ± SD and efflux ratios (B-to-A P_{app} / A-to-B P_{app}) were calculated. All calculations were made by

using the samples taken after 120 minutes of incubation as sink conditions were maintained. Raltegravir showed significantly higher transport in the B-to-A direction (P_{app} = 13.4 ± 2.1) compared to the A-to-B direction (P_{app} = 7.3 ± 2.2, p = 0.02). The efflux ratio of raltegravir at 120 minutes was 1.9. The presence of tariquidar reduced the efflux ratio of raltegravir to 1.3, which removed the preference for B-to-A permeability (p = 0.30). The ABCB1 control substrate digoxin showed significantly higher transport in the B-to-A direction (P_{app} = 12.9 ± 0.6) compared to the A-to-B direction (P_{app} = 2.1 ± 0.3, p < 0.001). The efflux ratio of digoxin at 120 minutes was 6.3. The presence of tariquidar reduced the efflux ratio of digoxin to 0.9 which removed the preference for B-to-A permeability (p = 0.58).

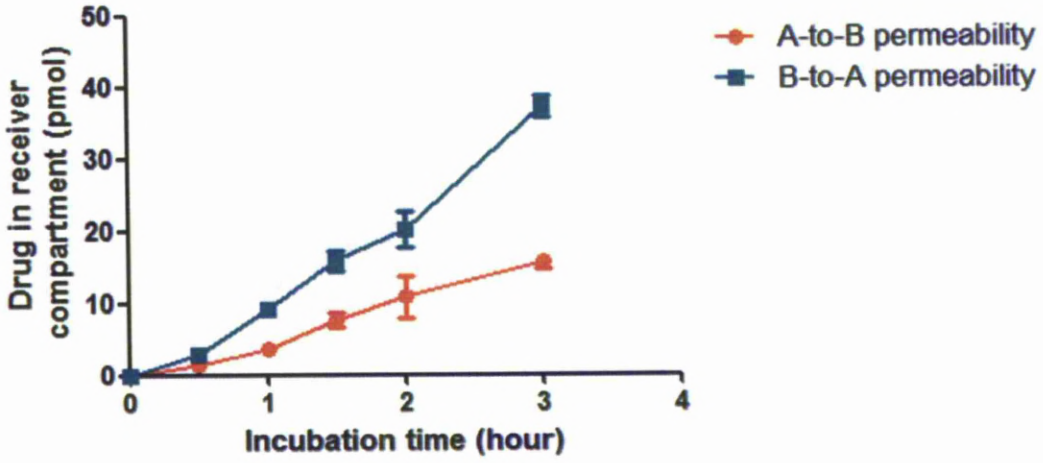

Figure 2.11. Raltegravir (1 μM) transport across a Caco-2 monolayer, showing A-to-B (●) and B-to-A (■) directions. Data are expressed as mean drug amount in receiver well (pmol, n = 3 experimental replicates) ± SD.

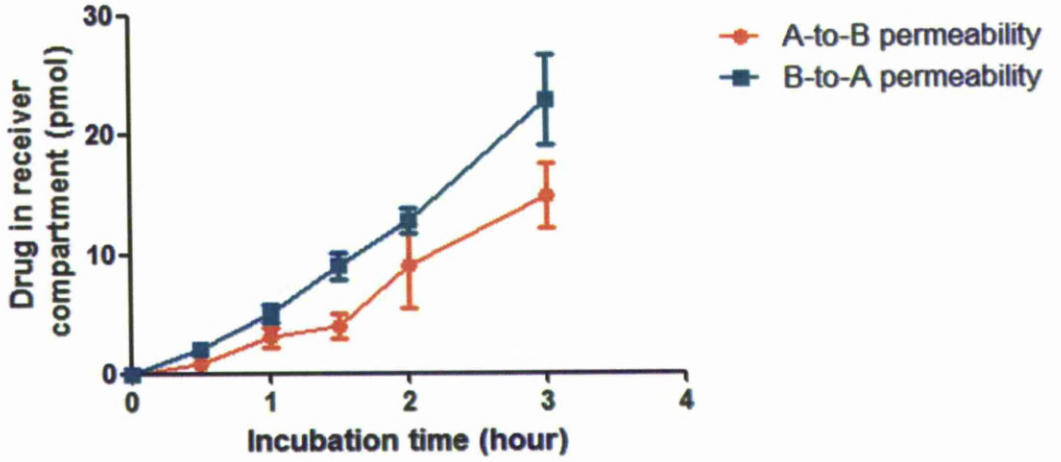

Figure 2.12. Raltegravir (1 μM) transport across a Caco-2 monolayer treated with 300 nM tariquidar, showing A-to-B (●) and B-to-A (■) directions. Data are expressed as mean drug amount in receiver well (pmol, n = 3 experimental replicates) ± SD.

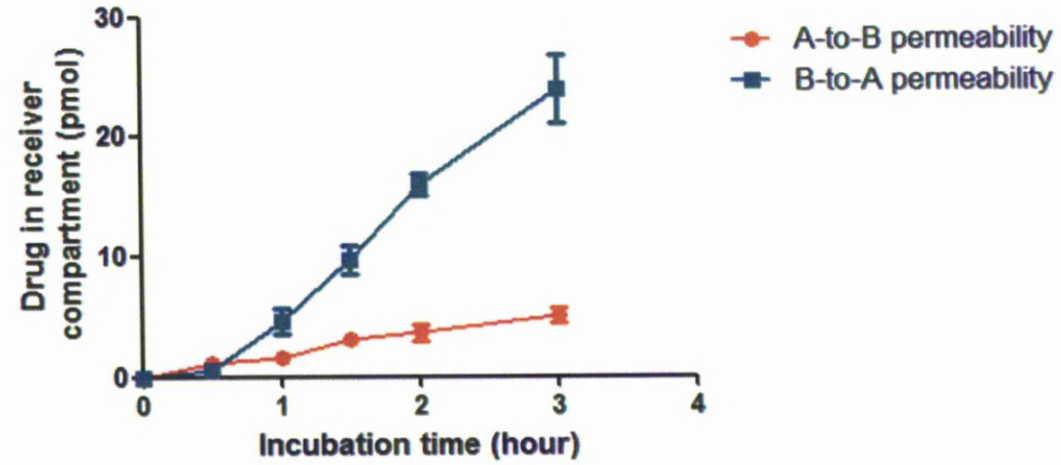

Figure 2.13. Digoxin (1 μM) transport across a Caco-2 monolayer, showing A-to-B (●) and B-to-A (■) directions. Data are expressed as mean drug amount in receiver well (pmol, n = 3 experimental replicates) ± SD.

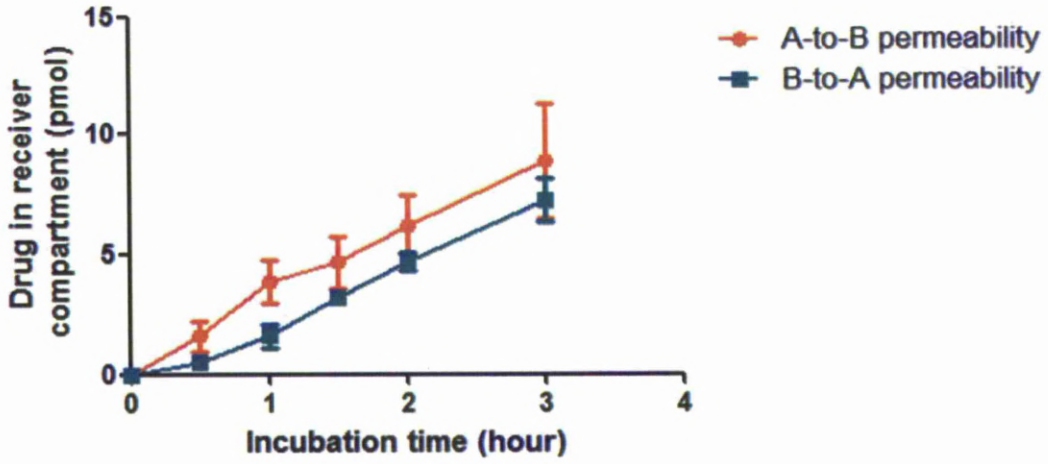

Figure 2.14. Digoxin (1 μM) transport across a Caco-2 monolayer treated with 300 nM tariquidar, showing A-to-B (●) and B-to-A (■) directions. Data are expressed as mean drug amount in receiver well (pmol, n = 3 experimental replicates) ± SD.

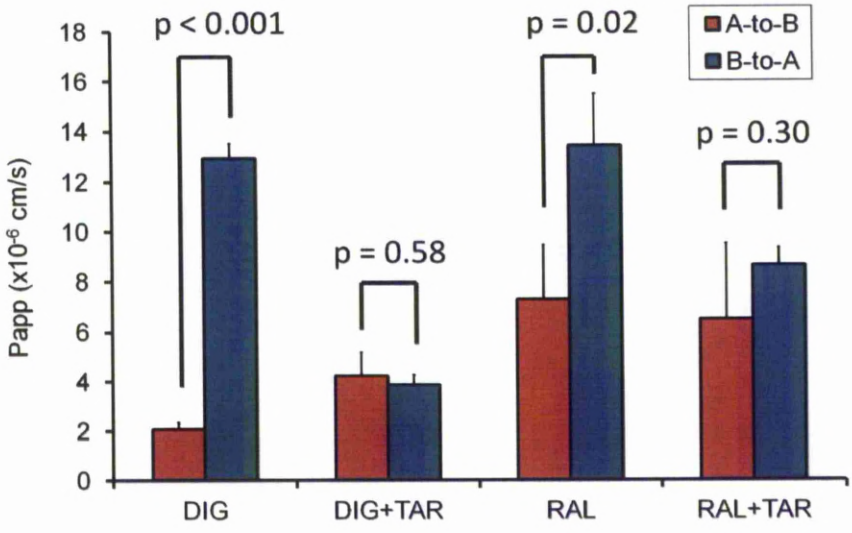

Figure 2.15. P_{app} of raltegravir (RAL) and digoxin (DIG) in the A-to-B (■) and B-to-A (■) directions across a Caco-2 transwell membrane, with and without the presence of 300 nM tariquidar (TAR). Data are expressed as mean P_{app} ($x10^{-6}$ cm/s; n = 3 experimental replicates) ± SD.

2.3.5 Accumulation of raltegravir in peripheral blood mononuclear cells and the influence of ABCB1 inhibition

Raltegravir accumulation in PBMCs from four human subjects was determined and tariquidar was used to determine the extent of raltegravir transport by ABCB1. Data are expressed as mean CAR ± SD and given in Figure 2.16. Raltegravir CAR was not significantly altered in tariquidar-treated cells compared to non-treated cells in subject 1 (3.76 ± 0.56 versus 3.78 ± 0.70, p = 0.83), subject 3 (2.52 ± 0.29 versus 3.03 ± 0.97, p = 1.0) or subject 4 (2.86 ± 0.93 versus 2.15 ± 0.30, p = 0.51). Raltegravir CAR was significantly higher in tariquidar-treated cells compared to non-treated cells in subject 2 (5.98 ± 2.12 versus 3.13 ± 0.22, p = 0.02). When combining the average results from each subject, raltegravir CAR was not significantly different in tariquidar-treated cells compared to non-treated cells (3.78 ± 1.56 versus 3.02 ± 0.67, p = 0.77).

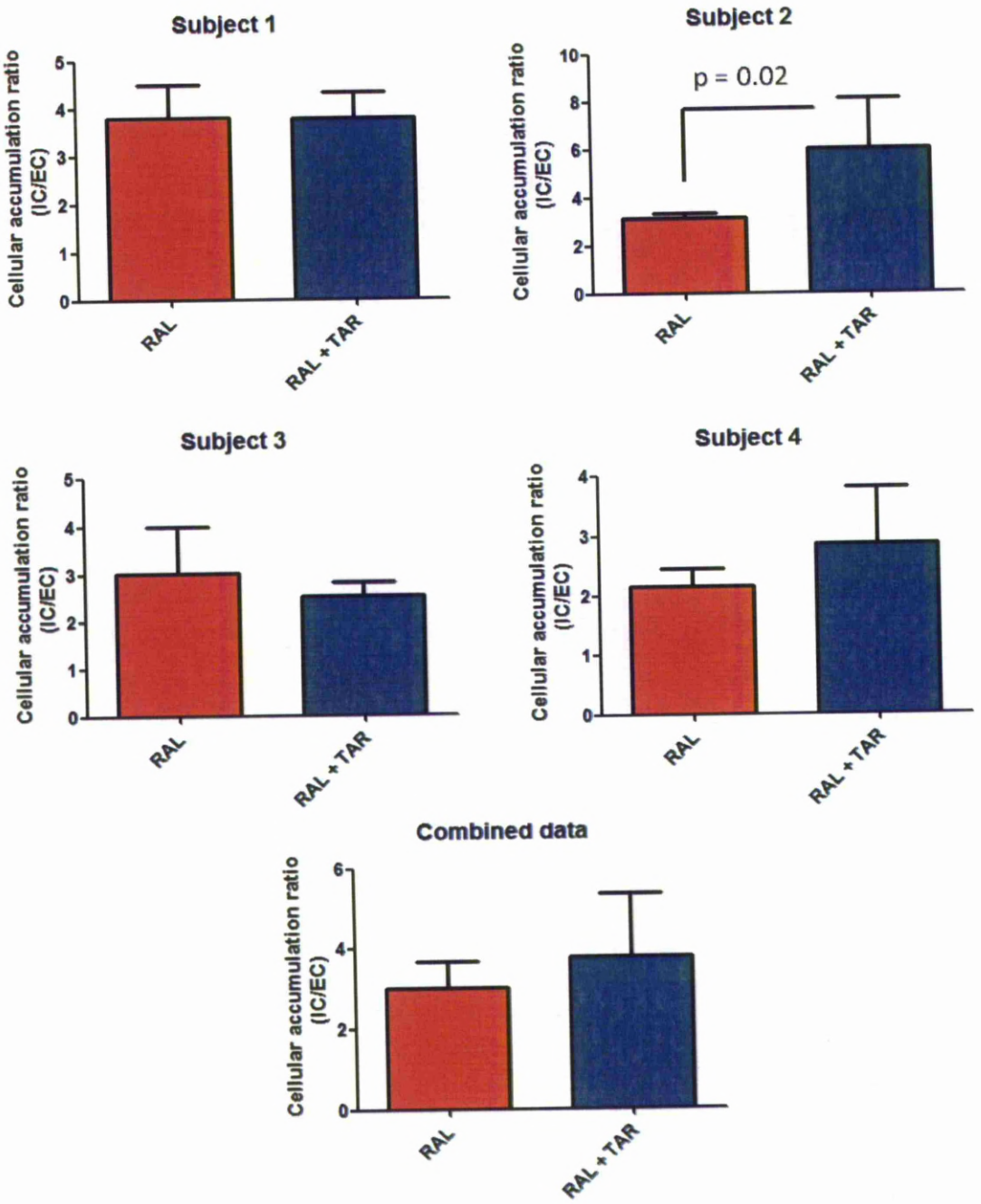

Figure 2.16. Raltegravir (1 μM) accumulation in PBMCs (■) and PBMCs co-incubated with 300 nM tariquidar (■). Data for subjects 1, 2, 3 and 4 are expressed as mean CAR ($n \geq 3$ experimental replicates) ± SD. Combined data are expressed as mean CAR ($n = 4$ biological replicates, $n \geq 3$ experimental replicates per biological replicate) ± SD.

2.3.6 Inhibition of ABCB1 by raltegravir, verapamil and tariquidar using CEM and CEM_{VBL100} cells

The ability of raltegravir to inhibit ABCB1-mediated drug transport was determined using CEM and CEM_{VBL100} cells. The CAR of ABCB1 substrate digoxin was determined in CEM, CEM_{VBL100} and CEM_{VBL100} co-incubated with raltegravir (2.5 μM, 25 μM or 250 μM), ABCB1 inhibitor tariquidar (300 nM) or non-specific transporter inhibitor verapamil (30 μM). Data are expressed as mean CAR (n = 3 experimental replicates) ± SD and are given in Figure 2.17. Digoxin CAR was significantly lower in ABCB1-overexpressing CEM_{VBL100} cells compared to CEM cells (0.49 ± 0.05 versus 1.19 ± 0.05, p = 0.046). Digoxin CAR in CEM_{VBL100} was unchanged when cells were incubated with 2.5 μM raltegravir (0.56 ± 0.05, p = 0.105), 25 μM raltegravir (0.46 ± 0.07, p = 0.268) or 250 μM raltegravir (0.52 ± 0.05, p = 0.268) but was significantly increased when CEM_{VBL100} cells were incubated with tariquidar (1.30 ± 0.24, p = 0.046) or verapamil (1.09 ± 0.09, p = 0.046).

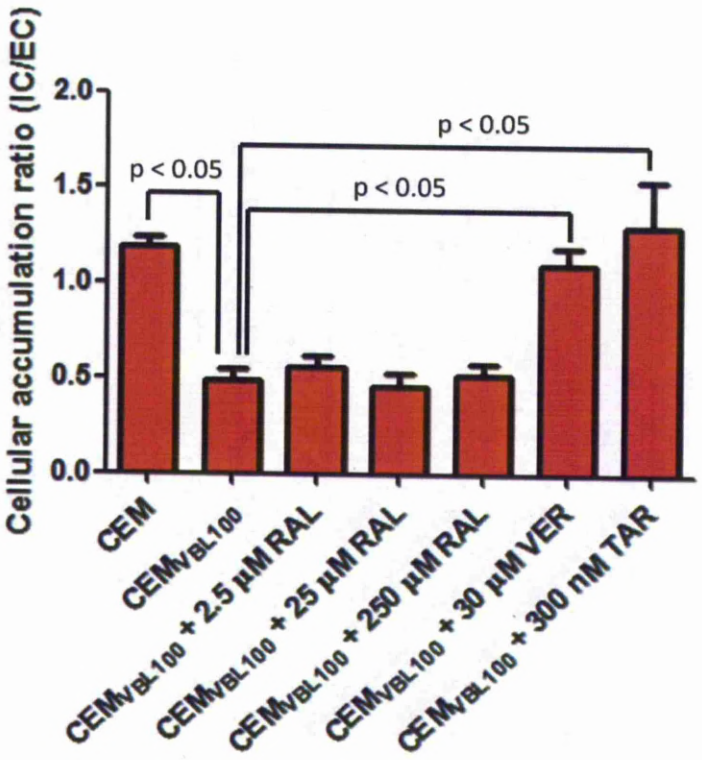

Figure 2.17. Digoxin (1 μM) accumulation in CEM, CEM_{VBL100} and CEM_{VBL100} co-incubated with raltegravir (RAL; 2.5 μM, 25 μM or 250 μM), ABCB1 inhibitor tariquidar (TAR; 300 nM) or non-specific transporter inhibitor verapamil (VER; 30 μM). Data are expressed as mean CAR (n = 3 experimental replicates) ± SD.

2.3.7 Modulation of vinblastine toxicity in CEM_{VBL100} cells by raltegravir

CEM_{VBL100} cells are resistant to vinblastine-induced toxicity due to greatly increased ABCB1 expression. The ability of raltegravir to increase vinblastine-induced toxicity over five day's incubation was determined. Data are expressed as percentage cell viability (mean percentage viability compared to vinblastine-free control cell incubations) ± SD and results are given in Figure 2.18 and converted to log scale in

Figure 2.19. Raltegravir did not appear to alter the susceptibility of CEM_{VBL100} cells to vinblastine-mediated toxicity at any concentration tested.

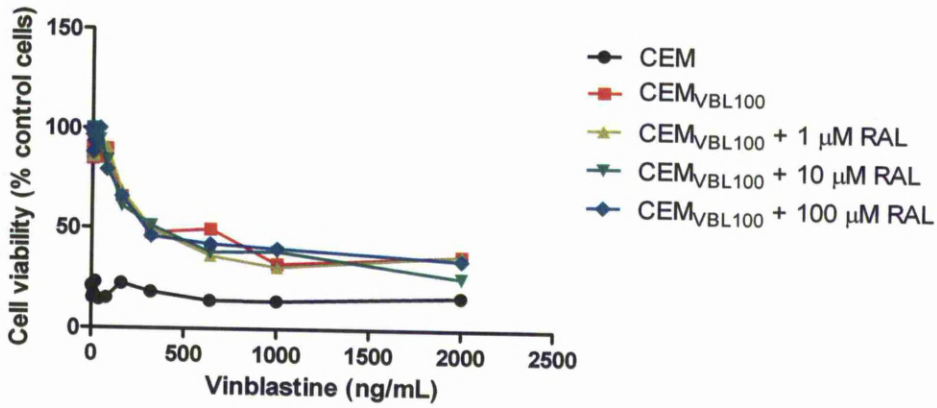

Figure 2.18. Cellular toxicity of vinblastine in CEM cells and CEM_{VBL100} cells co-incubated with 0-100 μM raltegravir. Data expressed as cell viability (percentage mean viability compared to drug-free control cell incubations, n = 6 experimental replicates) ± SD.

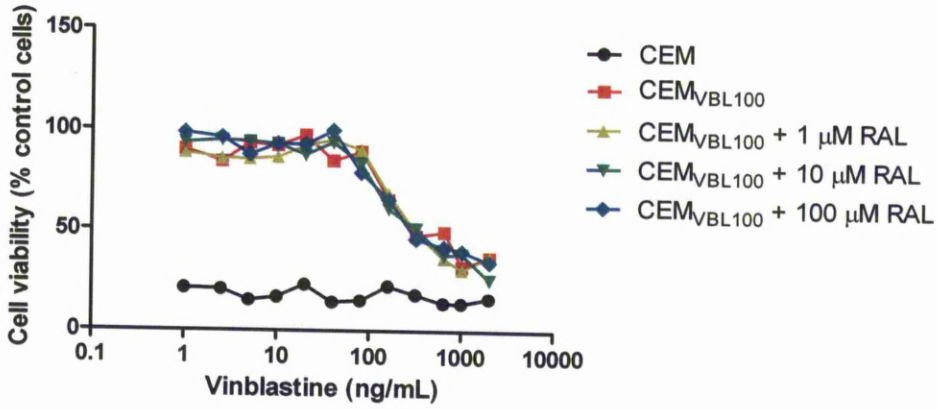

Figure 2.19. Log scale plot of cellular toxicity of vinblastine in CEM cells and CEM_{VBL100} cells co-incubated with 0-100 μM raltegravir. Data expressed as cell viability (percentage mean viability compared to drug-free control cells, n = 6 experimental replicates) ± SD.

2.3.8 Induction of ABCB1 by raltegravir in Caco-2 monolayers

The permeability of lopinavir, a confirmed ABCB1 substrate, through a Caco-2 monolayer was determined using control cells and cells pre-incubated for three days prior to the experiment with 20 μM raltegravir. Data are given as efflux ratios (B-to-A P_{app} / A-to-B P_{app}, n = 3 experimental replicates) ± SD and are shown in Figure 2.20. There was no significant difference in lopinavir efflux ratio between control cells (9.02 ± 0.85) and cells pre-incubated with raltegravir (8.81 ± 1.75, p = 1.0).

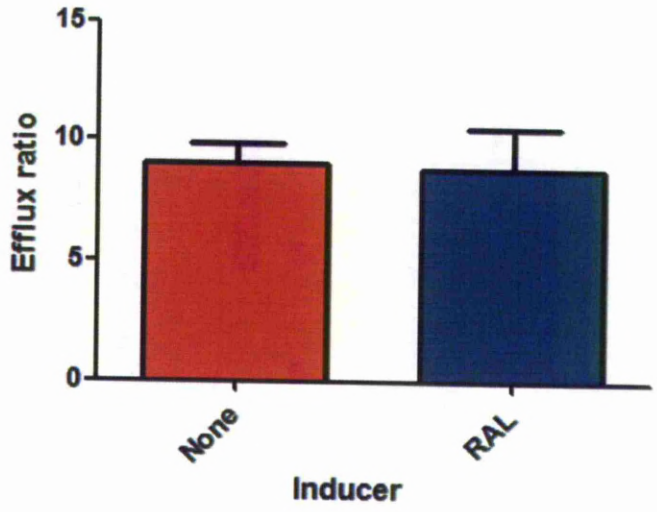

Figure 2.20. Efflux ratios of lopinavir across a Caco-2 monolayer with (■) and without (■) pre-incubation for three days with 20 μM raltegravir. Data are expressed as mean efflux ratio (B-to-A P_{app} / A-to-B P_{app}, n = 3 experimental replicates) ± SD.

2.4 DISCUSSION

After initially determining the toxicity of raltegravir in utilised cell lines, this chapter investigated how ABCB1 influences the cellular permeability and disposition of raltegravir. The ability of raltegravir to inhibit or induce ABCB1 activity was also investigated. Experiments utilised *in vitro* cell accumulation, permeability and toxicity models, as well as *ex vivo* models using isolated PBMCs.

The MTT assay (Mosmann, 1983) was modified and used to determine the toxicity of raltegravir in Caco-2 and CEM cell lines. Viable cells are able to convert yellow MTT, using mitochondrial reductase enzymes, to a dark blue formazan derivative. This process requires energy in the form of ATP and therefore non-viable cells are unable to convert MTT to formazan. Previous work in the Liverpool HIV pharmacology group has shown the PIs saquinavir, nelfinavir, indinavir, lopinavir, ritonavir and the NNRTI efavirenz caused toxicity in PBMCs at 10μM and higher concentrations (Chandler *et al.*, 2003).

Raltegravir showed no toxicity after five days in either Caco-2 or CEM cell lines at the highest concentration tested (100 μM) and the IC_{50} value of raltegravir could not be determined from the slope in either cell lines. This apparent lack of raltegravir toxicity at high concentrations *in vitro* suggests that raltegravir-induced cell toxicity is unlikely to affect experiments in this and subsequent chapters.

The expression of ABCB1 and ABCC1 on CEM and CEM_{VBL100} cell membranes was determined using specific monoclonal antibodies. Compared to CEM cells,

CEM_{VBL100} cells had 158-fold higher ABCB1 expression, confirming the use of CEM_{VBL100} cells in experiments requiring an ABCB1-overexpressing cell line. The lack of increased ABCC1 expression on CEM_{VBL100} cells suggests that vinblastine treatment has not increased expression of all drug transporters to the same degree as with ABCB1, although overexpression of an unchecked transporter cannot be ruled out. Drug accumulation studies in CEM and CEM_{VBL100} cells showed a small but significant decrease in raltegravir CAR in the ABCB1 over-expressing CEM_{VBL100} cells. The control ABCB1 substrates saquinavir and lopinavir showed a greater CAR decrease than was seen with raltegravir, suggesting that raltegravir is the weaker ABCB1 substrate. Raltegravir, saquinavir and lopinavir all showed increased CAR in CEM_{VBL100} cells co-incubated with ABCB1 inhibitor tariquidar and this increased CAR was comparable to the CAR obtained in wild type CEM cells. This supported the hypothesis that raltegravir is being actively transported by ABCB1 out of CEM_{VBL100} cells. The experiment was repeated four times to confirm the results.

In the bidirectional transport study using Caco-2 cells, the positive control substrate digoxin achieved an efflux ratio of 6.27 which was above the minimum efflux ratio of digoxin in Caco-2 monolayers suggested by the FDA (Huang *et al.*, 2007). Raltegravir achieved an efflux ratio of 1.85, which was reduced to 1.33 in the presence of tariquidar. This supported the hypothesis that raltegravir is being actively transported by ABCB1 in the B-to-A direction. However, unlike digoxin, raltegravir still showed preferential transport in the B-to-A direction in the presence of tariquidar (Figure 2.12). This presents the possibility that either tariquidar was not totally effective at preventing ABCB1 transport, or an as yet unidentified transporter expressed on the Caco-2 membrane is facilitating B-to-A transport of raltegravir, and

that this transporter is not fully inhibited by tariquidar. This could be facilitated by an efflux transporter on the apical surface (ABCC2, ABCC4) or possibly an uptake transporter on the basolateral surface (SLC22A1, SLC22A2) of the Caco-2 cell (Kis *et al.*, 2010a; Maubon *et al.*, 2007). However, the remaining active transport was small (Efflux ratio of 1.33) and therefore any transporter involved is unlikely to dramatically influence raltegravir absorption *in vivo*.

The extent of raltegravir transport by ABCB1 was small when compared to the transport of the positive control ABCB1 substrate, digoxin. Indeed, the FDA guidelines recommend that a drug should achieve an efflux ratio of at least 2 in Caco-2 cell monolayers and show greater than 50% reduction in efflux ratio when an ABCB1 inhibitor is used, in order for ABCB1 transport to be considered relevant *in vivo* (Huang *et al.*, 2008). In the Caco-2 monolayer experiments raltegravir only achieved an efflux ratio of 1.85 and a reduction in efflux ratio of 32% when tariquidar was used to inhibit ABCB1. The low rate of raltegravir transport by ABCB1 may explain the absence of major drug interactions with known potent ABCB1 inhibitors. This is consistent with a previous report that co-administration of ritonavir, a known ABCB1 inhibitor (Sankatsing *et al.*, 2004), had no clinically significant effect on raltegravir pharmacokinetics and no raltegravir dose adjustment is required in patients (Iwamoto *et al.*, 2008c).

Both the bidirectional transport study using Caco-2 cells and the cellular accumulation study using CEM and CEM_{VBL100} cells concluded that raltegravir was significantly transported by ABCB1. However, the extent of transport was not high, which was confirmed by the positive control substrates digoxin, saquinavir and

lopinavir showing greater levels of ABCB1-mediated transport. This does not support the previous data performed in-house by Merck, which gave an efflux ratio of 11.1 for raltegravir using LLC-PK1 cells overexpressing human ABCB1, where the positive control verapamil only gave an efflux ratio of 5.2. Verapamil was used as both an ABCB1 substrate and a competitive inhibitor of ABCB1 transport in laboratory experiments. The level of ABCB1 expression in the LLC-PK1 cells used by Merck may have been much higher than in the cell lines used in the author's experiments, which would explain the differences in the data. However, the level of ABCB1 expression detected on the surface of the CEM_{VBL100} cells was far greater than seen in wild type CEMs, confirmed by flow cytometry (Figure 2.3).

We cannot dismiss the possibility that CEM_{VBL100} cells over-express a transporter other than ABCB1 which potentially altered the results by increasing the CAR of raltegravir, therefore reducing the impact of ABCB1. Indeed, expression of the influx transporter SLCO1A2 was shown to be higher in CEM_{VBL100} cells compared to CEM cells, and SLCO3A1 expression was lower in CEM_{VBL100} cells (Janneh *et al.*, 2008). This emphasises the disadvantage of using a cell line subjected with high drug concentrations to induce transporter expression.

In order to assess the effect of physiologically relevant expression levels of ABCB1 on raltegravir cellular accumulation, experiments were conducted using PBMCs *ex vivo* from four healthy volunteers. Only PBMCs from one individual showed an increase in raltegravir accumulation once tariquidar was added. No significant change was seen in the other three volunteers. The expression level of ABCB1 on PBMCs is expected to vary between individuals, which may explain why the

addition of tariquidar had varying effects between volunteers. Although ABCB1 is expressed in PBMCs, expression is not as high as in the liver, kidney or gut (Bleasby *et al.*, 2006) and may have a lower expression level than ABCC transporters (Turriziani *et al.*, 2008). Considering that ABCB1-mediated raltegravir transport using ABCB1-overexpressing cell lines *in vitro* was low, it is unsurprising that ABCB1 appears not to alter raltegravir exposure in PBMCs.

Raltegravir failed either to reduce the accumulation of ABCB1 substrate digoxin or to increase the toxicity of vinblastine in CEM_{VBL100} cells. Both these data suggest that raltegravir does not inhibit ABCB1 *in vitro* and is unlikely to reduce ABCB1 activity *in vivo*. Also, pre-incubating a Caco-2 monolayer with 20 μM raltegravir for three days failed to alter the efflux ratio of lopinavir through the monolayer. Lopinavir is an ABCB1 substrate (Janneh *et al.*, 2007) and the lack of effect from raltegravir suggests that ABCB1 expression was not sufficiently induced or inhibited over the three day raltegravir incubation. However, lopinavir is also a known substrate of other drug transporters, including ABCC2 (Agarwal *et al.*, 2007) and SCLO1B1 (Hartkoorn *et al.*, 2010); it is possible that raltegravir is inhibiting multiple drug transporters with the effect of "cancelling out" any changes in lopinavir efflux ratio, although this is unlikely. Also, raltegravir may require longer than three days to induce ABCB1 and further experiments are required to conclusively show a lack of induction.

The results showing no effect of raltegravir on ABCB1 functionality *in vitro* support data from patients and trial volunteers, as there is evidence that raltegravir is unlikely to inhibit or induce ABCB1 *in vivo*. For example, raltegravir did not alter the

exposure of midazolam, a known ABCB1 substrate, in a PK study using healthy volunteers (Iwamoto *et al.*, 2008a).

In conclusion, raltegravir is a weak substrate of ABCB1 and does not appear to inhibit or induce the function of this transporter *in vitro*. If raltegravir was highly transported by ABCB1 *in vitro*, then drugs or other xenobiotics which significantly alter ABCB1 functionality or expression would be expected to cause contraindications *in vivo*. These interactions have not been observed and the results obtained in this chapter use *in vitro* and *ex vivo* systems to suggest that raltegravir transport by ABCB1 is lower than previous data indicates and is unlikely to be an important factor *in vivo*.

Chapter 3

Interactions between raltegravir and drug influx transporters

Table of Contents

3.1 INTRODUCTION

The primary route of raltegravir metabolism is glucuronidation via UGT1A1 and raltegravir is not a substrate or an inhibitor of the major cytochrome P450 enzymes (Iwamoto *et al.*, 2008a; Kassahun *et al.*, 2007). However, the involvement of human drug transporters in raltegravir absorption, disposition, metabolism and excretion (ADME) has not been fully investigated. Raltegravir has shown higher concentrations (1.7-fold) in semen (Barau *et al.*, 2010) and lower concentrations (0.04 to 0.39-fold) in cerebrospinal fluid (Calcagno *et al.*, 2010; Yilmaz *et al.*, 2009) compared to plasma (Section 1.6.5). These differences may be influenced by drug transporters present at membrane barriers.

There are important reasons why raltegravir should be screened for transport by known drug transporters. First, by regulating intracellular permeation, drug transporters could be an important factor in understanding the lack of a clear pharmacokinetic-pharmacodynamic (PK-PD) relationship, such as the similar virological response observed in patients given a wide range of raltegravir doses (Cattaneo *et al.*, 2012; Markowitz *et al.*, 2006). Second, an understanding of the mechanisms that control raltegravir disposition may help rationalise or even anticipate drug interactions in the clinic. Raltegravir represents the first member of a new drug class, possessing a unique chemical structure containing a diketo acid derivative (Summa *et al.*, 2008): class-specific trends in drug transport may be evident such as those reported for protease inhibitors with ABCB1 (Lee *et al.*, 1998; van der Sandt *et al.*, 2001) or for nucleoside reverse transcriptase inhibitors with organic anion and cation transporters (Takeda *et al.*, 2002; Uwai *et al.*, 2007).

Finally, knowing which transporters are involved in raltegravir ADME will identify candidate genes for future pharmacogenetic studies.

The interactions between raltegravir and the efflux transporter ABCB1 were investigated in Chapter 2. However, the interactions between raltegravir and influx transporters are unknown and could be an important determining factor in raltegravir ADME. Antiretroviral drugs are known to interact with several influx transporters, including members of the organic anion and cation transporters of the SLCO and SLC22A gene subfamilies (Roth *et al.*, 2012).

The SLCO transporters are believed to be important in the transport of antiretroviral drugs in the liver, intestine, kidney, placenta, central nervous system, as well as other tissues. SLCO1A2, SLCO1B1 and SLCO1B3 are known to transport PIs and maraviroc *in vitro* and lopinavir and maraviroc plasma concentrations are influenced by the SLCO1B1 521T>C polymorphism (rs4149056) (Hartkoorn *et al.*, 2010; Siccardi *et al.*, 2010). Furthermore, several PIs are able to inhibit SLCO activity *in vitro* (Campbell *et al.*, 2004), which could potentially result in drug-drug interactions with co-administered SLCO substrates.

The SLC22A transporters play a role in exposure of several antiretroviral drugs, particularly NRTIs (Takeda *et al.*, 2002), and are expressed throughout the body with highest expression in the kidney and liver. SLC22A1 activity is inhibited *in vitro* by nelfinavir and ritonavir (Jung *et al.*, 2008), although the inhibitory potential of raltegravir and other new antiretroviral drugs on SLC22A1 activity has yet to be determined and was investigated in this chapter. It can be seen that influx

transporters are able to influence drug ADME properties and this emphasises the importance of assessing the *in vitro* interactions between raltegravir and influx transporters of the SLCO and SLC22A subfamlies.

The aim of this chapter was to increase our understanding of the interactions between influx drug transporters and newer antiretroviral compounds, with particular focus on raltegravir. This information will help to explain variability in raltegravir PK and may aid in the prediction and, hopefully, avoidance of potential transporter-mediated drug-drug interactions. First, the transport of raltegravir and other new antiretroviral drugs by a selection of influx transporters was evaluated using the *Xenopus laevis* oocyte expression system. The influx transporters screened for drug transporting activity were SLCO1A2, SLCO1B1, SLCO1B3, SLC10A1, SLC15A1, SLC15A2, SLC22A1, SLC22A6 and SLC22A8 (see Section 1.5.2, Table 1.3 for transporter locations). Second, the ability of raltegravir and other antiretroviral drugs to inhibit SLC22A1 was determined using transfected SLC22A1-overexpressing KCL22 cells.

3.2 METHODS

3.2.1 Materials

SLC22A1-overexpressing KCL22 cells and mock-transfected KCL22 cells were donated by Athina Giannoudis, Department of Haematology, Royal Liverpool University Hospital (Liverpool, UK). Primary renal proximal tubule epithelial cells, renal cell basal medium and renal cell growth kit components were purchased from The American Type Culture Collection (Virginia, USA). [^{3}H]Raltegravir (specific activity = 32.85 Ci/mmol) and non-radiolabeled raltegravir sodium salt were gifts from Merck (New Jersey, USA). Etravirine was a gift from Janssen (Buckinghamshire, UK). [^{14}C]Darunavir (specific activity = 39.19 mCi/mmol), non-radiolabelled darunavir, [^{14}C]rilpivirine (specific activity = 20.00 mCi/mmol) and non-radiolabelled rilpivirine were gifts from Tibotec (Mechelen Belgium). Atazanavir was a gift from Bristol-Myers Squibb (New York, USA). Nevirapine was a gift from Boehringer Ingelheim (Berkshire, UK). Ritonavir was a gift from Abbott (Illinois, USA). Tenofovir, efavirenz and lamivudine were purchased from Toronto Research Chemicals (Toronto, Canada). Amprenavir was a gift from GlaxoSmithKline (Middlesex, UK). [^{3}H]Estrone 3-sulphate (specific activity = 50 Ci/mmol), [^{14}C]tetraethylammonium (specific activity = 55 mCi/mmol), [^{3}H]taurocholic acid (specific activity = 10 Ci/mmol), [^{3}H]glycyl-sarcosine (specific activity = 60 Ci/mmol) and [^{3}H]aminohippuric acid (specific activity = 5 Ci/mmol) were purchased from American Radiolabelled Chemicals (Missouri, USA). mMessage Transcription kits were purchased from Ambion Ltd. (Huntingdon, UK). Ultima Gold scintillation fluid was purchased from Perkin Elmer (Boston, USA).

Restriction enzymes were purchased from New England Biolabs (Hitchen, UK). Adult female *Xenopus laevis* frogs were purchased from Xenopus Express (Lyon, France). All other drugs and reagents were obtained from Sigma (Poole, UK).

3.2.2 Production of uptake transporter cRNA for Xenopus laevis oocyte injection

SLCO1A2, *SLCO1B1* and *SLCO1B3* transporter genes were previously cloned from cDNA extracted from Huh-7D12 and A549 cells (Hartkoorn *et al.*, 2010). Transporter DNA-containing plasmids were isolated from these clones, linearised using restriction enzymes and used as a template in cRNA production using a T3 mMessage mMachine RNA transcription kit (Ambion®) following the manufacturer's protocol. Following cRNA generation, plasmid DNA was degraded (1 µL Turbo DNase, 37°C, 15 minutes) and cRNA was concentrated using a lithium chloride precipitation method. Concentrated cRNA pellets were reconstituted in sterile water to a final concentration of 1 µg/mL for use in microinjection. SLC10A1, SLC15A1, SLC15A2, SLC22A1, SLC22A6 and SLC22A8 cRNA was provided at 1 µg/mL by Becton Dickinson (Oxford, UK).

3.2.3 Xenopus laevis maintenance

Adult female *Xenopus laevis* frogs were housed in fresh, filtered water and provided with shelter. Frogs were monitored daily to check for signs of ill health and were fed dried frog food pellets twice daily. Frogs were sacrificed using anaesthetic solution (MS222, 5 g/L, 45 minutes) following Schedule 1 procedures.

3.2.4 Xenopus laevis oocyte isolation, collagenase treatment and microinjection

Oocytes were harvested from sacrificed adult female *X. laevis* frogs and treated with modified Barth's solution minus calcium (88 mM NaCl, 1 mM KCl, 15 mM HEPES, 100 U penicillin, 100 µg/mL streptomycin, pH 7.4) containing collagenase (1 mg/mL, 22 °C, 60 rpm shaker, 1 hour). Cells were washed and transferred to Barth's solution containing calcium (88 mM NaCl, 1 mM KCl, 15 mM HEPES, 0.3 mM $CaCNO_3 \cdot 6H_2O$, 41 µM $CaCl_2 \cdot 6H_2O$, 0.82 mM $MgSO_4 \cdot 7H_2O$, 100 U penicillin, 100 µg/mL streptomycin, pH 7.4) and stored overnight in a cold room at 8°C. Healthy cells were selected and injected with transporter cRNA (50 ng per oocyte, 1 ng/nL) or sterile water (50 nL) and maintained in Barth's solution containing calcium to allow transporter expression (5 days for SLCO1B3-injected oocytes, 3 days for all other conditions, 18°C). Barth's solution was replaced daily and damaged oocytes were removed to maintain viability of the healthy oocytes.

3.2.5 Antiretroviral drug accumulation in transporter cRNA-injected Xenopus laevis oocytes

Drug accumulation studies using *Xenopus laevis* oocytes were performed as described previously with slight modifications (Hartkoorn *et al.*, 2010). Unless otherwise stated, radiolabelled drug was incubated in HBSS (pH 7.4) with ≥ 4 oocytes per condition in a 48-well nunc flat bottom plate (500 µL, 0.33 µCi/mL, 22°C, 60 rpm shaker, 1 hour). Radiolabelled positive control drugs were tested alongside radiolabelled antiretroviral drugs to ensure successful transporter expression. Drug concentrations used for raltegravir, darunavir, efavirenz and

rilpivirine were 1 μM, 10 μM, 26 μM and 25 μM, respectively (drug concentrations were usually dictated by the specific activity of the drug). Darunavir, efavirenz and rilpivirine were not used when measuring transport by SLCO1A2, SLCO1B1 or SLCO1B3 as this has been investigated previously (Hartkoorn *et al.*, 2010; Kwan *et al.*, 2007) and rilpivirine was only assessed when sufficient oocytes were available. Positive control drugs used were [^{3}H]estrone 3-sulphate (1 μM) for SLCO1A2, SLCO1B1, SLCO1B3 and SLC22A8, [^{3}H]aminohippuric acid (1 μM) for SLC22A6, [^{3}H]taurocholic acid (1 μM) for SLC10A1, [^{3}H]glycyl-sarcosine (1 μM) for SLC15A1 and SLC15A2, and [^{14}C]tetraethylammonium (6 μM) for SLC22A1. All incubations were terminated by transferring the oocytes to cell strainers and washing in ice cold HBSS to remove extracellular drug. Each oocyte was placed in a separate scintillation vial followed by 100 μL 10% SDS solution. After disintegration of the oocytes by the SDS, 4 mL scintillation fluid was added to all vials, which were then loaded into a liquid scintillation analyzer (TRI-CARB®). Results are expressed as the amount of drug per oocyte (pmol/oocyte) assuming that each oocyte had a volume of 1 μL (Hartkoorn *et al.*, 2010).

3.2.6 Culture of mock-transfected and SLC22A1-overexpressing KCL22 cells

KCL22 cells were maintained in cell culture medium (RPMI, 10% [vol/vol] FCS) prior to the experiment in a CO_2 incubator (37 °C, 5% CO_2). SLC22A1-overexpressing KCL22 cells and mock-transfected KCL22 cells were created previously by Athina Giannoudis at the Department of Haematology, Royal Liverpool University Hospital, Liverpool, UK (Giannoudis *et al.*, 2008). In this previous work, SLC22A1-overexpressing KCL22 cells were created by transfecting

pcDNA-hSLC22A1 plasmid into cells by nucleofection. Similarly, mock-transfected KCL22 cells were created by transfecting the empty vector pcDNA3.1 into cells by nucleofection. Transfected cells were selected using neomycin and stable cell lines were established. KCL22 cells were used for human SLC22A1 transfection because it expresses a low basal amount of SLC22A1 in comparison to other chronic myelogenous leukemia cell lines (Thomas *et al.*, 2004). All cell culture procedures were performed in a sterile environment. Frozen stocks of KCL22 cells were produced and thawed out using the same method as described for CEM cells in Section 2.2.2.3.

3.2.7 Evaluation of the effects of antiretroviral drugs on the accumulation of tetraethylammonium in SLC22A1-overexpressing KCL22 cells

SLC22A1-overexpressing KCL22 cells and mock-transfected KCL22 cells of a constant cell density (1 mL, 2.5 x 10^6 cells/mL) were incubated (37°C, 5% CO_2) for 30 minutes in cell culture medium (RPMI, 10% [vol/vol] FCS) containing SLC22A1 substrate [^{14}C]tetraethylammonium (5.4 μM, 0.3 μCi/mL). Separate incubation were undertaken where SLC22A1-overexpressing KCL22 cells were preincubated for 30 minutes prior to the substrate addition with cell culture medium (RPMI, 10% [vol/vol] FCS) containing one of a selection of co-incubated drugs, which included either 50 μM of SLC22A1 inhibitors prazosin or cepharanthine, or 50 μM of antiretroviral drug, which were also included during the 30 minutes of substrate incubation. The antiretroviral drugs examined as potential SLC22A1 inhibitors were atazanavir, lopinavir, amprenavir, indinavir, darunavir, ritonavir, nelfinavir,

lamivudine, tenofovir, zalcitabine, abacavir, zidovudine, stavudine, etravirine, nevirapine, rilpivirine, efavirenz and raltegravir.

Following incubation, cells were centrifuged (800 g, 1°C, 1 minute), 100μL supernatant aliquots taken, added to scintillation vials and used to calculate extracellular drug concentrations. The remaining supernatant was discarded and the cells were washed with ice-cold HBSS and centrifuged (800 g, 1°C, 1 minute). This HBSS wash was repeated a total of three times, after which the HBSS was discarded and 100 μL tap water was added to lyse the cells. The incubations were vigorously vortexed for five minutes and samples were added to scintillation vials. Four millilitres of scintillation fluid was added to scintillation vials, which were then loaded into a liquid scintillation analyzer (TRI-CARB®). Using intracellular radioactivity readings, cellular tetraethylammonium concentrations were determined in each cell line (μM ± SD, assuming 1 pL volume per cell).

Following this experiment, the procedure was repeated with modifications to produce IC_{50} data. Accumulation of [^{14}C]tetraethylammonium (5.4 μM, 0.3 μCi/mL) was determined when cells were co-incubated with a log range of antiretroviral drug concentrations (0, 1, 2.5, 5, 10, 25, 50, 100 μM). Antiretroviral drugs used in this experiment were drugs that showed good SLC22A1 inhibition at 50 μM and have either not been investigated in previous literature (darunavir and rilpivirine) or have shown conflicting results to those previously published (efavirenz) (Jung *et al.*, 2008; Jung *et al.*, 2009). Raltegravir, although not showing SLC22A1 inhibition at 50 μM, is integral to the work in this thesis and was tested to confirm a lack of SLC22A1 inhibition at 100 μM and below. Prazosin was used as a positive control SLC22A1

inhibitor. Data was plotted using Prism 5 and the slopes were used to calculate relative IC_{50} (the amount of drug needed to achieve 50% SLC22A1 as determined from the maximum and minimum extremes of the non-linear regression plot) and the absolute IC_{50} (the amount of drug needed to achieve 50% SLC22A1 as determined from the maximum of the non-linear regression plot and 0% accumulation).

3.2.8 Statistical analysis

Data were analysed using SPSS 15.0 for Windows. All data were tested for normality using the Shapiro-Wilk test. An independent *t* test was used to determine the significance of normally distributed data and the Mann Whitney U test was used for all other data. A two-tailed p value of < 0.05 was accepted as being statistically significant.

3.3 RESULTS

3.3.1 Antiretroviral drug accumulation in transporter cRNA-injected Xenopus laevis oocytes

The accumulation of raltegravir and several other newly developed antiretroviral drugs were determined in SLCO1A2 (Figure 3.1), SLCO1B1 (Figure 3.2), SLCO1B3 (Figure 3.3), SLC22A6 (Figure 3.4), SLC22A8 (Figure 3.5), SLC10A1 (Figure 3.6), SLC15A1 (Figure 3.7), SLC15A2 (Figure 3.8) and SLC22A1 (Figure 3.9) cRNA-injected *Xenopus laevis* oocytes. Darunavir, efavirenz and rilpivirine were not used when measuring transport by SLCO1A2, SLCO1B1 or SLCO1B3 as this has been investigated previously (Hartkoorn *et al.*, 2010; Kwan *et al.*, 2007) and rilpivirine was only used when sufficient oocytes were available (SLC22A6 and SLC22A8). Water-injected *Xenopus laevis* oocytes were also used in accumulation experiments to determine passive diffusion of drug into oocytes, and control substrates were used to validate transporter expression. The ratio of drug accumulation in transporter cRNA-injected oocytes compared to water-injected control oocytes was determined and is given in Table 3.1.

Raltegravir showed higher accumulation in SLC22A6 cRNA-injected oocytes (2.22-fold accumulation, $p < 0.001$) and SLC15A1 cRNA-injected oocytes (1.52-fold accumulation, $p = 0.003$) compared to water-injected oocytes. Darunavir showed higher accumulation in SLC22A6 cRNA-injected oocytes (1.29-fold accumulation, $p = 0.022$) and SLC22A1 cRNA-injected oocytes (1.20-fold accumulation, $p = 0.001$) compared to water-injected oocytes, although the increase was not large compared to control substrates. Efavirenz and rilpivirine did not show higher accumulation in

transporter cRNA-injected oocytes. Control substrates all showed higher accumulation in transporter cRNA-injected oocytes compared to water-injected oocytes (Table 3.1), confirming the activity of the transporter proteins.

Transporter	Drug	RNA-injected accumulation (pmol oocyte^{-1}) ± SD	Water-injected accumulation (pmol oocyte^{-1}) ± SD	RNA/water ratio	Significance (p value)
SLCO1A2	RAL	0.39 ± 0.14	0.35 ± 0.07	1.11	0.091
	E3S	1.48 ± 0.63	0.27 ± 0.09	5.48	**<0.001**
SLCO1B1	RAL	0.41 ± 0.05	0.38 ± 0.05	1.08	0.09
	E3S	2.68 ± 1.55	0.34 ± 0.17	7.97	**<0.001**
SLCO1B3	RAL	0.63 ± 0.19	0.65 ± 0.13	0.97	0.092
	E3S	0.56 ± 0.23	0.21 ± 0.03	2.60	**<0.001**
SLC22A6	RAL	0.44 ± 0.12	0.20 ± 0.03	2.22	**<0.001**
	DRV	4.31 ± 1.24	3.33 ± 1.05	1.29	**0.022**
	EFV	225.52 ± 72.48	244.80 ± 43.99	0.92	0.121
	RPV	54.8 ± 14.4	60.31 ± 7.94	0.91	0.083
	AHA	9.39 ± 2.64	0.17 ± 0.04	56.91	**<0.001**
SLC22A8	RAL	0.23 ± 0.04	0.20 ± 0.05	1.17	0.175
	DRV	5.95 ± 1.61	5.47 ± 0.32	1.09	0.895
	EFV	283.11 ± 62.13	265.27 ± 30.87	1.07	0.326
	RPV	62.67 ± 16.70	60.31 ± 7.94	1.04	0.674
	E3S	0.84 ± 0.44	0.19 ± 0.07	4.33	**0.016**
SLC10A1	RAL	0.20 ± 0.03	0.20 ± 0.03	1.03	0.566
	DRV	3.63 ± 1.21	3.33 ± 1.05	1.09	0.501
	EFV	248.02 ± 58.96	244.80 ± 43.99	1.01	1.000
	TCA	0.28 ± 0.10	0.08 ± 0.05	3.51	**<0.001**
SLC15A1	RAL	0.26 ± 0.12	0.17 ± 0.03	1.52	**0.003**
	DRV	4.77 ± 0.70	5.33 ± 1.94	0.89	0.51
	EFV	267.15 ± 57.13	291.87 ± 81.45	0.92	0.299
	GLY	0.45 ± 0.13	0.11 ± 0.05	4.22	**<0.001**
SLC15A2	RAL	0.19 ± 0.04	0.17 ± 0.03	1.08	0.157
	DRV	5.82 ± 2.20	5.33 ± 1.94	1.09	0.336
	EFV	251.15 ± 62.55	291.87 ± 81.45	0.86	0.114
	GLY	0.29 ± 0.19	0.11 ± 0.05	2.69	**<0.001**
SLC22A1	RAL	0.21 ± 0.03	0.17 ± 0.04	1.21	0.059
	DRV	7.29 ± 0.72	6.06 ± 0.47	1.20	**0.001**
	EFV	241.89 ± 74.38	239.91 ± 33.88	1.01	0.958
	TEA	0.34 ± 0.06	0.17 ± 0.04	1.99	**0.001**

Table 3.1. Accumulation of raltegravir, darunavir, efavirenz, rilpivirine and various positive control compounds in oocytes. Results are expressed as mean drug concentrations per oocyte (pmol/oocyte, $n \geq 4$ oocytes per condition) ± SD.

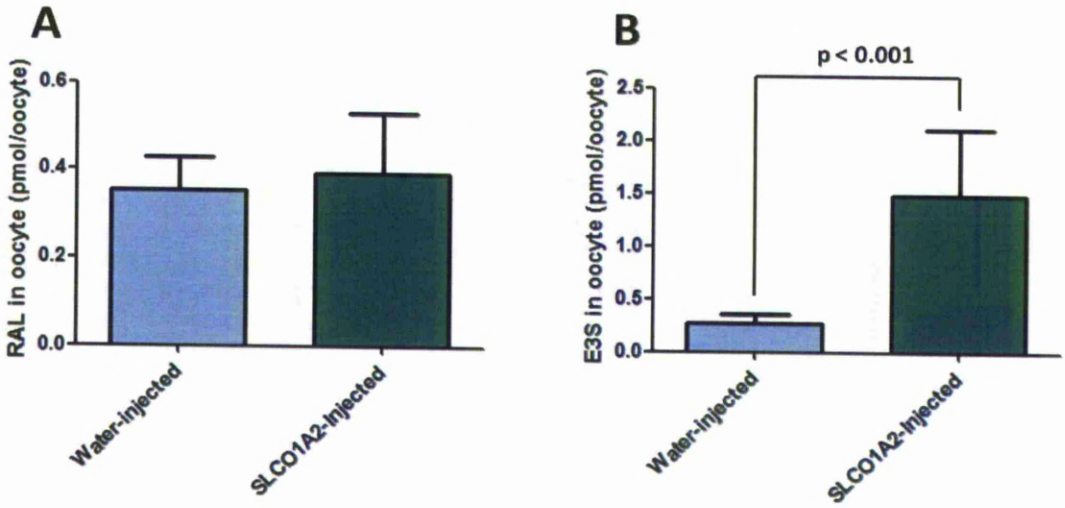

Figure 3.1. Accumulation of raltegravir (Figure 3.1A, 1 μM) and estrone 3-sulphate (Figure 3.1B, 1 μM) in water-injected and SLCO1A2 cRNA-injected oocytes. Data are presented as mean drug amount per oocyte (pmol/oocyte, n ≥ 19 oocytes) ± SD.

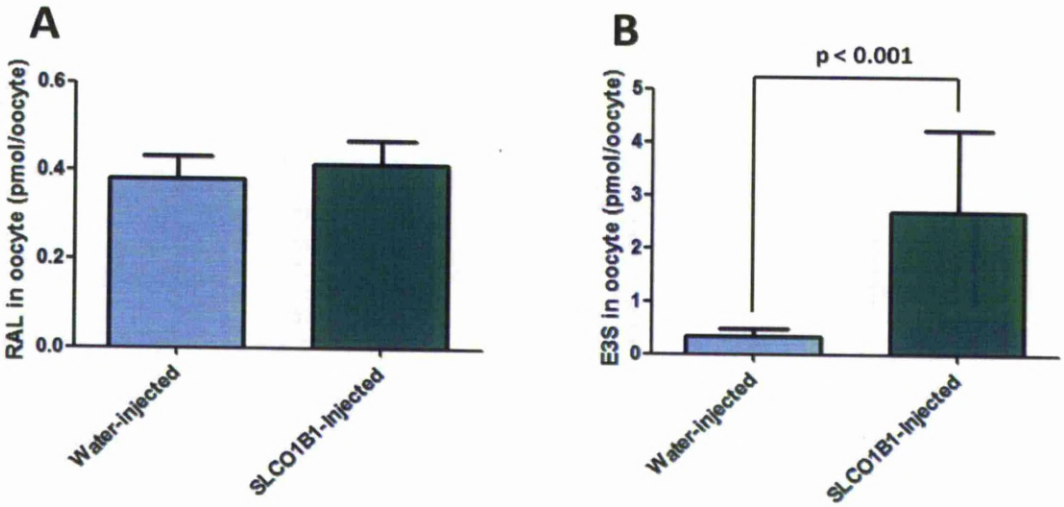

Figure 3.2. Accumulation of raltegravir (Figure 3.2A, 1 μM) and estrone 3-sulphate (Figure 3.2B, 1 μM) in water-injected and SLCO1B1 cRNA-injected oocytes. Data are presented as mean drug amount per oocyte (pmol/oocyte, n ≥ 21 oocytes) ± SD.

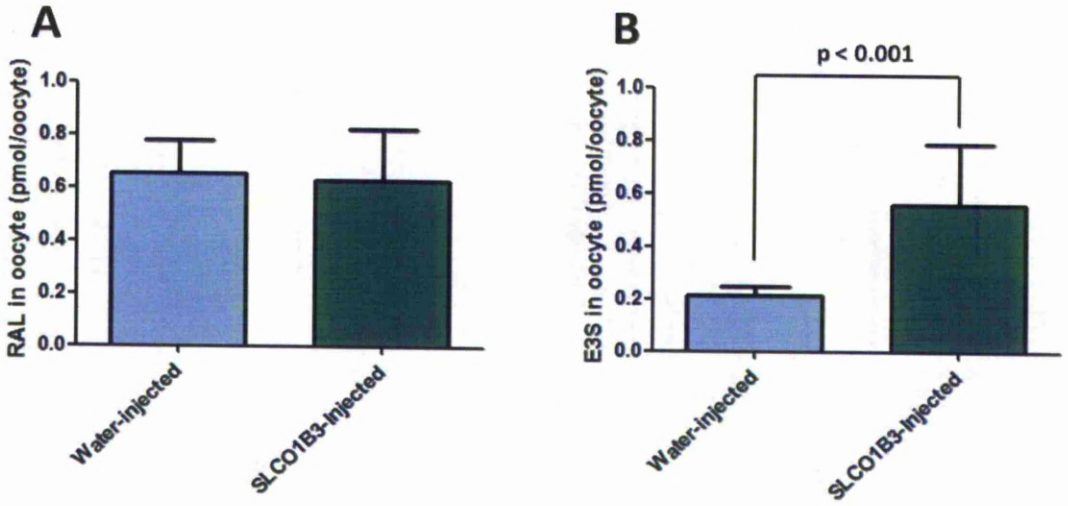

Figure 3.3. Accumulation of raltegravir (Figure 3.3A, 1 μM) and estrone 3-sulphate (Figure 3.3B, 1 μM) in water-injected and SLCO1B3 cRNA-injected oocytes. Data are presented as mean drug amount per oocyte (pmol/oocyte, $n \geq 23$ oocytes) ± SD.

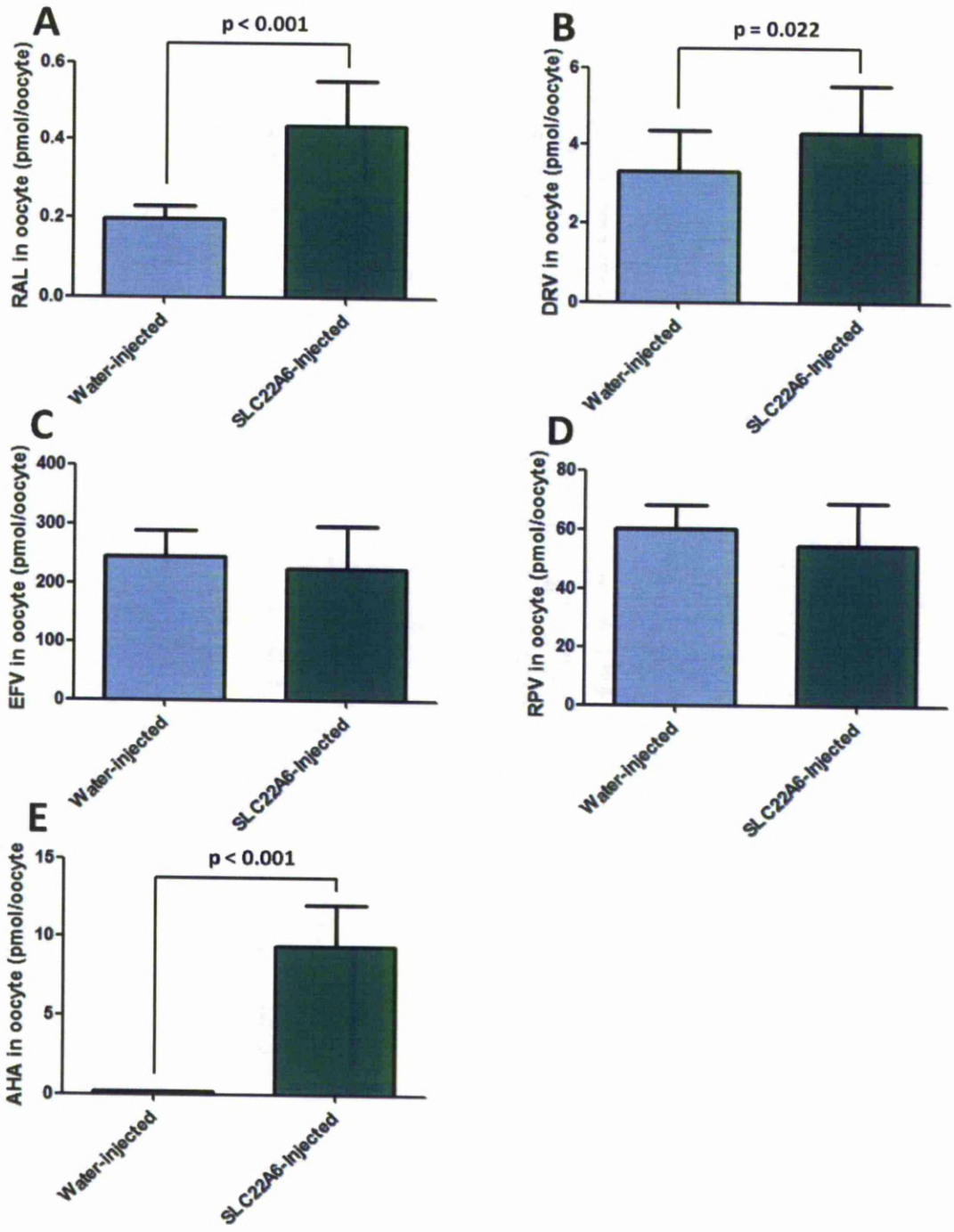

Figure 3.4. Accumulation of raltegravir (Figure 3.4A, 1 μM) darunavir (Figure 3.4B, 10 μM), efavirenz (Figure 3.4C, 26 μM), rilpivirine (Figure 3.4D, 20 μM) and aminohippuric acid (Figure 3.4E, 1 μM) in water-injected and SLC22A6 cRNA-injected oocytes. Data are presented as mean drug amount per oocyte (pmol/oocyte, $n \geq 17$ oocytes) ± SD.

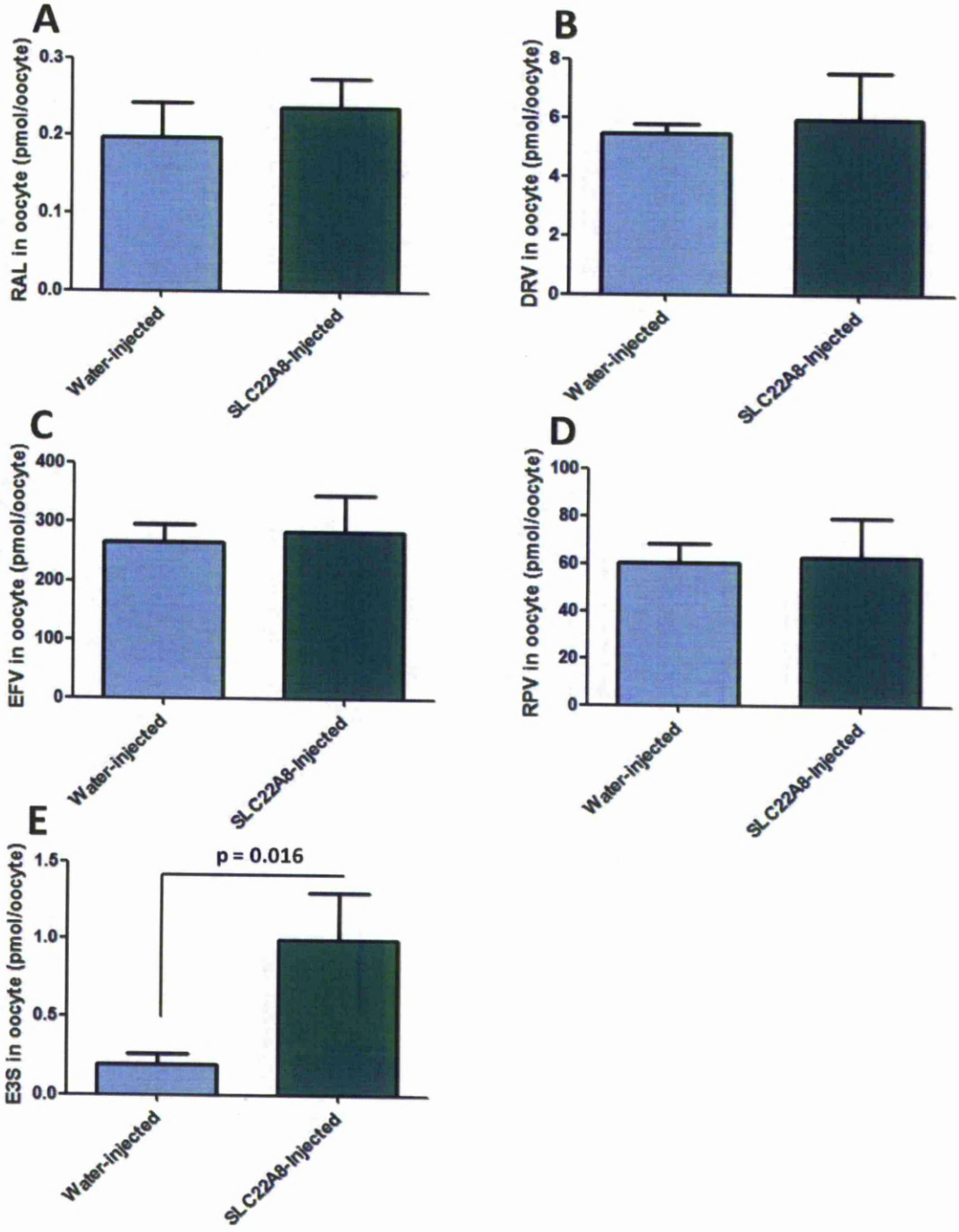

Figure 3.5. Accumulation of raltegravir (Figure 3.5A, 1 μM) darunavir (Figure 3.5B, 10 μM), efavirenz (Figure 3.5C, 26 μM), rilpivirine (Figure 3.5D, 20 μM) and estrone 3-sulphate (Figure 3.5E, 1 μM) in water-injected and SLC22A8 cRNA-injected oocytes. Data are presented as mean drug amount per oocyte (pmol/oocyte, $n \geq 4$ oocytes) ± SD.

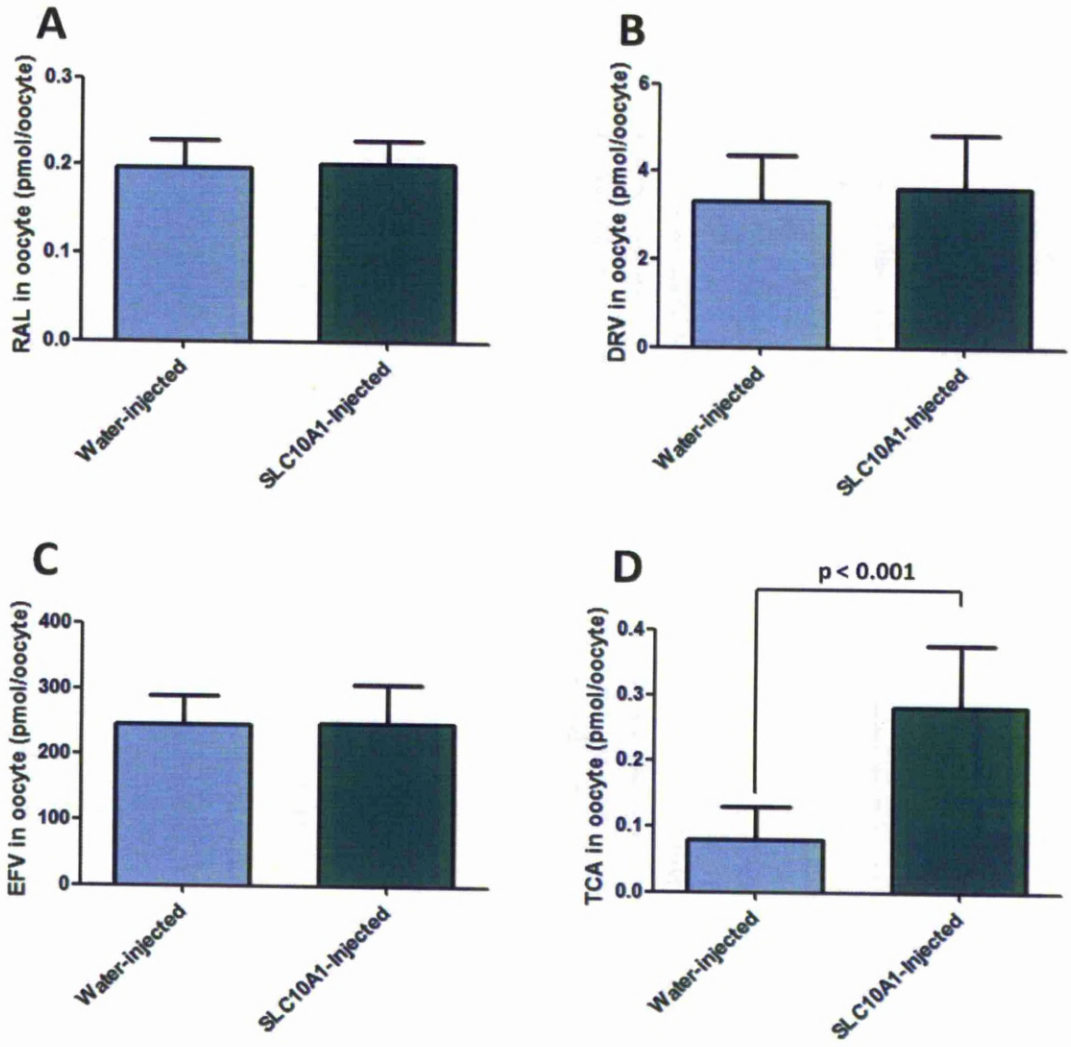

Figure 3.6. Accumulation of raltegravir (Figure 3.6A, 1 μM), darunavir (Figure 3.6B, 10 μM), efavirenz (Figure 3.6C, 26 μM) and taurocholic acid (Figure 3.6D, 1 μM) in water-injected and SLC10A1 cRNA-injected oocytes. Data are presented as mean drug amount per oocyte (pmol/oocyte, $n \geq 21$ oocytes) ± SD.

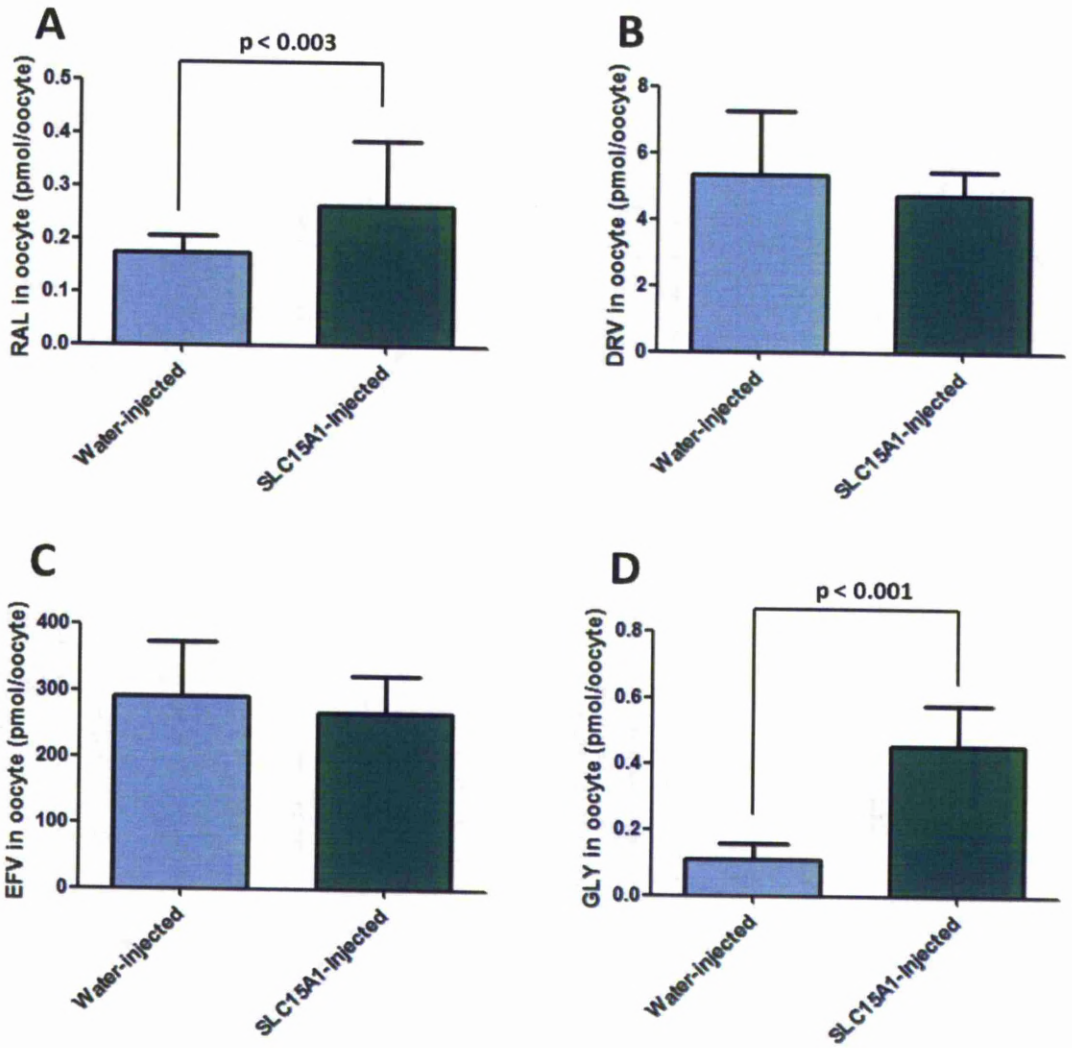

Figure 3.7. Accumulation of raltegravir (Figure 3.7A, 1 μM), darunavir (Figure 3.7B, 10 μM), efavirenz (Figure 3.7C, 26 μM) and glycyl-sarcosine (Figure 3.7D, 1 μM) in water-injected and SLC15A1 cRNA-injected oocytes. Data are presented as mean drug amount per oocyte (pmol/oocyte, $n \geq 21$ oocytes) ± SD.

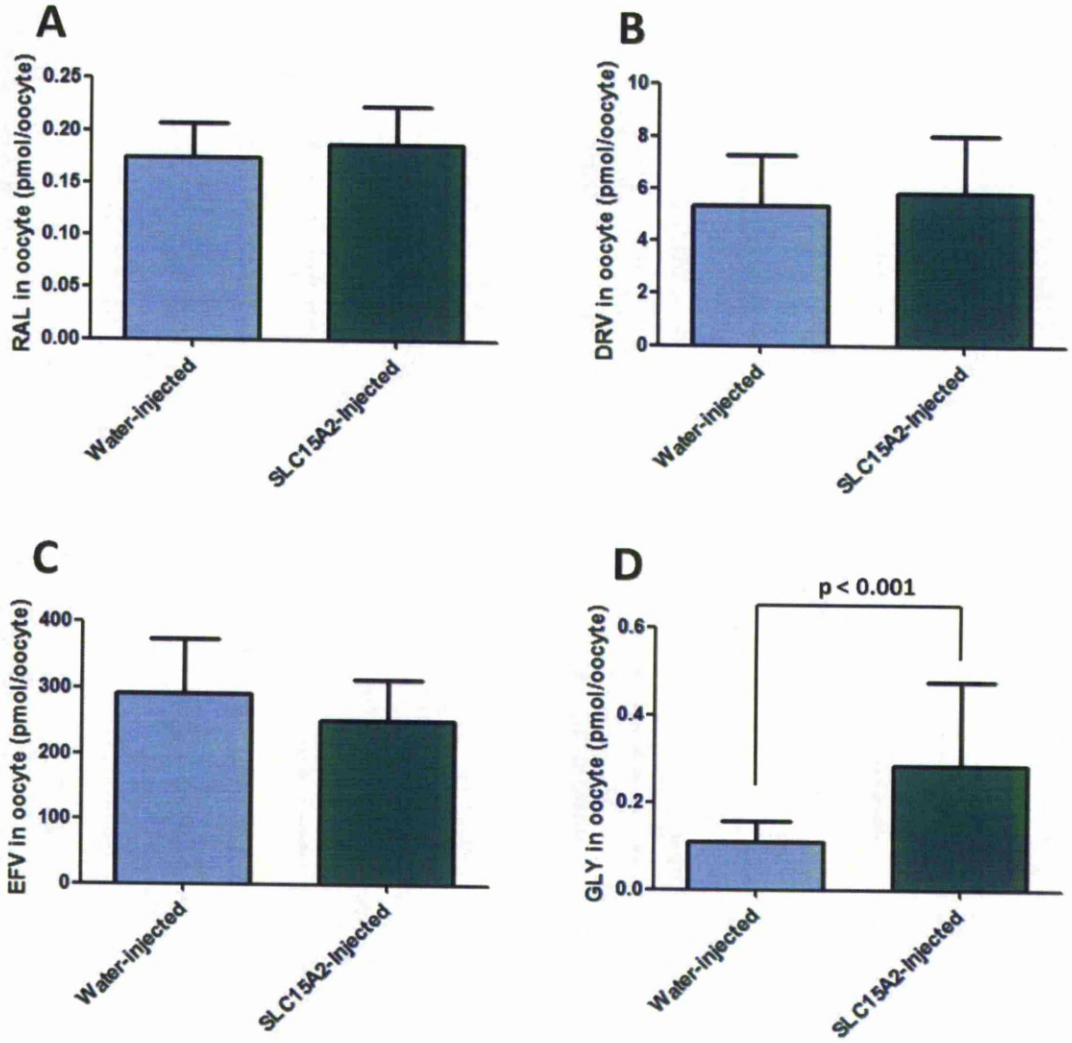

Figure 3.8. Accumulation of raltegravir (Figure 3.8A, 1 μM), darunavir (Figure 3.8B, 10 μM), efavirenz (Figure 3.8C, 26 μM) and glycyl-sarcosine (Figure 3.8D, 1 μM) in water-injected and SLC15A2 cRNA-injected oocytes. Data are presented as mean drug amount per oocyte (pmol/oocyte, $n \geq 18$ oocytes) ± SD.

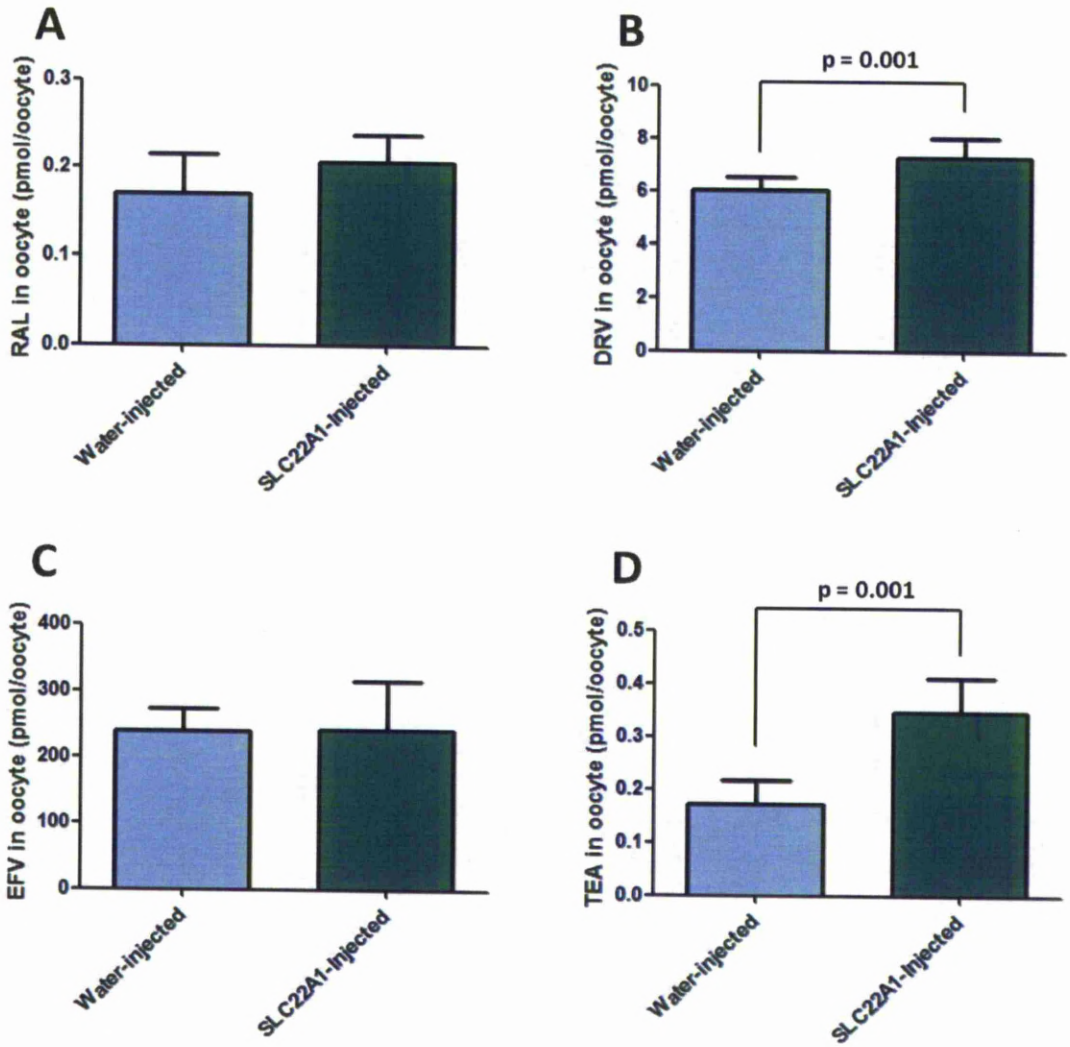

Figure 3.9. Accumulation of raltegravir (Figure 3.9A, 1 μM), darunavir (Figure 3.9B, 10 μM), efavirenz (Figure 3.9C, 26 μM) and tetraethylammonium (Figure 3.9D, 6 μM) in water-injected and SLC22A1 cRNA-injected oocytes. Data are presented as mean drug amount per oocyte (pmol/oocyte, $n \geq 7$ oocytes) ± SD.

3.3.2 Accumulation of tetraethylammonium in SLC22A1-expressing KCL22 cells co-incubated with antiretroviral drugs

The inhibition of SLC22A6-mediated tetraethylammonium transport by HIV PIs (Figure 3.10), NRTIs (Figure 3.11), NNRTIs (Figure 3.12) and raltegravir (Figure

3.12) was determined in transfected SLC22A1-overexpressing KCL22 cells. Prazosin and cepharanthine are control SLC22A1 inhibitors and were used to validate the experiment. Results are given as tetraethylammonium (TEA) concentration in cells after 30 minutes incubation (μM, n = 3 experimental replicates) ± SD.

Tetraethylammonium cellular accumulation was significantly higher in SLC22A1-expressing KCL22 cells compared to mock transfected control KCL22 cells (10.5 ± 0.6 μM versus 0.3 ± 0.004 μM, $p < 0.001$). Tetraethylammonium cellular accumulation was significantly reduced in SLC22A1-expressing KCL22 cells when cells were co-incubated with 50 μM lopinavir (7.2 ± 1.8 μM, $p = 0.018$), amprenavir (6.8 ± 1.6 μM, $p = 0.007$), indinavir (5.2 ± 0.6 μM, $p < 0.001$), darunavir (4.7 ± 0.4 μM, $p < 0.001$), ritonavir (4.0 ± 0.3 μM, $p < 0.001$), nelfinavir (3.1 ± 2.5 μM, $p = 0.033$), zalcitabine (9.1 ± 0.7 μM, $p = 0.042$), abacavir (8.8 ± 0.8 μM, $p = 0.027$), stavudine (7.6 ± 0.6 μM, $p = 0.001$), etravirine (8.2 ± 1.4 μM, $p = 0.032$), nevirapine (8.0 ± 1.5 μM, $p = 0.026$), rilpivirine (6.3 ± 0.2 μM, $p < 0.001$), efavirenz (5.4 ± 0.7 μM, $p < 0.001$), or control SLC22A1 inhibitors prazosin (2.1 ± 0.4 μM, $p < 0.001$) and cepharanthine (2.4 ± 0.2 μM, $p < 0.001$). Tetraethylammonium cellular accumulation was not significantly altered in SLC22A1-expressing KCL22 cells when cells were co-incubated with 50 μM atazanavir (10.2 ± 0.8 μM, $p = 0.649$), lamivudine (11.4 ± 0.6 μM, $p = 0.083$), tenofovir (9.7 ± 0.6 μM, $p = 0.158$), zidovudine (8.5 ± 3.1 μM, $p = 0.39$) or raltegravir (9.6 ± 1.4 μM, $p = 0.34$), indicating that these antiretrovirals do not inhibit this transporter.

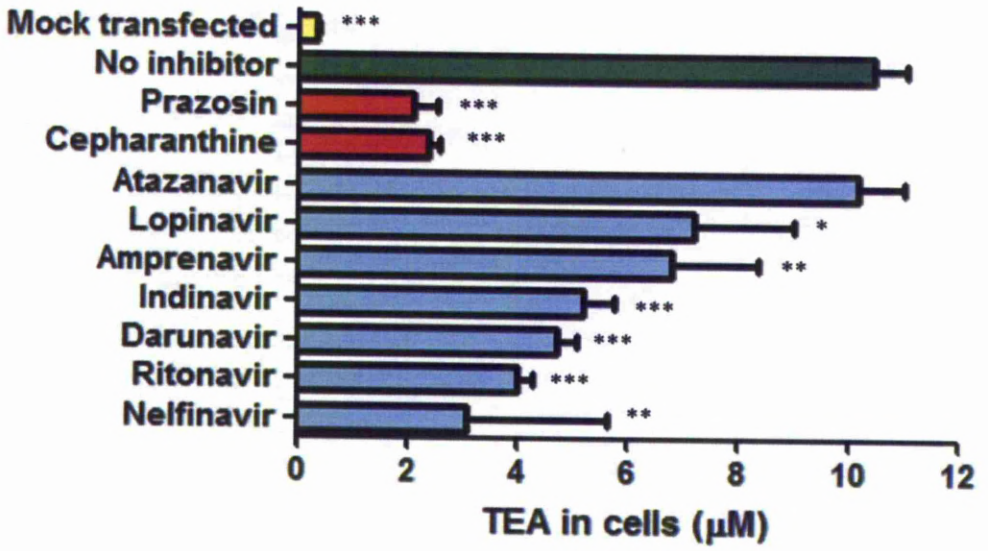

Figure 3.10. The effect of PIs on accumulation of tetraethylammonium in KCL22 cells. Yellow bar = mock transfected cells (no transfection-induced SLC22A1 expression). Green bar = SLC22A1-expressing transfected cells. Red bars = Transfected cells with 50 μM control SLC22A1 inhibitors present. Blue bars = Transfected cells with 50 μM PI drugs present. Results are given as tetraethylammonium (TEA) concentration in cells after 30 minutes incubation (μM, n = 3 experimental replicates) ± SD. * = $p<0.05$, ** = $p<0.01$, *** = $p<0.001$.

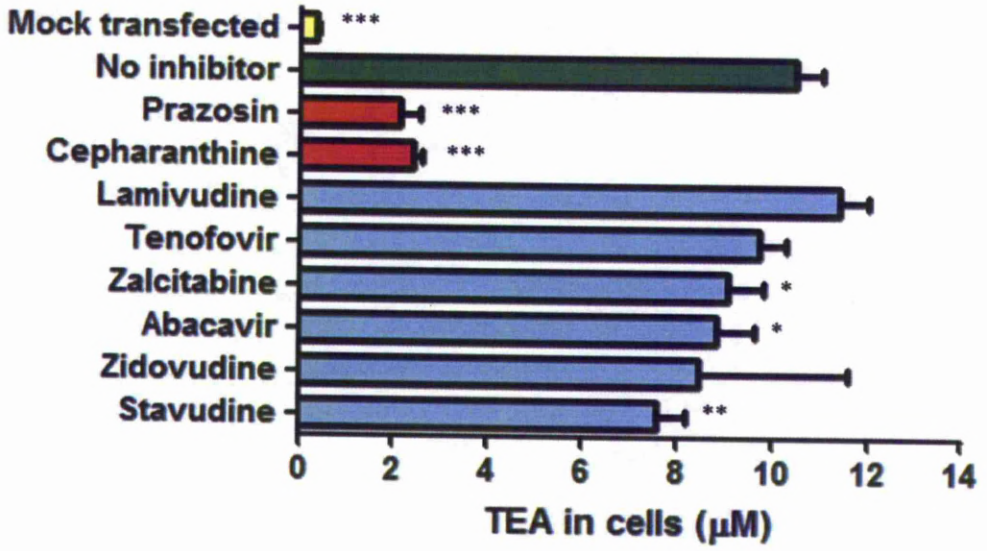

Figure 3.11. Effect of NRTIs on accumulation of tetraethylammonium in KCL22 cells. Yellow bar = mock transfected cells (no transfection-induced SLC22A1 expression). Green bar = SLC22A1-expressing transfected cells. Red bars = Transfected cells with 50 μM control SLC22A1 inhibitors present. Blue bars = Transfected cells with 50μM NRTI drugs present. Results are given as tetraethylammonium (TEA) concentration in cells after 30 minutes incubation (μM, n = 3 experimental replicates) ± SD. * = $p<0.05$, ** = $p<0.01$, *** = $p<0.001$.

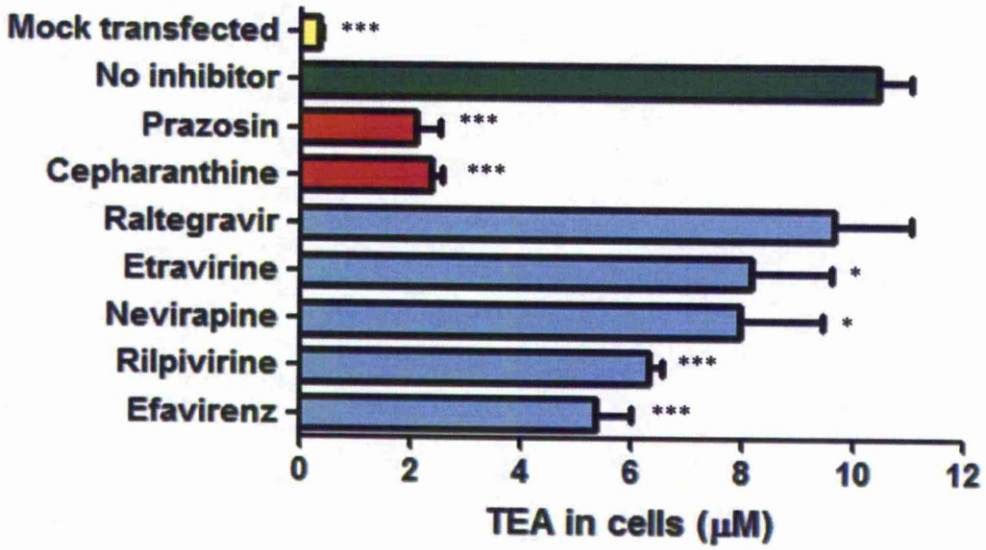

Figure 3.12. Effect of NNRTIs and raltegravir on accumulation of TEA in KCL22 cells. Yellow bar = mock transfected cells (no transfection-induced SLC22A1 expression). Green bar = SLC22A1-expressing transfected cells. Red bars = Transfected cells with 50 μM control SLC22A1 inhibitors present. Blue bars = Transfected cells with 50μM NNRTI drugs or raltegravir present. Results are given as TEA concentration in cells after 30 minutes incubation (μM, n = 3 experimental replicates ± SD). * = $p<0.05$, ** = $p<0.01$, *** = $p<0.001$.

3.3.3 SLC22A1 IC_{50} of antiretroviral drugs

The inhibition of SLC22A1 using a concentration range of antiretrovirals was used to determine IC_{50} values. Data are presented in Figure 3.13 and relative and absolute IC_{50} values were determined (Table 3.2). Control SLC22A1 inhibitor prazosin achieved an 84% reduction in cellular tetraethylammonium accumulation at 100 μM and a relative IC_{50} value of 2.3 μM, which is similar to values found in published literature (Minematsu *et al.*, 2010).

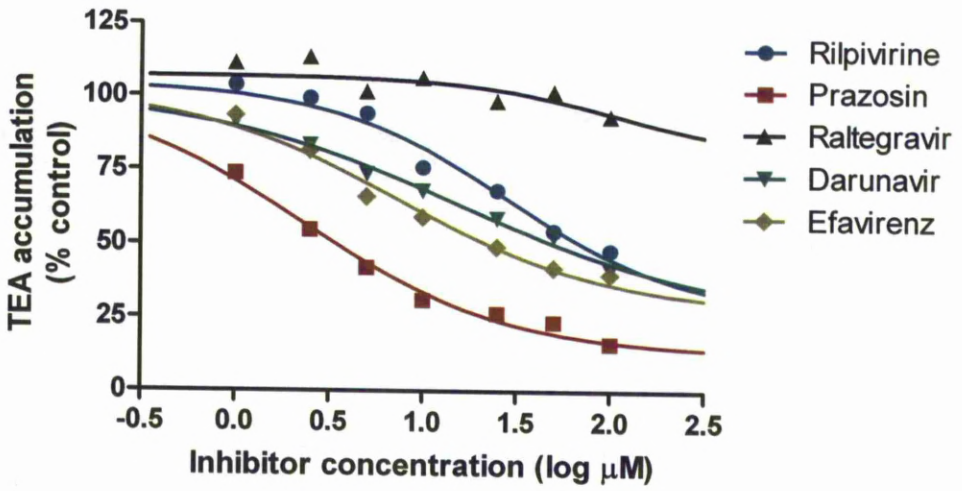

Figure 3.13. Inhibition of tetraethylammonium accumulation in SLC22A1-expressing KCL22 cells using a concentration range of raltegravir, rilpivirine, darunavir, efavirenz and control SLC22A1 inhibitor prazosin. Data are expressed as mean percentage tetraethylammonium (TEA) accumulation compared to accumulation in drug-free control cells (n = 3 experimental replicates).

Inhibitor	TEA accumulation when 100 μM inhibitor used (% compared to inhibitor-free control)	Relative IC_{50} (μM)	Absolute IC_{50} (μM)
Prazosin	16.1	2.3	2.8
Raltegravir	93.4	>100	>100
Rilpivirine	47.9	28.5	61.6
Darunavir	41.3	15.9	46.2
Efavirenz	39.7	7.4	21.8

Table 3.2. Maximum observed SLC22A1 inhibition and calculated relative IC_{50} values for raltegravir, rilpivirine, darunavir, efavirenz and control SLC22A1 inhibitor prazosin.

3.4. DISCUSSION

This chapter has investigated how raltegravir and several other antiretroviral drugs interact with a selection of influx drug transporters. The inhibition of SLC22A1 by a wide range of antiretroviral drugs, including raltegravir, was also determined.

The oocyte expression system was used to assess the transport of raltegravir, darunavir, efavirenz and rilpivirine by a selection of influx transporters. The only transporters which significantly increased raltegravir accumulation were SLC15A1 (52% increase) and SLC22A6 (120% increase). The peptide transporting protein SLC15A1 is highly expressed in the intestine (Daniel *et al.*, 2004) and acts by transporting substrate compounds from the lumen into the cells lining the intestine. This would suggest that SLC15A1 has the potential to increase the absorption of raltegravir from the intestine. However, the extent of raltegravir transport was only small and unlikely to have an important role *in vivo*. Furthermore, Caco-2 monolayers are known to express high levels of SLC15A1 (Hubatsch *et al.*, 2007) which are expressed on the apical surface, therefore transporting substrates in the A-to-B direction. Raltegravir Caco-2 monolayer permeability was predominantly in the B-to-A direction under normal experimental conditions detailed in Chapter 2, which does not support the hypothesis that SLC15A1 has a major effect on raltegravir in this model. The anion transporter SLC22A6 is predominantly expressed in the proximal tubule of the kidney but is also expressed in the brain, central nervous system, skeletal muscle and placenta (Roth *et al.*, 2012). The transport of raltegravir by SLC22A6 is investigated in further detail in Chapter 4.

Efavirenz oocyte accumulation was not increased by any influx transporter tested using the oocyte expression system. The impact of drug transporters on efavirenz is largely unknown, although efavirenz is not transported by ABCB1 *in vitro* (Janneh *et al.*, 2009). Efavirenz is a CYP2B6 substrate and efavirenz plasma concentrations have been linked to polymorphisms in CYP2B6, such as the 516G>T variant (rs3745274) (Haas *et al.*, 2004). Although not all possible transporters of efavirenz have been screened, our data suggest that active transport of efavirenz by the studied transporters is unlikely to be as important for its ADME properties as metabolism.

The only transporters which significantly increased darunavir oocyte accumulation were SLC22A1 (20% increase) and SLC22A6 (29% increase). However, both transporters only caused a small increase in oocyte accumulation in comparison to control substrates and, since in oocytes the transporters are likely to be more highly expressed than at physiological levels, it is unlikely that these transporters would play a major role in darunavir disposition *in vivo*.

The *Xenopus laevis* oocyte expression system has several advantages when investigating drug transport. The large size and high protein production of oocytes provides robust and reliable data. Also, expression of endogenous primary and secondary active xenobiotic transporters in oocytes is low (Sobczak *et al.*, 2010). However, there are disadvantages also. Temperature must be maintained at 18°C during protein expression and around room temperature during any accumulation experiments to avoid degradation and this may impact transporter kinetics. Also, as in other models, the expression of investigated transporters is super-physiological. Therefore, although they allow investigation of low-affinity or high permeability

substrates, this means that caution should be taken when extrapolating to in vivo observations.

The organic cation transporter SLC22A1 is predominantly expressed in the liver and is localised to the basolateral membrane of hepatocytes (Nies *et al.*, 2008) where it mediates the uptake of substrate from the blood and facilitates drug elimination. Raltegravir did not reduce the accumulation of tetraethylammonium, a confirmed SLC22A1 substrate, in SLC22A1-overexpressing KCL22 cells at 100 μM or below. Therefore, it is unlikely that raltegravir reduces the activity of SLC22A1 *in vivo*.

Several antiretroviral drugs inhibited SLC22A1 activity: all PIs apart from atazanavir were able to reduce tetraethylammonium accumulation. These findings agree with published data, where the PIs saquinavir, indinavir, ritonavir and nelfinavir were able to reduce tetraethylammonium accumulation in SLC22A1-overexpressing Hela cells (Zhang *et al.*, 2000) and atazanavir was found to have no SLC22A1-inhibiting ability *in vitro* (Jung *et al.*, 2008). There are no previous published data on the inhibition of SLC22A1 by darunavir or lopinavir and both were investigated. Lopinavir showed significant but only minor inhibition of SLC22A1 (29.4% reduction in SLC22A1 activity using 50 μM lopinavir) and darunavir showed more substantial SLC22A1 inhibition (53.9% reduction in SLC22A1 activity using 50 μM darunavir).

The NRTIs were not SLC22A1 inhibitors or only showed minor inhibition. Lamivudine did not inhibit SLC22A1 and this contradicts previous published data which showed significant inhibition (Jung *et al.*, 2008). However, Jung et al used 1-methyl-4-phenylpyridinium as the control SLC22A1 substrate and this could explain

the conflicting data. Indeed, it may suggest the existence of separate substrate binding sites on SLC22A1, only one of which is able to be inhibited by lamivudine.

The NNRTIs all showed some level of SLC22A1 inhibition although inhibition by etravirine and nevirapine was small (22.5% and 24.5% reduction in SLC22A1 activity, respectively, when using 50 μM drug). Efavirenz and rilpivirine showed more substantial SLC22A1 inhibition (50.0% and 41.2% reduction in SLC22A1 activity, respectively, when using 50 μM drug). Efavirenz did not show SLC22A1 inhibition in previous literature, which contradicts our data (Jung *et al.*, 2008). However, Jung et al used 1-methyl-4-phenylpyridinium as the control SLC22A1 substrate. Also, incubations were only 1 minute (compared to 30 minutes used in the author's experiments) and inhibition may therefore be time-dependent. Furthermore, the experiment in this thesis used multiple efavirenz concentrations to determine the IC_{50} and Jung et al only used efavirenz at a concentration of 5 μM. The inhibitory potential of efavirenz for SLC22A1 should be determined using a separate *in vitro* method to confirm results seen in this chapter. It is also important to note that efavirenz was not found to be a substrate for SLC22A1 in oocyte accumulation experiments detailed in this chapter.

All antiretroviral drugs showed less SLC22A1 inhibition than with prazosin (82.3% reduction in SLC22A1 activity using 50 μM prazosin). However, antiretroviral drugs may also inhibit other organic cation transporters important in drug disposition, such as SLC22A2 and SLC22A3. Indeed, certain antiretroviral drugs, such as ritonavir and nelfinavir, have been shown to inhibit both SLC22A1 and SLC22A2 *in vitro* (Jung *et al.*, 2008). The inhibition of SLC22A3 by antiretroviral drugs requires

investigation and the potential for drug-drug interactions *in vivo* needs to be evaluated.

In conclusion, of all transporters tested, only SLC15A1 and SLC22A6 showed significant raltegravir transport *in vitro*. The clinical significance of these observations need further study but SLC15A1-meiated raltegravir transport was low and an impact of this transporter *in vivo* seems unlikely. With the possible exception of SLC22A6, the studied drug transporter proteins do not appear to play a major role in raltegravir cellular permeation *in vitro*. Chapter 4 investigates the role of SLC22A6 in raltegravir cellular permeation in more detail and also details the competition between raltegravir and tenofovir for SLC22A6 transport.

Chapter 4

Competition between raltegravir and tenofovir for SLC22A6 transport

Table of Contents

4.1 INTRODUCTION

The human SLC22A influx transporter family currently contains 24 members on the Human Gene Nomenclature Committee website (http://www.genenames.org/), some of which are known to be important transporters of many endogenous and xenobiotic substances. Substrate specificity generally differs from ABCB1, as SLC22A substrates are usually negatively charged (anions) and less lipophilic.

The organic anion transporter, SLC22A6, is a membrane-bound protein of 550 amino acids and is predominantly expressed in the kidney, with low levels of mRNA also detected in retina, brain, choroid plexus, liver, pancreas, stomach, bladder, mammary glands, salivary glands and PBMCs (Bleasby *et al.*, 2006). Expression of SLC22A6 in the kidney is localised to the basolateral (blood-facing) surface of the renal proximal tubule cells (Motohashi *et al.*, 2002), where it removes substrates from the blood and facilitates renal elimination. The importance of SLC22A6 for drug transport in other human tissues has not been fully determined. Figure 4.1 gives the expression and location of several transporter proteins in renal proximal tubule cells (Daniel *et al.*, 2003; Kis *et al.*, 2010a). The mRNA of several other transporters, such as ABCG2 (Huls *et al.*, 2008), have also been detected in renal proximal tubule cells (Hilgendorf *et al.*, 2007), although the importance of these transporters in renal drug elimination is not fully understood.

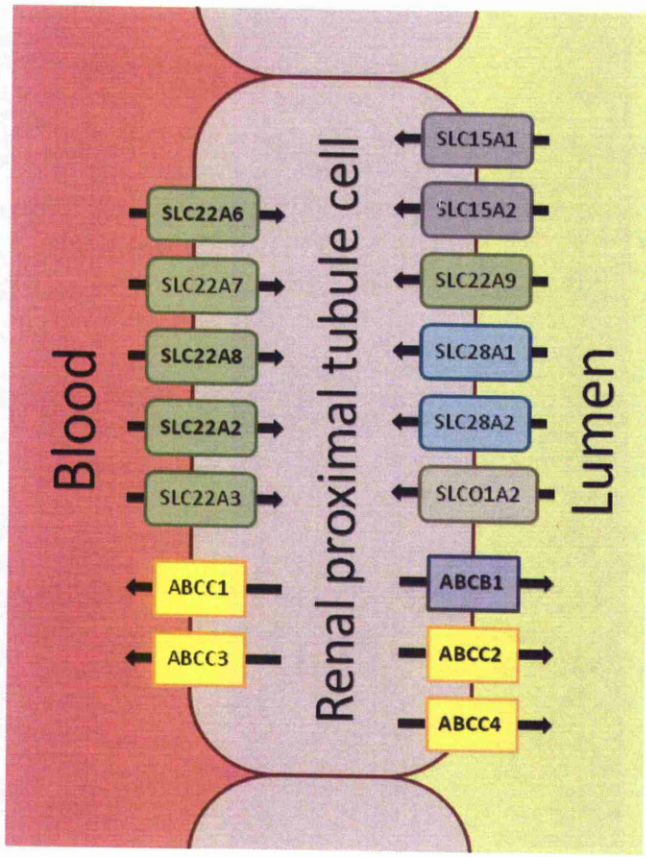

Figure 4.1. The expression and location of several drug-transporting proteins in renal proximal tubule cells (Daniel *et al.*, 2003; Kis *et al.*, 2010a). Transporters displayed in bold typeface are the transporters with highest expression.

SLC22A6 has been shown to transport a wide range of currently prescribed drugs, including some diuretics, statins, antibiotics and antivirals (including anti-HIV drugs) (Burckhardt *et al.*, 2011). The anti-herpes simplex virus acyclic nucleoside analogues acyclovir (K_m of 342 μM) and ganciclovir (K_m of 896 μM) were found to be low affinity SLC22A6 substrates *in vitro* (Takeda *et al.*, 2002). Several anti-HIV NRTIs and NtRTIs are also SLC22A6 substrates, including didanosine, lamivudine, stavudine, zalcitabine, zidovudine and tenofovir (Burckhardt *et al.*, 2011).

There is a low frequency of SLC22A6 polymorphisms, suggesting an important endogenous role for the wild type transporter (Fujita *et al.*, 2005). However, polymorphisms have been described which are known to alter SLC22A6 functionality. Increased affinity (K_m) but reduced maximum rate (V_{max}) for tenofovir transport has been reported by SLC22A6 in oocyte expression experiments using the arginine/histidine SLC22A6 polymorphism (rs11568626) (K_m of 14.4 μM and V_{max} of 27.1 pmol/oocyte/20 min) compared to wild type SLC22A6 (K_m of 21.1 μM and V_{max} of 60.3 pmol/oocyte/20 min) (Bleasby *et al.*, 2005).

Drug interactions have been observed which are believed to involve SLC22A6-mediated, and possibly SLC22A8-mediated, transport. Probenecid is a potent inhibitor of SLC22A6 and was created to reduce the renal excretion of β-lactam antibiotics such as penicillin (Overbosch *et al.*, 1988) and various cephalosporins (Brown, 1993). Probenecid was also able to reduce the renal excretion of methotrexate in humans (47% increase in half-life compared to control patients) (Aherne *et al.*, 1978) and published *in vitro* data supports the involvement of SLC22A6 in this interaction (probenecid inhibited methotrexate transport by rat Oat1 with a K_i of 15.8 μM) (Uwai *et al.*, 2000). The elimination half-life of the diuretic furosemide was increased when co-administered with probenecid (69% increase compared to control patients) and caused prolonged diuretic drug action (Vree *et al.*, 1995). Nonsteroidal anti-inflammatory drugs (NSAIDs) are also potent inhibitors of SLC22A6 and were shown to reduce methotrexate transport by rat Oat1 *in vitro* (indomethacin inhibited methotrexate transport by rat Oat1 with a K_i of 4.2 μM) (Uwai *et al.*, 2000). Adefovir accumulation and cytotoxicity in SLC22A6-expressing CHO cells was reduced by NSAIDs *in vitro* (Mulato *et al.*, 2000) and the authors

suggested that NSAIDs may reduce adefovir nephrotoxicity *in vivo*. It is clear that SLC22A6 is important in the elimination of several drugs and that drug interactions involving SLC22A6 are possible *in vitro* and *in vivo*.

Wenning *et al* (2008) studied the interaction of raltegravir (400 mg twice-daily) and tenofovir (300 mg once-daily). The study showed increased raltegravir AUC (49%) and C_{max} (64%), but no effect on raltegravir C_{min}, and a decrease in tenofovir AUC (10%), C_{max} (23%) and C_{min} (13%) (Wenning *et al.*, 2008). Investigations in Chapter 3 showed that 1 μM raltegravir was significantly transported by SLC22A6 over a one hour accumulation time course using SLC22A6-expressing *Xenopus laevis* oocytes. Given that tenofovir has previously been shown to be an SLC22A6 substrate/inhibitor, competition between raltegravir and tenofovir for SLC22A6 transport may reduce raltegravir renal elimination.

To better understand the affinity of raltegravir for SLC22A6, time-dependent and concentration-dependent kinetics experiments were undertaken and results are given in this chapter. The potential for raltegravir-drug interactions involving SLC22A6 were also evaluated. The K_m and V_{max} of raltegravir and tenofovir were calculated using the *Xenopus laevis* oocyte expression system. The competition between these drugs for SLC22A6 transport was also determined. Aminohippuric acid is a prototypical SLC22A6 substrate and was used to validate experiments. The impact of SLC22A6 on raltegravir accumulation in PBMCs and cultured primary renal cells was also determined.

4.2 METHODS

4.2.1 Materials

[^{3}H]Raltegravir (specific activity = 32.85 Ci/mmol) and non-radiolabeled raltegravir sodium salt were gifts from Merck (New Jersey, USA). [^{3}H]Tenofovir (specific activity = 3.4 Ci/mmol) was purchased from Moravek (California, USA). Non-radiolabelled tenofovir was a purchased from Toronto Research Chemicals (Toronto, Canada). [^{3}H]Aminohippuric acid (specific activity = 5 Ci/mmol) was purchased from American Radiolabelled Chemicals (Missouri, USA). mMessage mMachine RNA Transcription kits were purchased from Ambion Ltd. (Huntingdon, UK). Ultima Gold scintillation fluid was purchased from Perkin Elmer (Boston, USA). Restriction enzymes were purchased from New England Biolabs (Hitchen, UK). Adult female *Xenopus laevis* frogs were purchased from Xenopus Express (Lyon, France). IMAGE clones of SLC22A6 were purchased from Geneservice (Nottingham, UK). GC5™ competent *E.coli* cells, SOC medium, Genelute™ plasmid miniprep kits and Genelute™ PCR clean-up kits and TRI reagent® were purchased from Sigma (Poole, UK). The Taqman® reverse transcriptase kit and Taqman® custom array plates were purchased from Invitrogen UK (Paisley, UK). Ficoll-Paque PLUS was purchased from GE Healthcare (Buckinghamshire, UK). All other drugs and reagents were obtained from Sigma (Poole, UK).

4.2.2 Transformation of a SLC22A6-containing plasmid into competent E.coli

An IMAGE clone of the wild-type human SLC22A6 gene (clone number 5190748) was purchased from Geneservice (Nottingham, UK) and transformed into GC5™ competent *E.coli* cells using the following protocol. Cells (50 μL) were thawed and incubated on ice with 50 ng pCMV-SPORT6 plasmid containing the wild type human SLC22A6 gene (30 minutes). Cells were briefly heat shocked in a water bath (37°C, 45 seconds) before being returned to ice (2 minutes). SOC medium (450 μL) was added to each transformation reaction and cells were placed in a shaking incubator (225 rpm, 37°C, 1 hour). Transformation reactions were plated onto agar containing ampicillin (100 μg/mL) using a sterile spreader and incubated (37°C, 18 hours) to select for successful transformants (pCMV-SPORT6 plasmid contains an ampicillin resistance gene). A successful clone was selected and grown in LB containing ampicillin (100 μg/mL, 37°C, 8 hours) and aliquots were stored at -80°C in freezing solution (80% LB, 20% glycerol) for future use.

4.2.3 Production of SLC22A6 cRNA for Xenopus laevis oocyte injection

The pCMV-SPORT6 plasmid containing the SLC22A6 gene was isolated from transformed GC5™ *E.coli* using a Genelute™ plasmid miniprep kit as described in the manufacturer's protocol. The pCMV-SPORT6 plasmid was linearised with the XhoI restriction enzyme (1 x NEB buffer 4, 1 x BSA, 1 μg plasmid DNA, 37°C, 1 hour) and purified using a Genelute™ PCR clean-up kit as described in the manufacturer's protocol. An SP6 mMessage mMachine RNA transcription kit

(Ambion®) was used to generate SLC22A6 cRNA from linear plasmid DNA as described in the manufacturer's protocol. Following cRNA generation, plasmid DNA was degraded (1 μL Turbo DNase, 37°C, 15 minutes) and cRNA was concentrated using a lithium chloride precipitation method. Concentrated cRNA pellets were reconstituted in sterile water to a final concentration of 1 μg/mL for use in microinjection.

4.2.4 Xenopus laevis maintenance

Adult female *Xenopus laevis* frogs were housed in fresh, filtered water and provided with shelter. Frogs were monitored daily to check for signs of ill health and were fed dried frog food pellets twice daily. Frogs were sacrificed using anaesthetic solution (MS222, 5 g/L, 45 minutes) following Schedule 1 procedures.

4.2.5 Xenopus laevis oocyte isolation, collagenase treatment and microinjection

Oocytes were harvested from sacrificed adult female *X. laevis* frogs and treated with modified Barth's solution minus calcium and prepared for microinjection as described in Section 3.2.4. Healthy cells were selected and injected with SLC22A6 cRNA (50 ng per oocyte, 1 ng/nL) or sterile water (50 nL) and maintained in Barth's solution containing calcium to allow transporter expression (3 days, 18°C). Barth's solution was replaced daily and damaged oocytes were removed to maintain viability of the healthy oocytes.

4.2.6 Determination of raltegravir and tenofovir K_m and V_{max} using SLC22A6-injected oocytes

Unless otherwise stated, radiolabelled drug was incubated in HBSS (pH 7.4) with ≥ 4 oocytes per condition in a 48-well nunc flat bottom plate (500 µL, 0.33 µCi/mL, 22°C, 60 rpm shaker). Time-dependent SLC22A6-mediated transport of [^{3}H]raltegravir, [^{3}H]tenofovir and control SLC22A6 substrate, [^{3}H]aminohippuric acid, was investigated by incubating each drug with SLC22A6- and water-injected oocytes at a standard concentration of 1 µM for various lengths of time (1, 2, 5, 10, 15, 30, 60, 120, 180 or 240 minutes) and terminating incubations as described in Section 3.2.5. Results are shown in Figures 4.2, 4.3 and 4.4 and from these results an incubation time was chosen that gave a high accumulation rate in SLC22A6 cRNA-injected oocytes compared to the water-injected controls and also allowed enough radiolabelled drug to enter the oocytes for it to be detectable (1 hour incubations were chosen for both drugs). Kinetics experiments were then performed in which [^{3}H]raltegravir and [^{3}H]tenofovir were incubated with SLC22A6- and water-injected oocytes for one hour using a range of drug concentrations (0.1, 0.3, 1, 3, 10, 30, 100, 300 and 1000 µM for raltegravir and 0.3, 1, 3, 10, 30, 100, 200 and 300 µM for tenofovir). All incubations were terminated and processed as described in Section 3.2.5. Transport of drug by SLC22A6 was determined by subtracting drug accumulation in water-injected oocytes from drug accumulation in SLC22A6 cRNA-injected oocytes. The K_m and V_{max} values were calculated by plotting initial rate of drug transport by SLC22A6 (pmol/oocyte/hr) against drug incubation concentration (µM). Intrinsic clearance (Cl_{int}) was calculated by dividing V_{max} by K_m.

4.2.7 Determination of competition between raltegravir and tenofovir for SLC22A6 transport

[^{3}H]raltegravir (0.33 μCi/mL, 1 μM) was incubated for 1 hour with SLC22A6 cRNA-injected oocytes with varying concentrations of non-radiolabelled tenofovir (1, 3, 10, 30, 100 and 300 μM) and the effect on [^{3}H]raltegravir uptake was determined. [^{3}H] raltegravir (0.33 μCi/mL, 1 μM) was also incubated with water-injected cells with and without 300 μM tenofovir in order to confirm the role of SLC22A6. This experiment was repeated using [^{3}H]tenofovir as the substrate and non-radiolabelled raltegravir as the competitor drug, using the same concentration ranges. All incubations were terminated and processed as described in Section 3.2.5. Relative IC_{50} values were generated for both drugs using Prism 5.0.

4.2.8 Isolation of peripheral blood mononuclear cells from healthy volunteer human blood

Venous blood samples (60 mL) were obtained from healthy volunteers (n = 4) via venipuncture. PBMCs were isolated from blood and prepared for accumulation experiments as described in Section 2.2.7.

4.2.9 Cellular accumulation of raltegravir in peripheral blood mononuclear cells

Accumulation of raltegravir in PBMCs was determined using the same method as used in Section 2.2.8, with modifications. Briefly, cells of a constant cell density (1 mL, 5 x 10^6 cells/mL) were incubated (37 °C, 5% CO_2) for 30 minutes in cell culture medium (RPMI, 10% [vol/vol] FCS) containing [^{3}H]raltegravir (1 μM, 0.2 μCi/mL).

Separate incubations were undertaken where cells were pre-incubated with cell culture medium (RPMI, 10% [vol/vol] FCS) containing either the competitive SLC22A6 inhibitor probenecid (1 mM, 30 minutes) or the competitive SLC15A1 inhibitor glycyl-sarcosine (1 mM, 30 minutes), which were also included during the 30 minutes of substrate incubation. Cells were washed and treated for analysis as described in Section 2.2.8. Using supernatant fraction and intracellular radioactivity readings, CARs were calculated for raltegravir as described in Section 2.2.5. Data are expressed as mean CAR ($n = 4$ biological replicates, $n \geq 3$ experimental replicates per biological replicate) ± SD.

4.2.10 Culture of human primary renal proximal tubule epithelial cells

Human primary renal proximal tubule epithelial cells ("renal cells") were maintained in complete growth medium. Complete growth medium was supplemented with 0.5% [vol/vol] FCS, 10 nM triiodothyronine, 10 ng/mL Epidermal growth factor, 100 ng/mL hydrocortisone hemisuccinate, 5 μg/mL insulin, 1 μM epinephrine, 5 μg/mL transferring, 2.4 mM L-alanyl-L-glutamine and 100 μg/mL penicillin/streptomycin. Once a cell confluence of approximately 95% was reached, renal cells were washed three times with HBSS (37°C) and incubated with trypsin-EDTA solution (37°C, 5 minutes). Flasks were gently tapped to remove renal cells and supplemented complete growth medium was added to neutralise the trypsin. Cells were added to a 50 mL skirted tube and centrifuged (800 g, 4°C, 5 minutes). Supernatant fraction was removed and replaced with fresh supplemented complete growth media to a final density of 5×10^5 cells/mL. Cells were seeded onto new culture flasks at a density of 1×10^5 cells/cm^2.

4.2.11 Cellular accumulation of raltegravir, tenofovir and aminohippuric acid in primary renal proximal tubule epithelial cells

When confluent, renal cells (passage 4) were seeded onto polyester membrane transwells at a density of 5 x 10^5 cells/cm^2. Media was replaced daily and plates were used in experiments after five days. On the day of the experiment, media was replaced with buffered HBSS (25 mM HEPES, pH 7.4) containing either [^{3}H]raltegravir (1 μM, 0.6 μCi/mL), [^{3}H]tenofovir (1 μM, 0.6 μCi/mL) or the control SLC22A6 substrate [^{3}H]amminohippuric acid (1 μM, 0.6 μCi/mL) and incubated (3 hours, 37°C, 5% CO_2). A separate incubation was undertaken where the cells were pre-incubated prior to substrate addition with buffered HBSS (25 mM HEPES, pH 7.4) containing the SLC22A6 inhibitor probenecid (1 mM, 30 minutes), which was also included during the three hours of substrate incubation. We also investigated the competition between raltegravir and tenofovir by incubating [^{3}H]raltegravir (1 μM, 0.6 μCi/mL) with 100 μM tenofovir and incubating [^{3}H]tenofovir (1 μM, 0.6 μCi/mL) with 100 μM raltegravir (3 hours, 37°C, 5% CO_2). Once incubations were complete, extracellular samples were taken and incubations were terminated by washing each well with cold HBSS (4°C, 3 mL) three times to remove excess drug. Cells were lysed with 0.5 mL tap water and contents were analysed by liquid scintillation as described in Section 2.2.5.

4.2.12 Determination of transporter mRNA expression in primary renal proximal tubule cells and whole kidney

Messenger RNA (mRNA) from primary renal proximal tubule cells were isolated using TRI reagent® according to the manufacturer's protocol. Specifically, TRI

reagent was added to cells (1mL for every $10cm^2$ cell monolayer culture) and thoroughly mixed using a pipette. Cell homogenate was incubated (5 minutes, 22°C), added to 1-bromo-3-chloropropane (BCP, 100 µL for every 1 mL TRI reagent) and further incubated (15 minutes, 22°C). Mixtures were centrifuged (12000 g, 15 minutes, 4°C) and supernatant fraction was transferred to a new tube. Isopropanol was added to samples (500 µL for every 1 mL TRI reagent) and tubes were mixed and incubated (10 minutes, 22°C). Tubes were centrifuged (12000 g, 8 minutes, 4°C) and supernatant fraction was discarded. The mRNA pellets were resuspended in 75%/25% ethanol/water mixture (1mL for every 1 mL TRI reagent) and centrifuged (7000 g, 5 minutes, 22°C). Supernatant fraction was discarded and RNA pellets were allowed to air dry (5 minutes, 22°C) before being resuspended in nuclease-free water for use in reverse transcriptase experiments.

The mRNA was reverse transcribed using the TaqMan® Reverse Transcription kit according to the manufacturer's protocol. Specifically, the ingredients of a 20 µL reaction were: 2 µL 10X TaqMan reverse transcriptase buffer, 4 µL 25 mM magnesium chloride, 4 µL 10 mM deoxyNTP mixture, 0.5 µg random hexamers, 0.5 µL RNase inhibitor, 0.5 µL MultiScribe Reverse Transcriptase (50 U/µL) and 2 µg mRNA. Reactions were incubated at 42°C (15 minutes) followed by a denaturing incubation at 95°C (5 minutes).

TaqMan® array plates (custom designed and containing primers for a selection of transporter genes) were loaded with reverse-transcribed cDNA (40ng) and used to quantify mRNA expression by standard real-time PCR methodology. Specifically, the ingredients of a 20 µL reaction were: 10 µL TaqMan Master Mix, 50 ng cDNA

and DNase-free water (to make up 20 μL volume total). Real-time polymerase chain reactions (RT-PCR) were run using the following times: 50°C for 2 minutes, 95°C for 10 minutes, followed by 40 cycles of [95°C for 15 seconds, 60°C for 1 minute).

This process was repeated and mRNA quantification obtained for whole kidney purchased from Ambion (UK), which was created from a pool of three individuals. Transporters were quantified using the δδCt method and included *SLC22A6*, *SLC22A1*, *SLC22A2*, *SLC22A3*, *ABCC1*, *ABCC2*, *ABCC3*, *ABCC4* and *ABCC10*. *GAPDH* was used as the housekeeping gene.

4.2.13 Statistical analysis

Data were analysed using SPSS 15.0 for Windows. All data were tested for normality using the Shapiro-Wilk test. An independent *t* test was used to determine the significance of normally distributed data and the Mann Whitney U test was used for all other data. A two-tailed p value of < 0.05 was accepted as being statistically significant.

4.3 RESULTS

4.3.1 Time-dependent accumulation of raltegravir, tenofovir and aminohippuric acid in SLC22A6-injected oocytes

All drugs tested had a greater accumulation rate in SLC22A6-injected oocytes compared to water-injected oocytes (Figures 4.2, 4.3 and 4.4). Raltegravir concentrations continued to increase in SLC22A6-injected oocytes throughout the four hour incubation whereas saturation was reached in water-injected oocytes after around two hours. Both tenofovir and aminohippuric acid showed virtually no accumulation in water-injected oocytes over the four hour incubation.

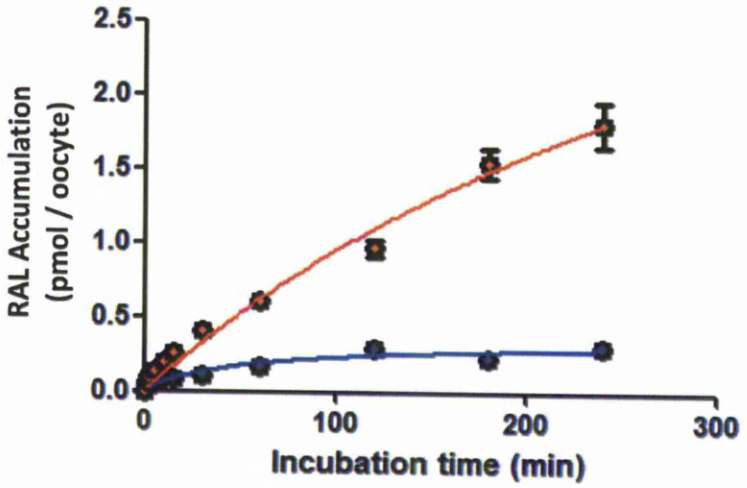

Figure 4.2. SLC22A6-injected (orange circle) and water-injected (blue circle) oocyte uptake of [^{3}H]raltegravir over a four hour incubation. Data are expressed as mean [^{3}H]raltegravir accumulation (pmol/oocyte, n = 5 experimental replicates from one biological replicate) ± SE.

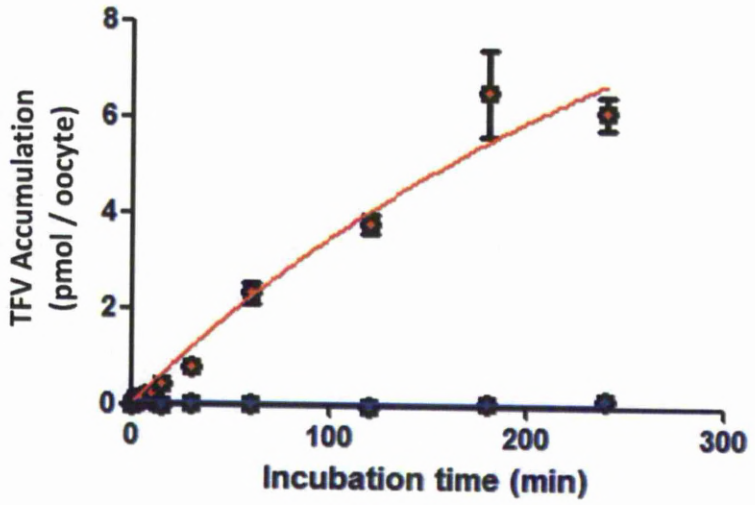

Figure 4.3. SLC22A6-injected (orange circle) and water-injected (blue circle) oocyte uptake of [^{3}H]tenofovir over a four hour incubation. Data are expressed as mean [^{3}H]tenofovir accumulation (pmol/oocyte, n = 5 experimental replicates from one biological replicate) ± SE.

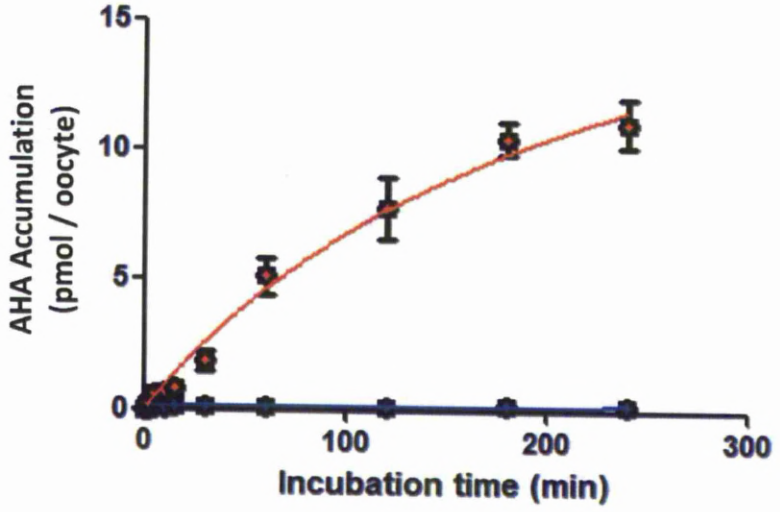

Figure 4.4. SLC22A6-injected (orange circle) and water-injected (blue circle) oocyte uptake of [^{3}H]aminohippuric acid over a four hour incubation. Data are expressed as mean [^{3}H]aminohippuric acid accumulation (pmol/oocyte, n = 5 experimental replicates from one biological replicate) ± SE.

4.3.2 Raltegravir and tenofovir K_m and V_{max} values using SLC22A6-injected oocytes

An incubation of one hour was chosen for subsequent kinetic studies. Raltegravir and tenofovir kinetics were determined for SLC22A6 in the oocyte expression system (Figures 4.5 and 4.6). Raltegravir K_m and V_{max} were calculated to be 150 μM and 36 pmol/oocyte/hr, respectively. Raltegravir Cl_{int} (V_{max}/K_m) was calculated as 0.2 μL/oocyte/hr. Tenofovir K_m and V_{max} were calculated as 25 μM and 129 pmol/oocyte/hr, respectively. The determined K_m value for tenofovir was similar to a previously published value of 21.1 μM using the *Xenopus laevis* oocyte expression system (Bleasby *et al.*, 2005). Tenofovir Cl_{int} was calculated as 5.2 μL/oocyte/hr.

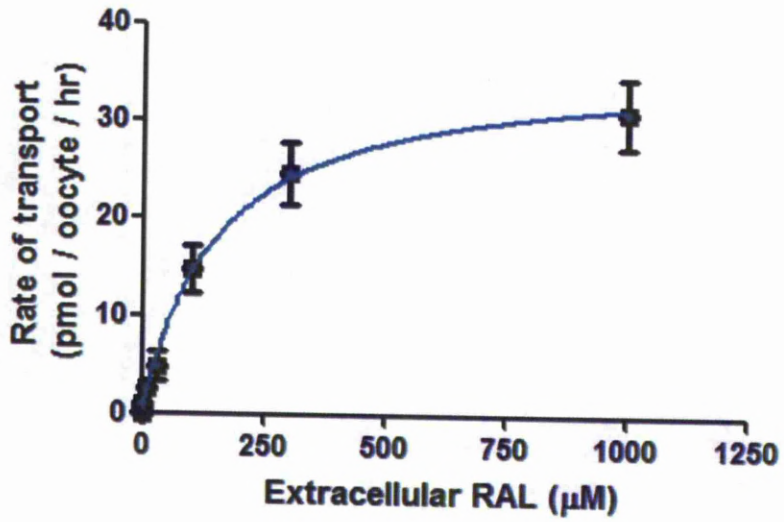

Figure 4.5. Concentration dependency of the uptake of raltegravir by SLC22A6. Data are expressed as mean rate of raltegravir transport (pmol/oocyte/hour, $n \geq 4$ experimental replicates from one biological replicate) ± SE.

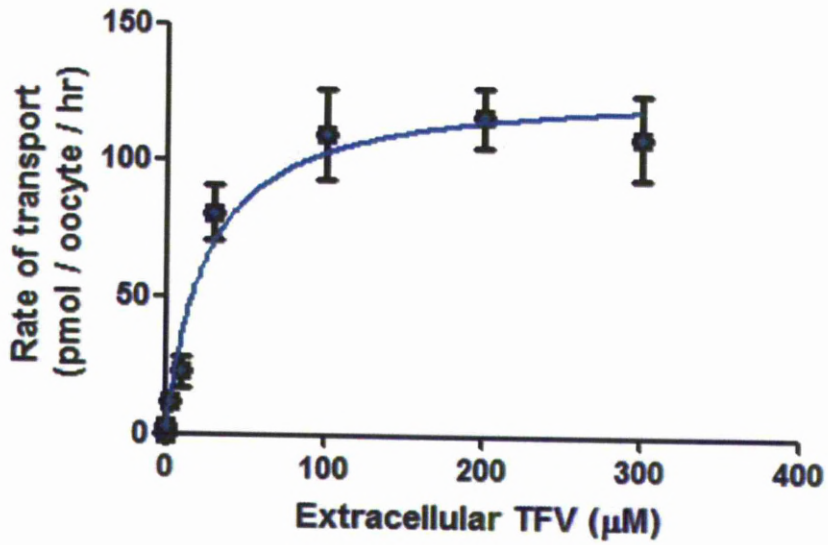

Figure 4.6. Concentration dependency of the uptake of tenofovir by SLC22A6. Data are expressed as mean rate of tenofovir transport (pmol/oocyte/hour, n ≥ 4 experimental replicates from one biological replicate) ± SE.

4.3.3 Competition between raltegravir and tenofovir for SLC22A6 transport

When incubated at 1 μM for one hour, raltegravir showed significantly higher accumulation in SLC22A6 cRNA-injected oocytes than in water-injected oocytes (1.73 ± 0.46 pmol/oocyte versus 0.54 ± 0.06 pmol/oocyte, n = 5, p = 0.014) (Figure 4.7A). The co-incubation of raltegravir with 1, 3, 10, 30, 100 and 300 μM tenofovir resulted in levels of raltegravir in SLC22A6-injected oocytes of 1.78 ± 0.41 pmol/oocyte, 1.63 ± 0.62 pmol/oocyte, 1.48 ± 0.58 pmol/oocyte, 1.28 ± 0.27 pmol/oocyte, 0.96 ± 0.28 pmol/oocyte and 0.83 ± 0.31 pmol/oocyte, respectively (Figure 4.7B). There was a statistically significant decrease ($p < 0.05$) in raltegravir accumulation when concentrations of 100 μM tenofovir and higher were added to the incubation mixture.

Similar results were seen when tenofovir accumulation was investigated in the presence of various concentrations of raltegravir. When incubated at 1 μM for one hour, tenofovir showed significantly higher accumulation in SLC22A6 cRNA-injected oocytes than in water-injected oocytes (2.11 ± 0.37 pmol/oocyte vs 0.03 ± 0.01 pmol/oocyte, $n = 5$, $p < 0.01$) (Figure 4.7C). The co-incubation of tenofovir with 1, 3, 10, 30, 100 and 300 μM raltegravir resulted in tenofovir accumulation in SLC22A6-injected oocytes of 2.11 ± 0.14 pmol/oocyte, 2.07 ± 0.38 pmol/oocyte, 1.47 ± 0.43 pmol/oocyte, 0.78 ± 0.50 pmol/oocyte, 0.49 ± 0.06 pmol/oocyte and 0.28 ± 0.08 pmol/oocyte, respectively (Figure 4.7D). There was a statistically significant decrease ($p < 0.05$) in tenofovir accumulation when concentrations of 10 μM raltegravir and higher were added to the incubation mixtures.

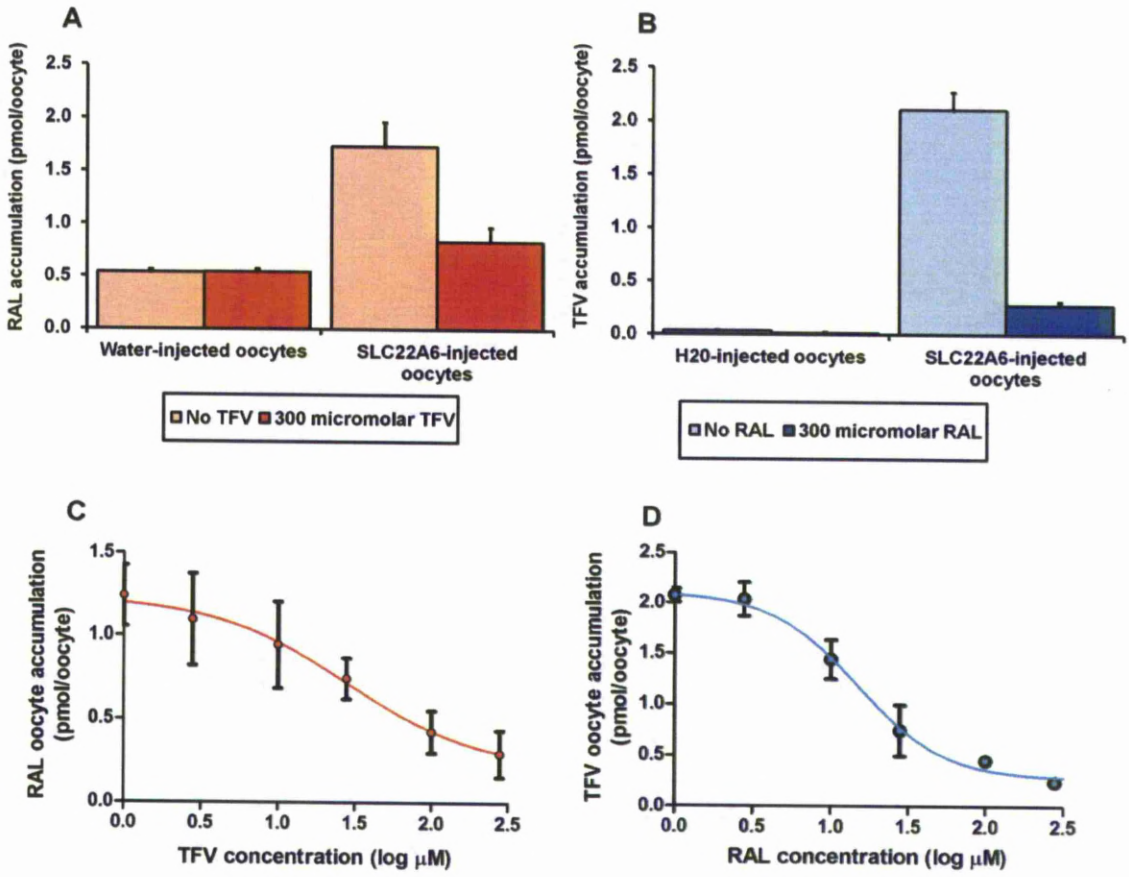

Figure 4.7 (A) Accumulation of 1 μM raltegravir in SLC22A6- and water-injected oocytes with and without the addition of 300 μM tenofovir. **(B)** Accumulation of 1 μM tenofovir in SLC22A6- and water-injected oocytes with and without the addition of 300 μM raltegravir. Data in A and B are expressed as mean drug concentration per oocyte (pmol/oocyte) (n = 5 experimental replicates from one biological replicate) ± SE. **(C)** Determination of IC_{50} for inhibition of 1 μM raltegravir SLC22A6 transport by tenofovir. Data are expressed as mean raltegravir oocyte concentration (pmol/oocyte) (n = 5 experimental replicates from one biological replicate) ± SE. **(D)** Determination of IC_{50} value for inhibition of 1 μM tenofovir SLC22A6 transport by raltegravir. Data are expressed as mean tenofovir oocyte concentration (pmol/oocyte) (n = 5 experimental replicates from one biological replicate) ± SE.

4.3.4 Effect of SLC22A6 and SLC15A1 inhibitors on the accumulation of raltegravir in peripheral blood mononuclear cells

Raltegravir accumulation in PBMCs from four healthy human subjects was determined (Figure 4.8). Probenecid and glycyl-sarcosine were used to determine the extent of raltegravir transport by SLC22A6 and SLC15A1, respectively. Data are expressed as mean CAR ± SD. Raltegravir CAR was not significantly altered in glycyl-sarcosine-treated cells compared to non-treated cells in subject 1 (3.47 ± 0.36 versus 3.78 ± 0.70, p = 0.513), subject 2 (4.54 ± 1.62 versus 3.13 ± 0.22, p = 0.146), subject 3 (2.70 ± 0.53 versus 3.03 ± 0.97, p = 0.564) or subject 4 (2.33 ± 0.57 versus 2.15 ± 0.30, p = 0.827). Raltegravir CAR was not significantly altered in probenecid-treated cells compared to non-treated cells in subject 1 (2.83 ± 0.85 versus 3.78 ± 0.70, p = 0.127), subject 3 (3.90 ± 0.80 versus 3.03 ± 0.97, p = 0.149) or subject 4 (2.27 ± 0.21 versus 2.15 ± 0.30, p = 0.513), but was significantly higher in probenecid-treated cells compared to non-treated cells in subject 2 (3.94 ± 0.57 versus 3.13 ± 0.22, p = 0.042). When combining the average results from each subject, raltegravir CAR was not significantly different in glycyl-sarcosine-treated cells compared to non-treated cells (3.23 ± 0.83 versus 3.02 ± 0.67, p = 0.77) or in probenecid-treated cells compared to non-treated cells (3.26 ± 0.98 versus 3.02 ± 0.67, p = 0.77).

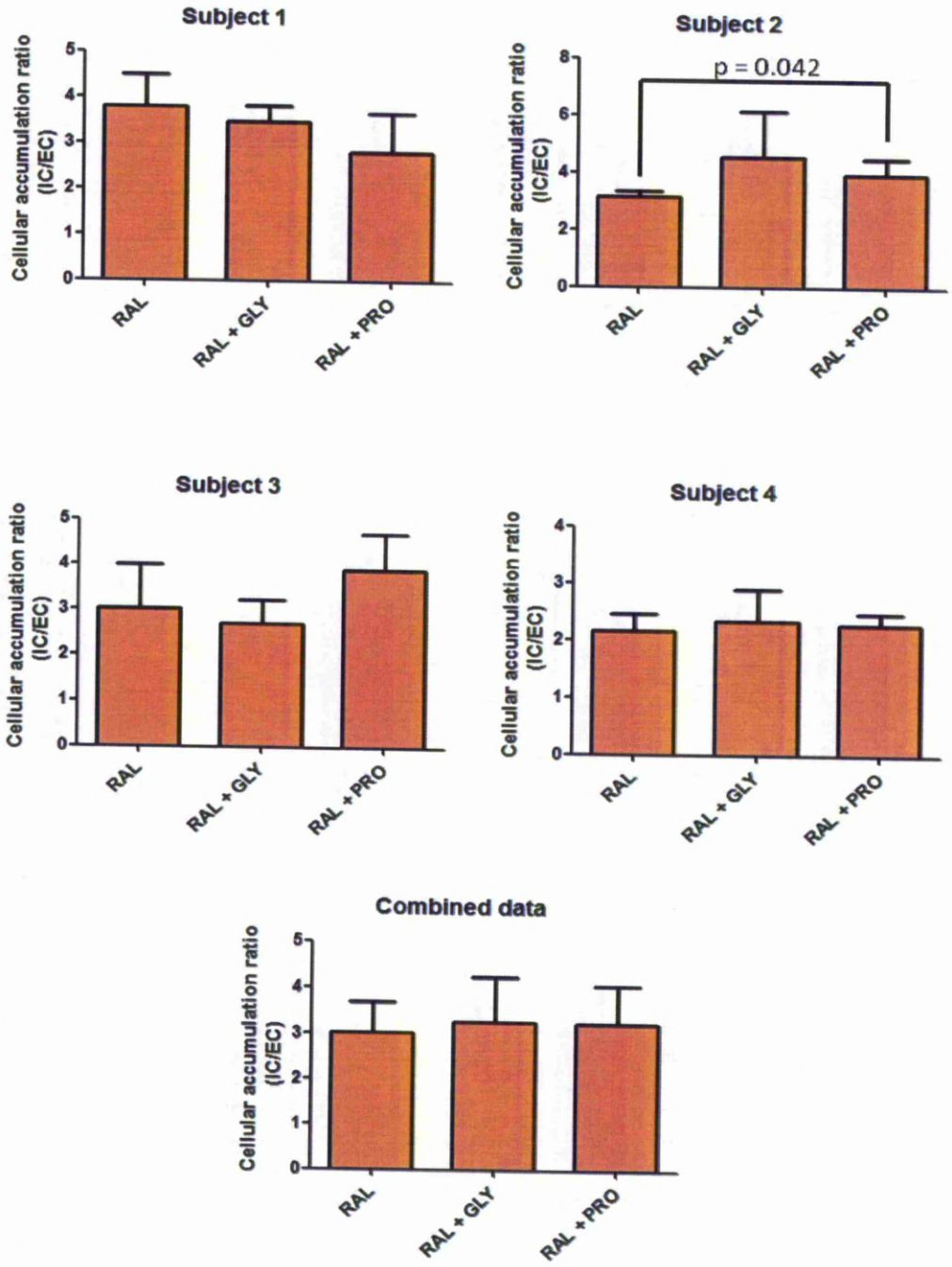

Figure 4.8. Raltegravir (RAL; 1 μM) accumulation in PBMCs and PBMCs co-incubated with 1 mM glycyl-sarcosine (GLY; SLC15A1 inhibitor) or 1 mM probenecid (PRO; SLC22A6 inhibitor). Data for subjects 1, 2, 3 and 4 are expressed as mean CAR ($n \geq 3$ experimental replicates) ± SD. Combined data are expressed as mean CAR ($n = 4$ biological replicates, $n \geq 3$ experimental replicates per biological replicate) ± SD.

4.3.5 Cellular accumulation of raltegravir, tenofovir and aminohippuric acid in primary renal proximal tubule epithelial cells

The cellular accumulation of raltegravir (CAR = 2.01 ± 0.20) (Figure 4.9A), tenofovir (CAR = 3.45 ± 0.76) (Figure 4.9B) and aminohippuric acid (CAR = 0.50 ± 0.02) (Figure 4.9C) were determined in renal proximal tubule epithelial cells. Raltegravir cellular accumulation was not significantly altered by 1 mM probenecid (CAR = 2.19 ± 0.45, $p = 0.56$) or 100 μM tenofovir (CAR = 2.07 ± 0.08, $p = 0.66$). Tenofovir showed a high level of cellular accumulation, which was not significantly altered by treatment with 1 mM probenecid (CAR = 2.59 ± 0.56, $p = 0.19$) or 100 μM raltegravir (CAR = 3.15 ± 0.74, $p = 0.65$). For aminohippuric acid a trend was seen towards a lower level of cellular accumulation when incubated with 1 mM probenecid (CAR = 0.44 ± 0.03, $p = 0.08$).

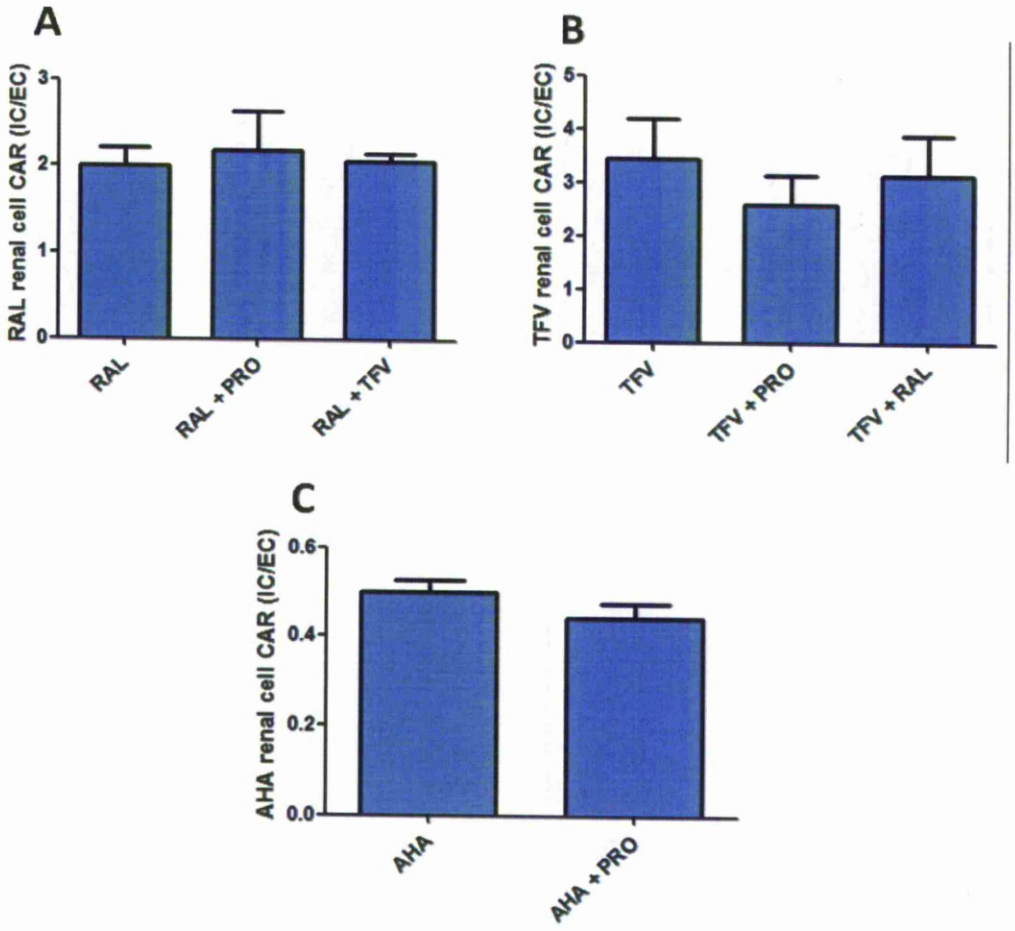

Figure 4.9. (A) Raltegravir (RAL; 1 μM) accumulation in primary renal proximal tubule cells alone or treated with 1 mM probenecid (PRO; SLC22A6 inhibitor) or 100 μM tenofovir (TFV). **(B)** Tenofovir (1 μM) accumulation in primary renal proximal tubule cells alone or treated with 1 mM probenecid or 100 μM raltegravir. **(C)** Aminohippuric acid (AHA; 1 μM) accumulation in primary renal proximal tubule cells alone or treated with 1 mM probenecid. Data are expressed as mean CAR (n = 3 experimental replicates) ± SD.

4.3.6 Transporter expression in cultured renal cells and kidney tissue

All transporters tested showed lower or undetectable expression in primary renal proximal tubule cells compared to whole kidney (Figure 4.10). Importantly, SLC22A6 was undetectable in the primary renal cells.

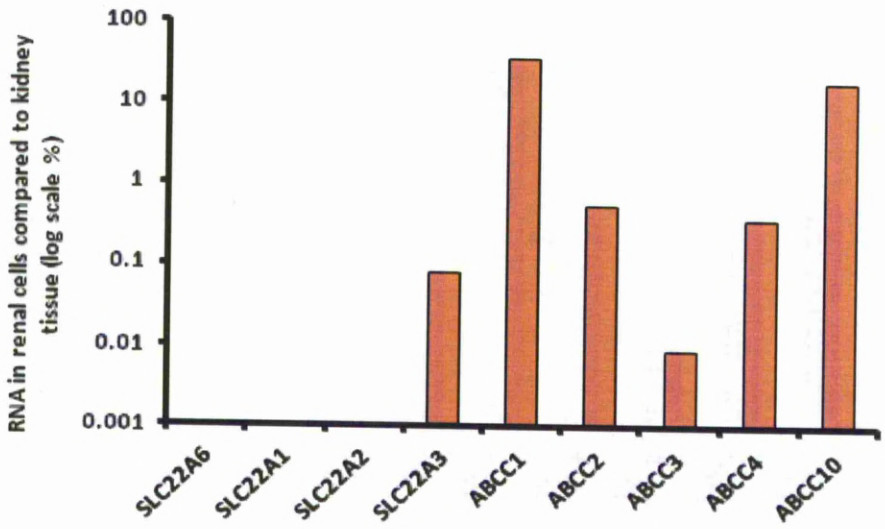

Figure 4.10. Relative abundance of transporter RNA in cultured renal proximal tubule cells compared to transporter RNA in whole kidney (log scale %, n = 1 experimental replicate).

4.4. DISCUSSION

This chapter investigated the affinity of raltegravir and tenofovir for influx transporter SLC22A6 using the *Xenopus laevis* oocyte expression system. Competition between raltegravir and tenofovir for SLC22A6 transport was also determined. In SLC22A6 cRNA-injected oocytes, raltegravir and tenofovir inhibited the accumulation of each other in a concentration-dependent manner (Figure 4.7). This competition was not observed in water-injected oocytes, which supports the hypothesis that raltegravir and tenofovir compete for SLC22A6 transport and are not having non-specific effects on oocyte membrane permeability.

Raltegravir accumulation in SLC22A6-expressing oocyte was inhibited by tenofovir with an IC_{50} value of 27.3 μM. Tenofovir accumulation in SLC22A6-expressing oocyte was inhibited by raltegravir with an IC_{50} value of 14.0 μM. The IC_{50} obtained for raltegravir was much lower than the observed K_m determined for SLC22A6 (IC_{50} of 14.0 μM versus a Km of 147 μM). This suggests that raltegravir is a more efficient SLC22A6 inhibitor than it is a substrate. Previous studies have indicated that SLC22A6 and SLC15A1 are absent from PBMCs (Bleasby *et al.*, 2006) and so these transporters are unlikely to explain the unusual PK–PD relationship for raltegravir. Indeed, our studies in PBMCs with known inhibitors of SLC22A6 and SLC15A1 revealed no significant interaction with raltegravir.

Wenning *et al* (2008) studied the interaction of raltegravir (400 mg twice-daily) and tenofovir (300 mg once-daily). The study showed increased raltegravir AUC (49%) and C_{max} (64%), but no effect on raltegravir C_{min}, and a decrease in tenofovir AUC

(10%), C_{max} (23%) and C_{min} (13%) (Wenning *et al.*, 2008). SLC22A6 is predominantly expressed in the proximal tubule of the kidney on the basolateral (blood-facing) surface, thereby facilitating removal of drugs out of the blood and into the urine (Rizwan *et al.*, 2007). Therefore, a possible mechanism of this interaction is inhibition of SLC22A6-mediated raltegravir transport at the kidney proximal tubule by tenofovir, resulting in increased raltegravir plasma concentrations.

In order to investigate interactions at the level of the kidney we conducted a number of experiments in primary renal proximal cells. No interaction between tenofovir and raltegravir was observed in these cells but neither was an interaction between positive control substrate aminohippuric acid and inhibitor probenecid. Subsequent analyses revealed expression of SLC22A6 mRNA to be undetectable in primary renal proximal cells, unlike in kidney tissue. Furthermore, all other transporters that were assessed were at lower expression than kidney tissue. It is possible that stimulating the primary cells to divide using Complete Growth Media results in reduced transporter expression. Indeed, the human kidney clear cell carcinoma cell line, Caki-1, has been shown to have undetectable SLC22A6 mRNA expression (Hilgendorf *et al.*, 2007). The same study showed significantly lower or absent mRNA expression of other several transporters in Caki-1, Caco-2 and HepG2 (liver) cell lines, emphasising the issue with using immortalised cell lines in transporter studies. The absence of a robust primary cell model for these studies is a limitation that precluded further *in vitro* investigation of this mechanism.

Since only a small percentage (around 30%) of raltegravir excreted via the kidney is in the parent form, with the remaining 70% being a glucuronide metabolite

(Kassahun *et al.*, 2007), it is important to determine if the raltegravir glucuronide is also transported by SLC22A6 and inhibited by tenofovir. It would also be interesting to investigate the transport and inhibitory potential of tenofovir diphosphate (fully phosphorylated tenofovir) or tenofovir disoproxil fumerate (prodrug of tenofovir) for SLC22A6 and whether this affects raltegravir transport to the same extent.

In conclusion, raltegravir and tenofovir show competition for SLC22A6 transport i*n vitro*, although the significance of this interaction requires further investigation *in vivo*. The reduced exposure of raltegravir in patients when co-administered with tenofovir may involve the SLC22A6 transporter. However, even if SLC22A6 is shown to influence raltegravir disposition in humans, it is unlikely that this will fully explain the large intra- and inter-patient variability seen in raltegravir PK.

Chapter 5

The impact of pH, metal binding and omeprazole on raltegravir physicochemistry and disposition

Table of Contents

5.1 INTRODUCTION

The pH of the GI tract is an important factor in the absorption of many drugs, potentially altering drug release, solubility, chemical stability, charge state and/or intestinal permeation (Charman *et al.*, 1997). Ionic drugs with a pKa within the physiological pH range are susceptible to alterations in GI pH because drugs with an ionic charge are less able to permeate the intestine wall without active transport. In healthy volunteers, raltegravir GMR for AUC, C_{max} and C_{12hr} increased 3.1, 4.2 and 1.5-fold, respectively, following five days of 20 mg once-daily omeprazole (Iwamoto *et al.*, 2009b); higher solubility at increasing pH was postulated as the mechanism of interaction (Brainard *et al.*, 2011c). However, GI pH was not measured in this study and there are no published data showing the effect of pH on raltegravir solubility *in vitro*. In a similar study using HIV-infected patients, raltegravir GMR for AUC, C_{max} and C_{12hr} was 1.4, 1.5 and 1.2-fold higher, respectively, following five days of 20 mg once-daily omeprazole and 1.5, 1.6 and 1.1-fold higher, respectively, following a single dose of 20 mg famotidine (Rhame *et al.*, 2009). HIV-infected patients, particularly those with advanced disease progression, have higher gastric pH than uninfected individuals (Shelton *et al.*, 2000) and this may explain why acid-reducing agents showed less impact on raltegravir PK in the study involving HIV-infected patients.

After ingestion of a meal, gastric pH is briefly elevated due to the buffering and diluting effect of the food (Charman *et al.*, 1997). The extent of gastric pH increase and the rate at which pH is lowered to fasting state levels depends on the volume of the food, the ability of the food to stimulate gastric acid secretion and the rate of gastric emptying. Other factors, such as fat and protein content of food, are also

important. In a steady-state food-effect study using healthy subjects, alterations in raltegravir exposure from a fasted state were shown for low fat (GMR of AUC, C_{max} and C_{12hr} of 0.54, 0.48 and 0.86, respectively), medium fat (GMR of AUC, C_{max} and C_{12hr} of 1.13, 1.05 and 1.66, respectively) and high fat (GMR of AUC, C_{max} and C_{12hr} of 2.11, 1.96 and 4.13, respectively) meals (Brainard *et al.*, 2011a). However, this study concluded that the effect of food was not clinically significant and recommended that raltegravir can be taken without regard to food.

Integrase strand transfer inhibitors work by chelating magnesium ions at the integrase enzyme active site, therefore preventing the insertion of viral DNA into the host cell's DNA (Espeseth *et al.*, 2000). Therefore, it is possible that by binding with free magnesium (and possibly other polyvalent cationic metals), the absorption of raltegravir may decrease. Indeed, interactions between integrase inhibitors and metal-containing products have been investigated. Raltegravir C_{12hr} and T_{max} were reduced by 67% and 1.75 hours, respectively, when taken with an antacid containing magnesium and aluminium, although the AUC and C_{max} were not significantly altered (Kiser *et al.*, 2010). Importantly, 75% of subjects taking antacids had a raltegravir C_{12hr} lower than 15 ng/mL (IC_{95} of raltegravir in 50% human serum). The authors hypothesised that this interaction may be mediated by an increase in raltegravir solubility with increased pH (decreasing the T_{max}) and binding of raltegravir to the metal ions in the antacid (decreasing C_{12hr}).

The investigations in this chapter aimed to establish the solubility, lipophilicity and pKa of raltegravir *in vitro* using a range of buffered pH solutions and solvents. The breakdown rate of raltegravir 400 mg tablets were determined in different pH

solutions to help explain delayed and double peaks in raltegravir PK profiles. The impact of pH, metal cations and omeprazole on raltegravir transcellular permeation across a a Caco-2 monolayer were also determined. Raltegravir is a substrate of ABCB1 *in vitro* (Moss *et al.*, 2011) (Chapter 2) and the interplay between pH and ABCB1 transport was investigated in cellular accumulation assays to ascertain whether active transport of raltegravir by ABCB1 was influenced by pH.

5.2 METHODS

5.2.1 Chemical reagents and materials

Caco-2 cells were purchased from the European Collection of Cell Cultures (Salisbury, UK). Raltegravir potassium salt, [^{3}H]raltegravir and standard 400 mg raltegravir tablets were gifts from Merck (New Jersey, USA). Lopinavir was a gift from Abbott (Illinois, USA). [^{3}H]Lopinavir was purchased from Moravek Biochemicals (California, USA). Tariquidar was purchased from Xenova (Sloane, UK). Acetonitrile was purchased from J. T Baker (Deventer, Holland). [^{14}C]Mannitol was purchased from American Radiolabelled Chemicals (Missouri, USA). All other reagents were obtained from Sigma (Poole, UK).

5.2.2 Creation of buffered pH solutions for solubility, lipophilicity, pKa and tablet breakdown experiments

Stock aqueous solutions were buffered to pH 1 (50 mM potassium chloride + 134 mM hydrogen chloride), 2 (50 mM potassium chloride + 13 mM hydrogen chloride), 3 (50 mM potassium hydrogen phthalate + 22.3 mM hydrogen chloride), 4 (50 mM potassium hydrogen phthalate + 0.1 mM hydrochloric acid), 5 (50 mM potassium hydrogen phthalate + 22.6 mM sodium hydroxide), 6 (50 mM monopotassium phosphate + 5.6 mM sodium hydroxide), 7 (50 mM monopotassium phosphate + 29.1 mM sodium hydroxide), 8 (50 mM tris hydroxymethyl aminomethane + 29.2 mM hydrogen chloride) and 9 (50 mM tris hydroxymethyl aminomethane + 5.7 mM hydrogen chloride). These stock solutions were used in experiments or were adjusted using 1 M hydrochloric acid or 1 M sodium hydroxide to create the required pH.

5.2.3 Determination of raltegravir solubility

Raltegravir solubility was determined at 1 mM and 10 mM (estimated range of drug concentrations in the stomach and duodenum of the gut following raltegravir dissolution) in a pH range of 1 to 8. Solutions were mixed on a mechanical shaker (120 rpm, 37°C, 2 hours) and vigorously mixed to allow maximum dissolution of raltegravir. Samples were then centrifuged to pellet undissolved drug (3000 g, 10 minutes, 22°C) and the supernatant carefully removed. Raltegravir concentrations in the supernatant were determined using LC-MS/MS analysis (Section 5.2.12)

5.2.4 Determination of raltegravir lipophilicity

Raltegravir lipophilicity was determined across a physiologically relevant pH range of 1 to 9 using the octanol:water Shake Flask Method. The organic solvent used was either 1-octanol, which allows hydrogen bonding, or cyclohexane, which does not allow hydrogen bonding. The aqueous and organic solvents were mutually saturated on a mechanical shaker (240 rpm, 24 hours, 22°C) before use. Raltegravir was added to the aqueous solvent at 10 μM (a concentration ensuring complete solubility in all pH solutions) before combining the aqueous and organic solvents in a 1:1 ratio and shaking the mixtures for 30 minutes. Mixtures were centrifuged (800 g, 30 minutes, 22°C) and a sample taken from the aqueous compartment for LC-MS/MS analysis (Section 5.2.12). Calculation of the apparent logP (also referred to as "logP" in this chapter) was based on the following equation:

$$\text{Apparent logP} = \log (C_{organic} / C_{aqueous})$$

Where $C_{aqueous}$ is the concentration of raltegravir in the aqueous solvent and $C_{organic}$ is the concentration of raltegravir in the organic solvent (estimated by deducting raltegravir in the aqueous compartment from the total amount in the mixture).

5.2.5 Determination of raltegravir pKa

Raltegravir pKa was determined using UV spectroscopy (Blanco *et al.*, 2005). Raltegravir was prepared in buffered pH solutions to a final concentration of 8 μM (a concentration giving an adequate signal for detection). The buffered pH solutions ranged between pH 3.5 and 9.5. Drug solutions were added to cuvettes and placed in a UV spectrophotometer (Perkin Elmer lambda 25 UV-vis) and allowed to acclimatise (25°C, 5 minutes). Following this, the UV-vis spectra were measured between 200 nm and 500 nm. The absorbance values were recorded at 300 nm (absorbance peak predominant at lower pH) and 333 nm (absorbance peak predominant at higher pH). For each pH the absorbance at 333 nm was divided by the absorbance at 300 nm and plotted to calculate the pKa.

5.2.6 Determination of raltegravir tablet breakdown rate

The breakdown rate of standard raltegravir 400 mg tablets were determined across a pH range of 1 to 8. The weight of each tablet was first recorded before the experiment. Tablets were then added to 150 mL pH buffer solution (roughly the volume of a fasted stomach) and gently rotated in an incubator to simulate the churning of the stomach (10 rpm, 37°C). Tablets were removed from solutions after 30 minutes incubation and allowed to completely dry (4 hours, 50°C). The weight of

each tablet was recorded and compared to the initial weight. Data was then used to calculate tablet dissolution rate (% of total tablet broken down/minute, n = 1 experimental replicate).

5.2.7 Caco-2 cell culture

Caco-2 cells were maintained in cell culture (37°C, 5% CO_2) by passaging at 70% confluence using cell culture medium (DMEM, 15% [vol/vol] FCS). The passage number of the cells used in this study was between 25 and 35. Caco-2 monolayers were cultured as previously described in Section 2.2.2.4 and were subsequently used to determine the effects of pH, metal salts and omeprazole on raltegravir monolayer permeation. Briefly, confluent Caco-2 cells were seeded onto polycarbonate membrane transwells at a density of 5 x 10^5 cells/cm^2. Media was replaced initially after 24 hours and then every 48 hours. Plates were used in the experiments 21 days after seeding. Monolayer integrity was checked on the day of the experiment using a MillicellERS (Millipore) to determine the TEER across the monolayer. A TEER of > 600 was deemed acceptable. In addition, radiolabelled [^{14}C]mannitol was added to separate wells on each plate (n = 3 replicates) to confirm monolayer integrity. [^{14}C]Mannitol samples were analysed by liquid scintillation counting (Beckman TRI-CARB®) and plates were only used for experiments if the average P_{app} of mannitol was less than 1 cm x 10^{-6} s^{-1}.

5.2.8 Impact of pH on raltegravir cell monolayer permeation

On the day of study, the TEER was assessed and the media in each plate was replaced with the appropriate pH-buffered incubation solutions. The pH in the basolateral compartments was maintained at pH 7.4 (HBSS containing 25 mM HEPES) and the pH in the apical compartments were maintained at pH 5, 6, 6.5 (HBSS containing 10 mM MES), 7, 7.4, 8 (HBSS containing 25 mM HEPES) or 8.5 (HBSS containing 10 mM Tricine). Compartments were allowed to equilibrate (37°C, 30 minutes). The incubation buffer in the apical (for apical to basolateral transport) and basolateral (for basolateral to apical transport) compartments were replaced with the appropriate incubation buffer containing raltegravir (50 μM) and plates were incubated (37°C, 5% CO_2). A concentration of 50 μM raltegravir, which was shown to be non-toxic to Caco-2 cells in Chapter 2, was used to ensure complete dissolution of drug at all pH solutions (as predicted by the solubility data) and to ensure drug concentrations in receiver compartments were sufficiently high to be quantifiable by LC-MS/MS. Samples were taken from the receiver compartments at 0, 30, 60, 90, and 120 minutes and replaced with fresh incubation buffer of the correct pH. Samples were analysed using LC-MS/MS (Section 5.2.12). Results were used to determine P_{app} (cm x 10^{-6} s^{-1}) for each direction and to determine the efflux ratio, as described in Section 2.2.6.

5.2.9 Impact of divalent and monovalent metals on raltegravir cell monolayer permeation

On the day of study, the TEER was assessed and the media in each plate was replaced with the appropriate pH-buffered incubation solution. The pH in the

basolateral compartments was maintained at pH 7.4 (HBSS without calcium chloride or magnesium sulphate (SIGMA code: H6648) containing 25 mM HEPES) and the pH in the apical compartments was maintained at pH 5 (HBSS without calcium chloride or magnesium sulphate containing 10 mM MES) or pH 7.4 (HBSS without calcium chloride or magnesium sulphate containing 25 mM HEPES). In the apical compartments at pH 5, magnesium chloride (1 mM, 10 mM or 25 mM), magnesium sulphate (25 mM), calcium chloride (25 mM) or potassium chloride (25 mM) were added. In the apical compartments at pH 7.4, magnesium chloride (1, 10 or 25 mM) was added. A maximum concentration of 25 mM was used for magnesium chloride as higher concentrations used in validation showed Caco-2 cell toxicity. Control apical compartments at pH 5 and pH 7.4 were also used, which were not supplemented with metal salts (other than those in the original buffer: 5.4 mM potassium chloride, 0.4 mM monopotassium phosphate, 4.2 mM sodium bicarbonate, 138 mM sodium chloride and 3.4 mM disodium phosphate). The pH in the basolateral compartments were maintained at pH 7.4 and were not supplemented with additional metal salts. A concentration of 1 μM was used for all test compounds in order to maximise the metal-to-drug ratio. Lopinavir was used as a negative control as there is no evidence that it binds to metals. The incubation buffer in the apical (for A-to-B transport) and basolateral (for B-to-A transport) compartments were replaced with the appropriate incubation buffer containing radiolabelled [^{3}H]raltegravir (1 μM, 0.5 μCi/mL) or [^{3}H]lopinavir (1 μM, 0.5 μCi/mL) and plates were incubated (37°C, 5% CO_2). Samples were taken from the receiver compartments at 0 and 30 minutes and were analysed by liquid scintillation counting (Beckman TRI-CARB®). The P_{app} and efflux ratios were calculated as described in Section 2.2.6.

5.2.10 Impact of omeprazole on raltegravir cell monolayer permeation

For induction studies using transwells, the cell monolayers were incubated with omeprazole (10 μM) for the last three days of the 21-day monolayer maturation. On the day of the experiment, the TEER was assessed and the media in each plate was replaced with warm incubation buffer (HBSS containing 25 mM HEPES, pH 7.4) and allowed to equilibrate (37°C, 30 minutes).

For inhibition studies, the incubation buffer contained omeprazole at 20 μM, as lower concentrations are known to inhibit CYP2C9 and CYP2C19 *in vitro*. The incubation buffer in the apical (for A-to-B transport) and basolateral (for B-to-A transport) compartments were replaced with incubation buffer containing the test substrate raltegravir (1 μM) with or without 20 μM omeprazole, and plates were incubated (37°C, 5% CO_2). A concentration of 1 μM raltegravir was used to avoid saturation of drug transporters (Hubatsch *et al.*, 2007). Samples were taken from the receiver compartments at 0 and 60 minutes and were analysed by liquid scintillation counting (Beckman TRI-CARB®). The P_{app} and efflux ratios were calculated as described in Section 2.2.6.

5.2.11 Cellular accumulation

Caco-2 cells were seeded (5 x 10^4 cells/mL) onto 6-well plates and grown for five days to reach the required confluence (DMEM, 15% [vol/vol] FCS, 37°C, 5% CO_2). Media was removed and cells were washed with warm HBSS and replaced with the appropriate pH-buffered incubation solution and allowed to equilibrate (37°C, 15

minutes). The pH in the wells was fixed at either pH 5, 6 (HBSS containing 10 mM MES), 7 or 8 (HBSS containing 25 mM HEPES). The test substrate raltegravir (1 μM) was added to the wells and plates were incubated (37°C, 5% CO_2, 10 minutes). A concentration of 1 μM raltegravir was used to avoid saturation of drug transporters (Hubatsch *et al.*, 2007). A separate incubation was undertaken where cells were pre-incubated (DMEM, 15% FBS, 37°C, 5% CO_2) prior to raltegravir addition with the potent non-competitive ABCB1 inhibitor, tariquidar (300 nM, 30 minutes), which was also included during the 10 minutes of raltegravir incubation. Following incubation, an extracellular sample was removed from each well for analysis, wells were washed three times with ice cold HBSS and 500 μL tap water was added to each empty well to lyse cells. Plates were frozen at minus 20°C overnight to aid removal of cells. Plates were thawed and 500 μL acetonitrile added to each well to release drug from protein. The well contents were transferred to separate 1.5 mL tubes for centrifugation (3000 g, 10 minutes, 22°C) and supernatant was removed. Supernatant fraction was vacuum-dried and reconstituted in HPLC-grade water for LC-MS/MS analysis (Section 5.2.12).

5.2.12 LC-MS/MS analysis

Samples from all studies using non-radiolabelled raltegravir (other than from cell accumulation studies) could be directly injected into the LC-MS/MS after dilution with HPLC-grade water. Samples from cell accumulation studies were prepared as described in the cellular accumulation method Section 5.2.11. The LC-MS/MS system used for sample analysis consisted of an autosampler model Surveyor, and LCQ DecaXP ion trap detector (Thermo, UK). Chromatographic separation was

performed at 30°C on a Fortis C-18 3 μm column (50 X 2.1 mm i.d., Fortis technologies, UK). Mobile phases were solution A (95% HPLC grade water, 5% acetonitrile, 0.05% formic acid) and solution B (10% HPLC-grade water, 90% acetonitrile, 0.05% formic acid) and flow rate was 0.4 mL / minute. Separation was achieved with a gradient elution beginning with 80% solution A and 20% solution B. Solution B was gradually increased to 100% over 0.5 minutes and maintained for a further 2 minutes. Solution A was increased to 80% over 0.1 minutes and maintained for 3.9 minutes, giving a total run time of 6.5 minutes. The retention time of raltegravir was 4.78 minutes and the lowest limit of quantification was 31.25 ng/mL. High quality control (QC) (2000 ng/mL) had an inter-day and intra-day accuracy of 98.2% and 97.1%, respectively, and an inter-day and intra-day precision of 97.0% and 93.1%, respectively. Medium QC (200 ng/mL) had an inter-day and intra-day accuracy of 96.8% and 99.1%, respectively, and an inter-day and intra-day precision of 89.1% and 89.2%, respectively. Low QC (100 ng/mL) had an inter-day and intra-day accuracy of 96.5% and 92.8%, respectively, and an inter-day and intra-day precision of 90.0% and 95.3%, respectively. All QC gave higher than 85% accuracy and precision, in accordance with FDA guidelines(*23*)(23) and the linear range for raltegravir quantification was 31.25-1000 ng/mL.

5.2.13 Statistical Analysis

Data were analysed using SPSS 15.0 for Windows. All data were tested for normality using the Shapiro-Wilk test. An independent t-test was used to determine significance of normally distributed data. The Mann Whitney U test was used for all other data. A two-tailed p value < 0.05 was accepted as being statistically significant.

5.3 RESULTS

5.3.1 Raltegravir solubility

Figure 5.1 shows raltegravir solubility in buffers ranging from pH 1 to 8. A concentration of 1 mM raltegravir was fully soluble across the pH range. However, 10 mM raltegravir was only fully soluble at pH 6.8, 6.9, 7 and 8 and achieved a mean supernatant concentration of 8.0 mM at pH 6.6, 6.3 mM at pH 6.4, 5.0 mM at pH 6.2, 3.7 mM at pH 6 and around 3 mM at pH 5 and below.

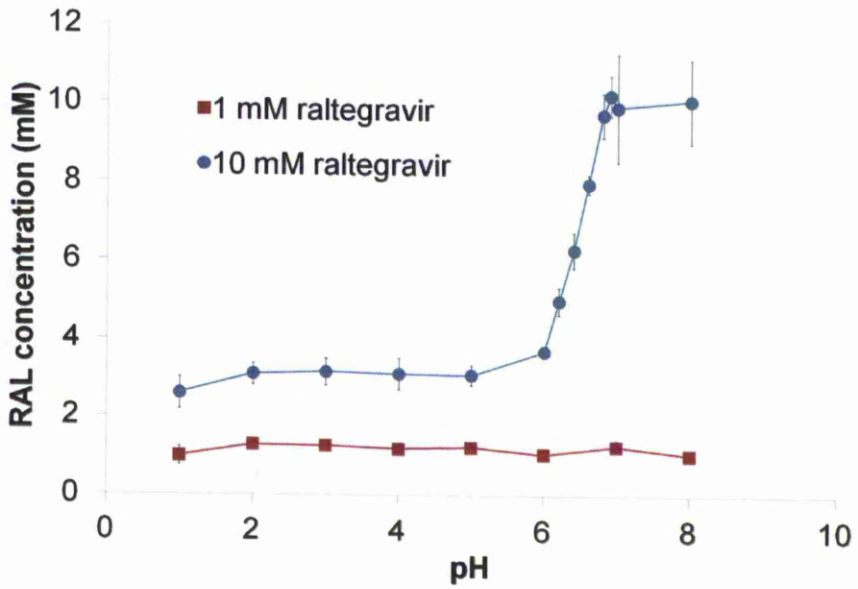

Figure 5.1. Raltegravir solubility at 1 mM (red squares ■) and 10 mM (blue circles ●) in a range of pH solutions. Data are expressed as mean raltegravir dissolved in solution (mM, n ≥ 3 experimental replicates) ± SD.

5.3.2 Raltegravir lipophilicity

When using cyclohexane as the organic solvent, raltegravir remained predominantly in the aqueous compartment (~90%) in all pH solutions, whereas using octanol resulted in low raltegravir concentrations (~7%) in the aqueous compartments of pH 5 or less (Figure 5.2). When using octanol as the organic solvent, raltegravir apparent logP was stable between aqueous pH 1 and 5 but decreased from 1.06 to -1.29 between pH 5 and 9 ($p < 0.05$, Figure 5.3). A negative logP is usually associated with poor cell membrane permeation (Goodwin *et al.*, 2001).

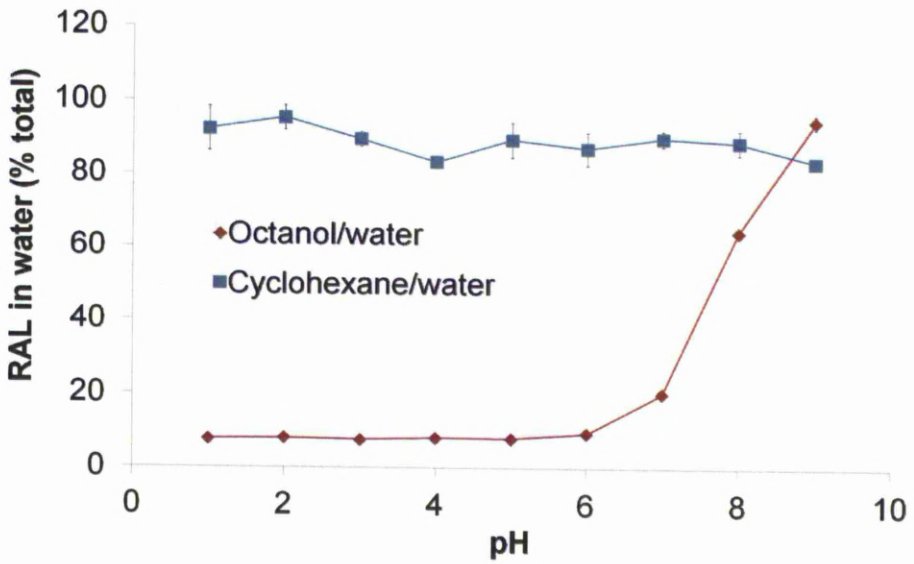

Figure 5.2. Partition of raltegravir (10 μM) between cyclohexane and water (blue squares ■, n = 4 experimental replicates) and between octanol and water (red diamonds ◆, n = 4 experimental replicates, n = 3 biological replicates) at different pH solutions. Data are expressed as mean percentage of raltegravir in water (% of total drug) ± SD.

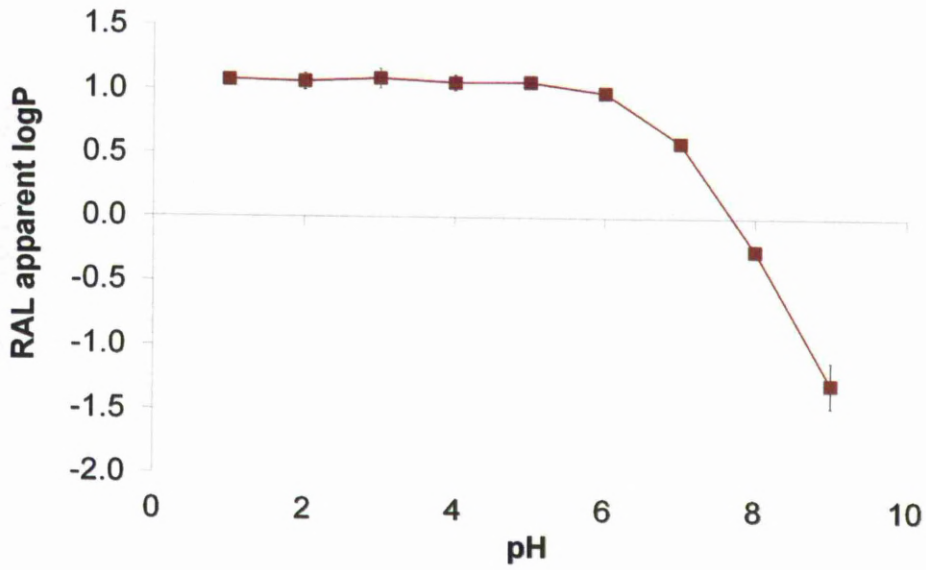

Figure 5.3. Apparent logP of raltegravir (10 μM) using octanol and water at different pH solutions. Data are expressed as mean log of raltegravir partition (logP, n = 4 experimental replicates, n = 3 biological replicates)) ± SD.

5.3.3 Raltegravir pKa

Figure 5.4 shows the relative absorbance at two wavelengths (333 nm versus 300 nm) as a function of the pH of the buffer solution. The most substantial change in the curve occurred between pH 6 and 8. Assuming this change in peak ratios was due to an alteration of the charge state of raltegravir, the pKa was calculated as 6.7.

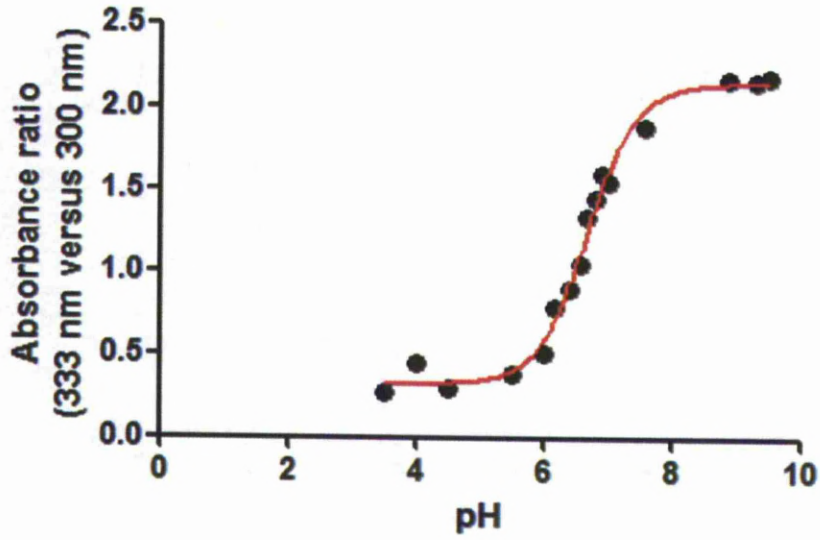

Figure 5.4. Determination of raltegravir pKa using UV spectroscopy. Data are expressed as relative absorbance at two wavelengths (333 nm versus 300 nm) as a function of the pH of the buffer solution (n = 1 experimental replicate).

5.3.4 Raltegravir tablet breakdown rate

The breakdown rate of standard raltegravir 400 mg tablets was determined across a pH range of 1 to 8 and was seen to increase as pH was increased (Figure 5.5). The loss of tablet weight was measured after 30 minutes and showed a 237% increase in weight loss as pH was increased from 1 to 8 (Figure 5.6). However, only a single replicate was performed for every pH solution, therefore statistical analysis could not be performed.

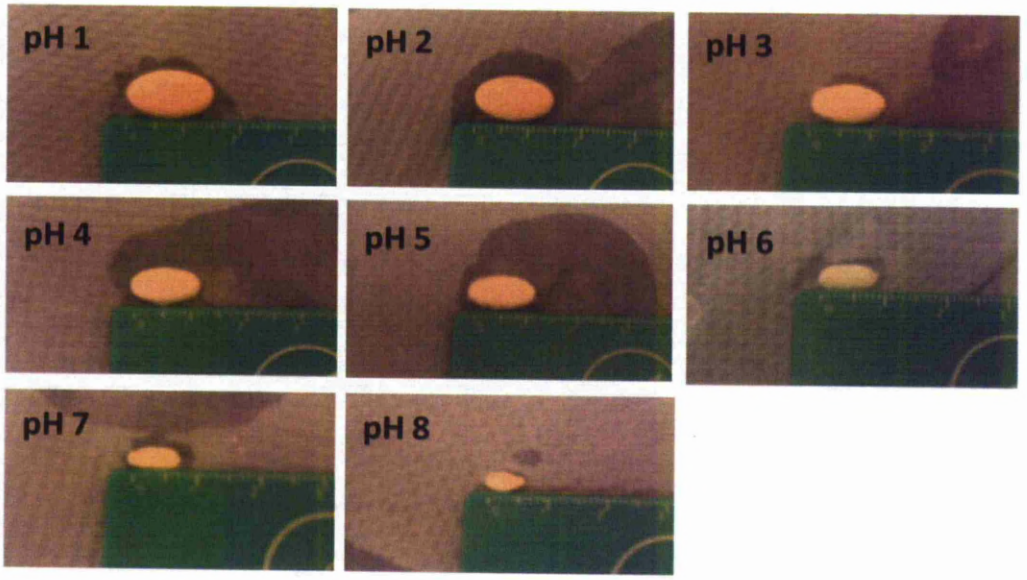

Figure 5.5. Photos of a raltegravir tablet after dissolving for 30 minutes in specified pH buffers. Tablets are places next to a centimetre ruler for comparison.

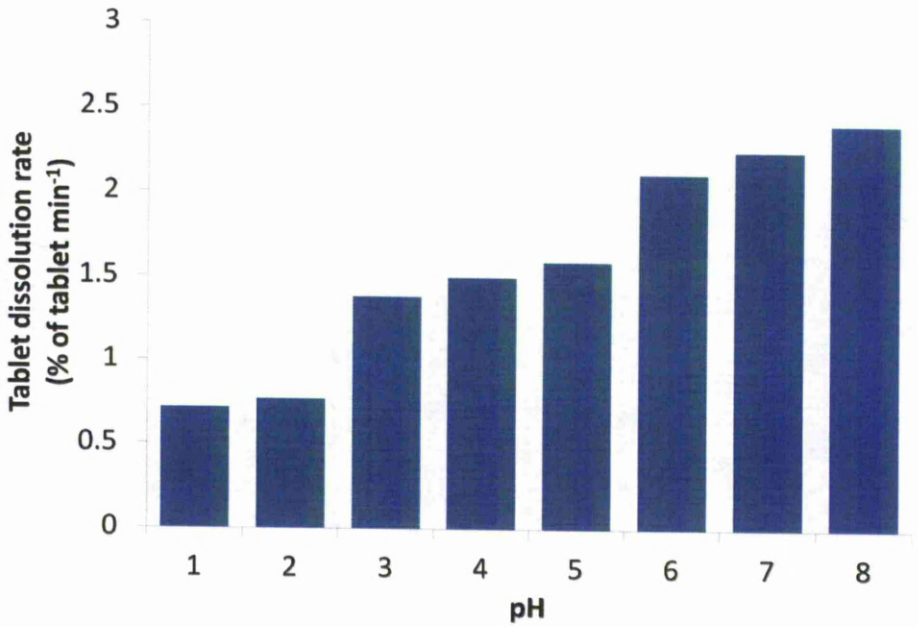

Figure 5.6. Dissolution rate of a 400 mg RAL tablet in a range of buffered pH solutions. Data are expressed as tablet dissolution rate (% of total tablet broken down/minute, n = 1 experimental replicate)

5.3.5 Impact of pH on raltegravir cell monolayer permeation

Figure 5.7 depicts the A-to-B raltegravir permeation through Caco-2 cell monolayers using various apical pH values. Increasing the apical pH from 5 to 8.5 decreased the rate and extent of raltegravir monolayer permeation in the A-to-B direction ($p < 0.05$). The P_{app} and efflux ratio of raltegravir at 60 minutes incubation is shown in Table 5.1. Raltegravir efflux ratio increased 12-fold as apical pH was increased from 5 to 8.5 ($p < 0.05$). When both apical and basolateral pH was 7.4 the efflux ratio was 2.5, suggesting active transport in the basolateral to apical direction. However, reducing apical pH to 6 or below caused raltegravir permeation to predominate in the apical to basolateral direction, suggesting that pH has the potential to overcome the effect of active drug transport.

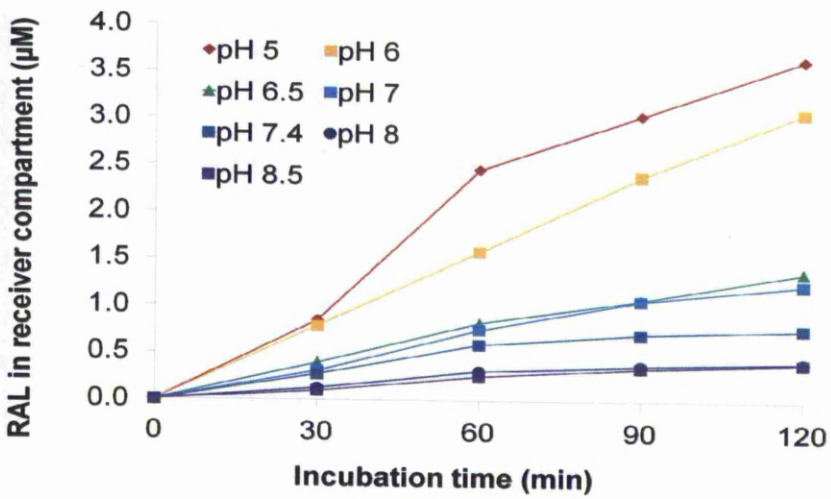

Figure 5.7. Time course experiment showing A-to-B permeation of raltegravir (50 µM) in Caco-2 monolayers over 120 minutes. Results are presented when using a range of apical pH buffers shown in the figure key. The basolateral pH was maintained at 7.4. Data are expressed as mean raltegravir accumulation in the basolateral (receiver) compartment (µM, n = 3 experimental replicates).

pH of apical compartment	A-to-B P_{app} (cm x 10^{-6} $second^{-1}$)	B-to-A P_{app} (cm x 10^{-6} $second^{-1}$)	Efflux ratio	Efflux ratio significance compared to p H5
5	27.3 ± 1.2	11.9 ± 1.5	0.4	-
6	17.6 ± 1.7	13.1 ± 2.3	0.7	$p < 0.05$
6.5	9.2 ± 1.1	14.5 ± 1.5	1.6	$p < 0.05$
7	8.4 ± 1.2	14.5 ± 2.1	1.7	$p < 0.05$
7.4	6.6 ± 0.8	16.4 ± 2.9	2.5	$p < 0.05$
8	3.5 ± 0.5	13.8 ± 0.7	3.9	$p < 0.05$
8.5	2.9 ± 0.3	14.1 ± 1.3	4.9	$p < 0.05$

Table 5.1. The effect of pH on raltegravir (50 μM) permeation using a Caco-2 monolayer. Column one gives the range of apical pH buffers used (basolateral pH was maintained at 7.4). Columns two and three give apparent permeation of raltegravir in the A-to-B and B-to-A directions, respectively. Data are presented as mean P_{app} (cm x 10^{-6} $second^{-1}$, n = 3 experimental replicates) ± SD. Column four gives the efflux ratio of raltegravir ($P_{app\ B\text{-}to\text{-}A}$ / $P_{app\ A\text{-}to\text{-}B}$). Column five compares the efflux ratio at pH 5 with other pH values (a significant difference was deemed to have a p value of < 0.05).

5.3.6 Impact of divalent and monovalent metals on raltegravir cell monolayer permeation

All P_{app} and efflux ratio calculations were made using samples taken after 30 minutes of incubation and sink conditions were maintained at this time point (Table 5.2). A positive correlation between concentration of magnesium chloride in the apical compartment and raltegravir efflux ratio is shown in Figure 5.8. When the apical compartment was pH 7.4, raltegravir efflux ratio was significantly increased when comparing control wells with no additional metal salt (efflux ratio = 1.3) to wells supplemented with 1 mM (efflux ratio = 1.6, $p < 0.05$), 10 mM (efflux ratio = 3.4, $p < 0.05$) or 25 mM (efflux ratio = 3.7, $p < 0.05$) magnesium chloride. Lopinavir efflux

ratio was unaltered when comparing control wells with no additional metal salt (efflux ratio = 5.1) to wells supplemented with 25 mM magnesium chloride (efflux ratio = 5.4, $p = 0.83$) illustrating that the effect of magnesium chloride on raltegravir cellular permeation was not a result of general changes in monolayer integrity.

When the apical compartment was pH 5, raltegravir efflux ratio was unchanged when comparing control wells with no additional metal salt (efflux ratio = 0.8) to wells supplemented with 1 mM magnesium chloride (efflux ratio = 0.7, $p = 0.28$), but a significant increase in efflux ratio was observed when supplemented with 10 mM (efflux ratio = 1.1, $p < 0.05$) or 25 mM (efflux ratio = 1.9, $p < 0.05$) magnesium chloride. Also, the effects of magnesium in a different salt form (magnesium sulphate), an additional divalent metal salt (calcium chloride) and a monovalent metal salt (potassium chloride) were investigated. Raltegravir efflux ratio was significantly increased when comparing control wells with no additional metal salt (efflux ratio = 0.8) to wells supplemented with 25 mM magnesium sulphate (efflux ratio = 1.6, $p < 0.05$) or 25mM calcium chloride (efflux ratio = 1.2, $p < 0.05$). The efflux ratio was unaltered when 25 mM potassium chloride was added to the apical compartment (efflux ratio = 0.8, $p = 0.83$). This supports the hypothesis that divalent metals, but not monovalent metals, have the potential to affect raltegravir cell membrane permeation.

Drug	Apical chamber pH	Metal salt added to apical chamber	Metal concentration (mM)	A-to-B P_{app} (cm x 10^{-6} $second^{-1}$)	B-to-A P_{app} (cm x 10^{-6} $second^{-1}$)	Efflux ratio (B-to-A / A-to-B)	Efflux ratio significance compared to no added salt
Raltegravir	5	none	0	22.8 ± 2.8	17.5 ± 1.0	0.8	-
		$MgCl_2$	1	18.6 ± 3.9	13.1 ± 2.0	0.7	p=0.28
			10	12.3 ± 0.8	13.2 ± 2.4	1.1	p<0.05
			25	7.8 ± 2.3	15.0 ± 0.3	1.9	p<0.05
		$MgSO_4$	25	10.2 ± 1.8	16.0 ± 0.9	1.6	p<0.05
		$CaCl_2$	25	14.7 ± 2.3	17.0 ± 4.2	1.2	p<0.05
		KCl	25	18.8 ± 2.8	14.7 ± 0.3	0.8	p=0.83
	7.4	None	0	11.5 ± 1.0	15.0 ± 0.5	1.3	-
		MgCl2	1	7.2 ± 1.1	11.5 ± 0.8	1.6	p<0.05
			10	4.0 ± 0.6	13.5 ± 0.5	3.4	p<0.05
			25	3.4 ± 0.8	12.5 ± 0.4	3.7	p<0.05
Lopinavir	7.4	none	0	9.9 ± 0.7	50.0 ± 4.6	5.1	-
		MgCl2	25	10.0 ± 0.8	54.4 ± 5.4	5.4	p=0.83

Table 5.2. The effect of metal cations on raltegravir (1 μM) permeation using a Caco-2 monolayer. Column four gives the concentration of metal salt used. Columns five and six give apparent permeation of raltegravir in the A-to-B and B-to-A directions, respectively. Data are presented as mean P_{app} (cm x 10^{-6} $second^{-1}$, n = 3 experimental replicates) ± SD. Column seven gives the efflux ratio of raltegravir (P_{app} B-to-A / P_{app} A-to-B). Column eight compares the efflux ratios with the the efflux ratio when no additional salt was added (a significant difference was deemed to have a p value of < 0.05).

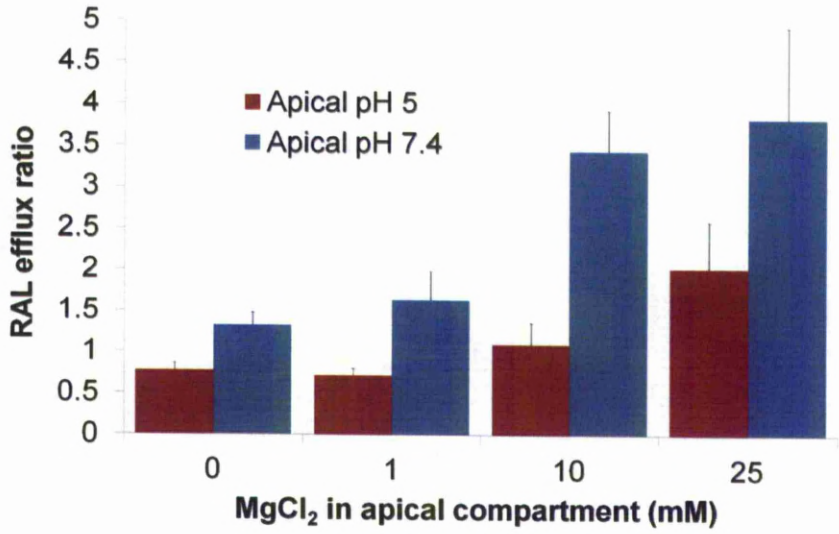

Figure 5.8. Efflux ratio of raltegravir (1 μM) in Caco-2 monolayers using a range of magnesium chloride concentrations in the apical compartment. The apical compartment was maintained at pH 5 (■) or pH 7.4 (■) and the basolateral compartment was maintained at pH 7.4. Data are expressed as mean drug efflux ratio (P_{app} B-to-A / P_{app} A-to-B, n = 3 experimental replicates) ± SD.

5.3.7 Impact of omeprazole on raltegravir cell monolayer permeation

Figure 5.9 depicts the efflux ratio of 1 μM raltegravir through Caco-2 cell monolayers in the presence and absence of omeprazole as an inhibitor (20 μM added during raltegravir incubation) or as an inducer (72 hour pre-incubation of cells with 10 μM omeprazole). All P_{app} and efflux ratio calculations were made using samples taken after 60 minutes of incubation and sink conditions were maintained. In inhibition studies, there was no significant difference in raltegravir efflux ratio between control cells and cells co-incubated with 20 μM omeprazole (efflux ratio of 2.7 versus 2.6, $p = 0.83$). Similarly, in induction studies there was no significant

difference in raltegravir efflux ratio between control cells and cells pre incubated for 72 hours with 10 μM omeprazole (efflux ratio of 2.7 versus 2.6, p = 0.51).

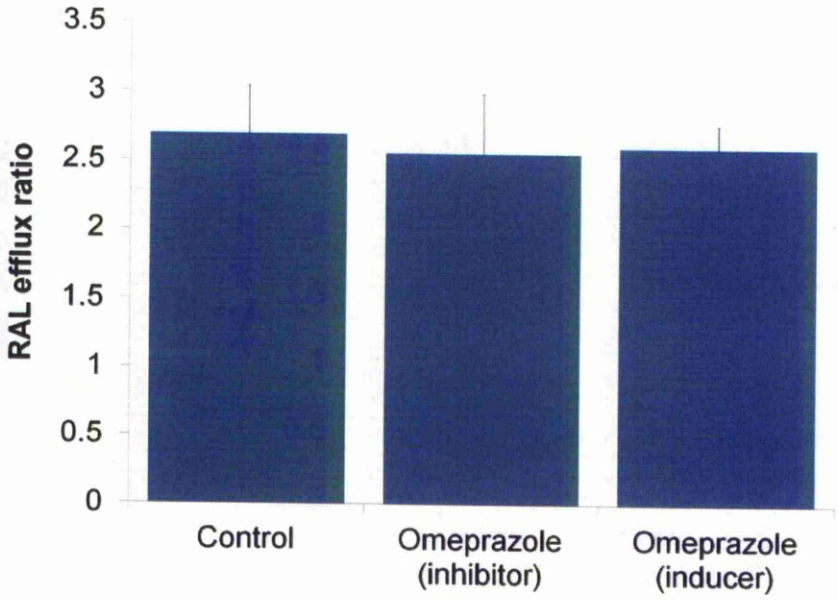

Figure 5.9. Efflux ratio of raltegravir (1 μM) in the presence of omeprazole (inhibitor study, 20 μM) or with cells pre-incubated with omeprazole for 3 days (induction study, 10 μM). Data are expressed as mean drug efflux ratio (P_{app} B-to-A / P_{app} A-to-B, n = 3 experimental replicates) ± SD.

5.3.8 Impact of pH and ABCB1 inhibition on raltegravir cellular accumulation

Figure 5.10 depicts the accumulation of raltegravir in Caco-2 cells using various pH buffers and using tariquidar to inhibit ABCB1. Raltegravir accumulation in Caco-2 cells increased 3.4-fold when incubation buffer pH was decreased from 8 to 5 ($p < 0.05$). This pH-related increase in raltegravir accumulation was also observed in cells treated with the ABCB1 inhibitor tariquidar (3.3-fold decrease, $p < 0.05$). Inhibiting ABCB1 led to increased raltegravir accumulation at pH 5 (1.4-fold, $p < 0.05$), 6 (1.5-

fold, $p < 0.05$), and 7 (1.4-fold, $p < 0.05$) but not significant at pH 8 ($p = 0.08$). These results suggest that pH impacts upon cellular permeation of raltegravir to a greater extent than ABCB1 transport and that ABCB1 transport of raltegravir is independent of pH.

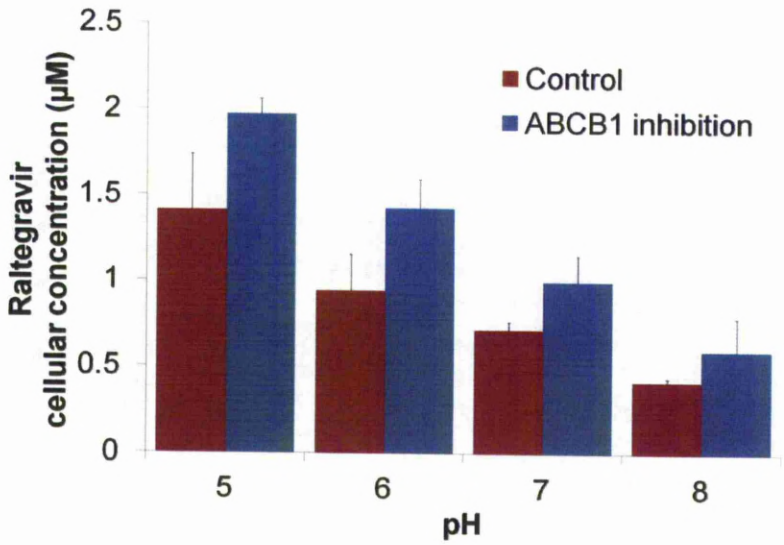

Figure 5.10. Accumulation of raltegravir (1 μM) in Caco-2 cells at extracellular pH of 5 to 8, with (■) and without (■) ABCB1 inhibitor tariquidar (300 nM). Data are expressed as mean intracellular raltegravir (μM, n = 3 experimental replicates) ± SD.

5.4 DISCUSSION

In this chapter the influence of pH on raltegravir solubility, lipophilicity, tablet breakdown and cellular permeation was investigated. Raltegravir exhibited solubility of less than 10 mM at pH 6.6 and below. It is likely that the drug obtains a negative charge at higher pH by deprotonation of the hydroxyl group at the 5-position of the 6-oxo-1,6-dihydropyrimidine ring (Figure 5.11). This negative charge would dramatically increase the solubility of the drug in aqueous buffer. Additionally, raltegravir logP was shown to decrease as pH was increased above 6, presumably due to the introduction of a charge to the drug. Indeed, the solubility and lipophilicity data were supported by the UV spectroscopy data, where raltegravir pKa was calculated at 6.7. This pKa is located within the pH range that would be encountered by the drug during passage through the GI tract. Also, raltegravir tablet breakdown rate was influenced by environmental pH, where increasing pH led to a more rapid dissolution. These investigations offer a convincing explanation for the large intra- and inter-patient variability of raltegravir PK in healthy and HIV-infected subjects (Cattaneo *et al.*, 2012).

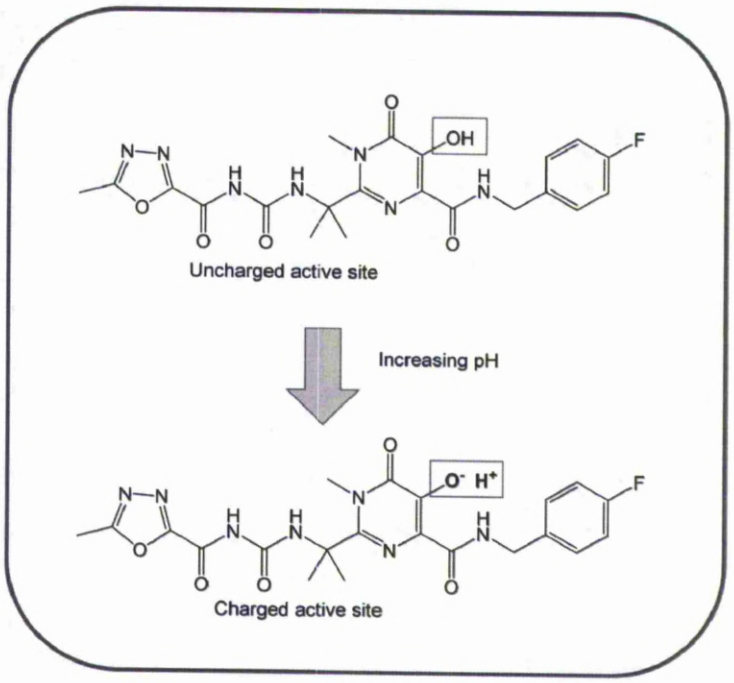

Figure 5.11. The hypothesised effect of increasing pH on the charge state of raltegravir.

In experiments assessing raltegravir cellular permeation, raltegravir was less able to cross a Caco-2 cell monolayer as the incubation buffer pH was increased from 5 to 8.5. This is most likely due to the introduced charge at the active site, preventing the drug from passing through the phospholipid bilayer of the cell membrane. Similar results were seen in accumulation studies, where less raltegravir was present in the cells when pH was increased from 5 to 8. ABCB1 inhibition had less impact on raltegravir intracellular concentrations than changes in extracellular pH. Permeation and accumulation were assessed using raltegravir concentrations from 1 μM to 50 μM and our solubility studies show that the drug was fully soluble at all pH values at these concentrations. Therefore, the introduction of a charge to raltegravir by increasing pH could have opposing consequences depending on the concentration of

the drug: At high drug concentrations the introduced charge would be predicted to increase dissolution and therefore absorption. Conversely, at lower concentrations solubility is unlikely to be an absorption-limiting factor and therefore the introduced charge may reduce the rate of absorption.

In previous clinical studies, co-administration of omeprazole and famotidine resulted in an increase in raltegravir C_{max} (Rhame *et al.*, 2009). This may result from the predicted increased solubility of raltegravir in the stomach and the duodenum, where drug concentrations would be highest. The C_{12hr} of raltegravir was only slightly higher or unchanged when taken with omeprazole or famotidine (Rhame *et al.*, 2009). It is tempting to speculate that over time raltegravir dissolution normalizes in all subjects and the benefit of increased gastric pH is overcome. Results from inhibition and induction studies using omeprazole indicated that there were no direct effects on raltegravir cellular permeation, indicating that the effect of omeprazole most likely results from its pH-altering properties.

Ingestion of a meal has been shown to result in an increase in gastric pH (Charman *et al.*, 1997), which would be predicted to increase raltegravir solubility. However, only high fat meals have been shown to increase raltegravir exposure with low fat meals resulting in a reduction (Brainard *et al.*, 2011a). It is possible that a high fat meal may dilute stomach acid to a greater extent or that the fat in the meal could increase the solubility of raltegravir.

Raltegravir cellular permeation decreased in the presence of the divalent cations magnesium and calcium in the incubation medium. This decrease was not found when the monovalent cation potassium was used. Raltegravir may bind to the divalent metals and form a metal-drug complex which is unable to cross the cell membrane. It is important to note that binding of raltegravir to a divalent metal (magnesium) is a prerequisite for inhibition of the HIV integrase enzyme (Loizidou *et al.*, 2009). Antacids containing magnesium caused no significant change in raltegravir C_{max} or AUC but did reduce C_{12hr}, resulting in 75% of patients having C_{12hr} less than the IC_{95} (Kiser *et al.*, 2010). The impact of antacids may be explained by a combination of the effects of pH and metal binding. It can be hypothesised that C_{max} remains unchanged while raltegravir solubility improves with increased pH but absorption is inhibited by magnesium binding. At later time points, when raltegravir solubility is no longer an issue, the elevated presence of magnesium in the gut may reduce the amount of raltegravir being absorbed, thus reducing raltegravir C_{12hr}. If true, co-administration of products containing polyvalent metal cations that do not alter gastric pH (e.g. multivitamin tablets) would be expected to reduce raltegravir exposure. This is certainly now worthy of empirical determination.

These data may also have implications for newer integrase strand transfer inhibitors, elvitegravir and dolutegravir. Elvitegravir and dolutegravir exposure have been shown to be reduced when taken with antacids containing magnesium and aluminium, being less marked when taken 2 hours before the antacid (Patel *et al.*, 2011; Ramanathan *et al.*, 2007a). In healthy subjects, elvitegravir and dolutegravir absorption have also been shown to be influenced by food according to fat content (German *et al.*, 2009; Song *et al.*, 2011) and it is recommended that elvitegravir is

taken with food (Ramanathan *et al.*, 2011). Interestingly, dolutegravir exposure has also been shown to be moderately reduced when taken with a multivitamin containing magnesium, calcium, iron, zinc and copper (Patel *et al.*, 2011).

In conclusion, the physicochemical properties of raltegravir are heavily influenced by pH. Both pH and polyvalent metals have the potential to alter the pharmacokinetics of raltegravir and these data help provide a rationale for the variability in raltegravir exposure seen in patients. The evaluation of how divalent metal-containing products, such as multivitamins that do not affect gastric pH, alter raltegravir pharmacokinetics in patients is now justified.

Chapter 6

Development of a population-based ADME simulator to predict raltegravir exposure

Table of Contents

6.1 INTRODUCTION

Raltegravir shows unusually large variability in PK both between patients and in the same patient over time. For example, Siccardi et al observed high variability in raltegravir C_{trough}, with median coefficient of variation (CV%) of 128% and 245% for inter- and intra-patient variability, respectively (Siccardi *et al.*, 2012b). This high variability has impeded the inclusion of raltegravir in therapeutic drug monitoring.

Over half (141 of 255) of patients who failed raltegravir therapy in a recent multicenter drug efficacy study had HIV with no detectable integrase resistance mutations (Geretti *et al.*, 2010). A smaller study found that 18% (2 of 11) of patients who failed raltegravir therapy had no evidence of HIV integrase mutations (da Silva *et al.*, 2010). These studies suggest that raltegravir therapy failure may occur independently of HIV resistance mutations. Raltegravir PK may be an influencing factor, although this could not be shown as patient PK samples were not obtained in the studies.

A statistically significant correlation between raltegravir PK and virological response has recently been demonstrated in patients. The QDMRK study investigated the PK parameters of raltegravir 400 mg twice-daily versus 800 mg once-daily in treatment-naive HIV-infected patients, and whether PK was predictive of virological efficacy (Rizk *et al.*, 2012). Results showed the once-daily treatment was less effective than the twice-daily treatment at achieving HIV RNA < 50 copies/mL (83% versus 89%). No correlation between raltegravir PK and virological response was found in patients taking 400 mg twice-daily raltegravir, possibly due to high PK variability, whereas C_{trough} was a predictor of raltegravir treatment failure in patients taking 800 mg once-

daily. Specifically, the lowest quartile C_{trough} in the once-daily arm (13.6 ng/mL) showed increased virological failure. Importantly, this C_{trough} was below 15 ng/mL, the IC_{95} of raltegravir against HIV-1 in 50% human serum. These data give evidence that raltegravir PK is potentially a determining factor in treatment success and that high inter-patient and inter-occasion variability (and often low patient numbers) in raltegravir PK studies may be the main issue in establishing a reliable raltegravir PK-PD relationship.

A population PK model has been published based on the data from six fasted healthy volunteers given a single 400 mg dose of raltegravir (Wang *et al.*, 2011). Another model has been published based on the data from 145 HIV-infected patients and 19 healthy volunteers (Arab-Alameddine *et al.*, 2012). The PK data used in both of these studies was highly variable and both concluded that the lack of information on factors with a potential effect on raltegravir absorption limits the interpretation of the results. This is the problem that this thesis has set out to tackle by investigating the impact of transporters, pH and various other factors on raltegravir disposition *in vitro*. However, *in vitro* data of this type is of only limited use to traditional population PK modelling, as the main sources of data for these models come from clinical studies and patient data. Therefore, a computational drug PK modelling system that combines both *in vitro* and *in vivo* data would be seen as the most productive option for raltegravir.

In vitro in vivo extrapolation (IVIVE) is the process of using *in vitro* data such as drug physicochemistry, permeability and metabolism to predict *in vivo* drug characteristics using PK simulation modelling. The Simcyp population-based ADME

simulator (Soldin *et al.*, 2011) utilises a "bottom-up" approach that integrates demographic factors (age, weight, height, sex, genetic polymorphisms, race, disease, etc), anatomical and physiological factors (organ size, blood flow, enzymes, transporters, plasma protein, gastric pH, transit time, etc) and drug-specific factors (molecular weight, pKa, logP, solubility, permeability, etc). These data are included in physiologically-based pharmacokinetic (PBPK) models, based on multi-compartmental equations that mimic the absorption, distribution, metabolism and elimination processes in the human body.

Oral absorption of a drug can be simulated using different approaches and taking into account the dynamic interplay of tablet disintegration, dissolution, solubility, intestinal permeation, and, for some drugs, metabolism. The Advanced Dissolution Absorption and Metabolism (ADAM) Model within Simcyp represents the GI tract as compartments based upon their physiological and anatomical characteristics and the relationship between permeability, metabolism and dissolution, amongst other factors, can be simulated (Darwich *et al.*, 2010).

.

This approach can be used to investigate drug disposition in drug discovery and development, such as PK profiling, drug-drug interactions, bioavailability and drug exposure in special populations (children, liver disease, kidney disease, etc). Moreover, design of a clinical trial can be optimized by IVIVE by determining how factors such as sample size, sex ratio and age may influence the final results.

The aim of this chapter was to develop an IVIVE model for simulating raltegravir PK and to investigate the role of GI pH and ingested magnesium using the ADAM

model. The influence of multiple dosing on raltegravir PK was also determined and compared to single dose. The model detailed in this chapter included data from previous clinical trials and also contained *in vitro* data generated during this project. This combined approach has provided a system to help determine which physiological and drug-based attributes are important in predicting raltegravir PK in virtual individuals.

6.2 METHODS

6.2.1 In vitro-in vivo extrapolation: drug parameters

Raltegravir PK properties were simulated using the full PBPK model implemented in the Simcyp Population-based Simulator (Version 11.0, Simcyp Limited, UK). Data describing raltegravir physiochemical and pharmacological properties were added to the model and were either derived from in-house *in vitro* data, literature sources or predicted by the Simcyp model (Figure 6.1) and are summarised in Table 6.1. Intrinsic solubility of raltegravir at pH 1-9 was predicted using ACD/PhysChem Suite (Toronto, Canada) and data were added to the Simcyp model (Figure 6.2).

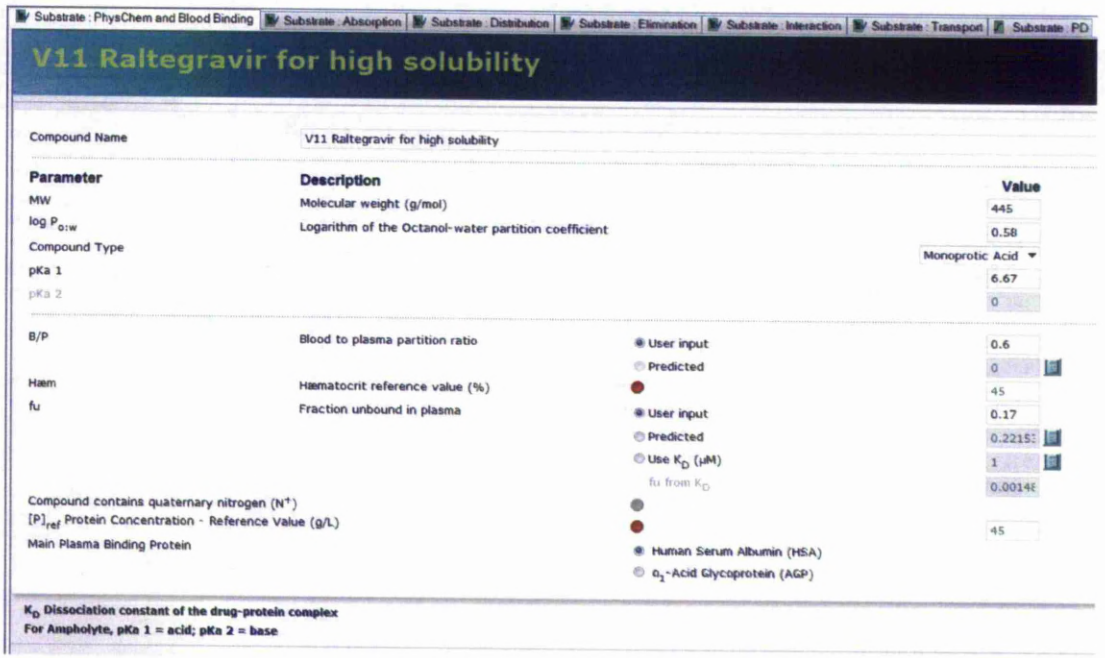

Figure 6.1. The interface screen of the Simcyp Population-based Simulator.

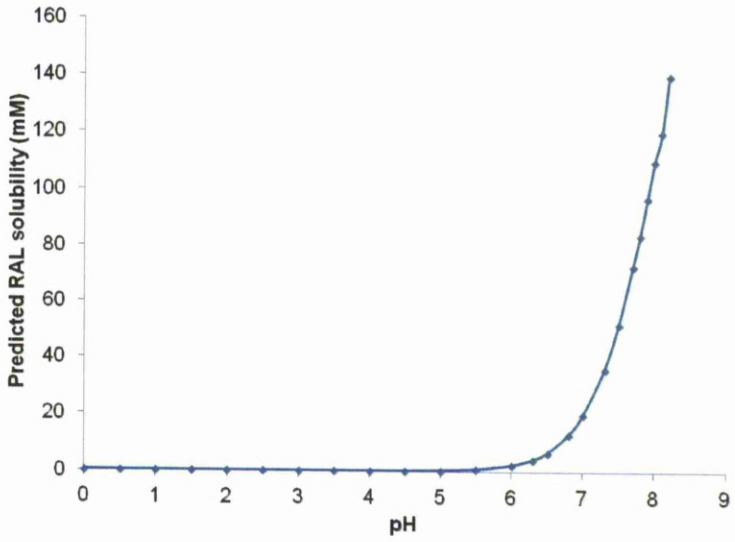

Figure 6.2. Predicted intrinsic solubility of raltegravir across a physiological pH range. Solubility was predicted using molecular structure, charge state and pKa using ACD/PhysChem Suite (Toronto, Canada) and data was added to the Simcyp model.

	Input parameters	Value	Reference
PhysChem	Molecular weight	445.16	(Summa *et al.*, 2008)
	$LogP_{O:W}$	0.58	In-house
	pKa	6.67	In-house
	B/P	0.6	(Laufer *et al.*, 2009)
	fu	0.17	(Laufer *et al.*, 2009)
Absorption	P_{app} pH 7.4 ($x10^{-6}$ cm/s)	6.6	In-house
	Tablet release rate	(see Figure 5.6)	In-house
	Solubility-pH profile	(see Figure 6.2)	Predicted
Distribution	Vss (L/kg)	0.308	SimCyp predicted
Elimination	Hepatic Cl_{int} (µL/min/10^6)	12.4	(Wang *et al.*, 2011)
	Cl_R (L/hr)	3.6	(Iwamoto *et al.*, 2008d)

Table 6.1. Input parameters detailing raltegravir properties. $LogP_{o:w}$ = Log partition coefficient between octanol and water (pH 7); B/P = blood to plasma drug ratio; fu = free drug fraction in plasma; P_{app} pH 7.4 = apical to basolateral apparent permeability in Caco-2 monolayer at pH7.4; Vss = volume of distribution (L/kg); Cl_{int} = intrinsic clearance (µL/min/10^6); Cl_R = renal clearance (L/hr).

6.2.2 *In vitro-in vivo* extrapolation: population parameters

All system parameters were taken from the North European Caucasian population library within Simcyp (Jamei *et al.*, 2009) with the exception of patient GI pH values, which were obtained from literature sources (Charman *et al.*, 1997; McCloy *et al.*, 1984; Rune *et al.*, 1969). All simulations except the simulation in Section 6.3.1 were performed in 5 separate groups of 50 healthy individuals, named Groups 1, 2, 3, 4 or 5. These groups contained individuals with the same physiological attributes to each other except for average GI pH values, which differed between groups and are shown in Table 6.2. All simulations consisted of 50% female subjects.

	Group 1 (very low pH)	Group 2 (low pH)	Group 3 (medium pH)	Group 4 (high pH)	Group 5 (very high pH)
Stomach residence time (hours)	0.4	0.4	0.4	0.4	0.4
Stomach pH	1	2.5	3	5	6
Intestine residence time (hours)	3.34	3.34	3.34	3.34	3.34
Duodenum pH	4	4.5	5	6	6.4
Jejunum pH	4.4	5	5.5	6.8	7
Ileum pH	6.4	6.8	7.4	7.6	8
Colon residence time (hours)	12	12	12	12	12
Colon pH	5	5.5	6	6.2	6.5

Table 6.2. Values for mean GI pH and residence time added to the model. Each pH value is the mean for a population representative and each segment had a CV% of 2% when determining pH for individuals in a group. Each residence time is the mean for a population representative and each segment had a CV% of 30% when determining GI transit time for individuals in a group.

6.2.3 In vitro-in vivo extrapolation: simulation design

Raltegravir (400 mg, single dose) PK was simulated in healthy volunteers (20-50 years old, 0.5 proportion female) over 12 hours. The number of simulated subjects in each group was initially investigated (5-75 individuals, Figure 6.3) and 50 individuals were chosen as the optimal population number for each group and used in all subsequent simulations. Simulated PK results were compared with actual PK in published data and used to calculate the geometric mean values for C_{max} (ng/mL), $AUC_{0\text{-}12hr}$ (ng/mL.hr), C_{trough} (ng/mL) and fa (fraction of dose absorbed), which were given with 5^{th} and 95^{th} percentiles. Median T_{max} (hours) was calculated and given with range.

A parallel trial was performed as described above to simulate the impact of elevated GI magnesium concentrations on raltegravir PK values. Drug parameters were altered so that Caco-2 monolayer P_{app} of raltegravir was reduced from 6.6 to 3.4 (obtained from data in Chapter 5), simulating the impact of 25 mM magnesium salt on raltegravir P_{app}.

In order to assess the effect of long-term multiple dosing on raltegravir PK, a parallel trial was performed where subjects were given 400 mg raltegravir every 12 hours for a total of five doses, simulating the current twice-daily dosing of patients in the clinical setting. PK values were determined for the final dose only and was compared with single dose raltegravir PK.

6.3 RESULTS

6.3.1 The impact of subject sample size on raltegravir exposure and result accuracy

In order to determine a suitable number of subjects to use in each simulation which balanced simulation run time with result reliability, an initial simulation was run to assess the impact of subject sample size on raltegravir $AUC_{0\text{-}12hr}$ using subjects from Group 3 (Figure 6.3). The geometric mean $AUC_{0\text{-}12hr}$ (ng/mL.hr, 95% CI) when 5, 10, 25, 50 or 75 subjects were used was 6141.3 (3807.2-9906.6), 7588.3 (5598.6-10285.2), 7927.5 (6771.5-9280.9), 8164.6 (7281.1-9155.4) and 8453.0 (7757.6-9210.7), respectively. Fifty subjects per group was chosen as the number to use in all subsequent simulations, as 95% CI were considered acceptable and the geometric mean $AUC_{0\text{-}12hr}$ for 50 subjects was not significantly different to when 75 patients were used ($p = 0.58$).

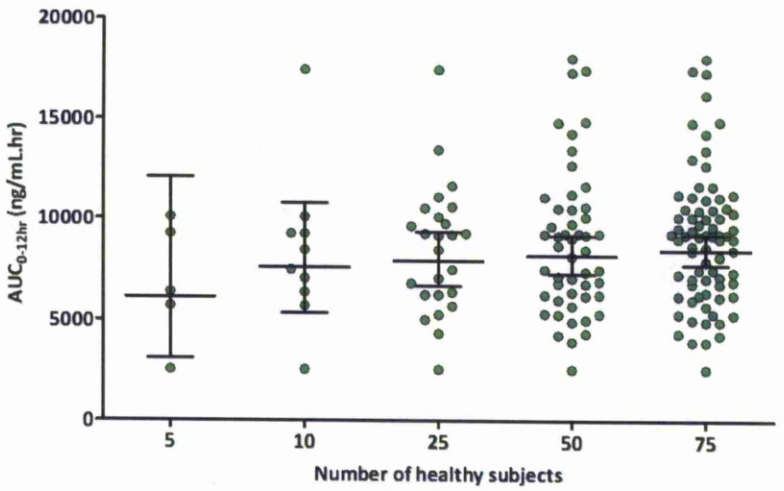

Figure 6.3. The effect of subject sample size on average simulated raltegravir exposure. Group 3 individuals were used and given a single 400 mg raltegravir tablet. Data are given as geometric mean $AUC_{0\text{-}12hr}$ (mg/mL.hr) with 95% CI.

6.3.2 The impact of GI pH on raltegravir solubility

The impact of pH on raltegravir solubility in the GI tract is shown in Table 6.3. A general trend towards increased raltegravir solubility in all GI segments can be observed by progressing from Group 1 to 5. The subjects between groups only differ in average GI pH values (Group 1 has very low GI pH, progressing to Group 5 with very high GI pH; see Table 6.2), therefore the increase in raltegravir solubility is likely a direct effect of increased GI pH.

	Group 1 (very low pH)	Group 2 (low pH)	Group 3 (medium pH)	Group 4 (high pH)	Group 5 (very high pH)
Solubility in stomach (mg/mL)	0.04	0.04	0.04	0.12	0.98
Solubility in duodenum (mg/mL)	0.04	0.08	0.12	0.98	2.4
Solubility in jejunum (mg/mL)	0.07	0.12	0.33	5.78	8.89
Solubility in ileum (mg/mL)	2.4	5.78	20.27	29.95	37.33
Solubility in colon (mg/mL)	0.12	0.33	0.98	1.57	2.93

Table 6.3. Raltegravir solubility in each segment of the GI tract. Results are shown as the mean solubility (mg/mL) for each group. Each group contained 50 individuals.

6.3.3 The impact of GI pH on raltegravir PK parameters

The impact of GI pH on raltegravir PK parameters in subject Groups 1 to 5 is shown in Table 6.4. A general trend towards increased raltegravir exposure can be observed by progressing from Group 1 (very low GI pH) to 5 (very high GI pH). Median T_{max} values are decreased as GI pH increased, which may be due to decreased tablet dissolution time and higher drug solubility during the earlier stages of the GI tract. Bivariate analysis showed that intestinal transit time strongly correlated with the fraction of raltegravir dose absorbed in individuals from each group ($p < 0.001$) and

that a decrease in intestinal transit time resulted in decreased raltegravir absorbance. The absorption rate of drug from individual GI segments, the total drug absorbed from each GI segment and the PK profile is given for Group 1 (Figure 6.4), Group 2 (Figure 6.5), Group 3 (Figure 6.6), Group 4 (Figure 6.7) and Group 5 (Figure 6.8).

	Group 1 (very low pH)	Group 2 (low pH)	Group 3 (medium pH)	Group 4 (high pH)	Group 5 (very high pH)
C_{max} (ng/mL)	1491.8	1980.0	2094.0	2541.3	2545.4
5^{th}-95^{th} percentile	(821.4-2835.7)	(1376.3-3402.9)	(1415.5-3657.4)	(1675.8-4382.6)	(1645.2-4147.9)
$AUC_{0\text{-}12hr}$ (ng/mL.hr)	5756.2	7285.4	8164.6	10136.7	11045.8
5^{th}-95^{th} percentile	(2485.5-12335.4)	(3769.7-14644.7)	(4308.2-16230.6)	(5320.9-18916.3)	(6169.1-19690.5)
T_{max} (hours) Range	3.7 (1.3-5.3)	3.3 (1.4-4.4)	3.2 (1.3-4.3)	2.3 (1.3-3.1)	2.1 (1.2-2.9)
C_{trough} (ng/mL)	30.9	51.4	113.2	153.2	188.2
5^{th}-95^{th} percentile	(8.4-60.9)	(21.6-93.6)	(58.4-210.1)	(87.3-254.7)	(95.4-312.8)
fa	0.39	0.49	0.55	0.69	0.75
5^{th}-95^{th} percentile	(0.16-0.60)	(0.26-0.67)	(0.34-0.73)	(0.45-0.86)	(0.54-0.91)

Table 6.4. Simulated PK values after a single dose of 400 mg raltegravir. Groups 1-5 each had 50 individuals and represented very low (Group 1) to very high (Group 5) GI pH. Geometric mean values for C_{max} (ng/mL), $AUC_{0\text{-}12hr}$ (ng/mL.hr), C_{trough} (ng/mL) and fa (fraction of dose absorbed) are given with 5^{th} and 95^{th} percentiles. Median T_{max} (hours) is given with range.

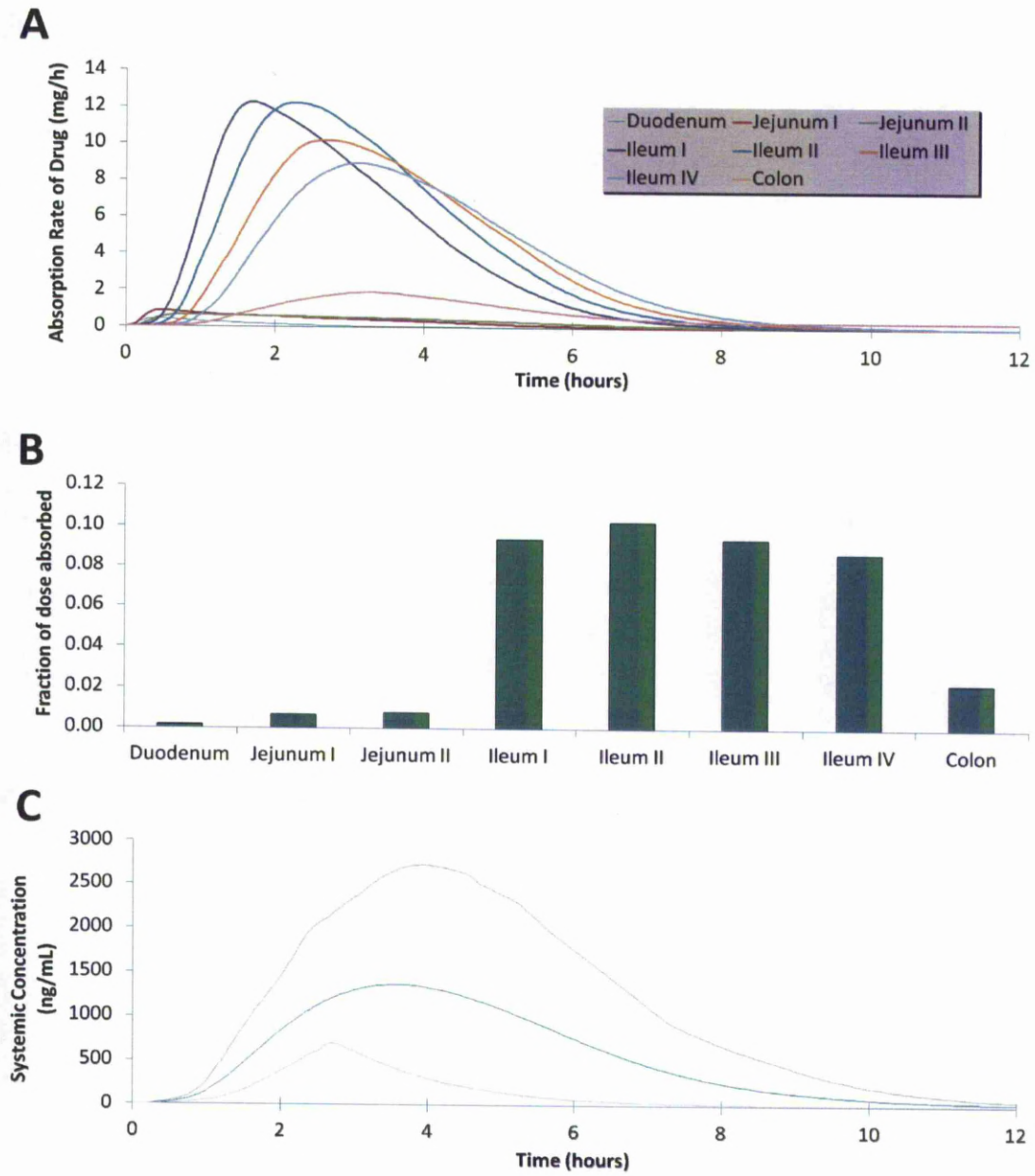

Figure 6.4. A. Mean simulated raltegravir absorption rate (mg/hour) in each GI segment from 50 Group 1 subjects. **B.** Mean simulated fraction of raltegravir absorbed (drug absorbed in segment/total drug) in each GI segment from 50 Group 1 subjects. **C.** Simulated raltegravir plasma concentration-time profile (ng/mL, green line) with 5th and 95th percentiles (grey lines) from 50 Group 1 subjects.

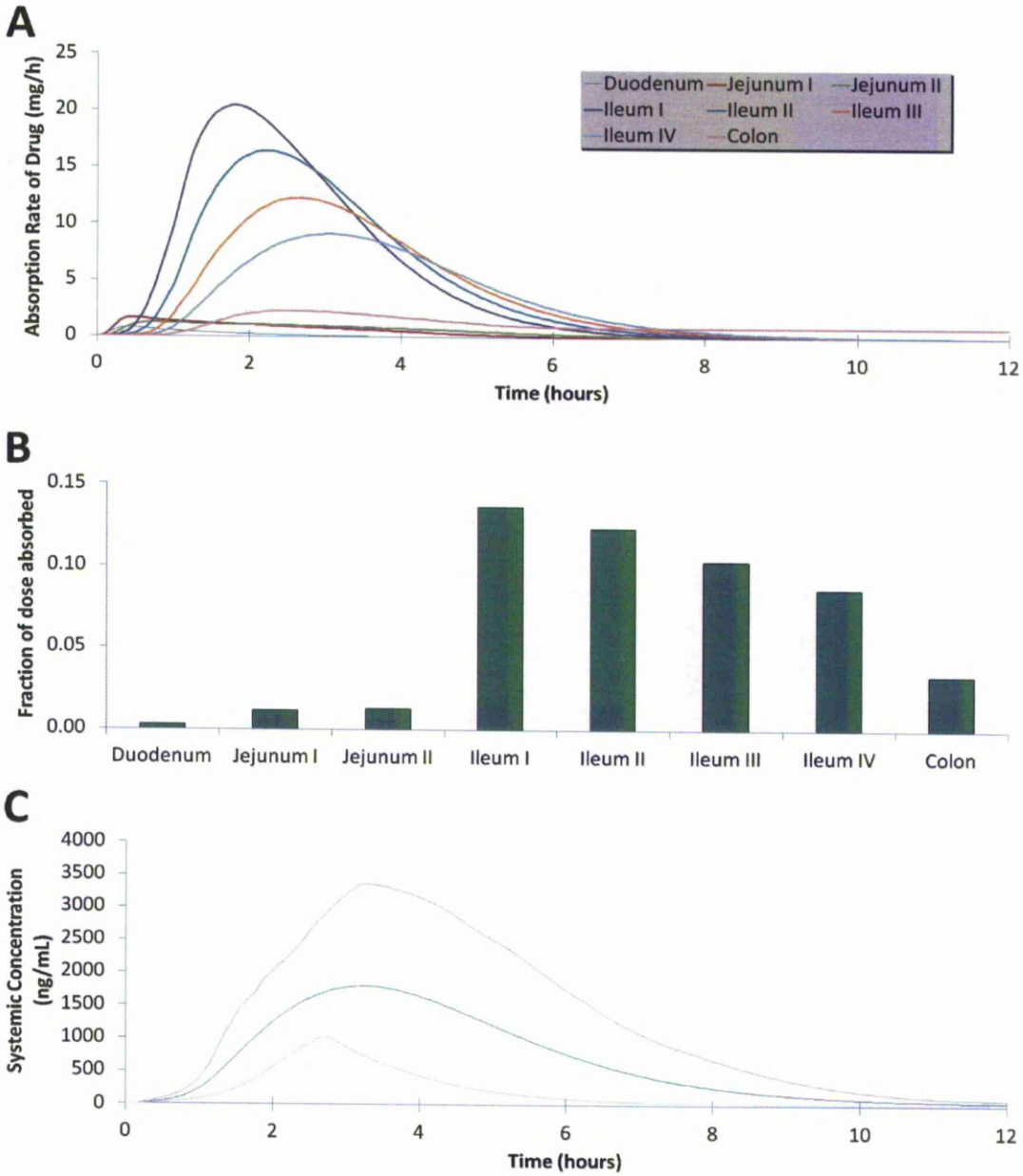

Figure 6.5. A. Mean simulated raltegravir absorption rate (mg/hour) in each GI segment from 50 Group 2 subjects. **B.** Mean simulated fraction of raltegravir absorbed (drug absorbed in segment/total drug) in each GI segment from 50 Group 2 subjects. **C.** Simulated raltegravir plasma concentration-time profile (ng/mL, green line) with 5th and 95th percentiles (grey lines) from 50 Group 2 subjects.

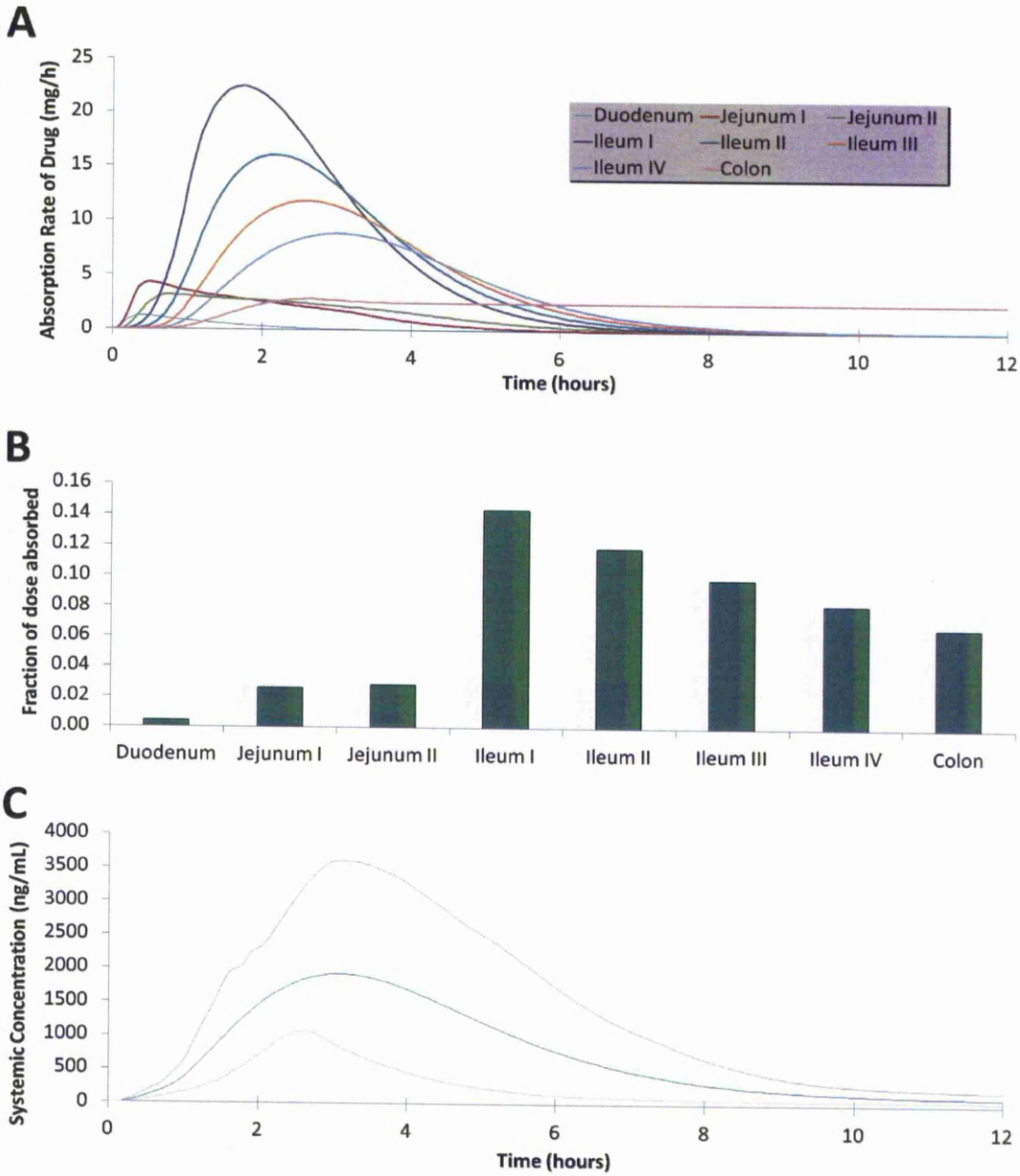

Figure 6.6. A. Mean simulated raltegravir absorption rate (mg/hour) in each GI segment from 50 Group 3 subjects. **B.** Mean simulated fraction of raltegravir absorbed (drug absorbed in segment/total drug) in each GI segment from 50 Group 3 subjects. **C.** Simulated raltegravir plasma concentration-time profile (ng/mL, green line) with 5th and 95th percentiles (grey lines) from 50 Group 3 subjects.

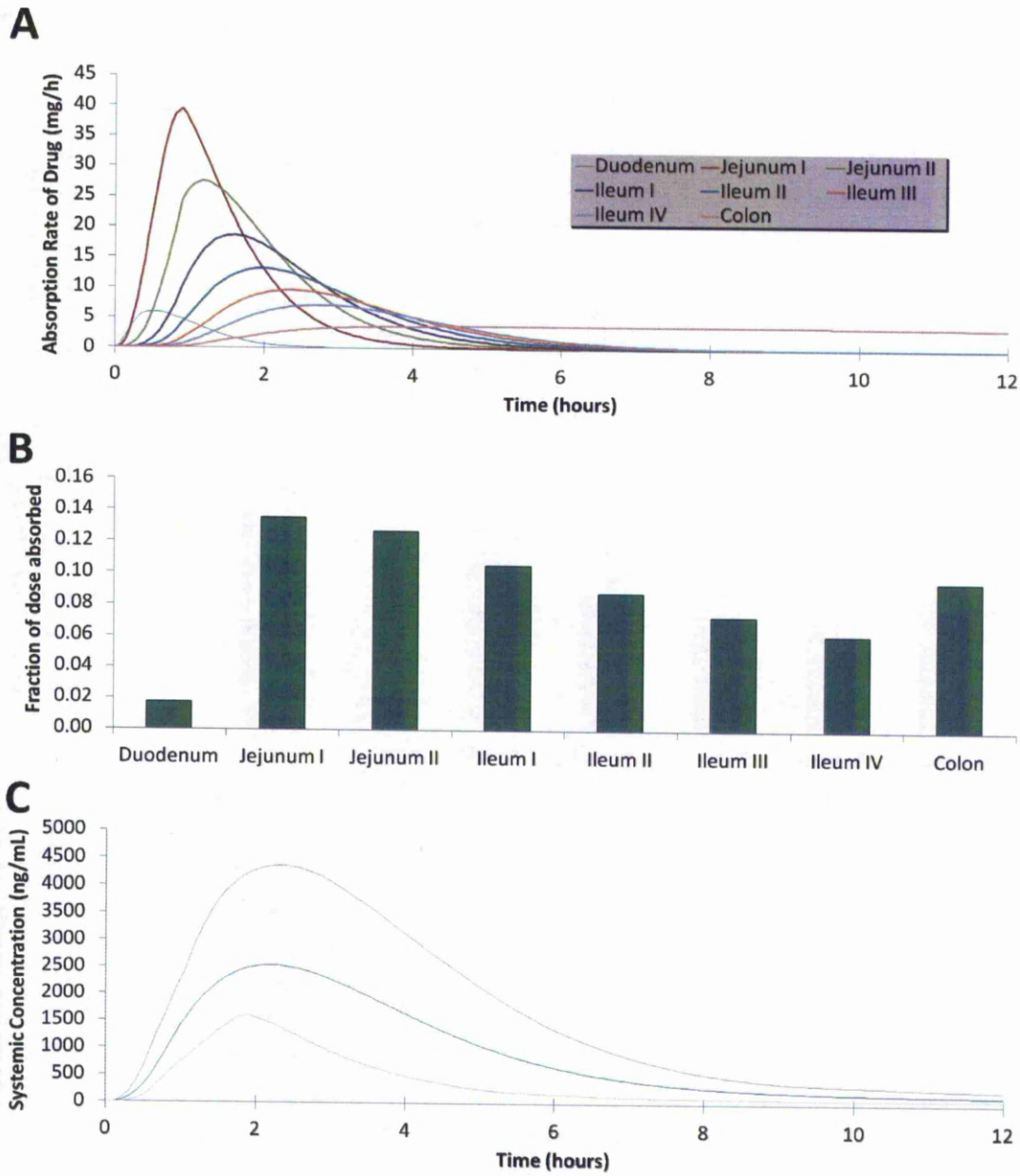

Figure 6.7. A. Mean simulated raltegravir absorption rate (mg/hour) in each GI segment from 50 Group 4 subjects. **B.** Mean simulated fraction of raltegravir absorbed (drug absorbed in segment/total drug) in each GI segment from 50 Group 4 subjects. **C.** Simulated raltegravir plasma concentration-time profile (ng/mL, green line) with 5th and 95th percentiles (grey lines) from 50 Group 4 subjects.

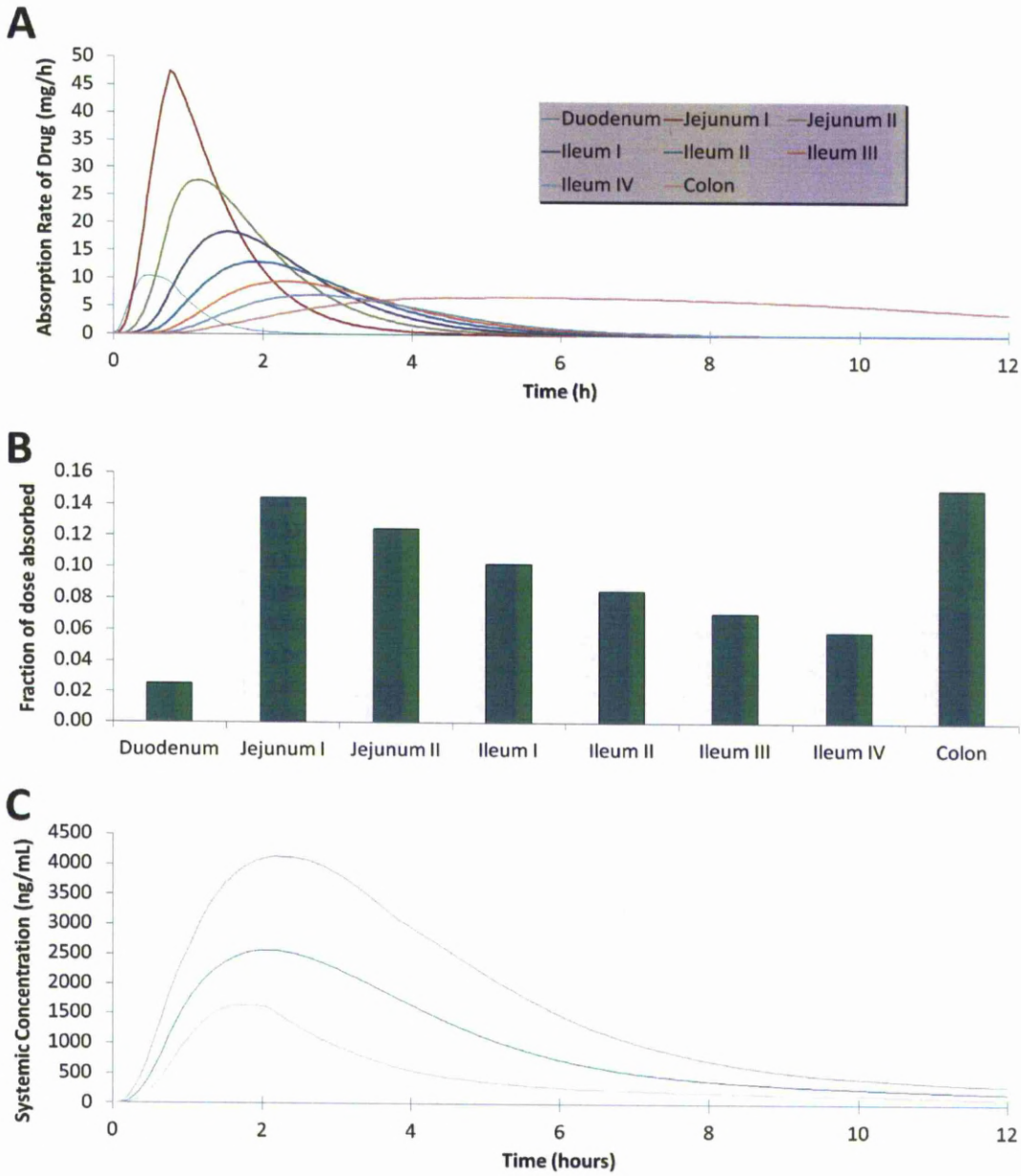

Figure 6.8. A. Mean simulated raltegravir absorption rate (mg/hour) in each GI segment from 50 Group 5 subjects. **B.** Mean simulated fraction of raltegravir absorbed (drug absorbed in segment/total drug) in each GI segment from 50 Group 5 subjects. **C.** Simulated raltegravir plasma concentration-time profile (ng/mL, green line) with 5th and 95th percentiles (grey lines) from 50 Group 5 subjects.

6.3.4 Comparison between reference and simulated raltegravir PK values

Reference PK values (mean ± SD) for C_{max} (2519 ± 1930 ng/ml), $AUC_{0\text{-}12hr}$ (7076 ± 4071 ng/ml) and C_{trough} (71 ± 50 ng/mL.h) are shown in Table 6.5 and are the averages of geometric mean values for fasted, healthy volunteers in selected previous studies (Brainard *et al.*, 2011a; Iwamoto *et al.*, 2009b; Iwamoto *et al.*, 2008d; Kassahun *et al.*, 2007; Kiser *et al.*, 2010; Wang *et al.*, 2011). All reference values displayed high inter-study variability, as shown by the large standard deviations, and this is why an average between studies was used. Simulated PK fell within the range of reference PK values. Group 2 displayed the best match with reference value $AUC_{0\text{-}12hr}$ (+4% deviation) and C_{trough} (-30% deviation), although the reference C_{max} value was most closely predicted in Group 4 (+3% deviation). Groups 2 and 4 reperesent populations with "low" and "high" GI pH values, respectively (Table 6.2).

	Reference value (± SD)	Group 1 (very low pH)	Group 2 (low pH)	Group 3 (medium pH)	Group 4 (high pH)	Group 5 (very high pH)
C_{max} (ng/mL)	2519 ± 1930	1466	1952	2101	2599	2654
% diff from real life	N/A	-42%	-23%	-17%	+3%	+5%
$AUC_{0\text{-}12hr}$ (ng/mL.hr)	7076 ± 4071	5783	7356	8454	10509	11788
% diff from real life	N/A	-18%	+4%	+19%	+49%	+67%
C_{trough} (ng/mL)	71 ± 50	29	50	112	152	200
% diff from real life	N/A	-60%	-30%	+57%	+113%	+180%

Table 6.5. Comparison of actual PK values with simulated PK values. Each simulated group contained 50 individuals. Geometric mean values for C_{max} (ng/mL), $AUC_{0\text{-}12hr}$ (ng/mL.hr), C_{trough} (ng/mL) and fa (fraction of dose absorbed) are given and the percentage difference of each simulated result to the reference value is calculated.

6.3.5 The impact of magnesium on raltegravir exposure

The impact of magnesium binding on raltegravir PK values in subject Groups 1 to 5 is shown in Table 6.6. GMR were generated which were the ratios between raltegravir PK values in the presence of elevated GI magnesium concentrations compared with the standard conditions given in Table 6.4. Simulated C_{max}, AUC and C_{trough} were all significantly ($p < 0.008$) reduced by the presence of magnesium in the GI tract. Raltegravir T_{max} was not significantly altered by magnesium in Groups 1 ($p = 0.49$), 2 ($p = 0.29$) or 3 ($p = 0.34$) but was significantly increased in Groups 4 (2.6 hours versus 2.3 hours, $p = 0.003$) and 5 (2.5 hours versus 2.1 hours, $p = 0.001$). The increased T_{max} in Groups 4 and 5 are likely a result of an inhibited rate of raltegravir absorption, caused by reduced tablet breakdown and lower drug solubility.

	Group 1 (very low pH)	Group 2 (low pH)	Group 3 (medium pH)	Group 4 (high pH)	Group 5 (very high pH)
C_{max} (ng/mL)	841.7	1215.3	1300.5	1603.9	1616.2
5th-95th percentile	(446.3-1610.8)	(831.4-2113.8)	(858.0-2330.8)	(1013.9-2842.4)	(1028.0-2671.5)
GMR	0.56	0.61	0.62	0.63	0.63
p value	< 0.001	< 0.001	< 0.001	< 0.001	< 0.001
$AUC_{0\text{-}12hr}$ (ng/mL.hr)	3435.7	4634.9	5208.0	6711.6	7358.9
Range	(1394.3-7542.3)	(2214.6-9766.6)	(2623.0-10697.6)	(3305.1-13023.4)	(3769.1-13570.3)
GMR	0.60	0.64	0.64	0.61	0.67
p value	< 0.001	< 0.001	< 0.001	< 0.001	< 0.001
T_{max} (hours)	3.8	3.5	3.3	2.6	2.5
Range	(1.4-5.7)	(1.4-4.7)	(1.4-4.5)	(1.3-3.5)	(1.3-3.4)
Median ratio	1.03	1.06	1.03	1.13	1.19
p value	0.49	0.29	0.34	0.003	0.001
C_{trough} (ng/mL)	21.9	33.3	66.2	90.3	152.1
5th-95th percentile	(4.6-58.2)	(11.8-63.2)	(32.5-119.8)	(48.4-153.5)	(88.9-253.6)
GMR	0.71	0.65	0.58	0.59	0.81
p value	0.008	< 0.001	< 0.001	< 0.001	0.005
fa	0.23	0.31	0.35	0.45	0.50
5th-95th percentile	(0.09-0.38)	(0.15-0.46)	(0.20-0.50)	(0.27-0.64)	(0.31-0.67)
GMR	0.59	0.63	0.64	0.65	0.67
p value	< 0.001	< 0.001	< 0.001	< 0.001	< 0.001

Table 6.6. Simulated raltegravir PK values in the presence of elevated magnesium GI concentrations. Each group contained 50 individuals. Geometric mean values for C_{max} (ng/mL), $AUC_{0\text{-}12hr}$ (ng/mL.hr), C_{trough} (ng/mL) and fa (fraction of dose absorbed) are given with 5^{th} and 95^{th} percentiles. Median T_{max} (hours) is given with range. Values in Table 6.6 have been divided by corresponding values in Table 6.4 to calculate the GMR (C_{max}, $AUC_{0\text{-}12hr}$, C_{trough} and fa) or median ratios (T_{max}). p values were calculated between values in Table 6.6 and Table 6.4.

6.3.6 The impact of multiple dosing on raltegravir exposure

The impact of multiple consecutive dosing on raltegravir PK values in subject Groups 1 to 5 is shown in Table 6.7. Subjects were given 400 mg raltegravir every 12 hours until a total of five doses had been taken and PK values in Table 6.7 are for

the final dose. GMR values were generated which were the ratios between raltegravir PK multiple dosing compared with the standard single dose given in Table 6.4. No significant change in raltegravir PK values was observed in any group on multiple dosing. This suggests no evidence of increased raltegravir exposure following multiple twice-daily dosing.

	Group 1 (very low pH)	Group 2 (low pH)	Group 3 (medium pH)	Group 4 (high pH)	Group 5 (very high pH)
C_{max} (ng/mL)	1465.9	1951.8	2100.7	2599.0	2654.3
5th-95th percentile	(879.0-2625.4)	(1335.7-3155.7)	(1440.0-3320.9)	(1719.2-4099.0)	(1765.7-4172.3)
GMR	0.98	0.96	1.01	1.04	1.04
p value	0.92	0.83	0.89	0.59	0.48
$AUC_{0\text{-}12hr}$ (ng/mL.hr)	5782.7	7355.9	8453.9	10508.9	11788.1
Range	(2890.1-12080.0)	(3927.8-14565.8)	(4430.7-16418.3)	(5613.8-18137.1)	(6867.5-20330.3)
GMR	1.00	1.01	1.04	1.04	1.07
p value	0.98	0.88	0.62	0.49	0.31
T_{max} (hours)	3.7	3.3	3.3	2.1	2.1
Range	(1.5-5.5)	(1.5-4.6)	(1.5-4.3)	(1.2-3.0)	(1.2-3.0)
Median ratio	1.00	1.00	1.03	0.91	1.00
p value	0.77	0.93	0.93	0.54	0.50
C_{trough} (ng/mL)	28.9	49.8	112.3	152.4	199.8
5th-95th percentile	(7.8-54.6)	(17.9-85.8)	(50.2-210.8)	(77.6-241.0)	(105.0-339.2)
GMR	0.94	0.97	0.99	0.99	1.06
p value	0.90	0.95	0.96	0.98	0.61
fa	0.39	0.49	0.56	0.69	0.78
5th-95th percentile	(0.17-0.59)	(0.26-0.67)	(0.35-0.73)	(0.45-0.87)	(0.46-0.96)
GMR	1.00	1.00	1.02	1.00	1.04
p value	0.70	0.99	0.77	0.76	0.21

Table 6.7. Simulated raltegravir PK values after five consecutive twice-daily doses. Each group contained 50 individuals. Geometric mean values for C_{max} (ng/mL), $AUC_{0\text{-}12hr}$ (ng/mL.hr), C_{trough} (ng/mL) and fa (fraction of dose absorbed) are given with 5^{th} and 95^{th} percentiles. Median T_{max} (hours) is given with range. Values in Table 6.7 have been divided by corresponding values in Table 6.4 to calculate the GMR (C_{max}, $AUC_{0\text{-}12hr}$, C_{trough} and fa) or median ratios (T_{max}). p values were calculated by comparing values in Table 6.7 and Table 6.4.

6.4. DISCUSSION

The IVIVE model developed in this chapter predicted the PK of raltegravir in virtual individuals with different GI pH profiles. The main PK variables were predicted with good accuracy compared with reference data, with each simulated PK parameter achieving less than a 2-fold difference in at least one of the groups (Table 6.5).

The simulations in Section 6.3.5 showed evidence of decreased raltegravir exposure when individuals were exposed to 25mM magnesium salt in the GI tract. This was simulated by using the permeability values determined in Chapter 5, where 25mM magnesium chloride significantly reduced raltegravir P_{app} through Caco-2 monolayers. This is not an ideal situation, as the concentration of GI magnesium in real life would fluctuate depending on compartment volume and magnesium absorption, thus the intestinal permeation of raltegravir would also fluctuate. However, it can be seen from the model that the rate of raltegravir absorption is a limiting factor in ultimate exposure. The data from these simulations support the hypothesis given in Chapter 5 that the combined effect of increased solubility and reduced intestinal permeability could explain the interaction observed between raltegravir and magnesium-containing antacid *in vivo* (Kiser *et al.*, 2010).

The simulations in Section 6.3.6 showed no evidence of increased raltegravir exposure following multiple twice-daily dosing, when compared to single dose. This partially agrees with published literature (Iwamoto *et al.*, 2008d). The study by Iwamoto *et al* compared the PK of steady-state raltegravir (400 mg twice-daily for 10 days) and single dose raltegravir (400 mg) in healthy subjects and found that the

steady-state/single dose ratio for C_{max}, $AUC_{0\text{-}12hr}$ and C_{trough} was 0.98, 1.05 and 1.48, respectively. Both C_{max} and $AUC_{0\text{-}12hr}$ ratios are similar to the results generated in the Simcyp model and show no evidence of increased exposure following multiple doses. The C_{trough} following multiple doses, however, was claimed to be 48% higher than single dose. This does not match the results from the Simcyp model, which showed no evidence of increased C_{trough} following multiple doses. However, a statistical comparison was not made on the C_{trough} data presented by Iwamoto *et al* and therefore the apparent increase may be due to sample variability. Furthermore, only 6 healthy subjects were used during the 400mg single and multiple dose studies and all these subjects were male. Being aware that the variability in raltegravir PK sampling is high, the small sample size and bias towards male subjects may have decreased the reliability of the data.

A recent study found a statistically significant 65% increase ($p = 0.01$) in raltegravir bioavailability in females compared to males(Arab-Alameddine *et al.*, 2012). Females have higher gastric pH and longer GI transit time than males (Soldin *et al.*, 2011) and results from the Simcyp model suggest both of these factors could potentially increase raltegravir exposure. However, the data from another study found that raltegravir C_{trough} was 58% lower in females compared to males ($p = 0.007$), with $AUC_{0\text{-}\infty}$ and C_{max} unchanged (Iwamoto *et al.*, 2008d). The discrepancy between these studies may be explained by the smaller female subject number in the study by Iwamoto et al (6 females) compared to the study by Arab-Alameddine et al (31 females). Also, the subjects used in the study by Arab-Alameddine et al were a combination of HIV-negative and HIV-positive subjects, with the majority being

HIV-positive (88%), whereas HIV-negative healthy subjects were included in the study by Iwamoto et al.

The IVIVE model has limitations and further *in vitro* data could potentially improve the model's predictive ability. Elimination of raltegravir from virtual subjects was determined by whole organ clearance obtained from published literature: information about the actions of individual metabolism enzymes was not included. The metabolism of raltegravir is well characterised and includes enzymes UGT1A1, UGT1A3 and UGT1A9 (Iwamoto *et al.*, 2008a). A model which included the actions of these individual enzymes on raltegravir metabolism, combined with known phenotypic variations and expression levels in the virtual population, could provide a more accurate model for determining raltegravir elimination. Similarly, the impact of drug transporters on raltegravir exposure *in vivo* is not fully understood and was not included in the final model.

Raltegravir PK profiles occasionally contain multiple peaks or delayed (>8 hours after dosing) peaks and, in an attempt to explain these peaks, it has been suggested that raltegravir is able to undergo enterohepatic recirculation via conversion of the raltegravir metabolite back to the parent form in the intestine and can subsequently be re-absorbed (Arab-Alameddine *et al.*, 2012). However, a PK study in healthy subjects using radiolabelled raltegravir did not support the theory, as there was no evidence of drug reabsorption (da Silva *et al.*, 2010). Therefore, enterohepatic recirculation of raltegravir was investigated in the validation process but was not included in the final model. Further investigation is needed to determine the extent of

raltegravir enterohepatic recirculation and these data would have the potential to further improve the Simcyp model.

In conclusion, the Simcyp population-based ADME simulator has been used to create a model simulating raltegravir PK parameters with acceptable accuracy to real life data. The most useful feature of this model is to investigate "what-if" scenarios, by directly altering subject physiological parameters such as GI pH and drug absorption rate and observing the effect on raltegravir PK. This also provides a tool for investigating other drugs, including HIV integrase inhibitors currently in development, which have also shown interactions with food and metal-containing products.

Chapter 7

General discussion

Table of Contents

7.1 SUMMARY OF EXPERIMENTAL DATA

The primary goal of this thesis was to identify factors influencing raltegravir pharmacokinetics and cellular exposure. Investigations have included the determination of raltegravir transport by known drug transporters *in vitro* (Chapters 2, 3 and 4), the effect of pH and metal binding on raltegravir physicochemical properties and cell permeation (Chapter 5), and the use of computer-based PK modelling to better understand how these *in vitro* characteristics may translate into patient PK (Chapter 6).

In Chapter 2, raltegravir transport by ABCB1 was confirmed *in vitro*. Transport of raltegravir by ABCB1 has also recently been confirmed *in vitro* by Minuesa et al, where a 47% reduction in raltegravir accumulation was observed in CEM_{VBL100} cells compared to CEM cells (de Kanter *et al.*, 2012). However, the impact of ABCB1 on raltegravir disposition *in vivo* has yet to be fully determined.

Evidence supporting a strong role for ABCB1 in influencing raltegravir PK is limited. Indeed, most studies have suggested no significant role for ABCB1 in raltegravir disposition *in vivo*. The potential effect of ABCB1 inhibitor ritonavir on raltegravir PK was examined in healthy subjects administered raltegravir alone (400 mg single-dose), followed by ritonavir (100 mg twice daily) for 16 days with a single dose of raltegravir (400 mg) on day 14. In the presence of ritonavir, raltegravir pharmacokinetics were not significantly affected: the GMR (90% CI) for C_{12hr}, AUC and C_{max} were 0.99 (0.70, 1.40), 0.84 (0.70, 1.01) and 0.76 (0.55, 1.04), respectively (Iwamoto *et al.*, 2008c). The *ABCB1* 3435C>T mutant variant (rs 1045642) has been reported to affect ABCB1 expression and in a recent study the effect of this mutation

on raltegravir PBMC and cerebrospinal fluid concentrations were assessed in healthy volunteers. Penetration into CSF and PBMC was not altered by *ABCB1* 3435C>T (Johnson *et al.*, 2012). The study also investigated 276 polymorphisms across *ABCC1, ABCC4, ABCC5, ABCG2, SLC15A1, SLC15A2, SLC22A2, SLC22A3, SLC22A6, SLC22A8, SLCO1A2, SLCO1C1, SLCO2B1,* and *SLCO3A1* and found no correlation between polymorphisms and concentrations of raltegravir in PBMC or CSF.

In Chapter 3, raltegravir was significantly transported by SLC22A6 and SLC15A1 using the *Xenopus laevis* oocyte expression system. Caco-2 monolayers express high levels of SLC15A1 on the apical cell membrane, facilitating A-to-B permeability of substrates (Behrens *et al.*, 2004) and results from Caco-2 monolayer permeability experiments in this thesis suggest there was no significant active transport of raltegravir in the A-to-B direction (efflux ratio of 2.5 when both chambers were pH 7.4) and that inhibition of ABCB1 in this system did not result in predominant A-to-B permeability. Therefore, SLC15A1 is unlikely to play a major role in luminal absorption predicted from the Caco-2 cell model. As such, further investigations of raltegravir transport by SLC15A1 were not conducted.

In Chapter 4, raltegravir and tenofovir were shown to compete for SLC22A6 using the *Xenopus laevis* oocyte expression system. Transport of tenofovir by SLC22A6 was reduced in the presence of raltegravir and this presents the possibility that raltegravir could reduce renal clearance of SLC22A6 substrates when co-administered. Raltegravir inhibited transport of tenofovir by SLC22A6 with an IC_{50} value of 14 μM. This figure is comparable to raltegravir plasma concentrations in a

PK study using healthy volunteers, where mean raltegravir C_{max} was 10.6 μM after administration of a single standard 400 mg tablet (Iwamoto *et al.*, 2008d). However, mean raltegravir C_{max} concentrations in most PK studies are substantially lower, for example 4.9 μM (Kassahun *et al.*, 2007), 2.9 μM (Iwamoto *et al.*, 2009b) and 2.0 μM (Kiser *et al.*, 2010) and therefore raltegravir is unlikely to achieve plasma concentrations which would substantially alter SLC22A6 activity at the kidney. However, it is possible that raltegravir is able to concentrate in the kidneys and achieve local concentrations higher than those detected in the plasma. Although possible, this seems unlikely because raltegravir is predominantly eliminated via the liver and only around 30% of total drug is excreted via the kidney (with only 30% of this being in the parent drug form). Furthermore, in a clinical study co-administered raltegravir did not alter tenofovir C_{24hr} and actually caused a minor but significant decrease in tenofovir C_{max} (23% reduction, $p < 0.05$), which contradicts the hypothesis that raltegravir can reduce the renal excretion of SLC22A6 substrates. Raltegravir concentration in the cerebrospinal fluid is more than 20-fold lower than in plasma (Yilmaz *et al.*, 2009) and it is possible that SLC22A6 (which his expressed on the apical surface of the blood-cerebrospinal fluid barrier) is actively removing raltegravir from the cerebrospinal fluid, although this remains a hypothesis and has not been demonstrated in this thesis.

To summarise this initial stage of the thesis, raltegravir has only shown interactions with drug transporters ABCB1, SLC22A6 and SLC15A1 *in vitro*. However, transport in each case was less than that observed for positive control substrates, and clinical evidence does not suggest a crucial role of these transporters in raltegravir PK. The minimal interaction of raltegravir with transporters may be seen as beneficial; much

like with the lack of interaction between raltegravir and cytochrome P450 enzymes. This reduces the risk of drug interactions and also reduces the risk of raltegravir exposure being altered by polymorphisms in transporters. If ABCB1 and SLC22A6 have a minor role in raltegravir disposition *in vivo*, the actions of these transporters would not be predicted to explain why patients receiving raltegravir display such large variation in exposure. It should be noted however that there are over 400 transporters coded for by the human genome (http://www.genenames.org/) and only relatively few have been characterised in any detail for drug transport.

Following transporter investigations in Chapter 2, 3 and 4, more fundamental physicochemical properties of raltegravir were investigated in relation to how these properties influence cellular exposure. There were several reasons why the focus of the investigations changed. First, no plausible transporters had been identified to explain the large intra- and inter- patient variability in raltegravir exposure and characterising the remaining transporters in the genome without a solid hypothesis was not feasible. Second, when initially validating Caco-2 monolayer experiments, the cellular permeability of raltegravir was observed to be sensitive to small changes to transport buffer pH. This suggested that pH could be a greater determining factor than ABCB1 in raltegravir Caco-2 cell permeability. Third, there has been steadily growing evidence from clinical studies that food and pH-altering agents could substantially alter raltegravir PK.

In Chapter 5, the effects of pH and metal binding on various pharmacological characteristics of raltegravir were investigated. Raltegravir was determined to be a weak acid with pKa of 6.67 and increasing pH above the pKa caused decreased logP,

increased solubility, increased tablet breakdown and (at lower drug concentrations) decreased cell membrane permeability. Additionally, the presence of divalent metals, but not monovalent metals, decreased raltegravir cell membrane permeability, presumably via the formation of metal-drug complexes. Figure 7.1 hypothesises how these factors may play a role in raltegravir absorption.

In Chapter 6, data generated in Chapter 5 was used to construct a computer model simulating raltegravir absorption, which was used to predict the effects of GI pH and metal binding on raltegravir bioavailability. Predictions were comparable to real subject PK data and have confirmed that environmental factors in the GI tract can play a significant role in raltegravir PK variation.

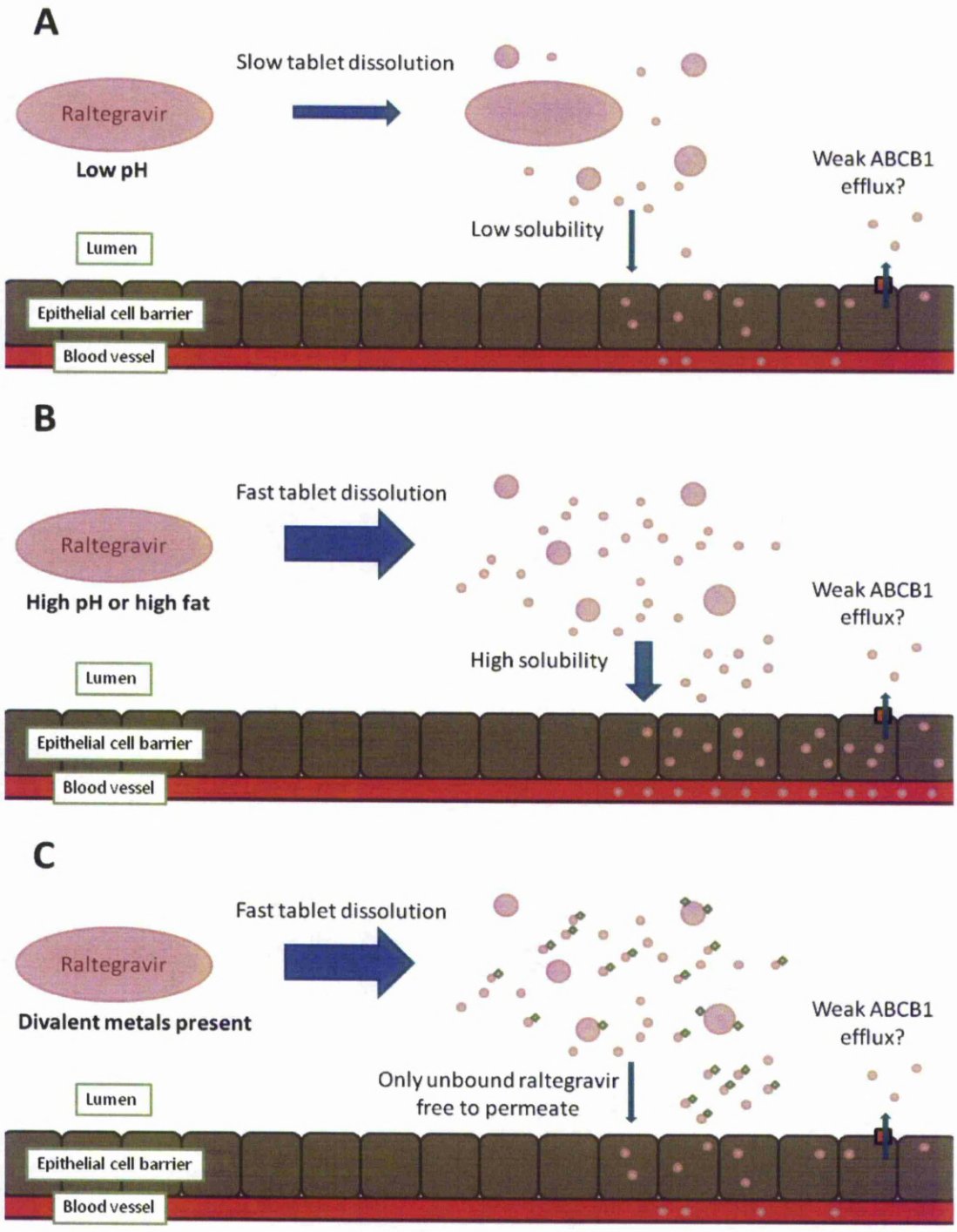

Figure 7.1. A hypothetical scenarios when a raltegravir tablet is taken by either a patient with low GI pH (Figure 7.1A), a patient having taken omeprazole (Figure 7.1B) or a patient having taken a divalent metal-containing antacid (Figure 7.1C). Figure 7.1A shows slow tablet dissolution and low luminal drug solubility caused by

the low pH environment. The raltegravir tablet may remain wholly or partially intact until later sections of the GI tract, where pH is higher. This may be the cause of the delayed or double peaks seen in some subject's PK profiles. Figure 7.1B shows rapid tablet dissolution and high luminal drug solubility, resulting from an increased pH environment and the addition of charge to the drug. Figure 7.1C shows rapid tablet dissolution and drug solubility caused by high GI pH, but low drug permeation through the gut wall. This reduced permeation results from raltegravir binding directly to the magnesium in the antacid, forming a drug-metal complex which is unable to permeate a cell membrane. As drug concentration in the lumen reduces as it passes through the intestine, drug solubility would no longer be a restricting factor, whereas the presence of ingested divalent metals will reduce drug absorption throughout the GI tract.

7.2 FUTURE INVESTIGATIONS

An investigational human trial to determine how metal-containing products affect raltegravir PK

Following the investigations in this thesis it is reasonable to ask; does this new information provide new avenues of investigation to improve clinical management with raltegravir, for example by increasing bioavailability or reducing PK variability?

Data in Chapters 5 and 6 show that divalent cation binding has the potential to reduce raltegravir cell membrane permeability *in vitro* and *in silico*. Clinical data also shows that divalent metal-containing antacids reduce the exposure of elvitegravir and dolutegravir. Therefore, the likelihood of an interaction between raltegravir and co-administered multivitamins *in vivo* is high and is certainly worthy of empirical determination. In this context, the author has recently secured funding to conduct a single centre, open label, three arm, five phase controlled study using 15 healthy subjects, investigating the impact of several co-administered metal-containing substances on the PK of subjects given a single dose 400 mg raltegravir tablet (Figure 7.2). Each subject will also have GI pH monitored by ingesting a radiotelemetric pH-recording capsule with the raltegravir tablet. Each phase will consist of a different treatment, as detailed in Figure 7.2.

Volunteers will be assigned into one of the three arms, ensuring that each treatment is performed by the completion of the trial. This assignment into separate arms will

help reduce any bias resulting from having identical order of treatments for each volunteer. Following the administration of treatment, blood samples will be taken across a 12 hour time course, which will be used to quantify raltegravir plasma concentration and create PK profiles. During the 12 hour blood sampling time course, the GI pH of volunteers will be monitored and data used to determine correlations between GI pH and raltegravir PK. The five phases will be separated by wash-out periods of four days to allow for total removal of raltegravir from the subject. As food has been shown to exacerbate raltegravir PK variability and increase or decrease raltegravir absorption depending on fat content, volunteers will fast overnight before beginning treatment.

The primary endpoint for the study will be the determination of a change in 400 mg raltegravir $AUC_{0\text{-}12hr}$, C_{12hr}, C_{max} and T_{max} following dosing of monovalent metal-containing antacid, divalent metal-containing antacid or multivitamin. The secondary endpoints will be the safety and tolerability of raltegravir with/without concomitant substances, the correlation between GI pH and raltegravir PK, the selection of an alternative antacid that does not cause a reduction in raltegravir C_{12hr} and the selection of an alternative dosing regimen which will allow divalent antacids and raltegravir to be co-administered and that does not cause a reduction in raltegravir C_{12hr}. The protocol for this trial has now been finalised and the trial is to be undertaken at the University of Liverpool with an expected start date of August 2012.

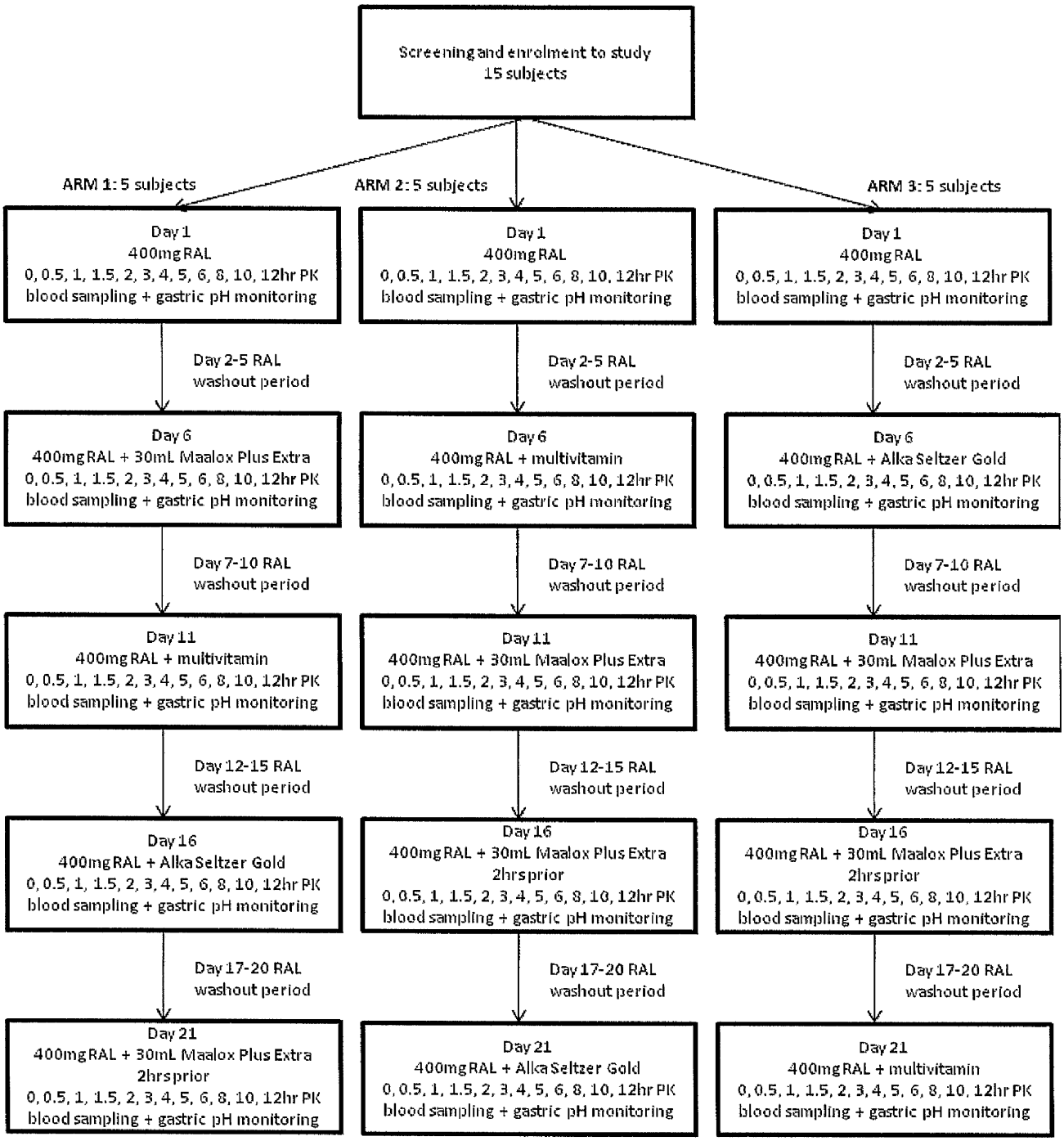

Figure 7.2. A study investigating the impact of several co-administered metal-containing substances on PK of subjects given a single dose 400 mg raltegravir tablet. The co-administered substances are; 1) Maalox Plus Extra, which raises gastric pH and contains divalent metals; 2) a standard multivitamin tablet, which contains several monovalent and polyvalent metals; 3) Alka Seltzer Gold, which

raises gastric pH and contains monovalent metals. The effect of taking Maalox Plus Extra two hours prior to taking the raltegravir tablet will also be investigated, as it is hypothesised that separating the treatments may prevent the drug interaction.

Utilising nanodispersed raltegravir to reduce drug pH sensitivity

Recent work at the University of Liverpool has indicated that the bioavailability of a number of PIs and NNRTIs can be enhanced using nanotechnology. Therefore, another possibility for future investigations is the use of raltegravir nanodispersions to overcome pH-determined solubility and to improve bioavailability. Using technology developed in Liverpool (Zhang *et al.*, 2008) a panel of raltegravir nanodispersions could be synthesised with controlled size, surface charge and polydispersity. These nanodispersions could then be characterised for their transcellular permeability across Caco-2 cell monolayers. Resulting P_{app} values would be used to simulate PK of the nanodispersions using the SimCyp population simulator to enable IVIVE, as in Chapter 6. The results from IVIVE could then be used to inform selection of appropriate doses for study in rodents. For this, adult male Wistar rats could be dosed with nanodispersions by oral gavage and plasma and tissue drug concentrations quantified by mass spectrometry. The PK properties could then be determined using NONMEM and used to provide an early risk/benefit assessment of the nanodispersion relative to an aqueous solution of raltegravir.

Nanodispersions of raltegravir are unlikely to be altered by pH, although this would need to be confirmed *in vitro*. This may represent a novel means of protecting the drug from pH changes and food effect in the GI tract. In addition, metal cations

would theoretically be excluded from the nanodispersion and therefore products with high metal contents (antacids, multivitamins, etc) would be unlikely to alter the absorption of nanoformulated raltegravir.

A previous clinical study by Dechamps et al provides an example of nanodispersions being used to protect megestrol acetate from influencing factors in the GI (Deschamps *et al.*, 2009). Megestrol acetate oral suspension, an appetite stimulant, is available as a standard formulation (MAOS) and a nanodispersion formulation (MA-ES). The PK of both was determined in healthy volunteers under both fed and fasted conditions. Both formulations achieved a similar C_{max} under fed conditions, whereas under fasted conditions MAOS C_{max} reduced by 86% and MA-ES only reduced by 30%, indicating that the nanodispersion PK was protected from the influence of fasting.

7.3 FINAL SUMMARY

In summary, the data within this thesis indicate that environmental factors such as the pH of the GI, the binding of raltegravir to divalent metals and food effects are major determinants of raltegravir cellular exposure. Drug transporters also appear to play a role but the contribution of the studied transporters to the large variability in raltegravir PK in the same patient appears to be minimal (Cattaneo *et al.*, 2012). However, distribution of raltegravir varies between tissues, with high drug concentrations in genital tract and low drug concentrations in CSF (Section 1.6.5). This variability in tissue penetration may be influenced by active transport across blood-tissue border membranes, but may also involve different affinities in tissue protein binding. Induction by rifampicin (Wenning *et al.*, 2009a) and inhibition by atazanavir (Iwamoto *et al.*, 2008b) of UGT1A1 both remain important causes of raltegravir-drug interactions (Figure 7.3).

The knowledge gained from these investigations can help to improve future integrase inhibitor design. Additionally, immediate investigations to determine the effects of divalent metal-containing products on raltegravir exposure in subjects are warranted. This is important because these interactions have the potential to reduce raltegravir C_{trough} to sub-optimal concentrations, as seen with divalent metal-containing antacids (Kiser *et al.*, 2010). Also, improved raltegravir formulation to prevent pH influencing tablet breakdown could provide a relatively simple strategy to reduce high patient PK variability.

The benefits of raltegravir include its low toxicity, rapid reduction in viral load and effectiveness against HIV resistant to other antiretrovirals. A successful once-daily regimen of raltegravir would be of great advantage. Although previous efforts failed to show non-inferiority of a once-daily raltegravir regimen, an improved knowledge of factors influencing raltegravir disposition provide a rational basis in which to achieve this goal.

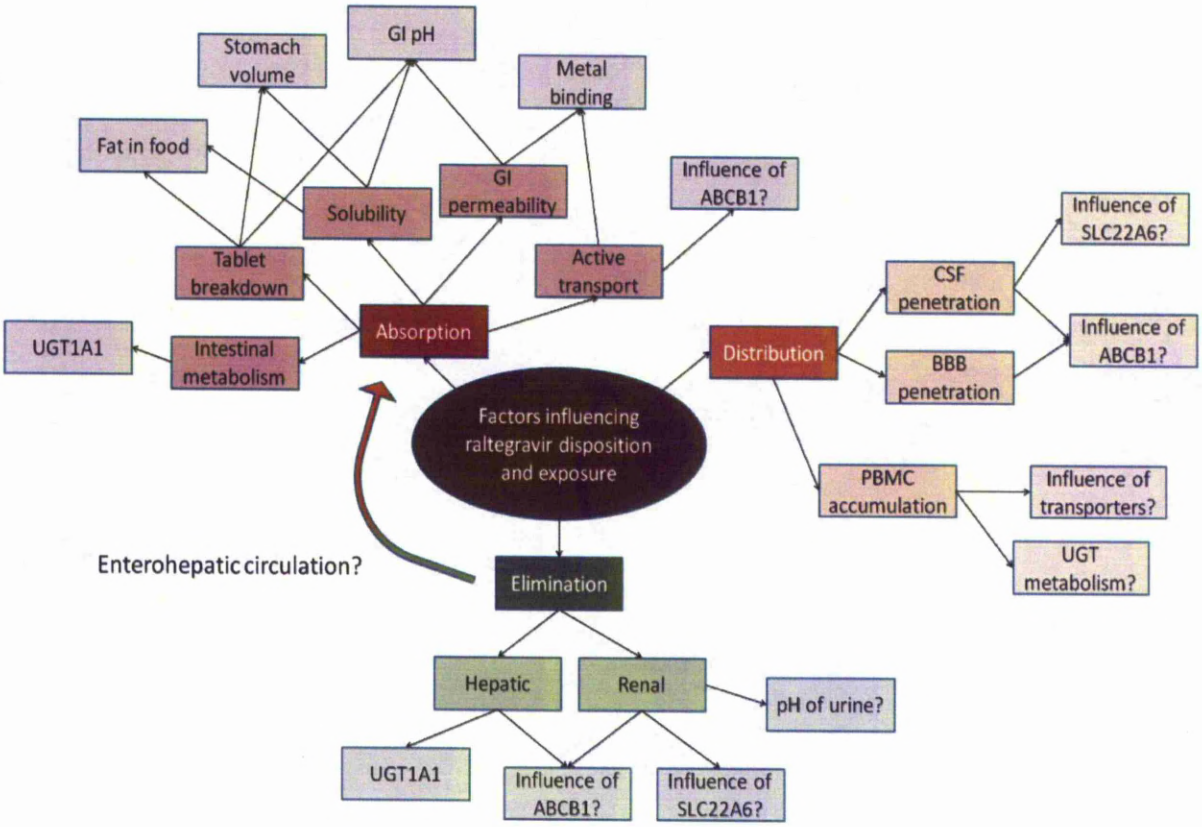

Figure 7.3. Some factors which may influence raltegravir absorption, distribution and elimination in humans. Factors include UGT1A1-mediated drug metabolism, pH-influenced drug absorption, drug-metal binding and drug transport. Both the existence of raltegravir enterohepatic recirculation and the main factors influencing raltegravir tissue distribution are not fully understood, but provide for exciting future research.

REFERENCES

Adamson CS (2012). Protease-Mediated Maturation of HIV: Inhibitors of Protease and the Maturation Process. *Mol Biol Int* Epub ahead of print: 604261, Jul 25.

Agarwal S, Pal D, Mitra AK (2007). Both P-gp and MRP2 mediate transport of Lopinavir, a protease inhibitor. *Int J Pharm* **339**(1-2): 139-147.

Aherne GW, Marks V, Mould GP, Piall E, White WF (1978). The interaction between methotrexate and probenecid in man [proceedings]. *Br J Pharmacol* **63**(2): 369P.

Aiken C (2006). Viral and cellular factors that regulate HIV-1 uncoating. *Curr Opin HIV AIDS* **1**(3): 194-9.

Ames BN, Profet M, Gold LS (1990). Nature's chemicals and synthetic chemicals: comparative toxicology. *Proceedings of the National Academy of Sciences of the United States of America* **87**(19): 7782-7786.

Anderson MS, Kakuda TN, Hanley W, Miller J, Kost JT, Stoltz R, *et al.* (2008a). Minimal pharmacokinetic interaction between the human immunodeficiency virus nonnucleoside reverse transcriptase inhibitor etravirine and the integrase inhibitor raltegravir in healthy subjects. *Antimicrob Agents Chemother* **52**(12): 4228-4232.

Anderson MS, Mabalot Luk JA, Hanley WD, Jin B, Riesenberg RA, Wenning LA, *et al.* (2010). Effect of raltegravir on the pharmacokinetics of methadone. *J Clin Pharmacol* **50**(12): 1461-1466.

Anderson MS, Sekar V, Tomaka F, Mabalot J, Mack R, Lionti L, *et al.* (2008b). Pharmacokinetic (PK) Evaluation of Darunavir/Ritonavir (DRV/r) and Raltegravir (RAL) in Healthy Subjects. 48th Interscience Conference on Antimicrobial Agents and Chemotherapy. Washington DC, USA, abstract A-962.

Anderson MS, Sekar V, Tomaka F, Mabalot J, Mack R, Lionti L, *et al.* (2008c). Pharmacokinetic (PK) Evaluation of Darunavir/Ritonavir (DRV/r) and Raltegravir (RAL) in Healthy Subjects. In: *48th Annual ICAAC*. Washington, DC.

Andrews E, Glue P, Fang J, Crownover P, Tressler R, Damle B (2010). Assessment of the pharmacokinetics of co-administered maraviroc and raltegravir. *British journal of clinical pharmacology* **69**(1): 51-57.

Arab-Alameddine M, Fayet-Mello A, Lubomirov R, Neely M, di Iulio J, Owen A, *et al.* (2012). Population Pharmacokinetic Analysis and Pharmacogenetics of Raltegravir in HIV-Positive and Healthy Individuals. *Antimicrob Agents Chemother* **56**(6): 2959-2966.

Asante-Appiah E, Seeholzer SH, Skalka AM (1998). Structural determinants of metal-induced conformational changes in HIV-1 integrase. *J Biol Chem* **273**(52): 35078-35087.

Asante-Appiah E, Skalka AM (1997). A metal-induced conformational change and activation of HIV-1 integrase. *J Biol Chem* **272**(26): 16196-16205.

Back DJ, Khoo SH, Gibbons SE, Merry C (2001). The role of therapeutic drug monitoring in treatment of HIV infection. *Br J Clin Pharmacol* **52**(S1): 89S-96S.

Barau C, Delaugerre C, Braun J, de Castro N, Furlan V, Charreau I, *et al.* (2010). High concentration of raltegravir in semen of HIV-infected men: results from a substudy of the EASIER-ANRS 138 trial. *Antimicrob Agents Chemother* **54**(2): 937-939.

Barre-Sinoussi F, Chermann JC, Rey F, Nugeyre MT, Chamaret S, Gruest J, *et al.* (1983). Isolation of a T-lymphotropic retrovirus from a patient at risk for acquired immune deficiency syndrome (AIDS). *Science* **220**(4599): 868-871.

Behrens I, Kamm W, Dantzig AH, Kissel T (2004). Variation of peptide transporter (PepT1 and HPT1) expression in Caco-2 cells as a function of cell origin. *Journal of pharmaceutical sciences* **93**(7): 1743-1754.

Bisgrove D, Lewinski M, Bushman F, Verdin E (2005). Molecular mechanisms of HIV-1 proviral latency. *Expert Rev Anti Infect Ther* **3**(5):805-814.

Blanco SE, Almandoz MC, Ferretti FH (2005). Determination of the overlapping pKa values of reorcinol using UV-visible spectroscopy and DFT methods. *Spectrochimica Acta* **61**: 93-102.

Bleasby K, Castle JC, Roberts CJ, Cheng C, Bailey WJ, Sina JF, *et al.* (2006). Expression profiles of 50 xenobiotic transporter genes in humans and pre-clinical species: a resource for investigations into drug disposition. *Xenobiotica; the fate of foreign compounds in biological systems* **36**(10-11): 963-988.

Bleasby K, Hall LA, Perry JL, Mohrenweiser HW, Pritchard JB (2005). Functional consequences of single nucleotide polymorphisms in the human organic anion transporter hOAT1 (SLC22A6). *J Pharmacol Exp Ther* **314**(2): 923-931.

Boffito M, Back DJ, Blaschke TF, Rowland M, Bertz RJ, Gerber JG, *et al.* (2003). Protein binding in antiretroviral therapies. *AIDS research and human retroviruses* **19**(9): 825-835.

Bousquet L, Roucairol C, Hembury A, Nevers MC, Creminon C, Farinotti R, *et al.* (2008). Comparison of ABC transporter modulation by atazanavir in lymphocytes and human brain endothelial cells: ABC transporters are involved in the atazanavir-limited passage across an in vitro human model of the blood-brain barrier. *AIDS research and human retroviruses* **24**(9): 1147-1154.

Bouyac-Bertoia M, Dvorin JD, Fouchier RA, Jenkins Y, Meyer BE, Wu LI, *et al.* (2001). HIV-1 infection requires a functional integrase NLS. *Mol Cell* **7**(5): 1025-1035.

Bow DA, Perry JL, Simon JD, Pritchard JB (2006). The impact of plasma protein binding on the renal transport of organic anions. *J Pharmacol Exp Ther* **316**(1): 349-355.

Brainard DM, Friedman EJ, Jin B, Breidinger SA, Tillan MD, Wenning LA, *et al.* (2011a). Effect of low-, moderate-, and high-fat meals on raltegravir pharmacokinetics. *J Clin Pharmacol* **51**(3): 422-427.

Brainard DM, Kassahun K, Wenning LA, Petry AS, Liu C, Lunceford J, *et al.* (2011b). Lack of a clinically meaningful pharmacokinetic effect of rifabutin on raltegravir: in vitro/in vivo correlation. *J Clin Pharmacol* **51**(6): 943-950.

Brainard DM, Wenning LA, Stone JA, Wagner JA, Iwamoto M (2011c). Clinical pharmacology profile of raltegravir, an HIV-1 integrase strand transfer inhibitor. *J Clin Pharmacol* **51**(10): 1376-1402.

Brainard LM, AS Petry AS, Fang L, Liu C, Breidinger SA, DeNoia EP, *et al.* (2009). Lack of a Clinically Important Effect of Rifabutin (RFB) on Raltegravir (RAL) Pharmacokinetics. In: *49th Annual ICAAC*. San Francisco, CA.

Briggs JA, Grunewald K, Glass B, Forster F, Krausslich HG, Fuller SD (2006). The mechanism of HIV-1 core assembly: insights from three-dimensional reconstructions of authentic virions. *Structure* **14**(1): 15-20.

Brown GR (1993). Cephalosporin-probenecid drug interactions. *Clinical pharmacokinetics* **24**(4): 289-300.

Burckhardt G, Burckhardt BC (2011). In vitro and in vivo evidence of the importance of organic anion transporters (OATs) in drug therapy. *Handbook of experimental pharmacology*(201): 29-104.

Calcagno A, Bonora S, Bertucci R, Lucchini A, D'Avolio A, Di Perri G (2010). Raltegravir penetration in the cerebrospinal fluid of HIV-positive patients. *AIDS (London, England)* **24**(6): 931-932.

Campbell SD, de Morais SM, Xu JJ (2004). Inhibition of human organic anion transporting polypeptide OATP 1B1 as a mechanism of drug-induced hyperbilirubinemia. *Chem Biol Interact* **150**(2): 179-187.

Cattaneo D, Gervasoni C, Meraviglia P, Landonio S, Fucile S, Cozzi V, *et al.* (2012). Inter- and intra-patient variability of raltegravir pharmacokinetics in HIV-1-infected subjects. *J Antimicrob Chemother* **67**(2): 460-464.

Chan DC, Kim PS (1998). HIV entry and its inhibition. *Cell* **93**(5): 681-684.

Chandler B, Almond L, Ford J, Owen A, Hoggard P, Khoo S, *et al.* (2003). The effects of protease inhibitors and nonnucleoside reverse transcriptase inhibitors on p-glycoprotein expression in peripheral blood mononuclear cells in vitro. *Journal of acquired immune deficiency syndromes (1999)* **33**(5): 551-556.

Charman WN, Porter CJ, Mithani S, Dressman JB (1997). Physiochemical and physiological mechanisms for the effects of food on drug absorption: the role of lipids and pH. *Journal of pharmaceutical sciences* **86**(3): 269-282.

Cherepanov P, Maertens G, Proost P, Devreese B, Van Beeumen J, Engelborghs Y, *et al.* (2003). HIV-1 integrase forms stable tetramers and associates with LEDGF/p75 protein in human cells. *J Biol Chem* **278**(1): 372-381.

Chiu TK, Davies DR (2004). Structure and function of HIV-1 integrase. *Curr Top Med Chem* **4**(9): 965-977.

Choo EF, Leake B, Wandel C, Imamura H, Wood AJ, Wilkinson GR, *et al.* (2000). Pharmacological inhibition of P-glycoprotein transport enhances the distribution of HIV-1 protease inhibitors into brain and testes. *Drug Metab Dispos* **28**(6): 655-660.

Christ F, Voet A, Marchand A, Nicolet S, Desimmie BA, Marchand D, *et al.* (2010). Rational design of small-molecule inhibitors of the LEDGF/p75-integrase interaction and HIV replication. *Nat Chem Biol* **6**(6): 442-448.

Cianfriglia M, Dupuis ML, Molinari A, Verdoliva A, Costi R, Galluzzo CM, *et al.* (2007). HIV-1 integrase inhibitors are substrates for the multidrug transporter MDR1-P-glycoprotein. *Retrovirology* **4:** 17.

Clarke D, Acosta E, Bryson D, Persaud D, Cababasay M, Fenton T, *et al.* (2012). Raltegravir (RAL) pharmacokinetics (PK) and safety in neonates: washout PK of transplacental RAL (IMPAACT P1097). 13th International Workshop on Clinical Pharmacology of HIV Therapy. Barcelona, Spain, Abstract O_22.

Clavel C, Peytavin G, Tubiana R, Soulie C, Crenn-Hebert C, Heard I, *et al.* (2011). Raltegravir concentrations in the genital tract of HIV-1-infected women treated with a raltegravir-containing regimen (DIVA 01 study). *Antimicrob Agents Chemother* **55**(6)**:** 3018-3021.

Clavel F, Guetard D, Brun-Vezinet F, Chamaret S, Rey MA, Santos-Ferreira MO, *et al.* (1986). Isolation of a new human retrovirus from West African patients with AIDS. *Science* **233**(4761)**:** 343-346.

Cocohoba J, Dong BJ (2008). Raltegravir: the first HIV integrase inhibitor. *Clin Ther* **30**(10)**:** 1747-1765.

Corbeau P, Reynes J (2009). CCR5 antagonism in HIV infection: ways, effects, and side effects. *Aids* **23**(15)**:** 1931-1943.

Cordon-Cardo C, O'Brien JP, Casals D, Rittman-Grauer L, Biedler JL, Melamed MR, *et al.* (1989). Multidrug-resistance gene (P-glycoprotein) is expressed by endothelial cells at blood-brain barrier sites. *Proceedings of the National Academy of Sciences of the United States of America* **86**(2)**:** 695-698.

Crauwels H, Stevens M, De La Rosa G, Boven K (2012). Absence of Pharmacokinetic Interaction between the NNRTI Rilpivirine (TMC278) and the Integrase Inhibitor Raltegravir. 19th Conference on Retroviruses and Opportunistic Infections. Seattle, USA

da Silva D, Van Wesenbeeck L, Breilh D, Reigadas S, Anies G, Van Baelen K, *et al.* (2010). HIV-1 resistance patterns to integrase inhibitors in antiretroviral-experienced patients with virological failure on raltegravir-containing regimens. *J Antimicrob Chemother* **65**(6): 1262-1269.

Daar ES, Kesler KL, Petropoulos CJ, Huang W, Bates M, Lail AE, *et al.* (2007). Baseline HIV type 1 coreceptor tropism predicts disease progression. *Clin Infect Dis* **45**(5): 643-649.

Daniel H, Kottra G (2004). The proton oligopeptide cotransporter family SLC15 in physiology and pharmacology. *Pflugers Archiv : European journal of physiology* **447**(5): 610-618.

Daniel H, Rubio-Aliaga I (2003). An update on renal peptide transporters. *American journal of physiology. Renal physiology* **284**(5): F885-892.

Darwich AS, Neuhoff S, Jamei M, Rostami-Hodjegan A (2010). Interplay of metabolism and transport in determining oral drug absorption and gut wall metabolism: a simulation assessment using the "Advanced Dissolution, Absorption, Metabolism (ADAM)" model. *Curr Drug Metab* **11**(9): 716-729.

de Kanter C, Blonk M, Colbers A, Fillekes Q, Schouwenberg B, Burger DM (2012). Influence of the HCV Protease Inhibitor Boceprevir on the Pharmacokinetics of the HIV Integrase Inhibitor Raltegravir. 19th Conference on Retroviruses and Oppurtunistic Infections. Seattle, USA.

Decker CJ, Laitinen LM, Bridson GW, Raybuck SA, Tung RD, Chaturvedi PR (1998). Metabolism of amprenavir in liver microsomes: role of CYP3A4 inhibition for drug interactions. *Journal of pharmaceutical sciences* **87**(7): 803-807.

Decloedt EH, McIlleron H, Smith P, Merry C, Orrell C, Maartens G (2011). Pharmacokinetics of lopinavir in HIV-infected adults receiving rifampin with adjusted doses of lopinavir-ritonavir tablets. *Antimicrob Agents Chemother* **55**(7): 3195-3200.

DeJesus E, Berger D, Markowitz M, Cohen C, Hawkins T, Ruane P, *et al.* (2006). Antiviral activity, pharmacokinetics, and dose response of the HIV-1 integrase inhibitor GS-9137 (JTK-303) in treatment-naive and treatment-experienced patients. *Journal of acquired immune deficiency syndromes* **43**(1): 1-5.

Deng H, Liu R, Ellmeier W, Choe S, Unutmaz D, Burkhart M, *et al.* (1996). Identification of a major co-receptor for primary isolates of HIV-1. *Nature* **381**(6584): 661-666.

Deschamps B, Musaji N, Gillespie JA (2009). Food effect on the bioavailability of two distinct formulations of megestrol acetate oral suspension. *Int J Nanomedicine* **4**: 185-192.

Dixit V, Hariparsad N, Li F, Desai P, Thummel KE, Unadkat JD (2007). Cytochrome P450 enzymes and transporters induced by anti-human immunodeficiency virus protease inhibitors in human hepatocytes: implications for predicting clinical drug interactions. *Drug Metab Dispos* **35**(10): 1853-1859.

Doranz BJ, Rucker J, Yi Y, Smyth RJ, Samson M, Peiper SC, *et al.* (1996). A dual-tropic primary HIV-1 isolate that uses fusin and the beta-chemokine receptors CKR-5, CKR-3, and CKR-2b as fusion cofactors. *Cell* **85**(7): 1149-1158.

Drach D, Zhao S, Drach J, Mahadevia R, Gattringer C, Huber H, *et al.* (1992). Subpopulations of normal peripheral blood and bone marrow cells express a functional multidrug resistant phenotype. *Blood* **80**(11): 2729-2734.

Elsby R, Surry DD, Smith VN, Gray AJ (2008). Validation and application of Caco-2 assays for the in vitro evaluation of development candidate drugs as substrates or inhibitors of P-glycoprotein to support regulatory submissions. *Xenobiotica; the fate of foreign compounds in biological systems* **38**(7-8): 1140-1164.

Eisele E, Siliciano RF (2012). Refefining the Viral Reservoirs that Prevent HIV-1 Eradication. *Immunity* **37**(3): 377-88.

Ernest S, Rajaraman S, Megyesi J, Bello-Reuss EN (1997). Expression of MDR1 (multidrug resistance) gene and its protein in normal human kidney. *Nephron* **77**(3): 284-289.

Espeseth AS, Felock P, Wolfe A, Witmer M, Grobler J, Anthony N, *et al.* (2000). HIV-1 integrase inhibitors that compete with the target DNA substrate define a unique strand transfer conformation for integrase. *Proceedings of the National Academy of Sciences of the United States of America* **97**(21): 11244-11249.

Farnet CM, Bushman FD (1997). HIV-1 cDNA integration: requirement of HMG I(Y) protein for function of preintegration complexes in vitro. *Cell* **88**(4): 483-492.

Fassati A, Gorlich D, Harrison I, Zaytseva L, Mingot JM (2003). Nuclear import of HIV-1 intracellular reverse transcription complexes is mediated by importin 7. *EMBO J* **22**(14): 3675-3685.

Fauci A, Bartlett JG, Goosby E (1998). Early treatment of HIV-1 infection. *Lancet* **352**(9144): 1935; author reply 1936.

Fayet Mello A, Buclin T, Franc C, Colombo S, Cruchon S, Guignard N, *et al.* (2011). Cell disposition of raltegravir and newer antiretrovirals in HIV-infected patients: high inter-individual variability in raltegravir cellular penetration. *J Antimicrob Chemother* **66**(7): 1573-1581.

Feng Y, Broder CC, Kennedy PE, Berger EA (1996). HIV-1 entry cofactor: functional cDNA cloning of a seven-transmembrane, G protein-coupled receptor. *Science* **272**(5263): 872-877.

Foisy MM, Yakiwchuk EM, Hughes CA (2008). Induction effects of ritonavir: implications for drug interactions. *The Annals of pharmacotherapy* **42**(7): 1048-1059.

Forni DD, Stevens MR, Lori F (2010). Strategies to improve efficacy and safety of a novel class of antiviral hyper-activation-limited therapeutic agents: the VS411 model HIV/AIDS. *Br J Pharmacol* **161**(4): 830-843.

Fox E, Bates SE (2007). Tariquidar (XR9576): a P-glycoprotein drug efflux pump inhibitor. *Expert review of anticancer therapy* **7**(4): 447-459.

Fujita T, Brown C, Carlson EJ, Taylor T, de la Cruz M, Johns SJ, *et al.* (2005). Functional analysis of polymorphisms in the organic anion transporter, SLC22A6 (OAT1). *Pharmacogenet Genomics* **15**(4): 201-209.

Geretti A, Fearnhill E, Ceccherini-Silberstein F (2010). Prevalence and patterns of raltegravir resistance in treated patients in Europe. HIV and Hepatitis Drug Resistance Workshop. Abstract 51. Dubrovnik, Croatia.

German P, Warren D, Wei L, Zhong L, Hui J, Kearney BP (2009). Effect of food on pharmacokinetics of elvitegravir, emtricitabine, tenofovir and the pharmacoenhancer GS-9350 as a fixed dose combination tablet. *49th Interscience Conference on Antimicrobial Agents and Chemotherapy, San Fransisco, USA.*

Giannoudis A, Davies A, Lucas CM, Harris RJ, Pirmohamed M, Clark RE (2008). Effective dasatinib uptake may occur without human organic cation transporter 1 (hOCT1): implications for the treatment of imatinib-resistant chronic myeloid leukemia. *Blood* **112**(8): 3348-3354.

Goodwin JT, Conradi RA, Ho NF, Burton PS (2001). Physicochemical determinants of passive membrane permeability: role of solute hydrogen-bonding potential and volume. *J Med Chem* **44**(22): 3721-3729.

Granfors MT, Wang JS, Kajosaari LI, Laitila J, Neuvonen PJ, Backman JT (2006). Differential inhibition of cytochrome P450 3A4, 3A5 and 3A7 by five human immunodeficiency virus (HIV) protease inhibitors in vitro. *Basic Clin Pharmacol Toxicol* **98**(1): 79-85.

Grinsztejn B, Nguyen BY, Katlama C, Gatell JM, Lazzarin A, Vittecoq D, *et al.* (2007). Safety and efficacy of the HIV-1 integrase inhibitor raltegravir (MK-0518) in treatment-

experienced patients with multidrug-resistant virus: a phase II randomised controlled trial. *Lancet* **369**(9569): 1261-1269.

Haas DW, Ribaudo HJ, Kim RB, Tierney C, Wilkinson GR, Gulick RM, *et al.* (2004). Pharmacogenetics of efavirenz and central nervous system side effects: an Adult AIDS Clinical Trials Group study. *Aids* **18**(18): 2391-2400.

Hanley WD, Wenning LA, Moreau A, Kost JT, Mangin E, Shamp T, *et al.* (2009). Effect of tipranavir-ritonavir on pharmacokinetics of raltegravir. *Antimicrob Agents Chemother* **53**(7): 2752-2755.

Hare S, Gupta SS, Valkov E, Engelman A, Cherepanov P (2010). Retroviral intasome assembly and inhibition of DNA strand transfer. *Nature* **464**(7286): 232-236.

Hariparsad N, Nallani SC, Sane RS, Buckley DJ, Buckley AR, Desai PB (2004). Induction of CYP3A4 by efavirenz in primary human hepatocytes: comparison with rifampin and phenobarbital. *Journal of clinical pharmacology* **44**(11): 1273-1281.

Hartkoorn RC, Kwan WS, Shallcross V, Chaikan A, Liptrott N, Egan D, *et al.* (2010). HIV protease inhibitors are substrates for OATP1A2, OATP1B1 and OATP1B3 and lopinavir plasma concentrations are influenced by SLCO1B1 polymorphisms. *Pharmacogenet Genomics* **20**(2): 112-120.

Hasan S, Antoniou T, Loutfy M, Kovacs C, Brunetta J, Smith G, *et al.* (2012). Comparative PK analysis of maraviroc, darunavir, raltegravir, etravirine and ritonavir between blood and seminal plasma in HIV infected patients. 13th International Workshop on Clinical Pharmacology of HIV Therapy. Barcelona, Spain, Abstract P_24.

Hazuda DJ (2010). Resistance to inhibitors of the human immunodeficiency virus type 1 integration. *Braz J Infect Dis* **14**(5): 513-518.

Hicks C, Gulick RM (2009). Raltegravir: the first HIV type 1 integrase inhibitor. *Clin Infect Dis* **48**(7): 931-939.

Hightower KE, Wang R, Deanda F, Johns BA, Weaver K, Shen Y, *et al.* (2011). Dolutegravir (S/GSK1349572) exhibits significantly slower dissociation than raltegravir and elvitegravir from wild-type and integrase inhibitor-resistant HIV-1 integrase-DNA complexes. *Antimicrob Agents Chemother* **55**(10): 4552-4559.

Hilgendorf C, Ahlin G, Seithel A, Artursson P, Ungell AL, Karlsson J (2007). Expression of thirty-six drug transporter genes in human intestine, liver, kidney, and organotypic cell lines. *Drug Metab Dispos* **35**(8): 1333-1340.

Hirano A, Ikemura K, Takahashi M, Shibata M, Amioka K, Nomura T, *et al.* (2011). Lack of Correlation Between UGT1A1*6, *28 Genotypes, and Plasma Raltegravir Concentrations in Japanese HIV Type 1-Infected Patients. *AIDS research and human retroviruses*.

Hiscott J, Kwon H, Genin P (2001). Hostile takeovers: viral appropriation of the NF-kappaB pathway. *J Clin Invest* **107**(2): 143-151.

Huang L, Wring SA, Woolley JL, Brouwer KR, Serabjit-Singh C, Polli JW (2001). Induction of P-glycoprotein and cytochrome P450 3A by HIV protease inhibitors. *Drug Metab Dispos* **29**(5): 754-760.

Huang SM, Strong JM, Zhang L, Reynolds KS, Nallani S, Temple R, *et al.* (2008). New era in drug interaction evaluation: US Food and Drug Administration update on CYP enzymes, transporters, and the guidance process. *Journal of clinical pharmacology* **48**(6): 662-670.

Huang SM, Temple R, Throckmorton DC, Lesko LJ (2007). Drug interaction studies: study design, data analysis, and implications for dosing and labeling. *Clinical pharmacology and therapeutics* **81**(2): 298-304.

Hubatsch I, Ragnarsson EG, Artursson P (2007). Determination of drug permeability and prediction of drug absorption in Caco-2 monolayers. *Nature protocols* **2**(9): 2111-2119.

Huls M, Brown CD, Windass AS, Sayer R, van den Heuvel JJ, Heemskerk S, *et al.* (2008). The breast cancer resistance protein transporter ABCG2 is expressed in the human kidney proximal tubule apical membrane. *Kidney international* **73**(2): 220-225.

Ingale KB, Bhatia MS (2011). HIV-1 integrase inhibitors: a review of their chemical development. *Antivir Chem Chemother* **22**(3): 95-105.

Isel C, Ehresmann C, Marquet R (2010). Initiation of HIV Reverse Transcription. *Viruses* **2**(1): 213-243.

Iwamoto M, Hanley WD, Petry AS, Friedman EJ, Kost JT, Breidinger SA, *et al.* (2009a). Lack of a clinically important effect of moderate hepatic insufficiency and severe renal insufficiency on raltegravir pharmacokinetics. *Antimicrob Agents Chemother* **53**(5): 1747-1752.

Iwamoto M, Kassahun K, Troyer MD, Hanley WD, Lu P, Rhoton A, *et al.* (2008a). Lack of a pharmacokinetic effect of raltegravir on midazolam: in vitro/in vivo correlation. *J Clin Pharmacol* **48**(2): 209-214.

Iwamoto M, Wenning LA, Mistry GC, Petry AS, Liou SY, Ghosh K, *et al.* (2008b). Atazanavir modestly increases plasma levels of raltegravir in healthy subjects. *Clin Infect Dis* **47**(1): 137-140.

Iwamoto M, Wenning LA, Nguyen BY, Teppler H, Moreau AR, Rhodes RR, *et al.* (2009b). Effects of omeprazole on plasma levels of raltegravir. *Clin Infect Dis* **48**(4): 489-492.

Iwamoto M, Wenning LA, Petry AS, Laethem M, De Smet M, Kost JT, *et al.* (2008c). Minimal effects of ritonavir and efavirenz on the pharmacokinetics of raltegravir. *Antimicrob Agents Chemother* **52**(12): 4338-4343.

Iwamoto M, Wenning LA, Petry AS, Laethem M, De Smet M, Kost JT, *et al.* (2008d). Safety, tolerability, and pharmacokinetics of raltegravir after single and multiple doses in healthy subjects. *Clinical pharmacology and therapeutics* **83**(2): 293-299.